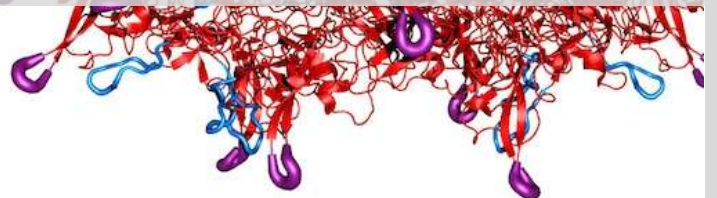


Virus Construction Kit – The Manual

Freiburg_Bioware iGEM 2010



Content

1	Overview	5
1.1	The Experimental System	5
1.2	Layers of specificity	6
2	Introduction to Adeno-Associated Virus Serotype 2.....	8
2.1	Biology of the AAV-2	8
2.1.1	Genomic organization	8
2.1.1.1	Organization of the Inverted Terminal Repeat Structure	9
2.1.2	Replication.....	9
2.1.2.1	Viral promoters	11
2.1.2.1.1	p5 promoter	12
2.1.2.1.2	p5 TATA-less promoter.....	12
2.1.2.1.3	p19 promoter	13
2.1.2.1.4	p40 promoter	14
2.1.3	Integration.....	14
2.1.4	Rescue	15
2.1.5	Rep proteins	16
2.1.5.1	Overview.....	16
2.1.5.1.1	Rep 78.....	18
2.1.5.1.2	Rep 68.....	19
2.1.5.1.3	Rep52.....	19
2.1.5.1.4	Rep40.....	20
2.1.6	VP proteins	20
2.1.6.1	VP1.....	21
2.1.6.2	VP2.....	24
2.1.6.3	VP3.....	25
2.1.6.4	Natural Tropism and HSPG motif	25
2.1.6.5	Assembly-activating protein.....	26
2.1.7	Trafficking.....	27
2.1.7.1	Endosomal transport and escape.....	29
2.2	Helper Genes.....	30
2.3	Recombinant Viruses and Mosaic Viruses.....	33
2.4	Gene Therapy	33
2.5	Immune Response.....	34
3	Components of our Virus Construction Kit.....	37
3.1	Modularization of the AAV-2.....	37
3.2	Arming	37
3.2.1	Thymidine kinase.....	37
3.2.2	Cytosine deaminase	38
3.3	Targeting.....	39
3.3.1	Loop Insertions	39
3.3.1.1	Modification of the Viral Capsid of the AAV2 using Viral Bricks	39
3.3.1.2	Cloning of Viral Bricks into capsid coding parts	40
3.3.1.3	Tagging	41
3.3.1.3.1	Specific Biotinylation via ViralBrick: The Biotinylation Acceptor Peptide.....	41

3.3.1.3.2	IMAC purification via Viral Brick: The Histidine Affinity Tag	42
3.3.1.4	Targeting.....	43
3.3.1.4.1	Targeting peptides via ViralBrick: The RGD Motif.....	43
3.3.1.4.2	Coupling Antibodies to the Viral Surface via ViralBrick: The Z34C Motif.....	44
3.3.2	N-terminal Fusion.....	45
3.3.2.1	VP1 insertion	47
3.3.2.2	Targeting molecules	48
3.3.2.2.1	Affibody Z _{EGFR:1907}	48
3.3.2.2.2	DARPin E_01.....	49
3.4	Favorite parts	53
4	Methods	56
4.1	Cloning.....	56
4.1.1	Polymerase Chain Reaction.....	56
4.1.2	Site-Directed Mutagenesis	56
4.1.3	Ligation	57
4.1.4	Transformation.....	57
4.1.5	PCR purification	58
4.1.6	Hybridisation of Oligos	58
4.1.7	Fill-in-reactions.....	59
4.1.8	DNA gel electrophoresis	59
4.1.9	Vector Dephosphorylation	60
4.1.10	Gel Extraction	61
4.1.11	Verification of Correct BioBrick Part Assembly	61
4.1.11.1	Test digestion	61
4.1.11.2	Colony PCR.....	61
4.1.12	Purification of Plasmid DNA	62
4.1.12.1	Miniprep	62
4.1.12.2	Midiprep	62
4.2	Cell Culture	63
4.2.1	Cell lines.....	63
4.2.1.1	HEK 293 cells	63
4.2.1.1.1	Overview	63
4.2.1.1.2	Establishing AAV-293 Cultures from Frozen Cells	64
4.2.1.1.3	Passaging of AAV-293 Cells	64
4.2.1.1.4	Transfecting the AAV-293 Cells	65
4.2.2	HT1080	66
4.2.3	A431.....	66
4.2.4	Flow Cytometry	66
4.2.4.1	Overview.....	66
4.2.4.2	Sample Preparation for Flow Cytometry.....	70
4.2.4.3	Cell Staining for Flow Cytometry.....	70
4.2.5	MTT Assay.....	71
4.2.5.1	Overview.....	71
4.2.5.2	Protocol	72
4.2.6	Quantitative real-time PCR.....	73
4.2.6.1	SYBR Green.....	74
4.2.6.2	Protocols.....	74
4.2.6.2.1	Genomic titer	75
4.2.6.2.2	Infectious titer	75
4.2.7	Fluorescence microscopy	77

5	Results.....	78
5.1	Modularization	78
5.1.1	Introduction to Modularization of Vector Plasmid	78
5.1.2	Recombinant and Modular Vectorplasmid Carrying GOI.....	78
	Recombinant and Modular Vector plasmid Carrying GOI.....	78
5.1.4	Cloning and Combination Strategies for the Vector Plasmid	80
5.1.5	Testing functionality of Assembled Vector Plasmid	84
5.1.5.1	Fluorescence Microscopy of Target Cells Demonstrates GOI Expression	84
5.1.5.2	Analysis of Target Cells by Flow Cytometry demonstrates GOI Expression.....	85
5.1.5.2.1	Influence of hGH terminator BioBrick on GOI Expression	85
5.1.5.2.2	Influence of <i>Beta-globin</i> intron Biobrick on GOI Expression.....	88
5.1.5.2.3	Functionality of the Full Assembled Vectorplasmid Demonstrated by GOI Expression	90
5.1.5.3	Conclusion	93
5.1.6	Modulatization of the RepCap plasmid	94
5.1.6.1	Overview Modularization: Overview.....	94
5.1.7	Modularization: Removing iGEM restriction sites and establishing loop insertion capability	95
5.1.7.1	Modifications in Rep.....	95
5.1.7.2	Modifications in VP123	96
5.1.7.3	Modularization: Adapting pSB1C3 to loop insertions – pSB1C3_001	99
5.1.7.4	Turning-off natural tropism: HSPG-knock-out	100
5.2	Targeting.....	102
5.3	Loop Insertions for Targeting, Purification, and Biotechnological Applications	102
5.3.1.1	IMAC purification via Viral Brick: The Histidin Affinity Tag	104
5.3.1.2	qPCR for infectious titer	105
5.3.2	His-Affinity Tag	106
5.3.2.1	Theory.....	106
5.3.2.2	Material and Methods:.....	107
5.3.2.3	Results and Discussion:	108
5.3.3	Biotinylation Acceptor Peptide (BAP).....	110
5.3.3.1	Theory.....	110
5.3.3.2	Materials and Methods:	111
5.3.3.3	Results and Discussion:	112
5.3.4	Miniaturized antibody binding domain (Z34C).....	113
5.3.4.1	Theory for Z34C	113
5.3.4.2	Material and Methods.....	113
5.3.4.3	Results and Discussion	114
5.4	N-terminal Fusion of Targeting Molecules for Targeting and Tumor Killing.....	118
5.4.1	Design of VP2 Fusion	118
5.4.2	Design of the VP1 Insertion.....	121
5.4.3	Colony PCR.....	124
5.4.4	Fluorescence analysis od viral stocks	125
5.4.5	Concentrating VP1UP_NLS_mVENUS_VP2/3 Viruses	125
5.4.6	Fluorescence microscopy	126
5.4.7	Flow cytometry.....	127
qPCR		137
5.4.8	Time laps.....	140
5.5	Arming: Suicide Genes as GOIs.....	142
5.5.1	Introduction.....	142

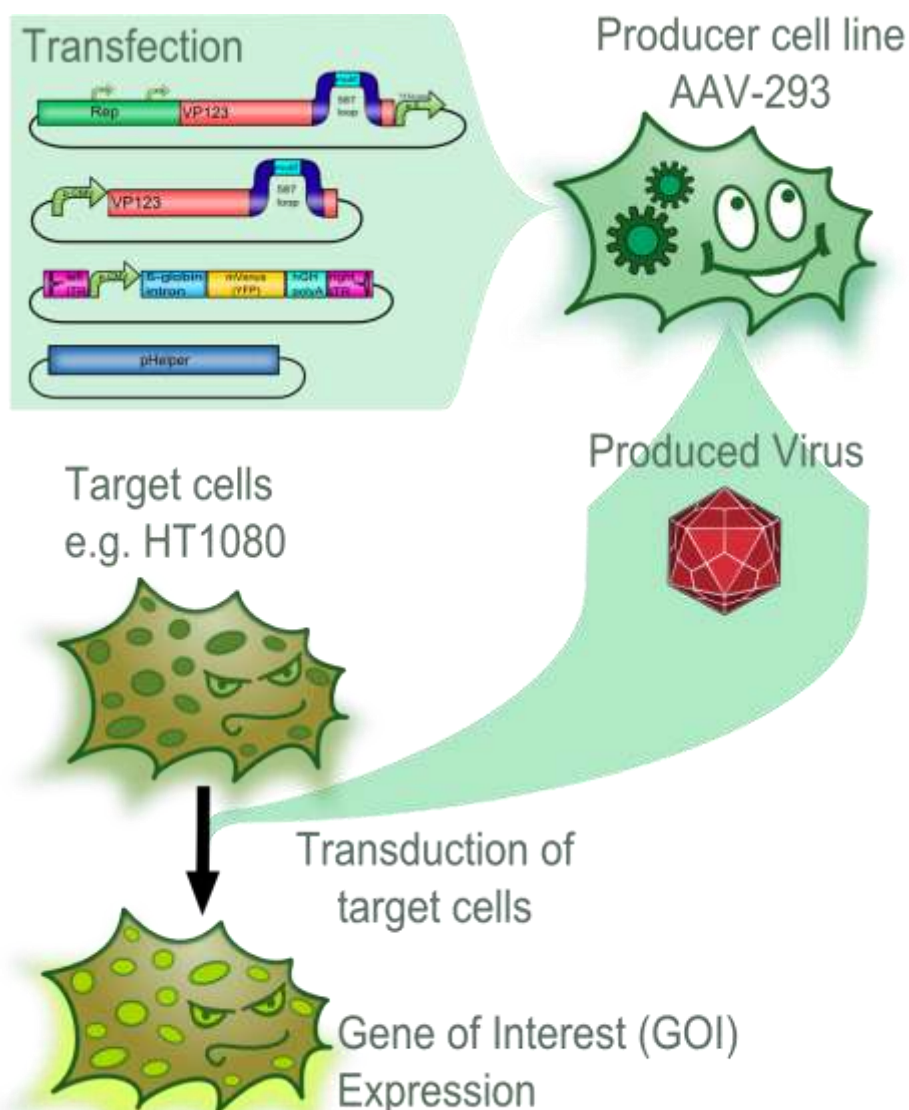
5.5.2	Successful Assembly of Vector Plasmids Carrying Suicide Genes via Cloning	142
5.5.3	Monitoring Efficient Tumor Killing by Phase-Contrast Microscopy	145
5.5.4	Quantitative Analysis of Cell Death by Flow Cytometry.....	146
5.5.5	Titration of Ganciclovir Concentrations for Efficient Cell Killing by Cytotoxicity Assays .	148
5.5.6	Killing Non-transduced Tumor Cells via Bystander Effect	152
5.5.7	Conclusions.....	154
5.6	Modeling.....	155
5.6.1	Model for Virus Production	155
5.6.1.1	Reaction Scheme	155
5.6.1.2	Reduced Reaction Scheme	157
5.6.1.3	Differential Equations.....	158
5.6.1.4	Methods and Simulation	159
5.6.1.5	Results and Discussion	163
6	Outlook	167
6.1	Other strategies.....	167
6.1.1	Evolutionary Self Coating Approach (ESCA)	167
6.1.2	RNA interference (RNAi) approach	167
7	Biosafety	Error! Bookmark not defined.
8	Appendix	169
8.1	<i>Dear diary</i> (– a Story on ITRs),	169
8.2	ITR Methods	170
8.3	Protocols.....	176
8.3.1	Recipes for stock solutions	176
8.3.1.1	Antibiotics.....	176
8.3.1.2	Buffers and Solutions	177
8.3.1.3	Media.....	178
8.3.1.4	E. coli culture	179
8.3.1.4.1	Competent E-coli-cells.....	179
8.3.2	Cell culture protocols	180
8.3.2.1	Establishing AAV-293 Cultures from Frozen Cells	180
8.3.2.2	Passaging of AAV-293 Cells	181
8.3.2.3	Transfecting the AAV-293 Cells	182
9	Acknowledgment.....	183
10	References:.....	184

1 Overview

1.1 The Experimental System

Therapies using viral vectors are a promising approach. In an first step the plasmids of the AAV-2 Helper-free System were genetically modified by converting it into BioBricks and inserting of targeting molecules into the constructs. These plasmids were then used to transfect the producer cell line AAV-293. After an incubation of three days the viral vectors were harvested and used to transduce different target cells. The succesful transduction can then for example be measured by detecting the fluorecence of fluorescent proteins in the target cells

The majority of the modifications that were introduced into the viral vector aimed to allow differential targeting of tumor cell over healthy off-target cells.



1.2 Layers of specificity

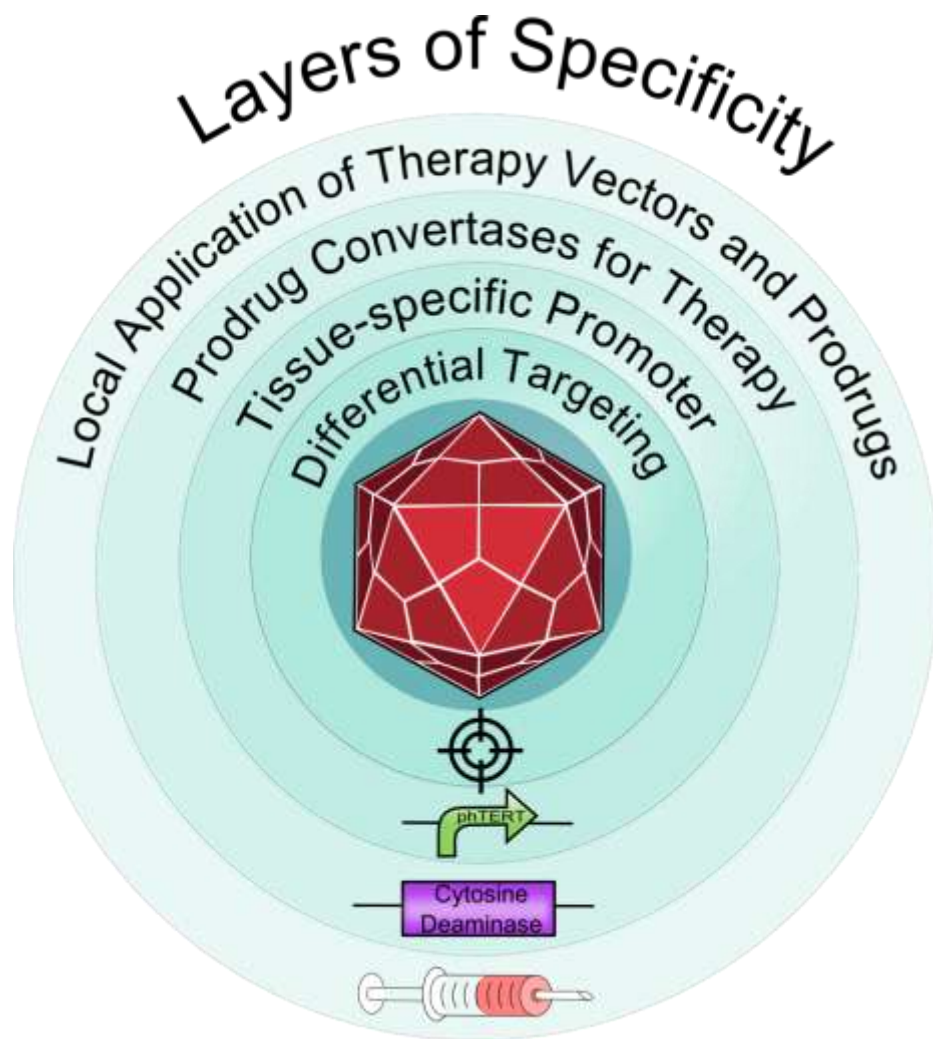
Employment of viral vectors for means of therapy is idea in the context of personalized medicine that gets more and more interest. In such applications the reduction of side effects and the safety of the patient in general is of the highest priority.

In order to satisfy this requirement we designed our Therapy Vector with several layers of Specificity:

The targeting of the viral vector towards the desired target cell (e.g. tumor cells) is the basic idea behind the employment of viral vectors for therapeutical means. There for the natural tropism has to be knocked down and a desired tropism has to be introduced that allows differential targeting of pathological but not of off-target cells. To fulfill this mission our Virus Construction Kit offers you different solutions.

Off-target cells that were transduced by mistake can be preserved from an undesired therapy effect when the therapeutic gene is controlled by a tissue specific promoter. For this mean a promoter has to be used that is as specific for the pathological tissue as possible. We included the human telomerase promoter ([phTERT](#)) which is often activated in tumor cells and is there for able to allow differential expression of a therapeutic gene product in pathological cells.

For reasons of safety Therapeutic vector do not directly trigger apoptosis in the successfully targeted cells. To include one further layer of specificity and safety we decided to arm our therapy vector with different prodrug convertases. Neither the single application of the harmless prodrug nor the single expression of the convertase has a noteworthy effect of the transduced cell. Only in cells that express the prodrug convertase and have a sufficient cytoplasmatic concentration of the belonging prodrug apoptosis is triggered. This dependency of the therapy on a prodrug can be employed to protect tissues or other persons that could come in contact with the therapeutical vector. This aspect was specially important for the development of a viral vector that is able to infect humans in the context of a undergraduate project for the iGEM competition. Therefore this approach gained our preference over other possibly equivalent arming possibilities described in the tumor therapy with viral vectors.



2 Introduction to Adeno-Associated Virus Serotype 2

2.1 Biology of the AAV-2

2.1.1 Genomic organization

The Adeno-associated virus serotype-2 (AAV-2) genome is a linear, single-stranded (ss) 4675 bp DNA virus. Due to its small size, gene genomic organization is condensed and gene regulation is complex. The viral nucleotide sequence consist of two open reading frames (ORFs) coding for Rep- and Cap proteins and are flanked on either side by identical inverted terminal repeat (ITR) structures which are palindromic and form hairpin structures.

The ITRs serve as primers for the host cells' DNA polymerase, which converts the single-stranded

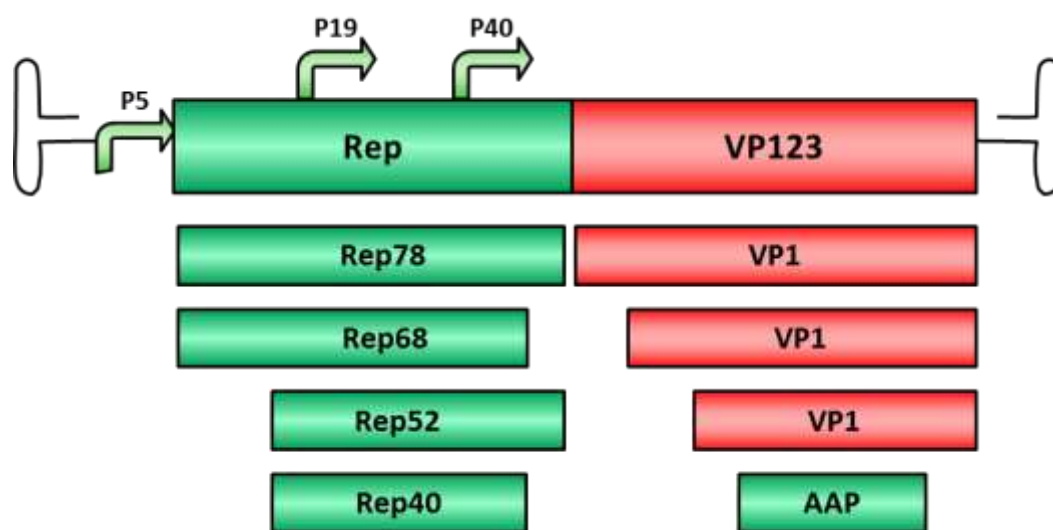


Figure 1: Genomic organization of the wt-AAV-2. The inverted terminal repeats (ITRs) flank the two open reading frames (ORFs). The four-nonstructural proteins encoded from the *rep* gene are driven by the p5 and p19 promoters, whereas the structural Cap proteins are regulated by the p40 promoter. Additionally, the Assembly Activating Protein (AAP) was found recently within the *cap* gene.

virus genome into double-stranded DNA (ds DNA) as a part of the viruses' replicative cycle. They also play important roles in viral genome integration into and rescue from the hosts genome, the formation of concatamers in the host cell nucleus and encapsidation of the viral genome into preformed capsids. Due to these essential functions, the ITR structures cannot be deleted from a viral vector and need to be delivered *in cis*.

2.1.1.1 Organization of the Inverted Terminal Repeat Structure

The inverted terminal repeat structures can be subdivided into several palindromic motives: A and A' form a stem loop which encases B and B' as well as C and C'. Those motives form both arms of the T-shaped structure. The functional motives on the ITR are two regions that bind Rep 68/78, called Rep-binding elements (RBE on the stem and RBE' on the B arm) and the terminal resolution site (trs) in which the rep proteins introduce single-stranded nicks. The 3' OH end of the A motive acts as a primer for DNA replication (D. S. Im & N Muzyczka 1990) (Lusby et al. 1980).

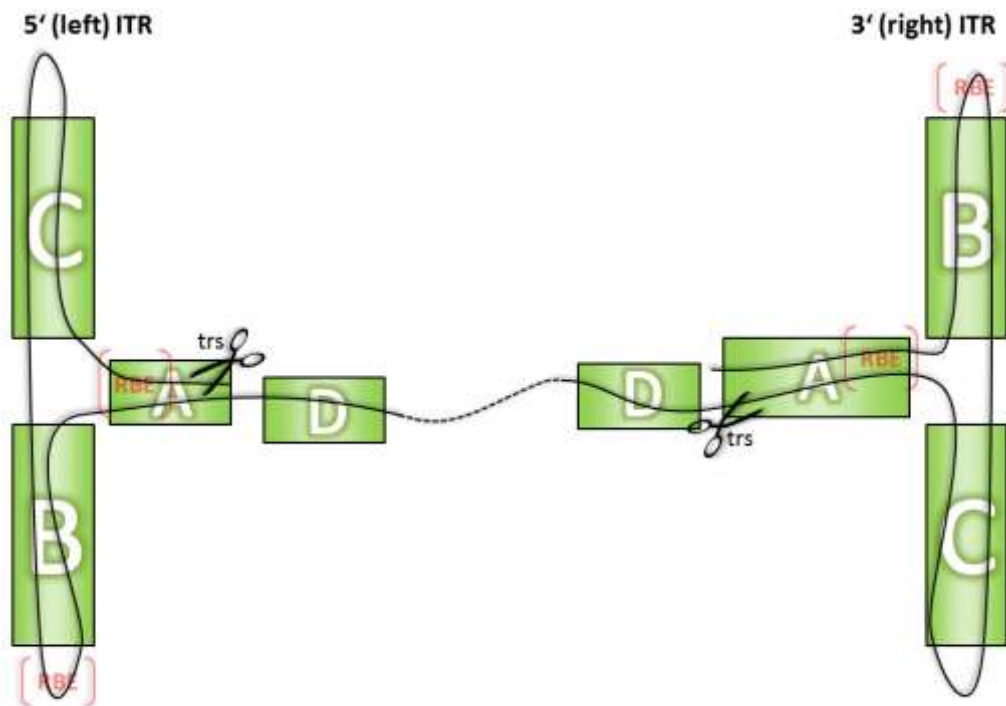


Figure 2: Organization of the ITRs, which are the only *cis*-required element in viral genome integration and replication.

2.1.2 Replication

The 3' OH end of the viral DNA folds onto itself as part of the inverted terminal repeat (ITR) structure and thus serves as a primer for elongation by the host cell's DNA polymerase. The polymerases strand displacement activity unfolds the opposite ITR structure and elongation continues until the 5' template end is reached (Lusby et al. 1980).

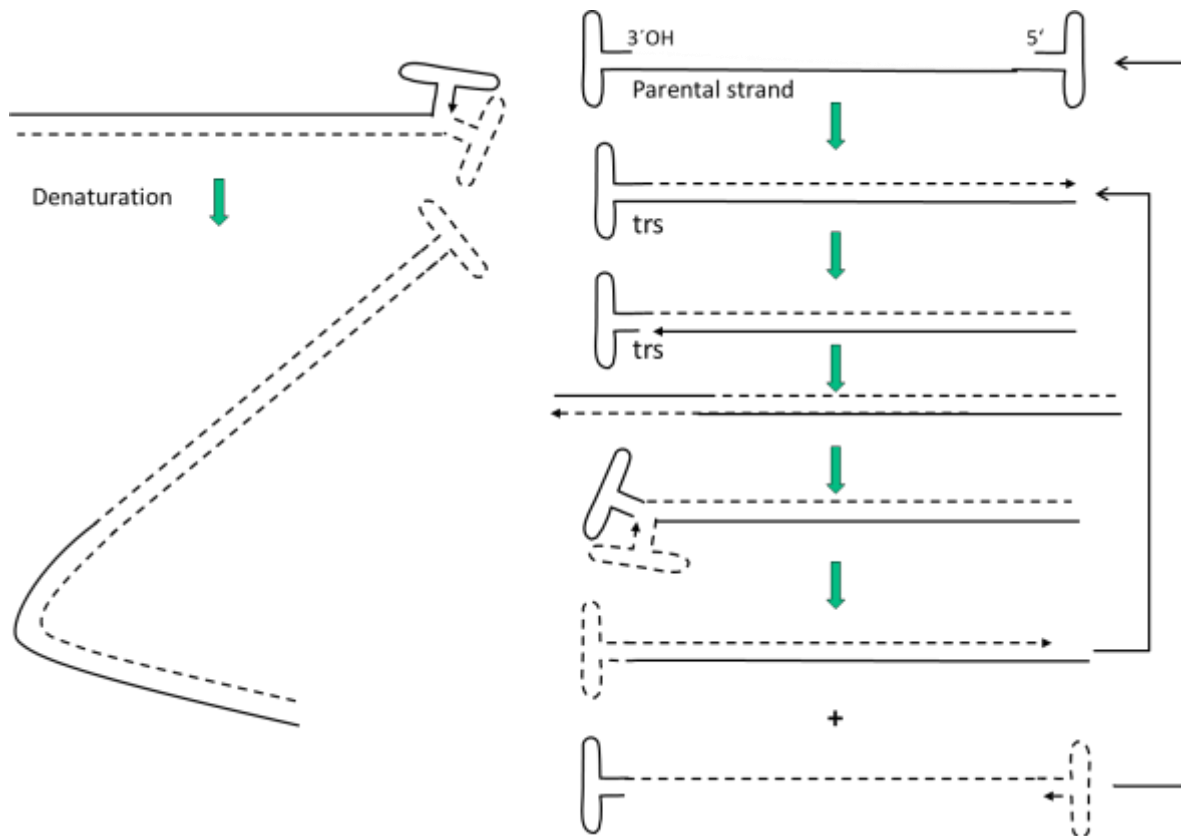


Figure 3: Schematic overview of AAV-2 replication.

The remaining hairpin structure that served as the origin of replication then acts as a target for the Rep 68/78 protein: It binds to the Rep-binding site (RBS) and unwinds the double-stranded DNA in a way that the terminal resolution site (trs) is being displayed in a single-stranded form on a stem loop. This enables the endonuclease catalytic domain of the Rep protein to introduce a nick of the parental strand at this site, which in turn serves as a new primer for DNA polymerase. The polymerase resolves the hairpin structure through strand displacement and copies the remaining end of the parental strand (D. S. Im & N Muzyczka 1990) .

Sometimes, nicking does not occur after polymerases have partially copied the virus DNA. In this case, the newly synthesized 3' end acts as a primer and the host cell's DNA polymerase copies the whole sequence once again, displacing the ITR strands in the middle of the sequence. This leads to a dsDNA containing the whole virus genome twice, called a duplex dimer (DD). Those dimers can be resolved back to duplex monomers (DM) by the Rep proteins

After replication, the dsDNA separates again forming new ssDNA in (+) and (-) polarity with hairpin structures at its ends. The Rep 40/52 proteins are involved in this process. Newly synthesized copies are either encapsidated into virus capsids or replicated again (Gonçalves, 2005a). Double-stranded genomes are formed as well through annealing of (+) - and (-) single strands. Both mechanisms occur during infection and contribute to transgene expression (Schultz & Chamberlain 2008).

If the double stranded virus DNA exists in an episomal form inside the nucleus, it tends to form linear as well as circular concatamers, which are formed by ligation of duplex monomers (Schultz & Chamberlain 2008).

2.1.2.1 Viral promoters

Three viral promoters are coordinating gene expression in the wildtype AAV-2. Each promoter regulates different open reading frames (ORFs) of regulatory proteins (p5 and p19 promoter) and structural proteins (p40 promoter). A general overview is provided in **Error! Reference source not found.** p5 and p19 promoters are repressed in absence of helper proteins provided by Ad or HSV whereas transactivation of p5 and p19 occurs in presence of helper viruses. Furthermore, the larger Rep proteins activate the p40 promoter. Since overexpression of Rep78 leads to cell cycle arrest, high levels of Rep78/68 lead to repression of the p5 promoter.

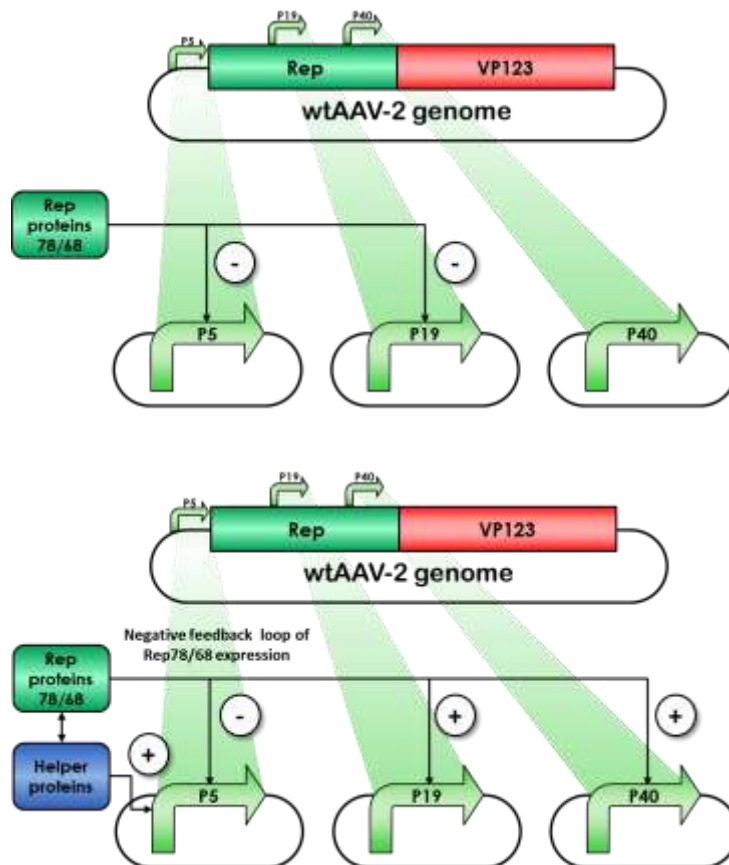


Figure 4: Regulation of the viral promoters located within the wt AAV-2 genome. In the absence of helper viruses, gene expression is suppressed, whereas activation of p5 and p19 occurs in the presence of helper proteins by interacting of Rep proteins with cellular and helper proteins.

2.1.2.1.1 p5 promoter

The p5 promoter, located downstream of the *rep* and *cap* ORF (Figure 5: The p5 promoter of the wtAAV-2 is located upstream of the rep and cap ORF and contains several elements, which interact with Rep and endogenous proteins.) of the wtAAV-2, regulates gene expression of the two larger non-structural proteins Rep 78 and Rep 68 that are essential in genome replication and viral genome integration into several hotspots of the human chromosome.

Several binding elements for cellular and viral proteins involved in regulation can be found in the p5 promoter (Figure 5) therefore playing an important role in gene transcription, integration and replication, dependent on the presence or absence of helper viruses such as adenovirus (Ad) or herpes simplex virus (HSV) (Murphy et al. 2007). Besides regulation of gene expression, the p5 integration efficient element (p5IEE) containing the rep binding element (RBE) and a terminal resolution site (*trs*) is responsible for mediating site specific integration into the human genome (Philpott et al. 2002).

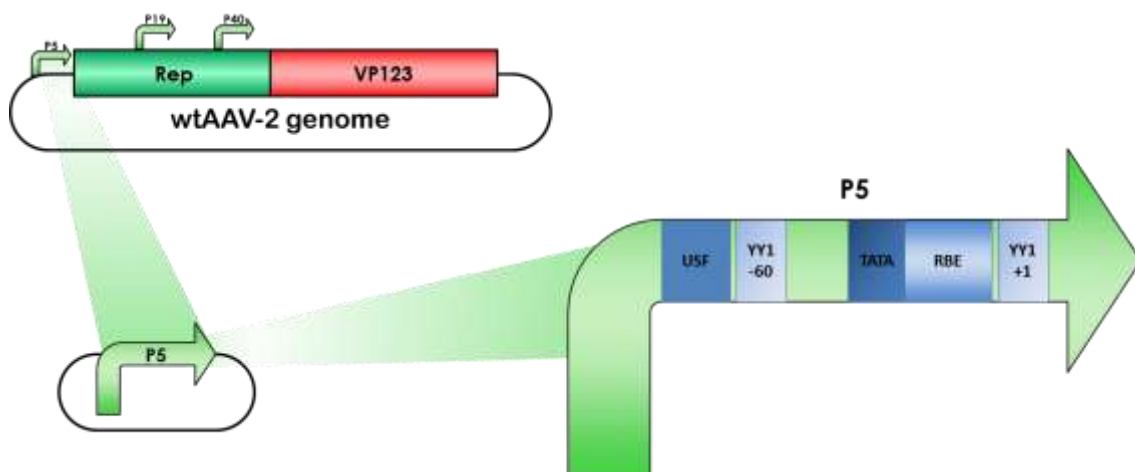


Figure 5: The p5 promoter of the wtAAV-2 is located upstream of the rep and cap ORF and contains several elements, which interact with Rep and endogenous proteins.

Containing two consensus sequences for binding immediate early E1A gene product from adenoviruses (Chang et al. 1989), p5 promoter is transactivated in the presence of helper viruses whereas suppression occurs in absence of adenoviral proteins by low levels of Rep proteins (Beaton et al. 1989). Regulating of Rep78/68 by its negative feedback loop is critical since overexpression leads to cell cycle arrest in the S-phase (Berthet et al. 2005) and suppression of cellular promoters (Jing et al. 2001).

2.1.2.1.2 p5 TATA-less promoter

In contrast to the natural location of the p5 promoter, the iGEM team Freiburg 2010 provides the RepCap plasmid with a relocated p5 promoter downstream of the *RepCap* genes (Figure 6).

Additionally the p5 promoter lacks the TATA box element (AVIGEN 1997). Those modifications result in an attenuated expression of the larger Rep proteins therefore leading to normal transcription of the Rep proteins driven by p19 promoter and enhanced expression of the Cap proteins, which are under the control of the p40 promoter. Additionally, removing the p5 promoter downstream of the *RepCap* genes and deletion of the TATA box eliminates contamination with wtAAVs. Hence, alteration of the p5 promoter is useful for enhanced production of recombinant viral particles attenuating repression of Rep78/68 and improving gene transcription of the capsid proteins and Rep proteins involved in genome packaging.

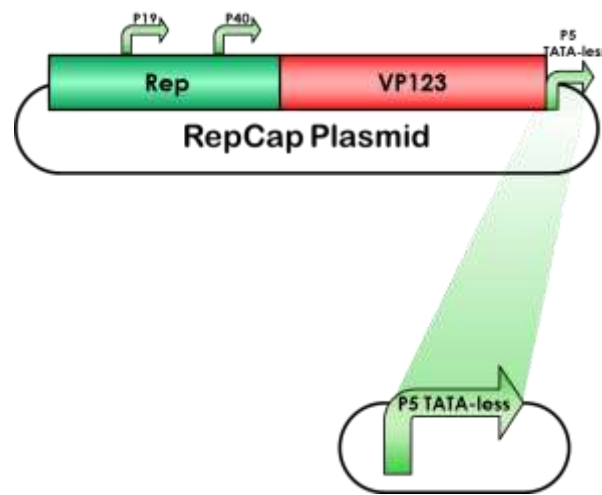


Figure 6: p5 TATA-less promoter is located downstream of the rep and cap ORF.

2.1.2.1.3 p19 promoter

p19 promoter drives gene expression of the smaller Rep proteins Rep52 and Rep40. In absence of a helper virus infection the promoter is inactive by repression of all four Rep proteins, but is transactivated by interaction of both the Sp1 site and Rep protein Rep78/68 bound to the Rep binding element (RBE) (Lackner & Nicholas Muzyczka 2002). By forming a DNA loop (Pereira & N Muzyczka 1997) and bringing the two promoters in proximal distance () additional cellular factors bound to p5 promoter interact with the p19 promoter leading to transcriptional activation of Rep52/40 (Lackner & Nicholas Muzyczka 2002).

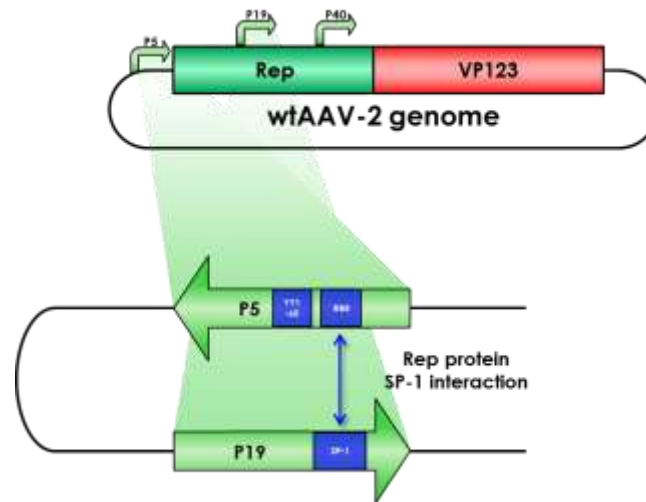


Figure 7: Forming of the DNA loop brings the p5 rep binding element in proximal distance to the Sp1 site found in the p19 promoter.

2.1.2.1.4 p40 promoter

The P40 promoter is derived from the adeno-associated virus serotype 2 (AAV2) genome, where it is located at 40 map units. It regulates the transcription of the capsid proteins VP1, VP2 and VP3 (Labow, Hermonat, & Berns, 1986; Cassinotti, Weitzand, & Tratschin, 1988).

Several sequence regions have been identified to be important for maximal promoter activity: Two Sp1 sites, which are located 250 (Sp1-50) and 270 (GGT-70) base pairs upstream of the transcriptional start point and to which Sp1 or Sp1-like proteins bind (Pereira & N Muzyczka 1997).

Referring to the virus genome, p40 can also be induced through transactivation by the Rep proteins. The Sp1-50, together with the CA_{RG}-140 site of the P19 promoter, are the main elements involved in this process. The Rep proteins, which bind to the Rep binding element in the terminal repeat or the P5 promoter, can induce P19 or P40 by interaction with their bound Sp1 proteins thereby forming a DNA-loop (Pereira & N Muzyczka 1997). In addition to that, the TATA box, located at 230, is also required for P40 activity. Furthermore the ATF-80 and the AP1-40 elements are also important for maximal promoter induction (Pereira & N Muzyczka 1997).

2.1.3 Integration

The AAV-2 is the only known mammalian virus that integrates into a specific location in the human genome in the presence of Rep78/68: Chromosome 19, 19q13.3-qter. The site of integration was termed AAVS1.

The mechanism of Rep-mediated integration into AAVS1 is not yet completely understood and seems to be imprecise and variable. Deletions or insertions often occur in the integration process (Schultz &

Chamberlain 2008). Linden et al. (1996) proposed a mechanism that is consistent with the observed patterns in which AAV exists in an integrated form:

AAVS1 bears a Rep-binding site (RBS) which is similar to the RBE in the virus genomes ITR. The Rep proteins are able to simultaneously bind to AAVS1 and the viral RBE, thereby bringing both strands into close proximity towards each other. After binding to the AAVS1 site, Rep acts as an endonuclease, the same way it does when binding to the AAV ITR, introducing a single strand-nick between two thymidine residues close to the binding site. This produces a free 3'-OH end which acts as a primer for the host cells' DNA polymerase. After replicating the displaced strand, the polymerase switches templates and replicates the AAV DNA, thereby linking AAVS1 and AAV together. Prior to integration, the AAV genome often exists in circular and/or concatameric form, resulting in multiple consecutive AAV copies in the host genome. Another explanation for this phenomenon could be a circularized AAV monomer that is being replicated several times in a rolling-circle manner before being integrated into the host genome.

Another template switch back to the AAVS1 sequence creates a second link between virus and host. This integration mechanism leaves single-stranded gaps that need to be repaired by cellular enzymes before integration is complete. Since successful integration of AAV depends on these cellular repair mechanisms, integration happens more frequently in dividing cells, in which repair functions are more active.

Recently, a sequence in the p5 promoter region that enhances site-specific integration through interaction with Rep78/68 has been identified, this motif was labeled p5 integration enhancer element (p5IEE). Apparently, p5IEE is sufficient to create the AAVS1 - Rep68/78 - Viral DNA -complex necessary for specific integration, even if the ITRs containing RBEs are not present.

2.1.4 Rescue

If the latently infected host cell is superinfected with adenovirus, the integrated virus genome can be rescued from the human chromosome and proceed its lytic lifecycle. Adenovirus gene products act as activators on AAV gene expression, leading to an excision of the viral sequences. Like in the integration process, the Rep 78/68 proteins catalyze the excision by introduction of single strand nicks at the terminal resolution sites within the terminal repeat structures flanking the AAV genome. DNA polymerase, displacing the single-stranded AAV sequence, then elongates the resulting free 3' OH ends. The incomplete single-stranded AAV sequence missing one terminal repeat primes upon itself at the homologous D motives, allowing DNA polymerase to copy it. This results in full-length, single-stranded AAV molecules, which are being able to re-enter the replicative cycle (Srivastava 2008), (R J Samulski 1993).

2.1.5 Rep proteins

2.1.5.1 Overview

The Adeno-associated virus (AAV) consists of two open reading frames (ORF), *rep* and *cap* ORF. The four non-structural *rep* genes are driven by two promoters located at map units 5 (

p5 promoter) and 19 (p19 promoter). Rep proteins are involved in genome encapsidation, regulation of gene expression and replication of the viral genome.

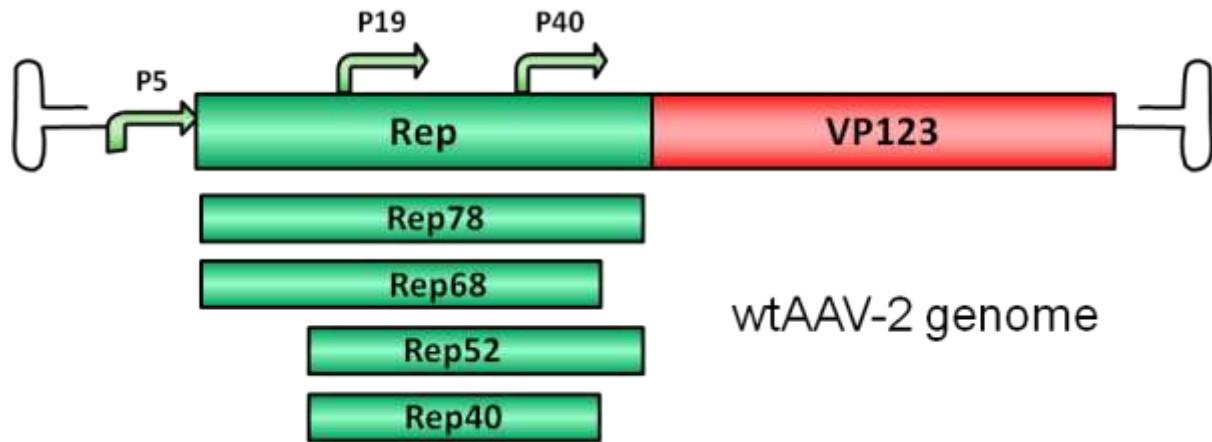


Figure 8: Genomic organization of the AAV-2 genome. The *rep* gene codes for four non-structural proteins – Rep40, Rep52, Rep68 and Rep78 – which are involved in gene regulation, genome encapsidation and viral DNA integration.

The two larger proteins Rep78/68 play an essential role in viral genome integration and regulation of AAV gene expression, whereas the smaller Rep proteins are involved in viral genome encapsidation. Rep proteins act both as repressors and activators of AAV transcription in respect to the absence and presence of helper viruses such as adenoviruses (Ad) or herpes simplex viruses (HSV) by interacting with several cellular proteins (Nash et al. 2009).

Furthermore, in the absence of Rep proteins, as it is the case in recombinant AAVs, integration of the viral genome into the human genome is rare and random. There are several hotspots for integration of wtAAV genomes such as the human chromosome 19q13.42, known as the AAVSI site, but as well some other accessible chromatin regions for preferred integration have been found (5p13.3 and 3p24.3). Integration into the human genome is mediated by the two regulatory proteins Rep68 and Rep78 driven by the AAV p5 promoter. The proteins bind to the Rep binding site (RBS) which is located within the inverted terminal repeats (ITRs). The minimal consensus Rep binding site (RBS) GAGT GAGC is found within the ITRs and in the p5 integration-efficient element (p5IEE) of the p5 promoter (Hüser et al., 2010). Rep78/68 proteins possess DNA-binding (reference), helicase (reference) and site-specific endonuclease activity located within the first 200 amino acids (M. D. Davis et al. 2000). Since the N-terminal region is unique to the larger Rep proteins, the two smaller Rep proteins possess other biological functions. Rep52/40 gene expression is driven by the p19 promoter which is located within *rep* ORF and the proteins are involved in encapsidating the viral genome into the preformed capsids. Gene expression of these proteins is suppressed in absence of

adenovirus infection by binding of Rep78/68 to the p5 promoter. Gene expression of p19 and p40 is transactivated by the Rep proteins Rep78/68 during coinfection.

2.1.5.1.1 Rep 78

Rep78 in a nutshell:

- 78 kDa
- Endonuclease activity
- ATPase and helicase activity
- Regulate viral gene expression
- Involved in genome integration into human chromosome

Regulated by the p5 promoter, Rep78 is the largest non-structural protein found in the wtAAV. Besides regulation of gene expression and viral genome replication, Rep78 has been found to play a functional role in AAV site-specific integration into the human genome (Hüser et al. 2010). In absence of Ad helper viruses, overexpression of Rep78 leads to cell cycle arrest by interacting with cell-cycle regulating phosphatases causing DNA damage by its intrinsic endonuclease activity (Berthet et al. 2005) and induces apoptosis. Due to its ability to bind to the Rep binding site (RBS) in the p5 integration-efficient element (p5IEE) of the p5 promoter, Rep78 mediates gene expression and retain a constant level of Rep proteins by suppressing transcriptional activity of the p5 promoter in absence of Ad viruses (Yue et al. 2010). Interaction of Rep78 with cellular factors such as transcription factors (Lackner & Nicholas Muzyczka 2002) provides the basis for gene regulation by Rep78 in associated with endogenous molecules.

2.1.5.1.2 Rep 68

Rep68 in a nutshell

- 68 kDa
- Endonuclease activity
- ATPase and helicase activity
- Regulate gene expression
- Involved in genome integration into human chromosome

Rep68 is a regulatory protein driven by the p5 promoter with an apparent molecular weight of 68 kDa lacking 92 amino acids from the carboxy terminus due to splicing of mRNA coding for the two larger Rep proteins.

The non-structural protein Rep68 belongs to the superfamily 3 (SF3) helicase found in other small DNA and RNA viruses such as simian virus 40 (SV40) and bovine papillomavirus (Mansilla-Soto et al. 2009). Formation of oligomeric complexes of Rep proteins provides the basis for the functional versatility of the two larger regulatory proteins. The AAA⁺ motor domain is known to function as an initiator for oligomerization of the Rep proteins. The cooperative effect of both domains appears to be further regulated by ATP binding as well as different DNA substrates such as dsDNA and ssDNA. Assembly of different nucleoprotein structures suggest that viral replication and genome integration is regulated and controlled by distinct Rep complexes which means that in presence of dsDNA Rep68 assembles to smaller complexes than in presence of ssDNA resulting in octamers.

2.1.5.1.3 Rep52

Rep52 in a nutshell

- 52 kDa
- ATPase and helicase activity
- Involved in genome encapsidation

Rep 52 is under the control of the p19 promoter and shares the same N-terminus with Rep78. It was shown that Rep52 possesses helicase and ATPase activity with 3'-5' polarity (R. H. Smith & Kotin 1998). Despite the helicase activity, Rep52 and Rep78 share a putative zinc-finger domain, which suggest interactions with diverse cellular factors (Nash et al. 2009) such as transcription factors (Lackner & Nicholas Muzyczka 2002) and TATA-binding proteins (P L Hermonat et al. 1998).

2.1.5.1.4 Rep40

Rep40 in a nutshell

- 40 kDa
- ATPase and helicase activity
- Involved in genome encapsidation

The smallest Rep protein (Rep40) possesses helicase and ATPase activity as well, but does not have strict requirements for DNA duplexes containing a 3' single-stranded end. Rep40 helicase activity requires bivalent ions such as Mg^{2+} or Mn^{2+} and is most active using ATP as substrate. Lacking the zinc finger domain, present in Rep52, Rep40 requires dimerization for functional helicase activity (Collaco et al. 2003). Rep40/52 proteins are required for translocation of the single-stranded, viral genomes into the preformed capsids proceeding with the 3' end of the DNA (King et al. 2001).

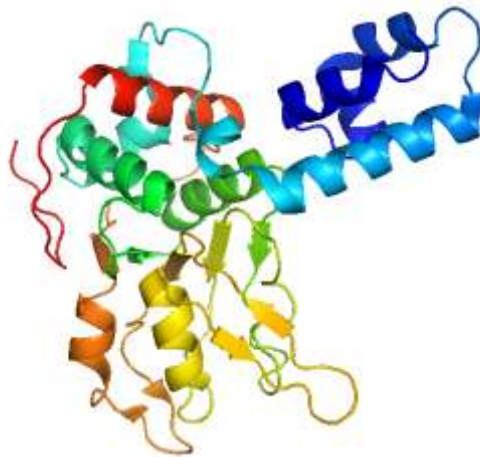
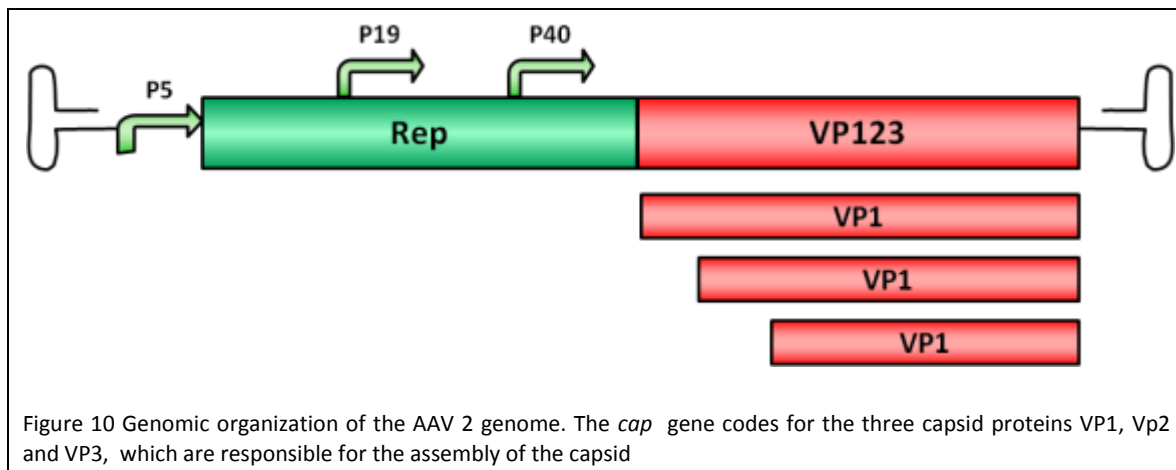


Figure 9: Crystal structure of the SF-3 helicase (PDB: 1SH9).

2.1.6 VP proteins

The AAV capsid consists of 60 capsid protein subunits composed of the three cap proteins VP1, VP2, and VP3, which are encoded in an overlapping reading frame. Arranged in a stoichiometric ratio of 1:1:10, they form an icosahedral symmetry. The mRNA encoding for the cap proteins is transcribed from p40 and alternative spliced to minor and major products. Alternative splicing and translation initiation of VP2 at a nonconventional ACG initiation codon promote the expression of the VP proteins. VP1, VP2 and VP3 share a common C terminus and stop codon, but begin with a different start codon. The N termini of VP1 and VP2 play important roles in infection and contain motifs that are highly homologous to a phospholipase A2 (PLA2) domain and nuclear localization signals (NLSs). These elements are conserved in almost all parvoviruses.



2.1.6.1 VP1

Whereas VP1 is translated from the minor spliced mRNA, VP2 and VP3 are translated from the major spliced mRNA. The minor spliced product is approximately 10-fold less abundant than the major spliced mRNA. Thus, there is much less VP1 than VP2 and VP3 resulting in a capsid stoichiometric ratio of 1:1:10. The N terminus of VP1 has an extension of 65 amino acids including an additional extension of 138 N-terminal amino acids forming the unique portion of VP1. It contains a motif of about 70 amino acids that is highly homologous to a phospholipase A2 (PLA2) domain. Furthermore, there are nuclear localization sequences (BR)(+) which are supposed to be necessary for endosomal escape and nucleareentry. (Bleker et al. 2006), (J. S. Johnson et al. 2010), (DiPrimio et al. 2008).

Phospholipases are enzymes that hydrolyze phospholipids into fatty acids and other lipophilic substances and can be found in mammalian tissues but also in insect and snake venom. They are subdivided into four major classes, termed A, B, C and D distinguished by the type of reaction they catalyse whereas the position of hydrolysis on the glycerol backbone defines the class of phospholipase.

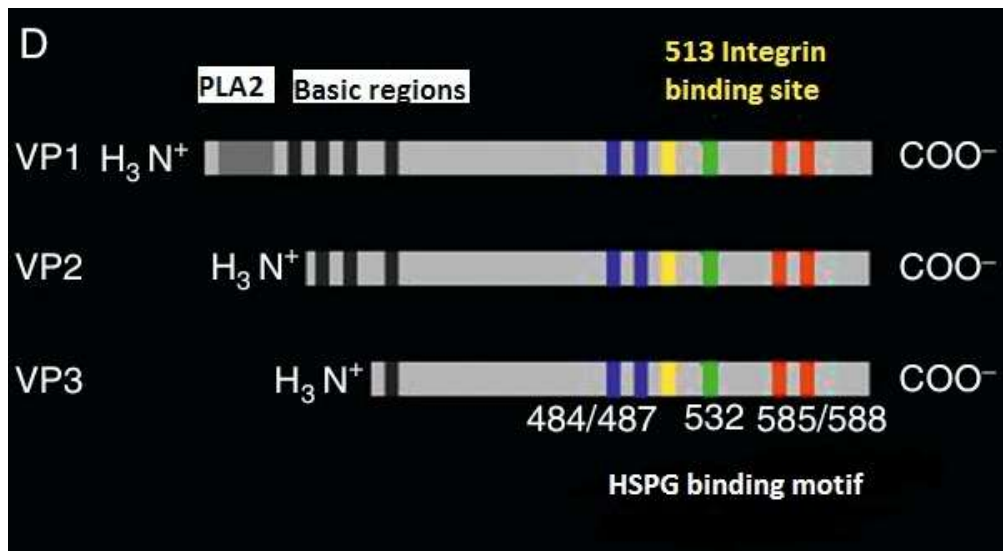


Figure 11: The schematic depiction of some AAV2 domains. VP1 contains a phospholipase A2 (PLA2) domain and four basic regions (BR1–4) located at the N-terminus of VP1 – VP3. The HSPG binding domain is generated by the basic residues at positions R484, R487, K532, R585, and R588 which are located near the C-terminus of the VP proteins. The NGR motif 511–513 forms an integrin $\alpha 5 \beta 1$ binding domain. Adapted from (Michelfelder & Trepel 2009)

It specifically recognizes and hydrolyzes the sn-2 acyl bond of phospholipids releasing arachidonic acid and lysophospholipids.

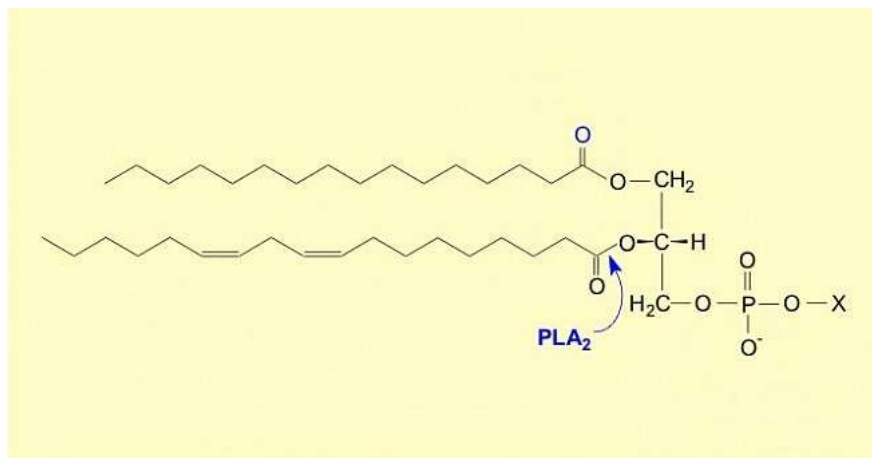


Figure 12: adapted from http://www.biochemtech.uni-halle.de/im/1182353660_397_00_800.jpg

The reaction mechanism will be depicted by the following image:

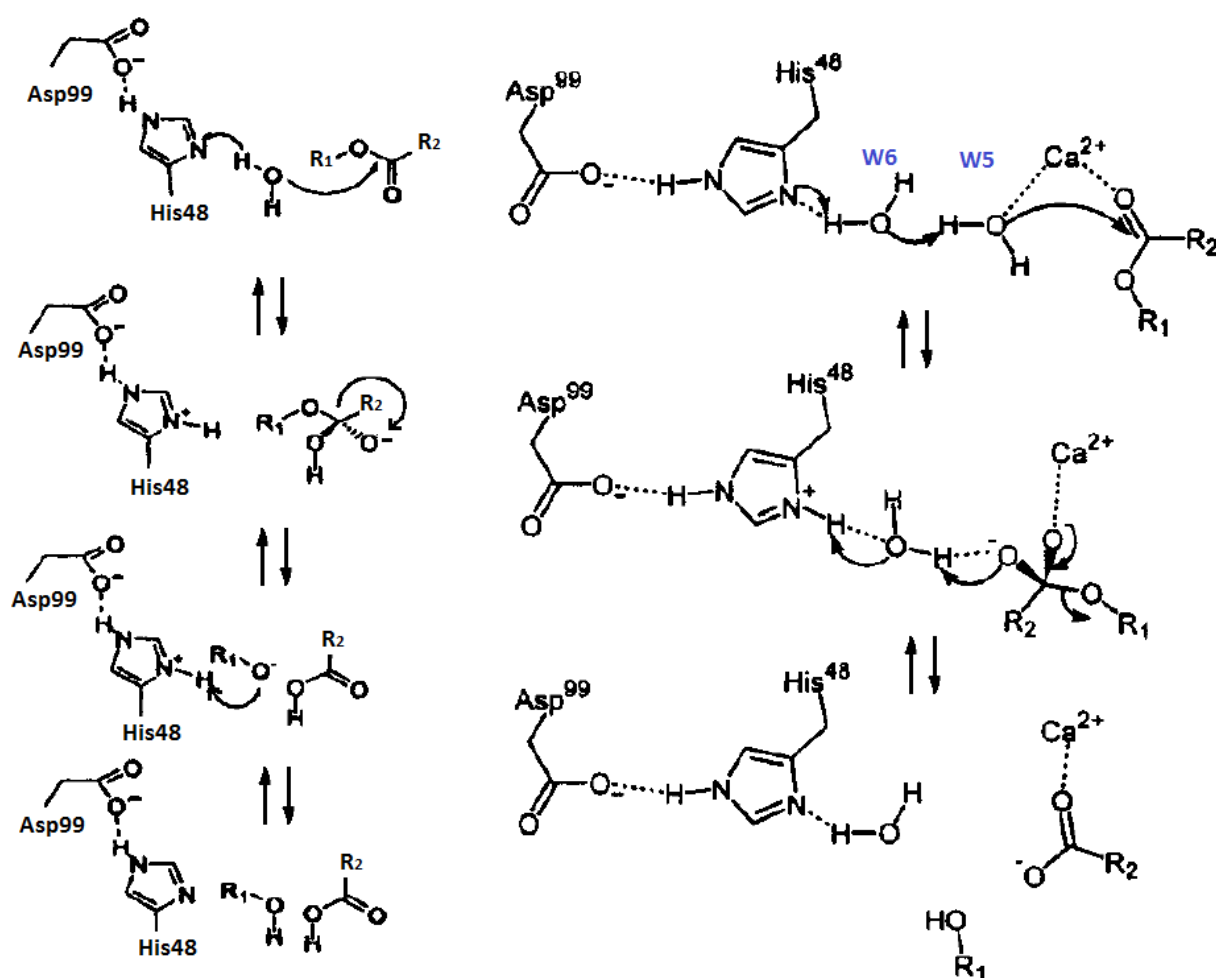


Figure 13 adapted from "Interfacial Enzymology: The Secreted Phospholipase A2-Paradigm"

There are two possible mechanism but the one on the right side has a lower transient state. The mechanism of sPLA2 on the right side is initiated by a His-48/Asp-99/calcium complex within the active site. The sn-2 carbonyl oxygen becomes polarized by the calcium ion while also influencing catalytic water molecule, w5..Via the bridging second water molecule w6 His-48 improves the nucleophilicity of the catalytic water. According to propositions two water molecules are needed to bypass the distance between the catalytic histidine and the ester.. Asp-99 is thought to enhance the basicity of His-48 through hydrogen bonding. Substituting the His-48 with an asparagine maintains wild-typ activity because the functional group on asparagines can function to lower the pKa of the bridging water molecule, too (Berg et al. 2001).

The phospholipase A2 is suggested to mediate membrane disruption of the vesicular compartment, which would allow escape of the virion into the cytosol, although this has not been demonstrated for AAV so far. The propensity of cellular PLA2 to cleave phospholipids is usually regulated by intracellular Ca²⁺ levels as well as phosphorylation of residues near the catalytic domain of the PLA2.

Not surprisingly, the N-terminus of VP1 contains a GXG binding site and several phosphorylation sites.

According to the structural modeling of VP1 the N-terminus can translocate through the 5-fold axis of symmetry in the capsid and expose the first 185 residues of VP1 (comment: experimental data also “strongly suggest that N-termini of VP1 harboring the PLA2 domain can be exposed on the capsid surface through the pores at the fivefold symmetry axes” (Girod et al. 2002)(Bleker, Sonntag & A. Kleinschmidt 2005). It only takes about 19 amino acids to reach through a phospholipid bilayer so this length would be sufficient for the presentation of the NLS and di-lysine sequences to the cytosol assuming the PLA2 domain had penetrated through an endosomal membrane or Golgi. (Michelfelder & Trepel 2009)

Analysing individual steps in the life cycle of several VP1up mutants and wtAAV-2 lead to the following conclusions: (i) mutations in VP1up did not affect DNA packaging or replication but resulted in a strong reduction of infectivity; (ii) this decrease in virus infectivity correlated with a loss in pvPLA2 activity; (iii) binding to the cell surface and entry into cells was not affected in VP1up mutants; (iv) however, these mutants showed obviously reduced and delayed Rep expression. (Girod et al. 2002) Summarizing these results the pvPLA2 activity is required for a step in the life cycle of the virus following perinuclear accumulation of virions but (Girod et al. 2002) before the onset of early gene expression.

Maybe future work will uncover whether the PLA2 domain in AAV performs optimally in a specific vesicular compartment, prefers a specific phospholipid substrate, operates at multiple cellular membranes such as the endosome and the nuclear envelope, or if its activity is regulated by cellular components.

2.1.6.2 VP2

The translation of VP2 from the major spliced mRNA is less efficiently compared to the translation of VP3 because it initiates at a Thr codon (ACG). VP2 and VP1 have an extension at the N terminus that remains internal when exposing the capsid to experimental conditions like low pH or heat. The N terminus of VP1 has an extension of 65 amino acids and similar to VP1 it has two functional elements: a phospholipase A2 (PLA2) domain and nuclear localization signals (BR)(+). The exact role of VP2 remains unknown, although the protein is thought to be nonessential for viral assembly and infectivity (J. S. Johnson et al. 2010), (DiPrimio et al. 2008).

2.1.6.3 VP3

Contained in VP1 and VP2, VP3 is the primary capsid protein that determines the surface topology of the AAV capsid. The capsid in turn dictates antigenicity and tropism. In comparison to the initiation of VP1 and VP2 the initiation of VP3 is because of a Met codon highly efficient (DiPrimio et al. 2008).

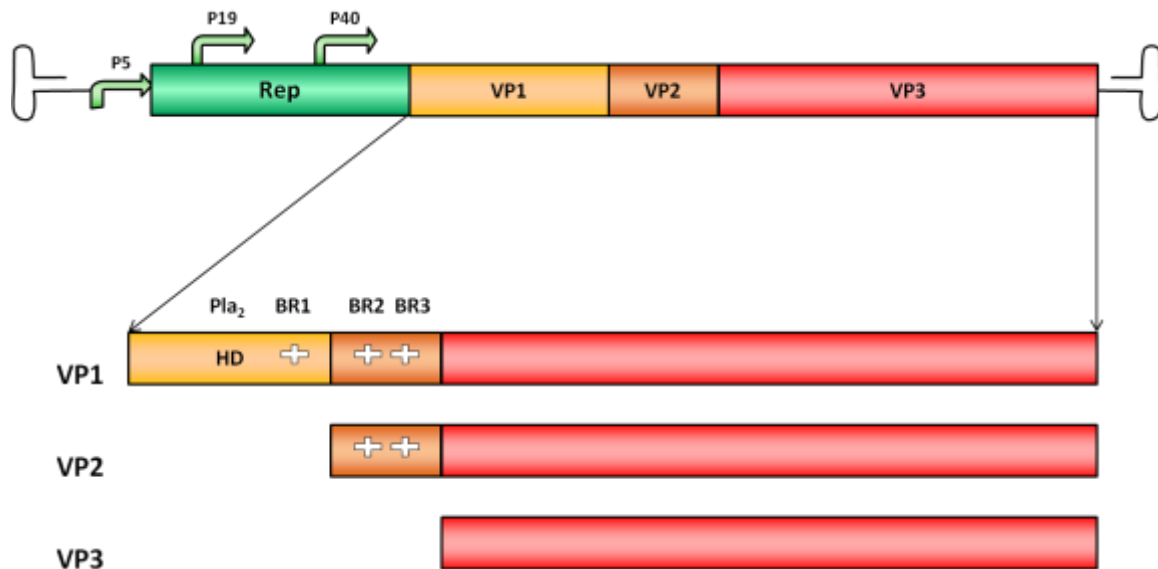


Figure 14: Genomic organization of the AAV-2 genome. The three capsid proteins VP1, VP2 and VP3 have a similar C terminus. The N termini of VP1 and VP2 contain a phospholipase A2 (PLA₂) domain and nuclear localization signals (BR)(+).

2.1.6.4 Natural Tropism and HSPG motif

The primary receptor of AAV-2 is the heparan sulfate proteoglycan (HSPG) receptor. Its binding motif consists of five amino-acids located on the capsid surface (Trepel, Vectors, et al. 2009).

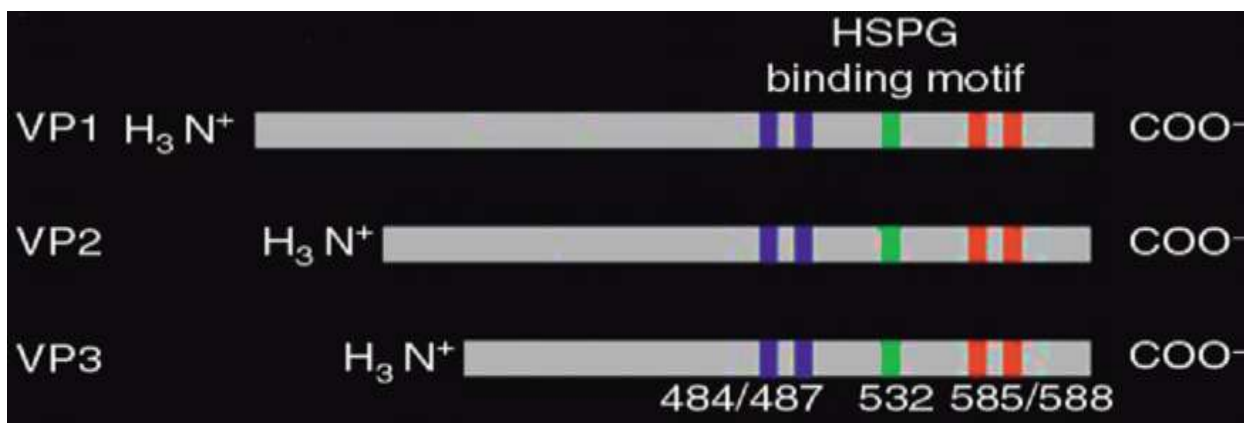


Figure 15: adapted from (Trepel, Vectors, et al. 2009). Schematic depiction of the 5 basic amino acids forming the HSPG motif: R484/R487, K532, R585/588. Other domains or binding motifs are not shown in this picture.

HSPG belongs to the glycosaminoglycans as well as heparin and consists of heparan sulfate glycosaminoglycan attached to a core protein and can be found on every human cell surface.

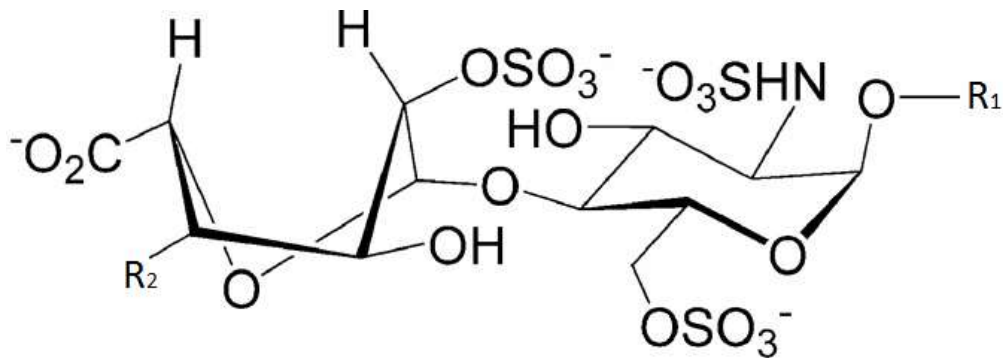


Figure 16: adapted from (Sinnis et al. 2007) amidosulfated disaccharid sequence in heparin.

Its acid residues bear negative charges and are therefore prone to electrostatic interactions with e.g. the positively charged HSPG binding motif of AAV-2. Other interactions with polar residues are possible, too.

Regarding AAV-2, two point mutations in AAV-2 (R585A and R588A) are sufficient to eliminate heparin binding (S. Opie et al. 2003). The biobricks with this knockout are annotated with „HSPG-ko“.

2.1.6.5 Assembly-activating protein

A gene encoding for the assembly-activating protein (AAP) was recently (in 2010) discovered in the Adeno-associated virus (AAV) serotype 2 genome. Its gene product is conserved among all AAV serotypes, illustrating its essential role in virus life cycle. Its functions comprise transport of the viral structural proteins to the nucleolus and involvement in following capsid assembly.

The AAP gene, located in the Cap coding region, is translated from an alternative open reading frame (ORF) with unconventional start codon. If modifications need to be introduced in the AAV capsid – for example for targeting approaches – the AAP has to be taken in account in order to prevent virus assembly impairment.

2.1.7 Trafficking

For creating efficient AAV2 vectors, precise knowledge of the events following virus transduction is necessary. The subsequent scheme and summary is intended to be an introduction into the complex process of virus transduction.

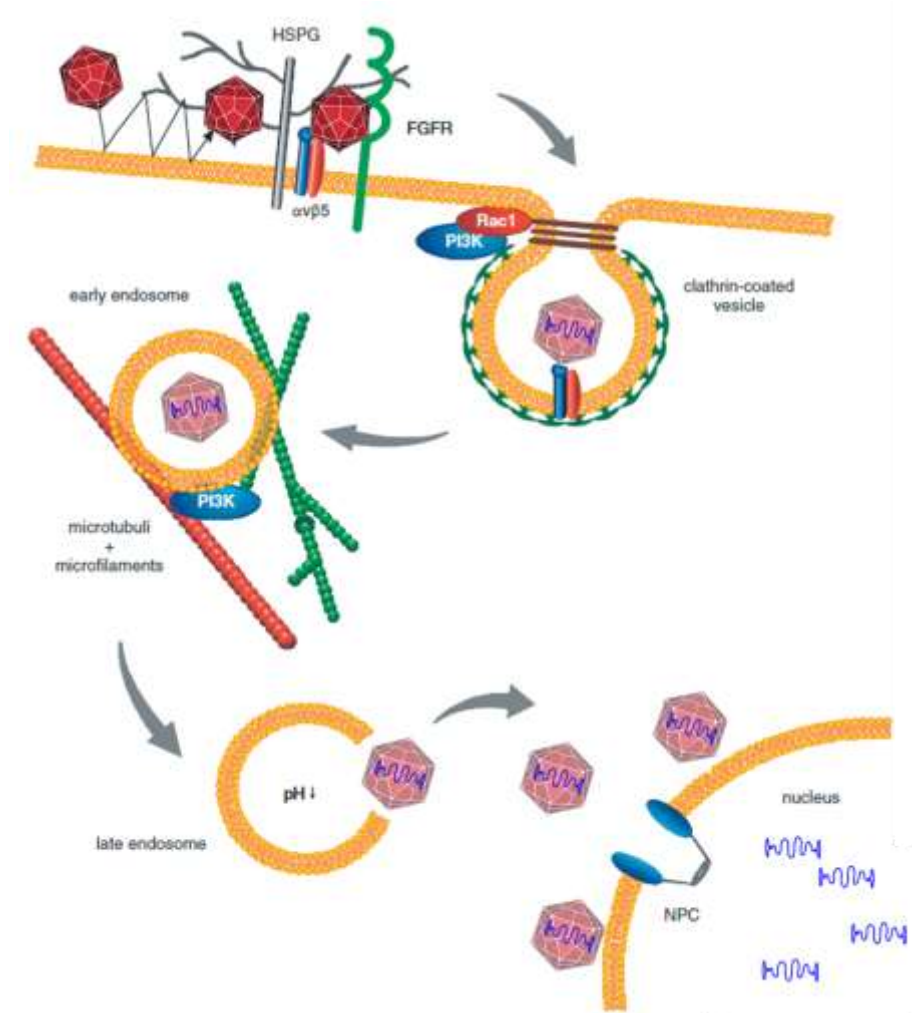


Figure 17: Adapted from (Hildegard Büning et al. 2008)

After several contacts with cellular structures like heperan sulphate proteoglycan (HSPG) the viral capsid proteins get rearranged. Clathrin-mediated endocytosis and cellular trafficking into the cell's center follows. After acidification and following endosomal escape, the viral genome is transferred into the nucleus and replicated (lytic phase) or integrated into the host genome (latent phase).

Before entering the cell, the viral particle has in average 4.4 contacts with the cellular surface. (Seisenberger et al. 2001) The main receptor of AAV2 is heperan sulfate proteoglycan (HSPG). After contact with HSPG the capsid structure gets rearranged (Levy et al. 2009). This is probably essential for interaction with other cofactors, which leads to endocytosis. The factors respectively co-

receptors of the cellular surface are known to enhance the initial binding affinity of HSPG: Fibroblast growth factor receptor 1 (FGFR-1), hepatocyte growth factor receptor (HGFR) and laminin receptor. It is known that AAVs affect both: $\alpha\text{V}\beta_5$ and $\alpha\text{V}\beta_1$ integrin. The $\alpha\text{V}\beta_1$ -binding site is an asparagine-glycine-arginine motif (Asokan et al. 2006). These integrins interact with intracellular molecules like Rho, Rac and Cdc42 GTPases. Figure 2 depicts the following cascade.

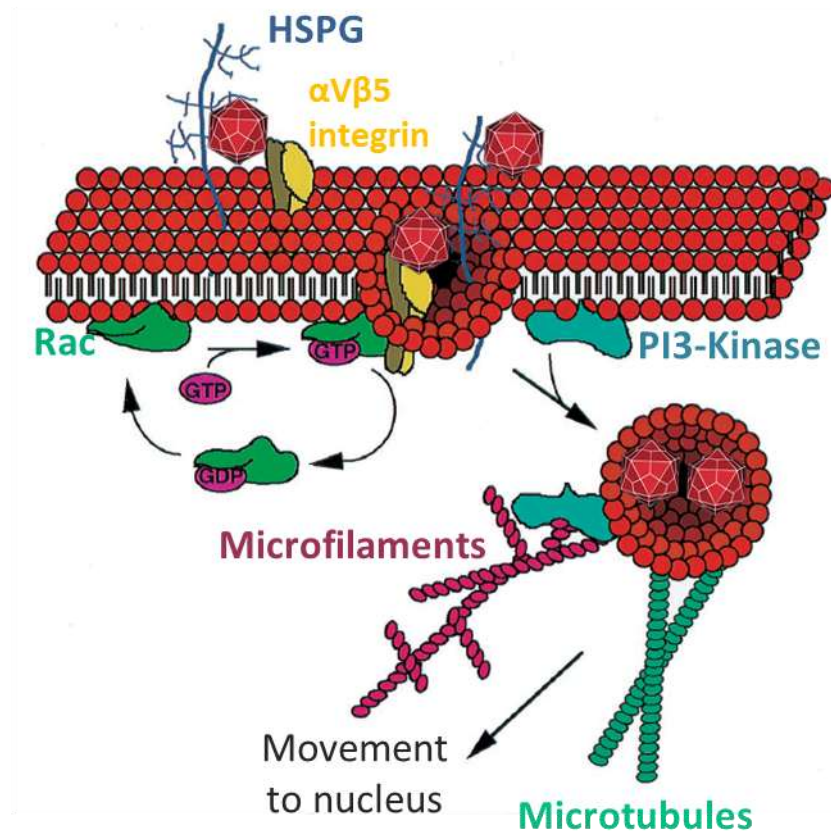


Figure 18: Adapted from (Sanlioglu, Benson, J. Yang, Atkinson, Reynolds & Engelhardt 2000a)

The initial contact with HSPG, FGFR-1, HGFR and/or laminin is followed by an interaction with $\alpha\text{V}\beta_5$ and/or $\alpha\text{V}\beta_1$ which probably leads to an intracellular activation of enzymes involved in the rearrangement of cytoskeletal proteins like actin, via PI3K-pathway (Kapeller & Cantley 1994), (E. Li et al. 1998). In general, the receptor-mediated endocytosis (RME) is a complex process proteins and co-factors form clathrin coated pits as shown in Figure 19.

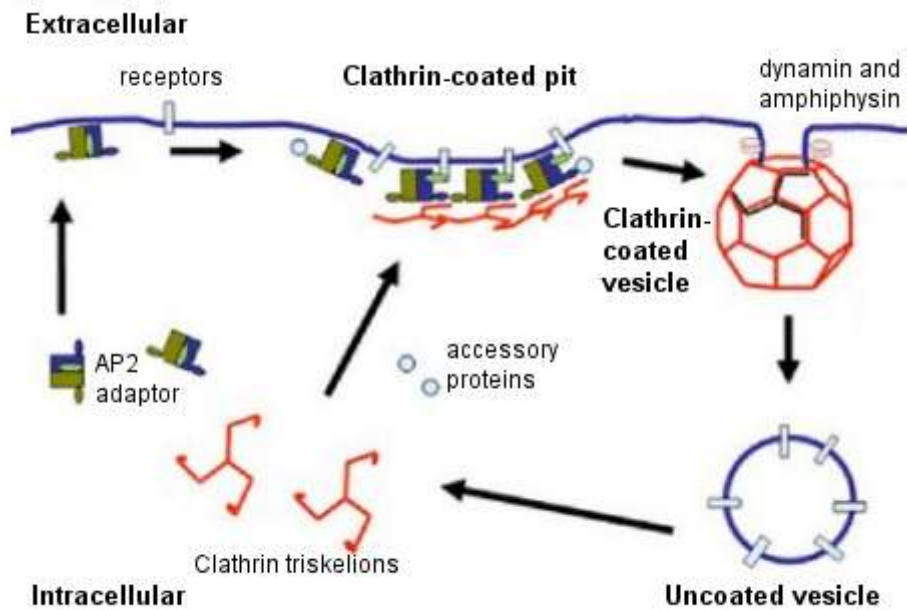


Figure 19: Intracellular trafficking.

The adaptor proteins (APs) AP1, AP2, AP3 and AP4 are complexes built of four subunits (Collins et al. 2002), (Asokan et al. 2006). Except for AP2, which requires GTP-bound-Arf1, the APs are linked via phosphatidylinositol (4,5)-bisphosphate (PIP2) to the cell membrane (Robinson 2004). APs recognize short cytoplasmatic motifs like YXX-phi (phi: bulky hydrophobic AA) of transmembrane receptors. In general, the recognition sites (mu-subunits) in the AP-complexes have to be phosphorylated by kinases (Ohno et al. 1995).

The actual scaffold of the endosome is build by the triskelion formed clathrins. The rigide backbone of clathrins is formed by three heavy chains (Ybe et al. 1999) and three light chains are regulating assembly competence (BRODSKY et al. 1991). After building the clathrin scaffold, dynamine is responsible for pinching-off the clathrin-coated pits (CCPs) from the cell's membrane (Summerford & R J Samulski 1998) (Sanlioglu, Benson, J. Yang, Atkinson, Reynolds & Engelhardt 2000b).

2.1.7.1 Endosomal transport and escape

Still there are possible additional entering pathways, for example knocking down microtubuli and microfilament arrangement does not prevent transduction completely (Kelley 2008). Currently it is thought that endosomal escape happens in the cytoplasm. After pinching off, the endosomes move via motor proteins along microtubuli and microfilaments towards the nuclear area. While trafficking through the cell the early endosoms getting acidulated (Sonntag et al. 2006).

Additional entering pathways were postulated for the virus, for example, it has been shown that proteasomal degradation via ubiquitination hampers transduction efficiency (Douar et al. 2001).

The first viral particles in the nuclear area can be detected after 15 minutes (Seisenberger et al. 2001) and an accumulation of virions takes place after 30 minutes post transfection. After arrival, the viral genomes are transported into the nucleus. It is not entirely clear in which way the transport is accomplished. The viral particles seem to use different pathways to enter the nucleus, either via the nuclear pore complexes with their maximal pore size of 23 nm. In this case, the viral capsid (25 nm diameter) has to be remodeled. Controversial results were published in the past, detecting intact viral particles (lu et al., 2000), but according to Lux et al. no intact capsids were detectable when lower amounts of viral particles were transduced (Lux et al. 2005).

Obviously further investigation of intracellular trafficking is essential for optimizing the AAV2 for medical applications.

2.2 Helper Genes

The AAV Helper-Free System by Stratagene (Waldbronn, Germany) is a modularized system for the production of infectious recombinant AAV-2 virion not depending on a coinfection with any helper virus. It is put into practice by the three plasmids pHelper, pAAV-RC, recombinant pAAV vector containing the gene of interest (GOI) and the recombinant cell line AAV-293.

The AAV-2 is a replication-deficient parvovirus, which originally needs a co-infection of adenovirus or herpes virus for replication. To realize a functional replication of AAV-2 without a co-infection, the AAV Helper-Free System allocates the pHelper plasmid and the AAV-293 host cells. The pHelper plasmid encodes for nearly all of the required adenovirus gene products for replication (VA, E2a, E4). The AAV-293 host cells express stably the remaining important replication genes (E1A, E1B).

Due to the fact that AAV-2 needs all relevant replication genes for productive infection and that the important replication-genes are dispersed, the AAV Helper-Free System describes a saver alternative to retroviral or adenoviral gene delivery (Stratagene n.d.).

The AAV-293 host cells contain the E1A and E1B genes. The E1A gene is the first gene to be expressed during an adenovirus infection. The E1A gene produces two different mRNAs resulting in two different proteins. The expressed E1A proteins transactivate and induce transcription of other early genes (like E2 and E4). In this case, E1A proteins do not bind directly onto control regions, but interact with other host proteins, which are binding to those regions (Chang et al. 1989) (Modrow et al. 2003).

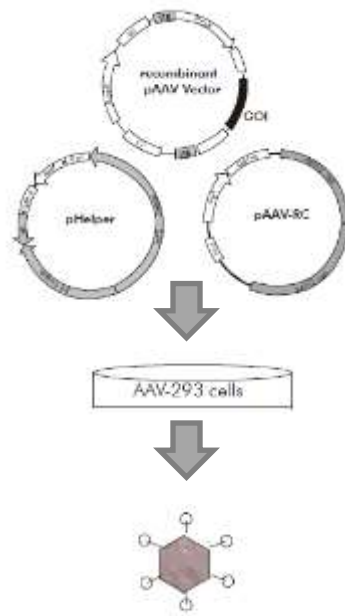


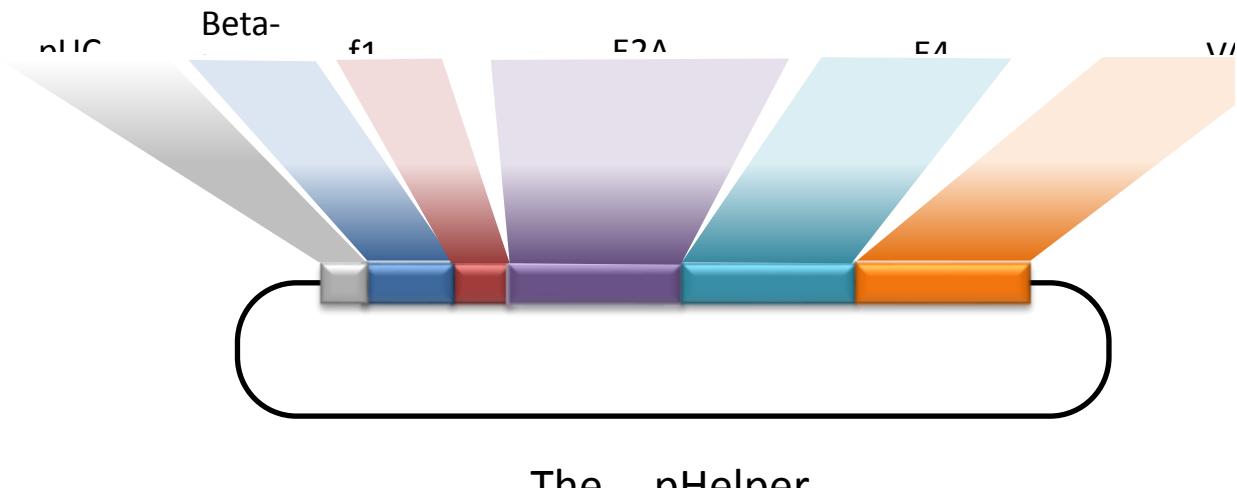
Figure 20: Schematic overview of the Helper Free System provided by Stratagene.

In the AAV-2 infection cycle, E1A proteins stimulate the expression of the p19 promoter and the p5 promoter, which are required to begin with the *rep*-gene transcription of the AAV(Chang et al. 1989) (Tratschin et al. 1984).

The E1B region encodes two polypeptides with overlapping reading frames, the major 21-Mr product and the 55-Mr moiety. It has been shown that only the 55-Mr polypeptide is required for effective helper function. It enables along with the E4orf6, a stable accumulation of AAV-specific cytoplasmic RNA, capsid proteins and DNA replication(R J Samulski & T Shenk 1988). In this context it has to be mentioned, that Stratagene deleted the E4orf6 out of its kit, because of its oncolytic activity. But it has been explained, that deletion of E4orf6 has no effect on virion production efficiency(Clark et al. 1999) .

The pHelper plasmid exists of the E2a gene, the E4 gene and the VA gene as well as a pUC ori and an f1 ori. The E2A gene encodes a 72 kD protein which is produced early in infection (Modrow et al. 2003). One helper function of E2A is to increase the processivity of replication. In the presence of E2A protein, short replication products, which are equivalent to break offs of the elongation strand of the template, are obviously reduced suggestion that E2A supports full-length replication of short

substrates. In immune-depletions, co-localizations between the E2A, the AAV Rep protein and the AAV DNA have been shown (Ward et al. 1998) .



It has been reported that E2A has affections on the AAV promoter regulation of spliced p5 and p19 as well as unspliced p40. E2A could also be responsible for the production of the AAV capsid proteins (Carter et al. 1992). To which extend it really takes elementary responsibility for any of the listed functions is not found out yet.

The VAI and VAI1 genes encode for two RNA-species, with a high GC-percentage and distinct secondary structure. The VAI RNA, which is implicated to have a helper function in AAV, usually plays a fundamental role in adenovirus' protein expression. There it blocks the phosphorylation of the initiation factor eIF-2, whereby the amino acid chain at the ribosome breaks off. (Modrow et al. 2003)

The expression of the AAV proteins may also be under the VAI adenovirus control. VAI may increase the AAV capsid production, but it also may play a role in RNA metabolism. (West et al. 1987)

The E4 gene exists of seven open reading frames. In this content, the proteins occurring from the gene are named E4-ORF1 up to E4-ORF7. All proteins are under the control of one promoter and arise from alternative splicing. The E4ORF6 is implicated to have a helper function in AAV. It promotes the formation of a dsDNA from the genomic ssDNA of the native virus.

2.3 Recombinant Viruses and Mosaic Viruses

2.4 Gene Therapy

Treating inherited and acquired diseases such as cancer is still one of the most challenging fields in today's biomedical research. Ever since Sidney Farber published a study in 1949 about several folic acid antagonists, which prevent tumor progression (FARBER 1949), cancer was treated with chemotherapy, surgery and radiation (Halperin 2006). Nevertheless, due to side effects caused by systemic applications and the lack of specificity, new treatments must be found for improved therapeutic efficacy and enhanced selectivity of the anticancer agents. One promising approach of treating cancer is suicide gene therapy or gene-directed enzyme prodrug therapy (GDEPT) including two steps of treatment: Targeted introduction of a gene encoding for enzymes into tumor cells, followed by the administration of a non-toxic prodrug which is converted into an anti-cancer metabolite.

Gene delivery using viral vectors to specifically target cells gained increasing attention in the last years being efficient in combination with suicide gene therapy. Several prodrug/enzyme systems have been reported (Greco & Dachs 2001). Ganciclovir (GCV)/herpes simplex virus thymidine kinase (HSV-TK), 5-fluorocytosine/cytosine deaminase (CD) and cyclophosphamide/cytochrome P450 systems have been widely used and their activity has been demonstrated in several preclinical studies (Greco & Dachs 2001).

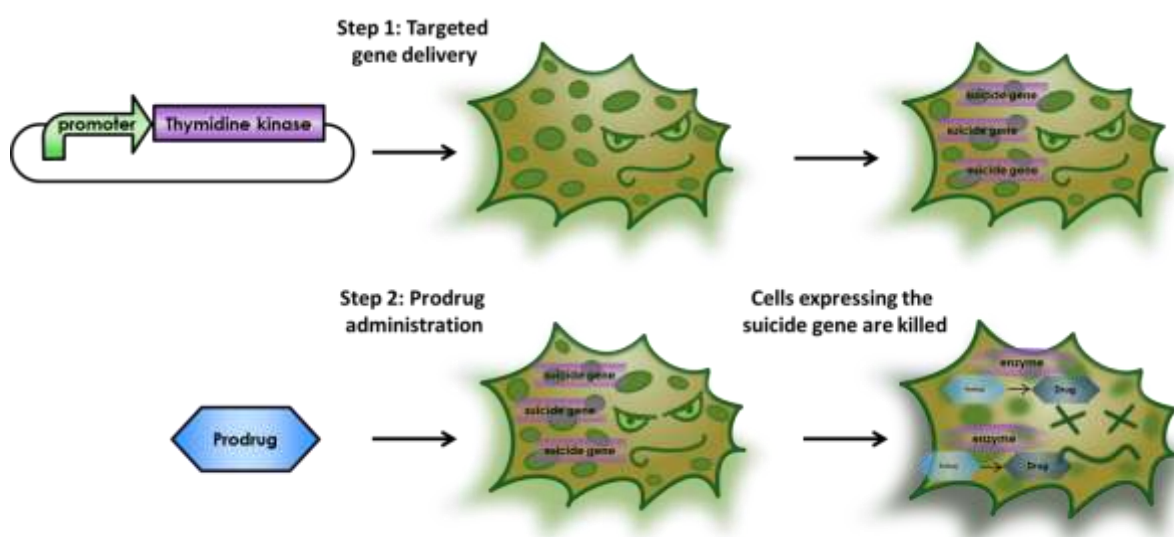


Figure 21: Schematic overview of gene-directed enzyme prodrug therapy (GDEPT). The suicide gene is introduced into the cancer cells. Administration of the prodrug leads to cell death in the cells expressing the enzyme, which converts the prodrug into the toxic product.

Using transgenic HSV – thymidine kinase or cytosine deaminase from *E. coli* for prodrug activation in tumor therapy several advantages can be found. Besides efficient killing of targeted tumor cells, neighboring, non-transduced cells are killed as well, providing an important effect in treating cancer. The bystander phenomenon was first reported by Moolten (1986) showing that HSV-TK negative cells surrounded by HSV-TK positive cells did not survive prodrug treatment.

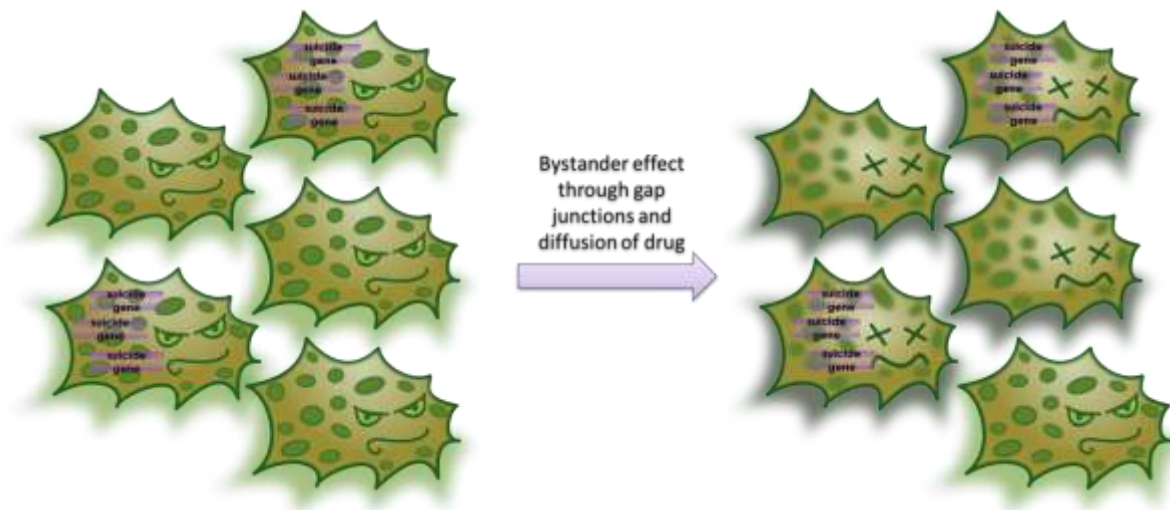


Figure 22: Efficient tumor killing is desired in cancer treatment. Locally administered prodrugs are converted to toxic metabolites by delivered enzyme in the infected cells. By passive diffusion, gap junction intercellular communication or immune-related response, non-transduced tumor cells are killed as well.

Transfer of toxic molecules between transduced and non-transduced cells can be achieved either through gap junctions (L. Yang et al. 1998) (Trepel, Stoneham, et al. 2009), via apoptotic bodies (Freeman et al. 1993) or by diffusion of soluble toxic substances (Huber et al. 1993).

2.5 Immune Response

Virus infections cause common human disease, including the familiar cold, influenza, mumps and measles. They are also associated with severe diseases, for example with Ebola or Marburg fever, with Hepatitis and AIDS. The immune system protects us from these infections by creating a barrier that prevents viruses from entering the body or by detecting and eliminating them in the corpus.

Every virus lives and reproduces in its own specific host. Reproduction can only take place in cell cytoplasm, whose components are needed in order to compensate for the lack of virus metabolism and biosynthesis-appliance. Viruses, which are located outside the cells, can be detected by antibodies, triggering an immune response by the members of the innate immune system, such as macrophages, neutrophils and natural killer-cells.

Inside a cell the virus can only be detected by cytotoxic T cells: While it uses the cellular machinery for reproduction, some of the viral proteins are degraded by proteasomes and become presented on

the cell surface by MHC-I-peptides. These exposed virus components are recognized by cytotoxic CD8+ T cells, which induce death of infected cells. The degraded viral proteins can also be accessible on MHC-II-peptides, which are detected by CD4+ T helper cells, which trigger and enforce the immune response for example by production of specific antibodies.

The Adeno-associated virus (AAV) is not associated with any human disease. Nevertheless, usage of recombinant AAV (rAAV) as therapeutic vector system harbors risks of immune responses.

AAV establishes a latent infection and often integrates at a specific site on q arm of chromosome 19, which is termed AAVSI site (Hernandez et al., 1999). This leads to several obstacles for usage of AAV vectors for therapeutic applications like gene silencing, insertions in gene sequences and immunotoxicity, a dangerous immune response to the vector or the transgene product (Mingozzi & High 2007). Humans are the only natural hosts for AAV-2 besides rhesus macaques. Due to wild-type AAV infections humans keep a population of antigen-specific memory CD8+ T cells (Mingozzi & High 2007). IgG antibodies are predominantly involved in the secondary immune response. 91% of Irish blood donors show a high repertoire of specific IgG1 and IgG2 subclasses and low doses of IgG3 (Madsen et al. 2009).

In vivo studies with AAVlacZ show that AAV vectors induce the secretion of chemokines and cytokines like gamma interferon (IFN- γ) (Zaiss et al. 2002). Studies in vitro show responses of IFN- γ , interleukin 10 (IL-10) and interleukin 13 (IL-13) after stimulation peripheral blood mononuclear cells (PBMC) from donors with AAV-2. This demonstrates a reaction of long-live CD4+ T helper-cells that are reactivated (Madsen et al. 2009). These results reveal that most Europeans are already infected with wildtype-AAV-2. Researchers suggest that more than 30% of mankind is already infected. In vitro studies from the United States support this hypothesis. One group found anti-AAV-antibodies in the blood sera at 80% of randomly chosen volunteers (Moskalenko et al. 2000). Other investigators show that 0,14% of the examined CD8+ T cells purified from PBMC are capsid specific for AAV-2 (Mingozzi, Maus, et al. 2007). These preexisting memory-CD8+ T cells could be responsible for the difference in vector-infusion outcome between humans (the natural host) and other species.

AAV-2 use distinct cellular receptors, e.g. heparin sulfate proteoglycan (HSPG), $\alpha V\beta 5$ integrin and human fibroblast growth factor receptor 1 (FGFR1) to become internalized (Favaro et al. 2009). These findings led researchers to the conclusion that the presence of an intact heparinbinding motif and the capsid t-cell responses are correlated. One group ablated the heparin-binding site in AAV-2 and observed no CD8+ T cell response. But it did not seem to influence T helper responses as measured by IgG isotypes and antigen-stimulated secretion of cytokines (Vandenberghe et al. 2006).

Approaches using peptides derived from the sequence of the VP1 viral capsid protein revealed a total of 59 t-cell epitopes. This demonstrates the difficulty to avoid the immune system by modifying the

AAV capsid (Madsen et al. 2009). Other approaches in mice reveal that different serotypes of AAV show the ability to cross-react with existing memory-T cells (Sabatino et al. 2005). Also in dogs different AAVs use some common peptides on their surface to activate the immune system (Wang et al. 2010). This shows the high conservation of the epitopes among multiple serotypes of AAV.

While proposing several possible solutions to avoid the immune system, the polymorphic nature of the human MHC and the high conservation of peptides on the surface of different serotypes of AAV may complicate these approaches (Mingozzi, Hasbrouck, et al. 2007). In general it can be said that the immune response to AAV is not severe as caused by other virus-types. This is due to the fact that AAVs fail to trigger inflammatory reactions dendritic cells need to differentiate into professional antigen-presenting cells (Mingozzi, Maus, et al. 2007). These antigen-presenting cells are needed for the activation of CD4⁺ T helper-cells which are needed for the completely feedback to the immune system. Nevertheless dendritic cells can be activated through the ability of AAV-2 to bind the HSPG binding motif with resultant AAV2 antigen inclusion, processing and MHC-I presentation (Wang et al. 2010). CD4⁺ T helper-cells can also be activated by other antigen-presenting cells therefore it is conceivable to block CD4⁺ cells during treatment with AAV. The activation of CD8⁺-t-cells through CD4⁺ T cells is depleted and the immune response is even more reduced than within the normal infection process.

Some researchers have found AAV vector DNA in the semen of dogs and fear the risk of germline transmission (Jiang et al. 2006) although these findings are controversially discussed. In a rabbit model it was demonstrated that semen was just positive for vector sequences following intravascular injection but not following intramuscular injection. Infectious vector particles were just detected up to four days after treatment and were undetectable thereafter. So the investigators suggest that AAV-2 presents a low risk of germline transmission for humans and there is no contemplation for male infertility so far (Favaro et al. 2009).

AAV vectors have been used in several phases of clinical trials for Leber's congenital amaurosis (LCA), hemophilia B, Cystic fibrosis, Arthritis, Muscular dystrophy, Parkinson's disease, Canavan's disease, Alzheimer's disease, Batten's disease and Hereditary emphysema.

3 Components of our Virus Construction Kit

3.1 Modularization of the AAV-2

3.2 Arming

Several prodrug/enzyme combinations were presented above. In our universal Virus Construction Kit we are using thymidine kinase/Ganciclovir and cytosine deaminase/5-fluorocytosine prodrug activation systems.

3.2.1 Thymidine kinase

Thymidine kinase (TK) (EC 2.7.1.21) is known to be involved in the salvage pathway of nucleosides to nucleotides (Andrei et al. 2005).

Due to its broader spectrum for different substrates, herpes simplex virus thymidine kinase (HSV-TK) is widely used in gene therapy approaches instead of endogenous thymidine kinases (Black et al. 1996). The transgenic introduced HSV-TK monophosphorylates nucleosides or nucleoside analogs such as ganciclovir (GCV) or acyclovir (ACV) followed by further phosphorylation through cellular kinases to nucleoside triphosphates. Incorporation of nucleotide analogs such as ganciclovir triphosphate or acyclovir triphosphates leads to DNA chain termination (Reardon 1989) and finally results in cell death.

Genetic modifications of the active site represented by a tripeptide motif in thymidine kinase increases the substrate affinity of HSV-TK towards GCV and ACV (Black et al. 1996). Two promising mutant HSV-TKs have been found by large mutagenesis screenings modifying several amino acids and conducting sensitivity assays for ganciclovir and acyclovir (Black et al. 2001).

The thymidine kinase mutant TK30 contains six modified amino acids (Black et al. 1996) created in a first screening showing enhanced affinity for ganciclovir and acyclovir, but reduced specificity for its natural substrate thymidine. In contrast to the TK30 mutant, the modified thymidine kinase SR39 obtained from a semi-random (SR) mutagenesis screening contains five modifications listed in Table 1 and provides further specificity for nucleoside analogs ganciclovir and acyclovir.

As efficient tumor killing and therefore ganciclovir activation is essential for successful tumor ablation, further improvements were conducted. Overexpression of transgenic thymidine kinase leads to accumulation of non-toxic intermediates, which cannot be phosphorylated sufficiently by endogenous guanylate kinase, the second enzyme in the salvage pathway of nucleotides. Overcoming this bottleneck was accomplished by fusing the mouse guanylate kinase (mGMK) to the N-terminus of both SR39 and TK30 mutants creating a fusion protein (mGMK_TK30 or mGMK_SR39) with enhanced GCV/ACV sensitivity *in vitro* and *in vivo* (Ardiani et al. 2010) and improved bystander activity. The effect of non-transfected tumor cell killing upon transfer of toxic metabolites through gap junctional intercellular communication (GJIC) or immune-mediated tumor ablation is essential in suicide gene therapy (Pope 1997). GCV-triphosphate is mainly transported through the central pore formed between connexin proteins from neighboring cells (Gentry et al. 2005), but immune-induced bystander effect seems to be likely as well (Grignat-Debrus et al. 2000).

3.2.2 Cytosine deaminase

Cytosine Deaminase (CD) (EC 3.5.4.1) in *E. coli* is encoded by *codA* and plays a crucial role in nucleotide synthesis due to deamination of cytosine to uracil. Subsequently, cytosine can be used for pyrimidine synthesis (Kilstrup et al. 1989). The expression of *codA* is regulated by the concentration of nitrogen in the media. In presence of either purines or pyrimidines, the expression is repressed, while lack of any nitrogen leads to overexpression of CD.

The CD's function is based on conversion of 5-Fluorocytosine (5-FCyt) to the highly toxic product 5-fluorouracil (5-FUra), which leads to cell death. *CodA* mutant *E. coli* as well as mammalian cells seem to be resistant to 5-FCyt due to the deficient metabolic activation. The resistance in *E. coli* arises because of the loss-of-function of cytosine permease *codB*, which is located adjacent to *codA*.

Due to this strong effect and the fact that mammalian cells do not express CD naturally (Koechlin et al. 1966) 5-FUra became a promising compound in suicide gene therapy. 5-FUra itself is metabolized to 5-fluorouridine-5'-triphosphate (FdUTP) and 5'-fluoro-2'-deoxyridine 5'-monophosphate (FdUMP) (Aghi et al. 1998), which in turn impair RNA as well as DNA synthesis and causes apoptosis

Table 1: Modified amino acid sequences of two mutant thymidine kinases.

Mutant	Modified amino acid sequence
wt HSV-TK	¹⁵² A ¹⁵⁹ L ¹⁶⁰ I ¹⁶¹ F ¹⁶⁸ A ¹⁶⁹ L
TK 30 (Black et al. 1996)	¹⁵² V ¹⁵⁹ I ¹⁶⁰ L ¹⁶¹ A ¹⁶⁸ Y ¹⁶⁹ F
SR39 (Black et al. 2001)	¹⁵² A ¹⁵⁹ I ¹⁶⁰ F ¹⁶¹ L ¹⁶⁸ F ¹⁶⁹ M

(Mullen et al. 1992; Damon et al. 1989). FdUMP inhibits thymidylate synthetase, which is responsible

for catabolism of deoxyuridylate into thymidylate. Consequently, treatment of cells with 5-FUra leads to failure of thymidylate synthetase and subsequently loss of dTTPs. Hence, during the DNA synthesis, both FdUTP as well as uridine throphosphate become incorporated into the DNA leading to the nick in the stand. dTTPs plays also crucial roles in repair events, thus dTTPs depletion is associated with repair failure and cell death. Another advantage of 5-FUra is its solubility and ability to freely diffuse into adjacent cells (Huber et al. 1994) therefore enhancing the bystander effect. Also, 5-FUra might interfere in the function or maturation events of RNA molecules, such as mRNA polyadenylation, tRNA methylation and processing of rRNA (Aghi et al. 1998).

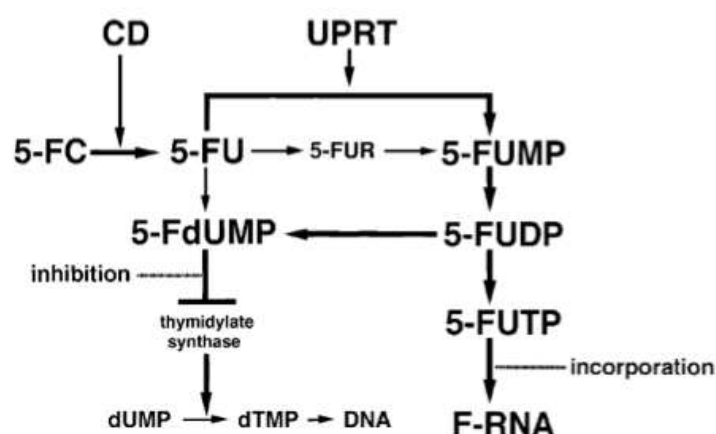


Figure 23: Fluorocytosine pathway (Adachi et al. 2000).

3.3 Targeting

The aims of our research are one the one hand, to knock down the natural tropism of the Adeno-associated virus particles and on the other hand, to specifically target tumor cells. This was achieved by genetically engineering the viral surface. For this purpose, two different strategies were developed, including insertion of motifs into surface-exposed loops or fusion to the N-terminus of the viral protein VP2.

3.3.1 Loop Insertions

3.3.1.1 Modification of the Viral Capsid of the AAV2 using Viral Bricks

For therapeutical applications in human gene transfer, the broad tropism for heparan sulfate proteoglycan (HSPG) has to be knocked-out and a novel tropism has to be inserted.

This retargeting can be achieved either by insertion of functional motifs into the two major surface exposed loops or by fusion of these motifs to the N-terminus of the viral coat proteins.

The graphic on the right shows parts of the three-dimensional structure of a viral coat protein. The parts of the loop regions that are coded in the ViralBricks are shown in purple for the **453 loop** and in blue for the **587 loop**.

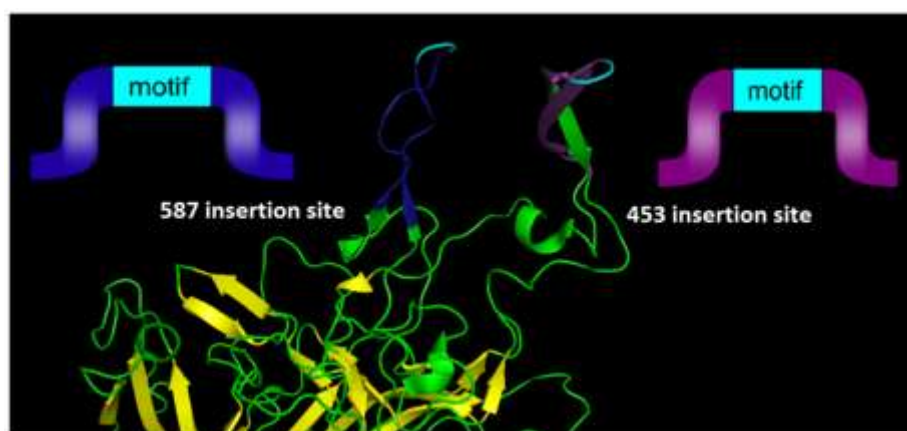


Figure 24: Three-dimensional representation of the AAV2 showing the amino acids of the 453 and 587 loops that are coded by the corresponding Viral Bricks.

3.3.1.2 Cloning of Viral Bricks into capsid coding parts

In order to make loop insertions more convenient the following restriction sites were inserted into all capsid coding parts and already existing restriction sites were removed from the constructs. The choice of these restriction sites was reasoned by enzyme performance, buffer compatibilities and the number of existing restriction sites that had to be removed at other positions. All restriction endonucleases were purchased from NEB.

Restriction Site	Enzyme	Recognition Site	Activity	Temp
Upstream 453	Sspl	5'... AATATT...3' 3'... TTATAA...5'	25;100;0;100	37°C
Downstream 453	Sal-HF	5'... GTCGAC...3' 3'... CAGCTG...5'	10;100;100;100	37°C
Upstream 587	BamHI-HF	5'... GGATCC...3' 3'... CCTAGG...5'	100;50;10;100	37°C
Downstream 587	PvuII-HF	5'... CAGCTG...3' 3'... GTCGAC...5'	0;25;0;100	37°C

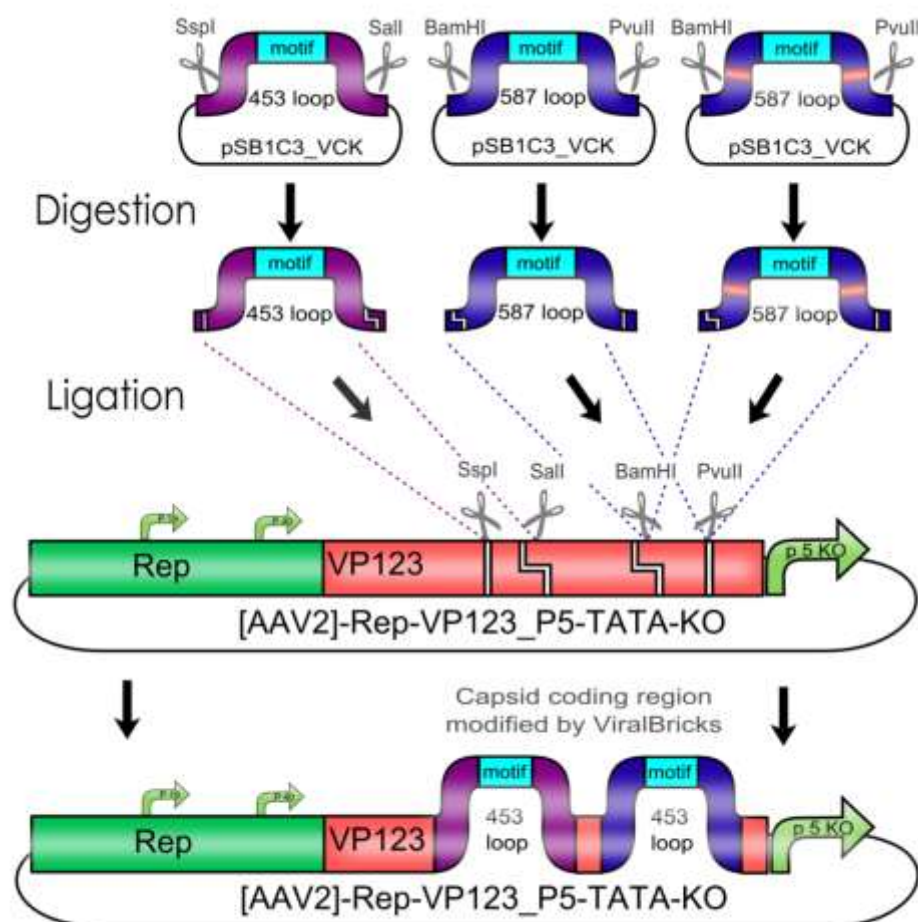


Figure 25:

3.3.1.3 Tagging

3.3.1.3.1 Specific Biotinylation via ViralBrick: The Biotinylation Acceptor Peptide

The BAP (Biotinylation Acceptor Peptide) that we included in our Virus Construction Kit is a 15 amino acid long peptide identified by Schatz J., 1993 in a library screening approach and published under the number #85. This peptide with the sequence 5' - GLNDIFEAQKIEWHE - 3' contains a central lysine that is specifically biotinylated by the prokaryotic enzyme biotin holoenzyme synthetase, encoded in the BirA gene of *E. coli*. Specific biotinylation of this peptide sequence can be performed in vivo by cotransfecting a plasmid with the BirA gene as described for the AAV in Arnold et al.; 2006 or by an in vitro coupling approach using the purified *Escherichia coli* enzyme biotin ligase (BirA). The purified BirA biotin ligase that was kindly provided by Avidity.

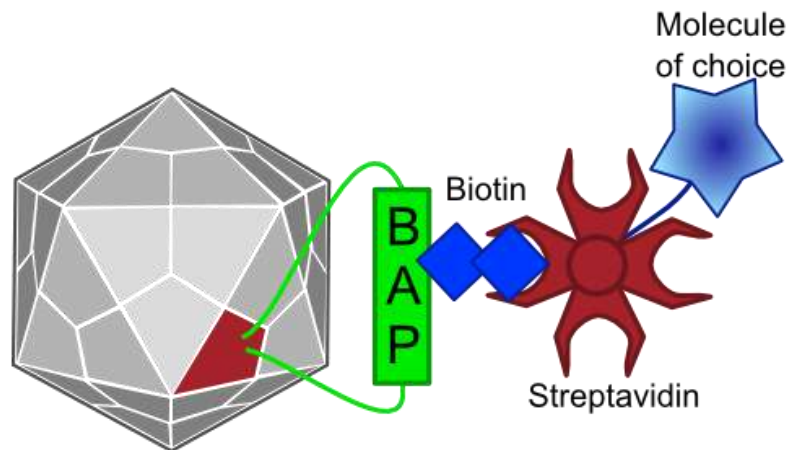


Figure 26: BAP

3.3.1.3.2 IMAC purification via Viral Brick: The Histidine Affinity Tag

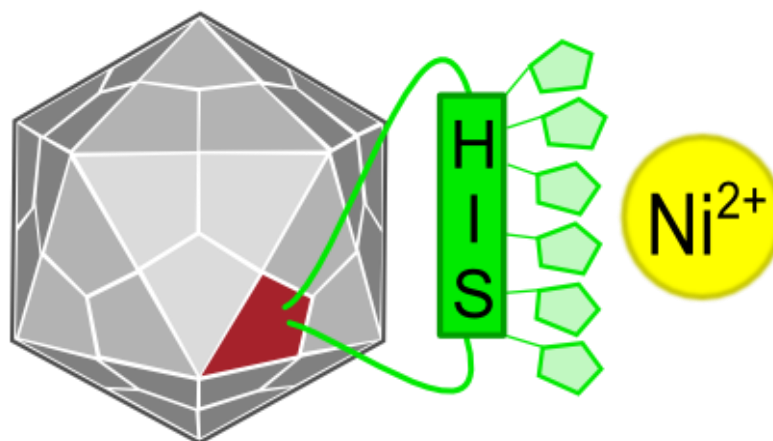


Figure 27: His

Protein tagging via histidine tags is a widely used method for protein purification: Multiple histidine residues (most commonly: Six) are fused to the end of the targeting protein.

The high binding affinity of histidine towards metal is being exploited for the purification of proteins via the so called “Immobilized Metal Ion Affinity Chromatography”(IMAC): Multiple histidine residues (most commonly: Six) are being fused to the end of the targeting protein. A cell extract containing the recombinant protein is then applied to a column containing immobilized Ni^{2+} -ions. The His-tags complex the Ni^{2+} -ions while other cellular proteins can be washed off the column. The purified proteins can then be eluted with imidazole, which displaces the histidine residues.(M. C. Smith et al. 1988), (Hoffmann & Roeder 1991)

Since the aim behind engineering therapeutic AAV vectors is a safe administration to human patients, it is important to consider a convenient way of purifying the virus particles. Contamination by cellular proteins could cause toxic side effects or a strong immune response. Koerber et al. have first inserted a His-tag into a surface-exposed loop at amino acid position 587 in the Cap protein and successfully purified recombinant viruses using IMAC (Koerber et al. 2007). For our Virus Construction Kit, we provide the His-tag motif in the ViralBrick standard, allowing for an easy insertion into the 453 and/or 587 loop. If the modified capsid bearing a His-tag is being cotransfected with a wild type capsid for the production of mosaic viruses, IMAC helps to not only purify the produced viral particles but also to enrich particles which actually contain the modified proteins.

3.3.1.4 Targeting

3.3.1.4.1 Targeting peptides via ViralBrick: The RGD Motif

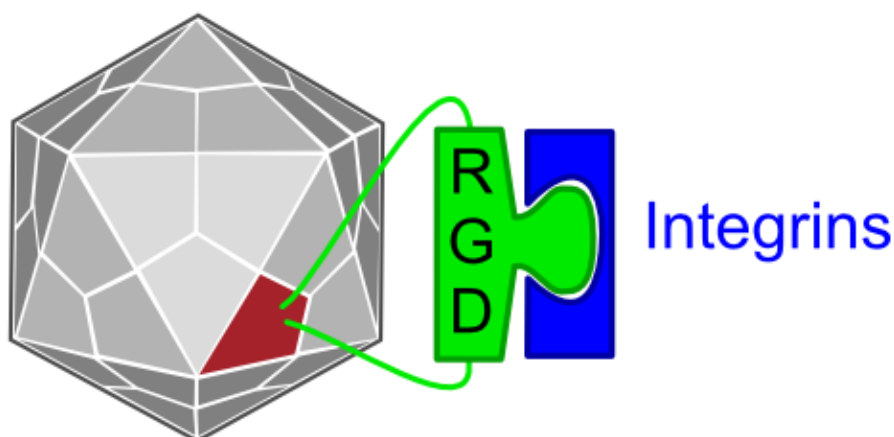


Figure 28: RGD motif

Integrins are transmembrane proteins that, among other functions, mediate cell attachment to surrounding tissues. They bind to a motif consisting of the amino acids arginine, glycine and aspartic acid (RGD in one-letter code). Because Integrin is highly expressed in many tumor cell lines (S. M. Albelda et al. 1990), (Damjanovich et al. 1992), (Lessey et al. 1995), (Smythe et al. 1995), (Gladson & Cheresch 1991), AAV particles displaying the RGD motif on various positions in their capsid proteins have been created by (Shi et al., 2003). Particles displaying RGD at amino acid positions 584 & 588 as well as 453 or 587 (Boucas et al., 2009) showed transduction efficiencies similar to wt AAV, even when the cells' HSPG receptors were blocked by heparin sulfate or when the natural HSPG binding motif on the capsid surface was knocked out. To further broaden the area of therapeutic application,

we created a ViralBrick containing the RGD motive to specifically target cells with low HSPG-/high Integrin expression.

3.3.1.4.2 Coupling Antibodies to the Viral Surface via ViralBrick: The Z34C Motif

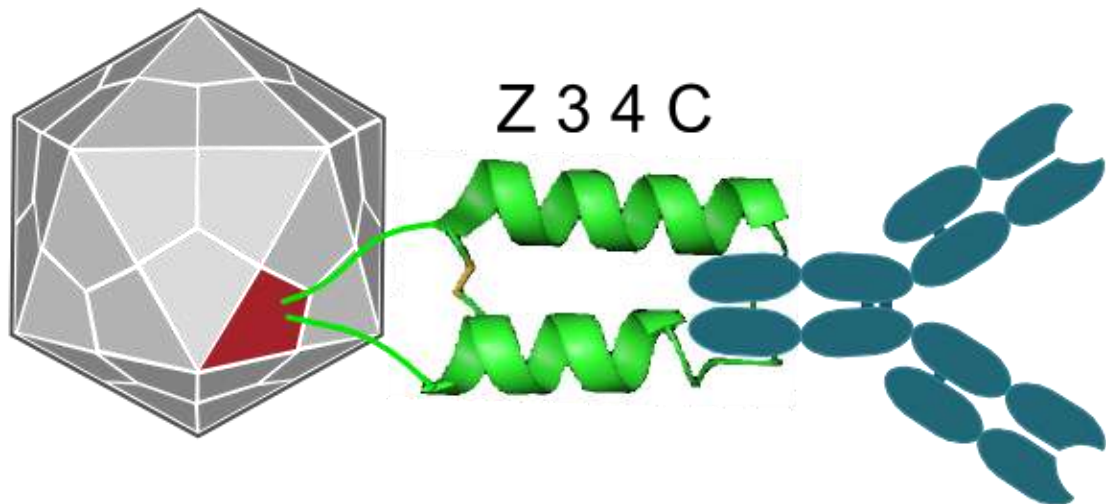


Figure 29: z34C motif

The idea of this targeting approach is to utilize a minimized fragment of the Staphylococcal Protein A that was first described in *Staphylococcus aureus*. These gram-positive bacteria have evolved the 508 amino acid long protein A that has a high affinity for the Fc-domain of antibodies to protect itself from the immune system. Binding to the constant region of the antibodies is accomplished by the Z-Domain of Protein A that is 58-59 amino acids long, has alone a high affinity ($K_d = 14,9 \text{ nM}$) for the antibodies and a three-helix bundle structure. In [Braisted & Wells; 1996] the authors reduced the secondary structure to an two-helix bundle. This size reduction has lead to an drastic reduction of the affinity for IgG ($>10^5$ fold) which could be recovered by 13 amino acid exchanges resulting in a 38 amino acid long peptide with an satisfying affinity for IgG ($K_d = 185 \text{ nM}$) termed Z38. This binding domain was subsequently improved in [Starovasnik et al.; 1997] by the insertion of a disulfide bridge connecting the ends of the helices leading to the binding domain Z34C which shows an increased affinity for IgG ($K_d = 20 \text{ nM}$).

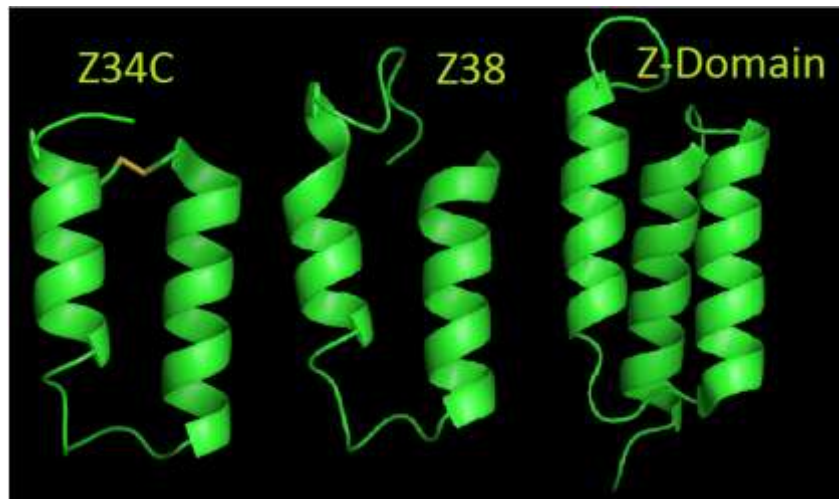


Figure 30: helix bundle

This engineered antibody binding domain of 34 amino acids was then inserted into capsids of different viral vectors amongst others also the AAV. In [Ried et al.; 2002] the Z34C domain was inserted at position 587 into the capsid of the AAV resulting in viral vector that can be targeted to different target cells without genetic engineering. This targeting approach was then improved in [Gigout et al.; 2005] by the creation of mosaic vectors that contain only ~25% of recombinant VP-Proteins what resulted in 4 to 5 orders of magnitude more infectiosity compared to all-mutant viruses.

3.3.2 N-terminal Fusion

Electron cryomicroscopy showed that the N-termini of VP1 and VP2 form globules in the interior of the capsid. However, the unique N-terminus of VP1 contains a Phospholipase A₂ domain which needs to be presented on the surface for endosomal release and therefore for successful infection. Immuno assays revealed that *in vitro* heat or urea treatment also leads to accessibility of the N-terminus of VP1 and possibly VP2 (Kronenberg et al. 2005). It is assumed that this surface exposure occurs via escape through channels at the fivefold symmetry axes of the capsid (Bleker, Sonntag & J. A. Kleinschmidt 2005). VP2 is expendable and fusion of larger motifs to its N-terminus does not affect viral assembly and genome packaging (K. H. Warrington et al. 2004). We expect that peptides fused to the N-terminus of VP2 become located on the virus surface either by transit through the channels or by exposure during capsid assembly.

In certain types of tumors, for example in breast (Walker & Dearing 1999), lung (Hirsch et al. 2003) and bladder (Colquhoun & Mellon 2002) carcinomas, the EGF receptor is overexpressed and therefore serves as a suitable target for cancer control or imaging.

The Z_{EGFR:1907} Affibody and the DARPin E01 were chosen as targeting molecules - two proteins which were engineered to specifically bind to the EGF receptor (Friedman et al., 2008; Steiner, Forrer, & Plückthun, 2008).

By N-terminal fusion to VP2 and therefore exposure of these motifs on the surface of the virus capsid we expect that EGFR overexpressing tumor cells can be transduced. Via additionally knocking down the natural tropism of the virus towards heparan sulfate proteoglycan (HSPG) infection of healthy cells is greatly reduced.

We couple these targeting peptides to a VP2/3 BioBrick according to the Freiburg assembly standard 25 with different kinds of linker, thus establishing a small linker library. Driven by the CMV promoter the resulting fusion protein is expressed *in trans* to the other structural and regulatory elements of the virus – the RepCap plasmid –, replacing 100 % of VP2 by start codon mutation. This allows titration and control of the amount of the VP2-targeting-subunit that becomes incorporated into the virus capsid.

We also want to investigate and provide further applications with our Virus Construction Kit: Fusion of a fluorescent protein or His-Tag enables tumor imaging or virus purification approaches.

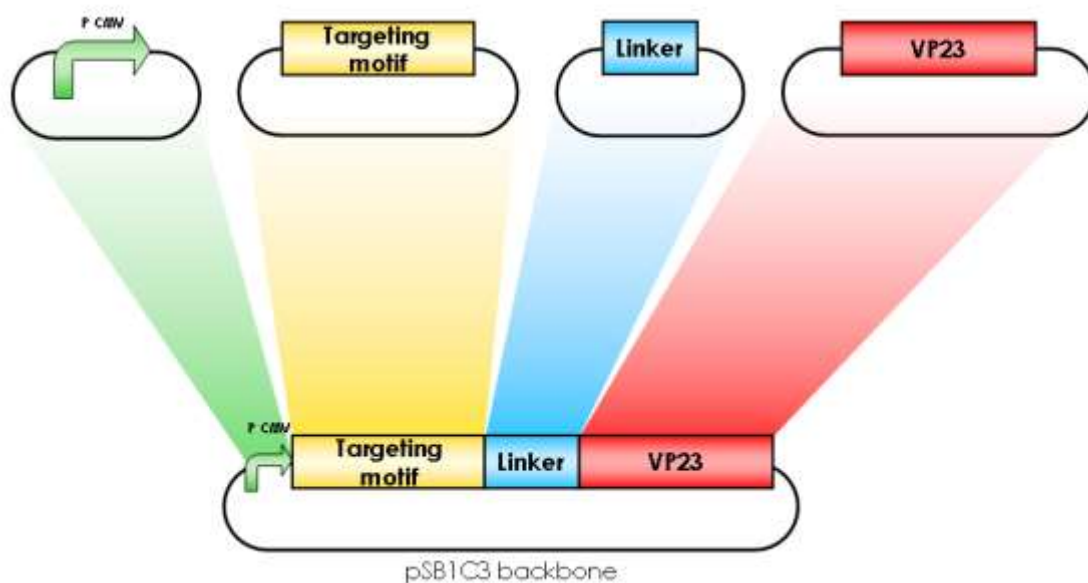


Figure 31: N-terminal fusion approach.

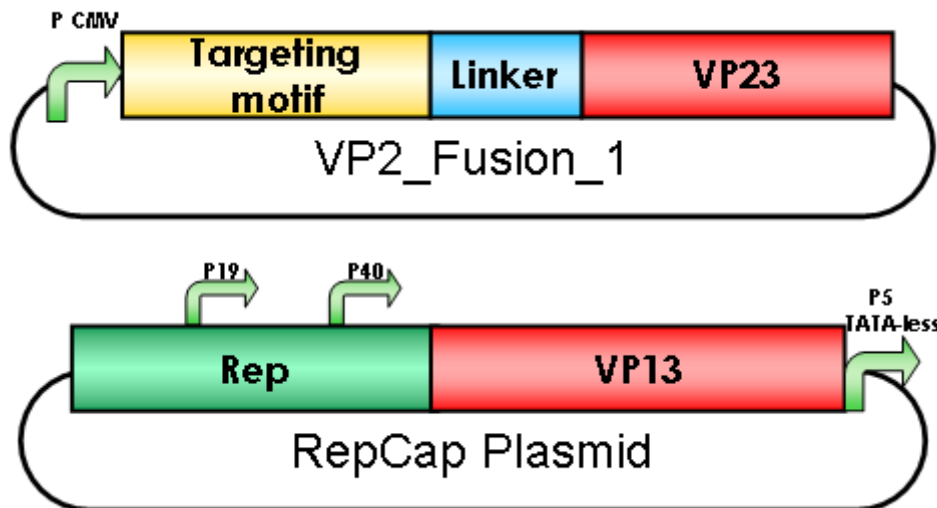


Figure 32: Cotransfected plasmids

3.3.2.1 VP1 insertion

We also designed an alternative strategy for integration of larger peptides into the virus capsid. The so called VP1 insertion is similar to the N-terminal fusion to VP2: Again the Affibody Z_{EGFR:1907} or the DARPin E01 is fused upstream to the VP2/3 BioBrick. In addition to that the unique N-terminal region of VP1 (VP1up) was fused to the targeting motifs, providing the essential phospholipase A₂ domain. For better infectivity, we expose a nuclear localization signal (NLS) on the capsid surface by inserting it between VP1up and the targeting peptide (Grieger et al. 2007). Again this fusion protein is driven by the CMV promoter and co-transfected to the RepCap plasmid –, in which this time the VP1 start codon is mutated.

As already described in the N-terminal VP2 fusion part above, we also want to test imaging and purification approaches. We perform transfections using different ratios of targeting-subunit plasmids to RepCap plasmids in order to find out which composition of the capsid allows optimal targeting of the tumor cells without affecting capsid assembly and packaging. By determining the amount of DNA-packaged capsids and transduced cells via quantitative real-time PCR and enzyme-linked immunosorbent assay (ELISA) we are able to determine the infectious titer of the re-targeted virus particles.

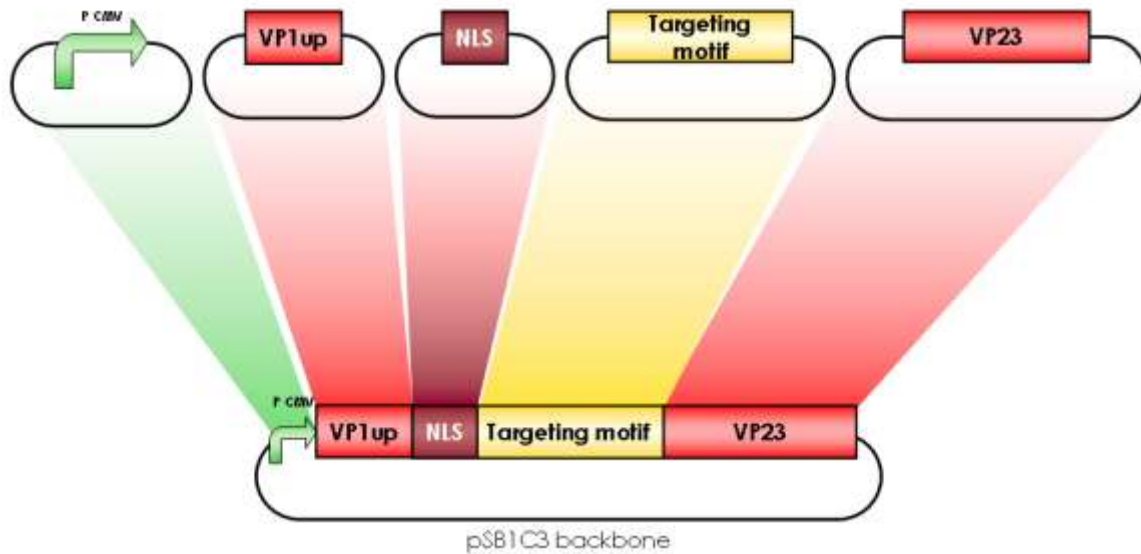


Figure 33:

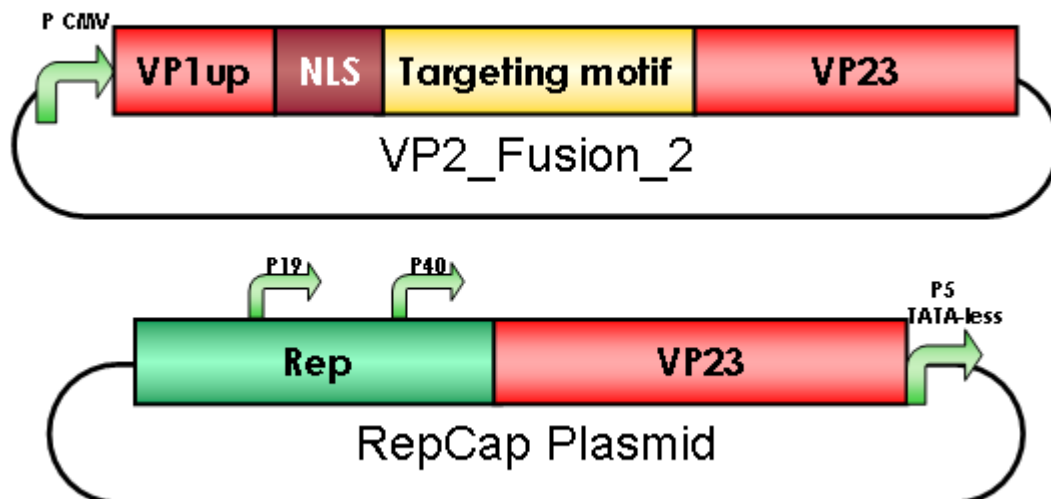


Figure 34:VP1 insertion

3.3.2.2 Targeting molecules

3.3.2.2.1 Affibody Z_{EGFR:1907}

Affibodies are small (6 kDa), soluble high-affinity proteins. They are derived from the IgG-binding B domain of the Staphylococcal protein A, which was engineered to specifically bind to certain peptides or proteins. This so-called Z domain consists of an antiparallel three-helix bundle and is advantageous due to its proteolytic and thermodynamic stability, its good folding properties and the ease of production via recombinant bacteria (Nord et al. 1997). Affibodies can be used for example for tumor

targeting (Wikman et al. 2004) and diagnostic imaging applications (Orlova et al., 2006; Orlova et al., 2007). The Z_{EGFR:1907} Affibody was engineered to specifically bind the EGF receptor with an affinity determined to be $K_D = 2.8$ nM (Friedman et al. 2008).

The EGF receptor is overexpressed in certain types of tumors, e.g. in breast (Walker & Dearing 1999), lung (Hirsch et al. 2003) and bladder (Colquhoun & Mellon 2002) carcinomas, and is therefore a suitable target for cancer imaging or therapeutic applications. Because of their good tumor uptake, and their property to become internalized into the target cells with an efficiency of 19 – 24% within one hour – compared to 45% of the natural ligand EGF – the Z_{EGFR:1907} Affibody was chosen for therapeutic applications by the Freiburg iGEM Team 2010 (Göstring et al. 2010; Friedman et al. 2008).

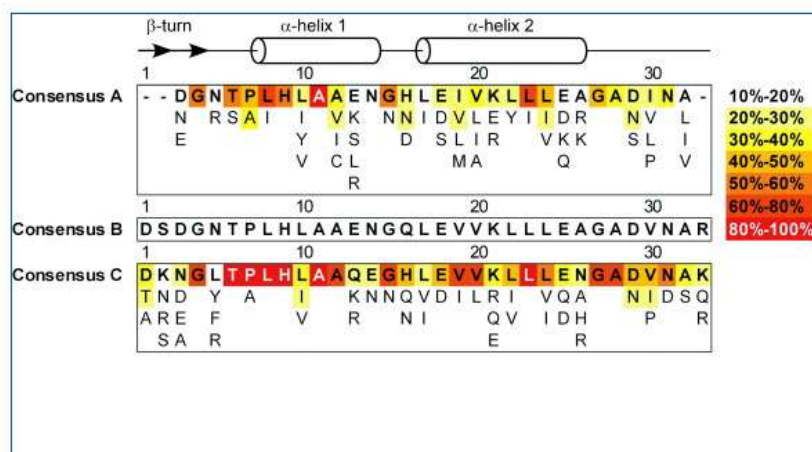


Figure 35: Nucleotide sequence of designed Z_{EGFR:1907}

3.3.2.2.2 DARPin E_01

Natural protein ankyrin repeat (AR) molecules are motifs that can be found commonly in proteins (Bork 1993). These motifs are mediating protein-protein interactions suggesting that AR proteins can be used for designing new binding molecules. Design of structural scaffolds with consensus regions and randomized positions of interacting residues leads to improved biophysical characteristics of targeting molecules (Binz et al. 2003) (Kohl et al. 2003).

A



B

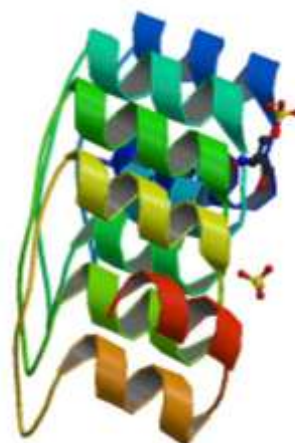


Figure 36: (A) Consensus sequence of ankyrin repeat proteins. (B) Three dimensional structure of ankyrin repeat proteins (N3C)

The repetitive nature of the ankyrin proteins allows modifications in their variable and modular binding surface. Therefore, consensus sequences of natural ankyrin proteins have been used to design novel and stable scaffolds for binding proteins.

Designed Ankyrin Repeat Proteins (DARPin) are well expressed, monomeric in solution, thermodynamically stable and have the ability to fold fast. In the publication of (Steiner et al. 2008) screening libraries were created by using the signal recognition particle (SRP) translocation pathway for phage display. The selected DARPin E_01 has very high affinities to the target protein ErbB1 and can be used as a potential targeting molecule for our approach by fusing the DARPin to N-terminal VP proteins.

Our designed ankyrin repeat protein consists of three internal binding repeats and the C- and N-terminal capping repeats. Each internal repeat module comprises one beta-turn and two hydrophobic alpha helices. The potential interaction residues are located in the beta-turn and the first alpha helix of the AR-proteins (Figure 37).

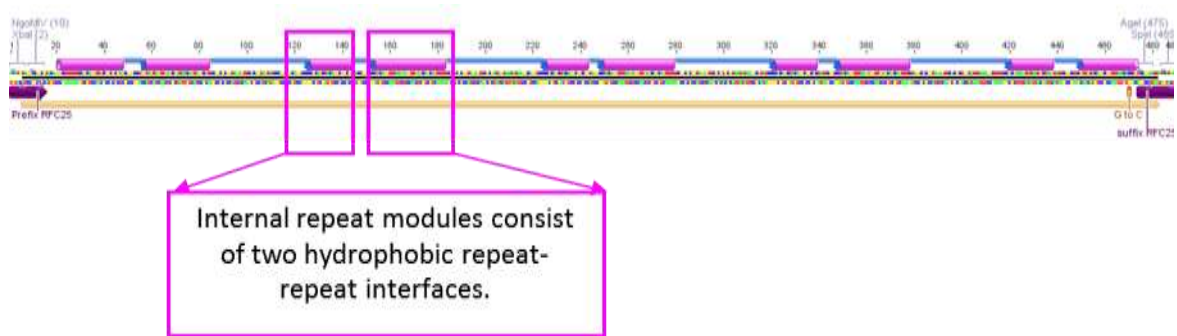


Figure 37: Schematic overview of the internal repeat modules of DARPins. These proteins contain two hydrophobic alpha helices.

Furthermore, there have been found several conserved motifs within the sequences (Figure 38).

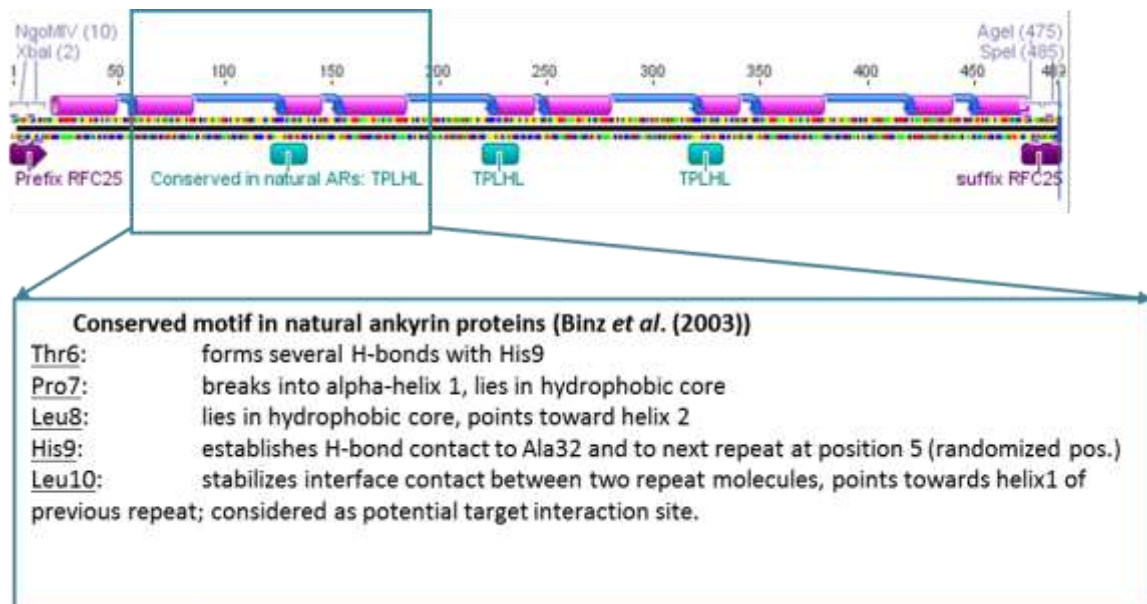


Figure 38: Conserved motifs found in DARPins.

Capping repeats:

- Capping repeats: N-terminal capping
- C-terminal capping

Exposed surface of capping modules is hydrophilic and is therefore needed for forming a stable, well folded AR domain.

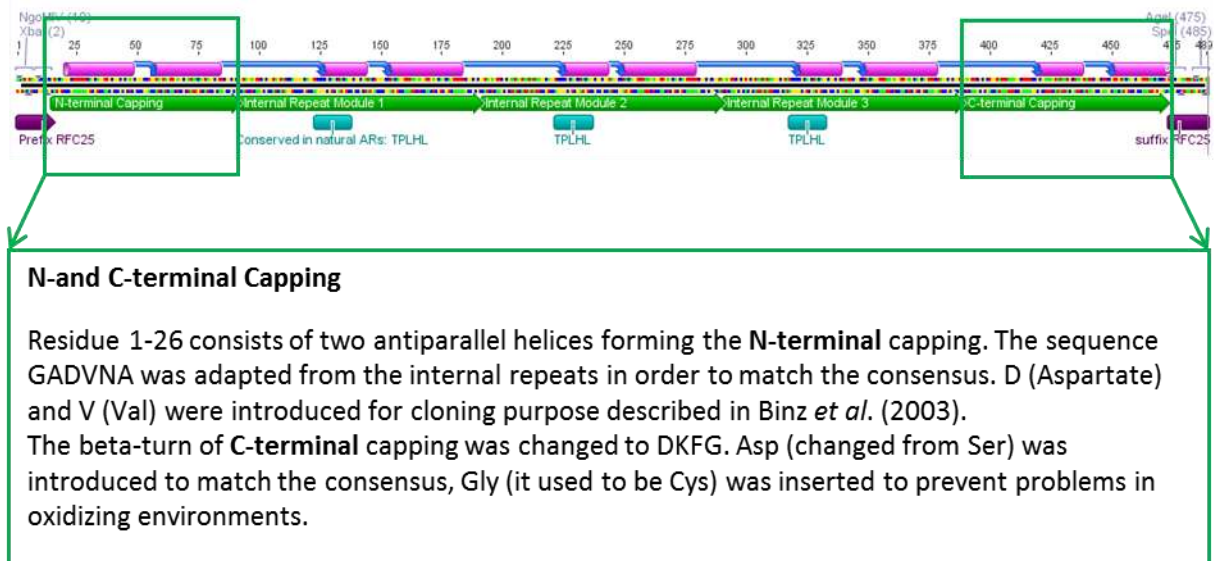
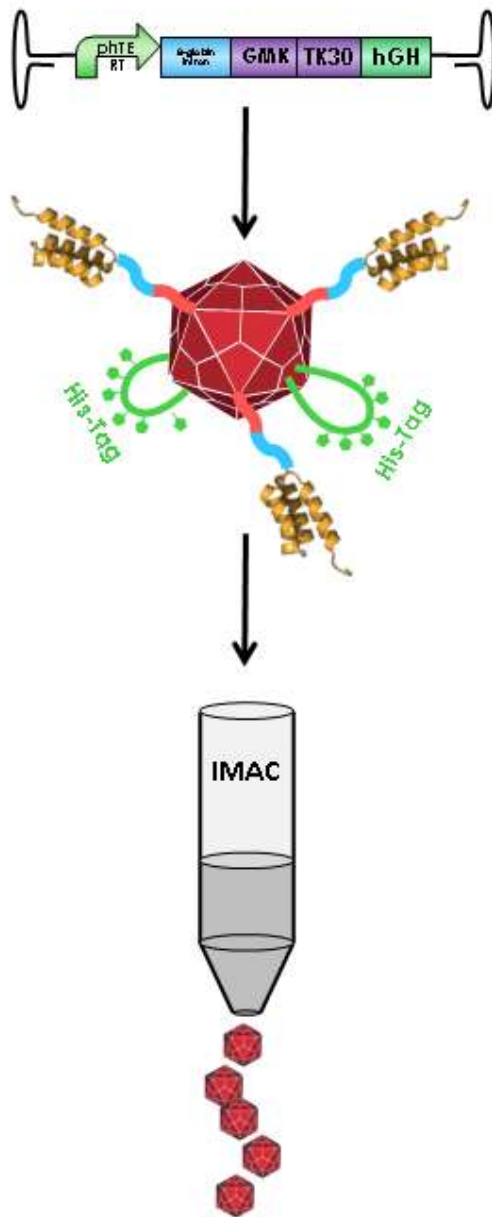
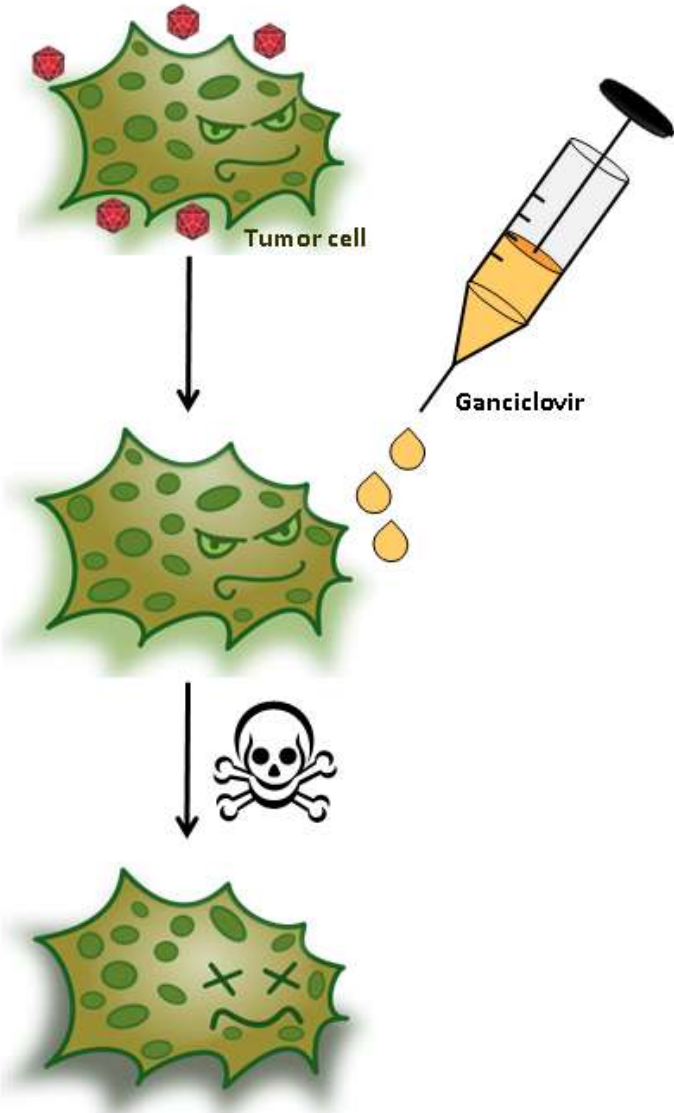


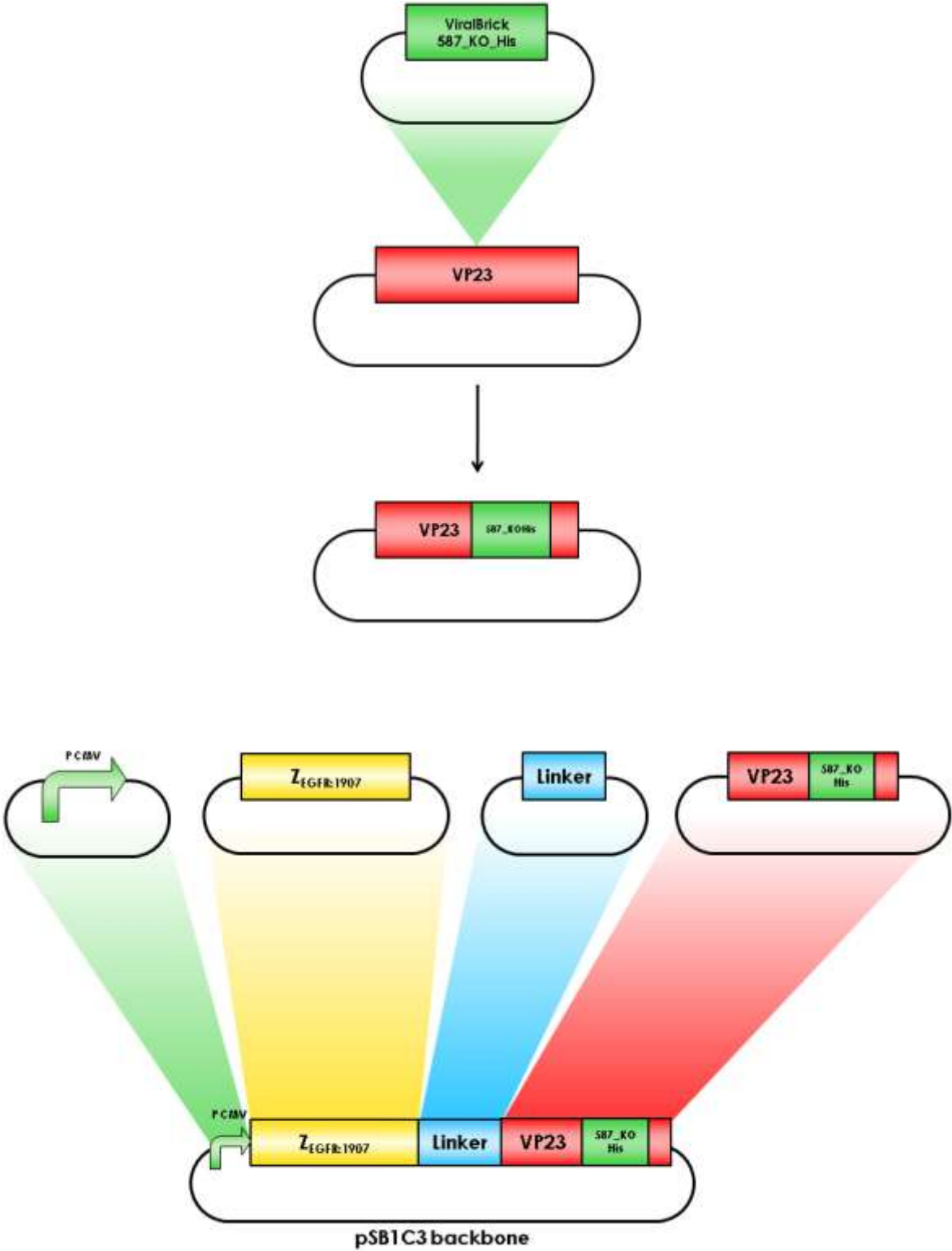
Figure 39: The capping modules of the DARPins.

3.4 Favorite parts



The main goal of our work is to create a re-targeted virus capsid against EGFR overexpressing tumor cells. By packaging a gene, coding for a prodrug-activating enzyme, which expression is under control of a tumor-specific promoter, these malignant cells can be killed. Furthermore the virus can be easily purified via capsid integrated His-Tags. By using a helper free system, these recombinant, therapeutic AAV2-particles are not able to reproduce.





4 Methods

4.1 Cloning

4.1.1 Polymerase Chain Reaction

The Polymerase Chain Reaction (PCR) is a technique to amplify specific DNA sequences delivered by a DNA template independent from a bacterial system. Especially designed primers encompass the desired sequence. These primers serve as docking regions for the polymerase which extends the newly synthesized DNA strand.

The DNA template strand is heat denaturated (98 °C, 1 minute) to produce single-stranded DNA. The next step requires the temperature to be lowered to a temperature at which forward and reverse primers are able to anneal to their complementary bases on the DNA template. This temperature is defined by the length and the GC content of the primers. With increasing temperature (72 °C) the polymerase binds the priming regions and elongates the primers. The temperature is raised again to denaturate the double strand and the cycle starts anew.

PCRs were performed using Mastercycler gradient (Eppendorf, Hamburg, Germany), Mastercycler personal (Eppendorf) and Px2 ThermoHybaid devices (Thermo Fisher, Waltham, MA, USA). Phusion™ Polymerase together with corresponding buffer and dNTP mix were obtained from New England Biolabs (New England Biolabs, Ipswich, MA, USA). Link to NEB: <http://www.neb.com>

4.1.2 Site-Directed Mutagenesis

The Site-Directed Mutagenesis (SDM) is used to mutate a specific base inside the plasmids sequence (Hutchison et al. 1978). Therefore, forward and reverse primers, which prime at the same site, containing a mismatch at the specific base in terms of the original structure are required. This mismatch defines the new base through which the original one is replaced.

As with Polymerase Chain Reaction, the site-directed mutagenesis works by amplifying the desired construct. The DNA double-strand is heat-denaturated which allows primers to bind to the single-stranded sequences after lowering the temperature. Designing a mismatch within the primers sequence leads to replacement of the unwanted base in later cycles of denaturing, annealing and elongation strands. After SDM program is finished, digestion with DpnI is necessary to digest parental methylated and hemi-methylated plasmid strands which do not contain the desired base pair exchange. For SDM, QuikChange Lightning Site-Directed Mutagenesis Kit (Agilent Technologies, Santa

Clara, CA, USA) and QuikChange Site-Directed Mutagenesis Kit (Agilent Technologies) were used. Link to Agilent: <http://www.genomics.agilent.com>

4.1.3 Ligation

Through restriction enzymes digested plasmid fragments can be reassembled into a new vector by ligation (see: Digestion). Ligase (Lehman 1974) connects complementary overhangs of fragments originated from digestion. The 5' phosphoryl group is bound to the hydroxyl group of the 3' end and therefore connects the fragments via ligase. This reaction requires energy whose form depends on ligase used. T4 DNA Ligase for example requires ATP.

This new vector now holds the genetic information of both the opened vector (minus the cut out fragment), and the insert.

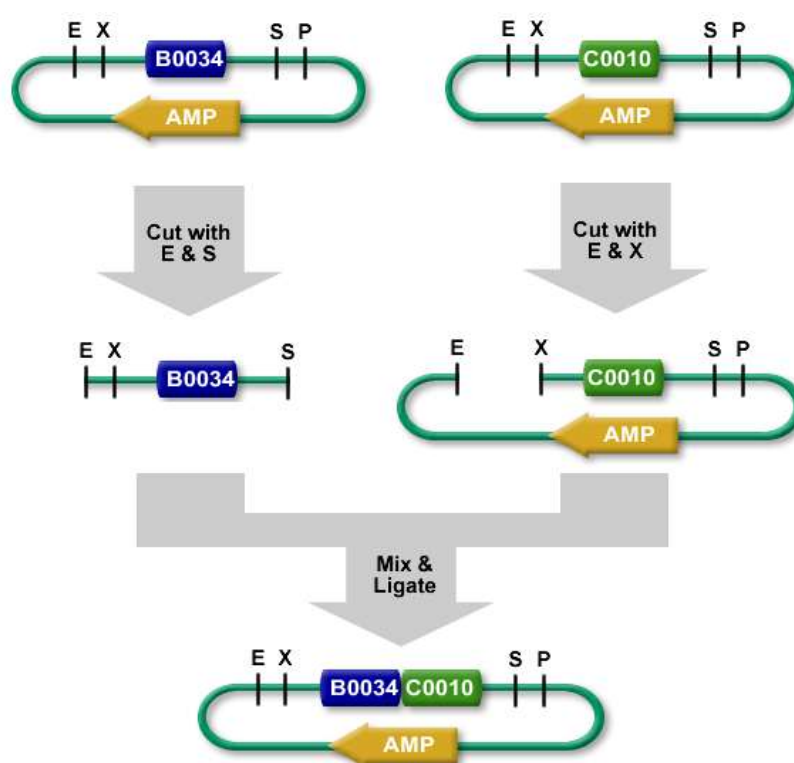


Figure 40:BioBrick assembly strategy

4.1.4 Transformation

Transformation is the process in which competent bacterial cells incorporate plasmid-DNA. DNA obtained from previous steps is added to competent cells. During incubation on ice, the plasmids attach to the cell surface. To make the cells assimilate the plasmids, the tubes are heat-shocked for a short time to 42 °C to allow the plasmids to pass the cell membrane. Although the mechanism is still

not fully understood, it is probably related to a decrease in the cell's membrane fluidity (Panja et al. 2008). After incubation on ice in order to regenerate the cells LB or DYT media is added and the tubes are incubated on a shaker at 37 °C to establish antibiotic resistance. After that, the cells are pelleted via centrifuging, the supernatant is discarded, and the pellet resuspended in the remaining rest of the media and plated on an agar plate containing the appropriate antibiotic. For transformation, BL21, XL1-blue and XL-10 Gold cells were used.

Table 2: Genotypic characterization of bacterial strains used for transformation.

Cell strain	genotype
BL21	<i>E. coli</i> B F ⁻ <i>dcm ompT hsdS</i> (r _B ⁻ m _B ⁻) <i>gal</i>
XL1-blue	<i>recA1 endA1 gyrA96 thi-1 hsdR17 supE44 relA1 lac</i> [F' <i>proAB lacI^qΔM15 Tn10</i> (Tet ^r)]
XL10-Gold	Tetr ^r Δ(<i>mcrA</i>)183 Δ(<i>mcrCB-hsdSMR-mrr</i>)173 <i>endA1 supE44 thi-1 recA1 gyrA96 relA1 lac Hte</i> [F' <i>proAB lacI^qΔM15 Tn10</i> (Tet ^r) Amy Cam ^r]

4.1.5 PCR purification

PCR purification is performed to purify the DNA sample from primers, salts, nucleotides, enzymes or other contaminations. This is based on different binding properties of these impurities on the membrane which is used within the purification. The PCR product together with a specific buffer which allows binding to the membrane is added on a column, which is centrifuged and the flow-through is discarded. Elution of the the PCR product is performed after washing the column several times For PCR purification, QIAquick PCR Purification Kit (QIAGEN, Hilden, Germany) was used.

Used protocol: QIAquick ® (QIAGEN, Hilden, Germany)

4.1.6 Hybridisation of Oligos

Renaturation and hybridization reactions lead to the pairing of complementary single-stranded nucleic acids. The main technique of a hybridization is that complementary strands of nucleic acids anneal after a heating and cooling down procedure. Denaturation of the double-stranded DNA unwinds it and separates it into single strands through the breaking of hydrogen bondings between the bases. In a renaturation step, the single strands finally hybridize and build double helices. Hybridisations can be performed using a Thermoblock or by running a PCR like we did in our experiments.

4.1.7 Fill-in-reactions

Fill-in reactions can be performed by PCR in order to blunt DNA. In comparison to a conventional PCR, the product is not obtained by amplification, but by fill-in 5'-overhangs of ssDNA using the Klenow-fragment [Figure]. This protein fragment is a product of the DNA polymerase I from *E. coli*, when cleaving it enzymatically by the protease subtilisin. It retains a 5' → 3' polymerase activity and a 5' → 3' exonuclease activity, but is lacking the 3' → 5' exonuclease activity. Therefore, the protein fragment is useful for many applications like DNA labeling by fill-in 5'-overhangs or strand displacement amplification (in this method the exo- klenow-fragment extends the 3'-end of a nicked strand and displaces the downstream DNA strand). After starting the PCR program, the samples are heated for 15 minutes at 94°C following an incubation time of 3 minutes at 94 °C. As soon as the samples are cooled down at 37 °C 1 µl Klenow-fragment (NEB, Frankfurt am Main) is added. The reaction is carried out usually in the same buffer as used for the digestion. While incubating the samples at 37°C for one hour, the fill-in reaction is finally running.

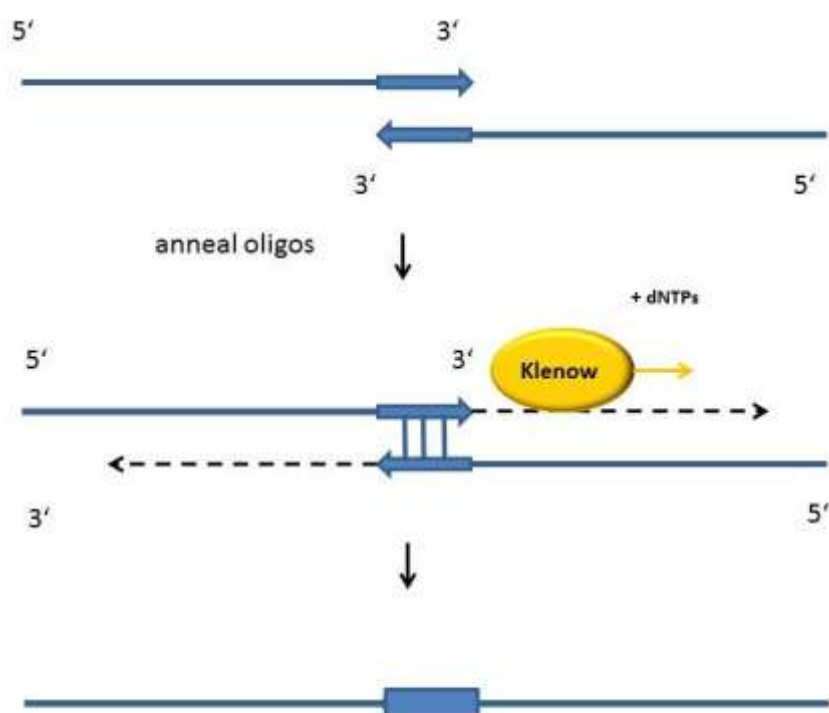


Figure 41: Fill-in reaction of two annealed long oligonucleotides by using the Klenow-fragment.

4.1.8 DNA gel electrophoresis

Agarose gel electrophoresis and polyacrylamide gel electrophoresis are common analytical techniques to identify, quantify and purify nucleic acids. The usage of the two types of gels depends

on the size of the fragments. Whereas an agarose gel is used to separate relatively long DNA molecules from 100 kDa up to 500 kDa, a polyacrylamide gel can also be used molecules shorter than 100 kDa. For our experiments we separated the DNA fragments by 1% - 1,5 % Agarose gel electrophoresis (Thermo EC Classic Series, Thermo Scientific) using Gelred™ (Hayward, USA) for staining. Gelred™ is a fluorescent nucleic acid gel stain which intercalates with nucleic acid and replaces the usage of the highly toxic ethidium bromide (EtBr) bit by bit.

[<http://www.biotium.com>] As a DNA ladder we used the GeneRuler™ DNA Ladder Mix (Fermentas, Germany).

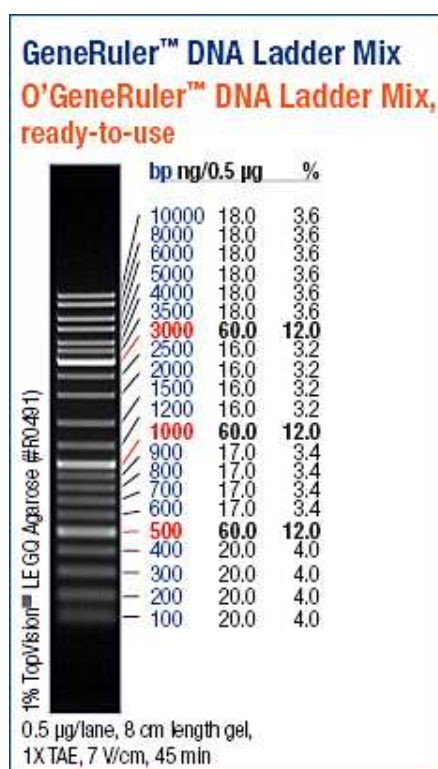


Figure 42: GeneRuler DNA ladder mix provided by Fermentas.

4.1.9 Vector Dephosphorylation

A higher amount of vector backbone in cloning strategies can be reached by using a Phosphatase like the Antarctic Phosphatase (NEB, Frankfurt am Main, Germany). This enzyme catalyzes the removal of 5' phosphate groups from DNA, RNA, rNTPs and dNTPs.

[<http://www.neb.com>].

Dephosphorylated fragments cannot religate due to the lack of 5' phosphoryl termini which are required by ligases. The dephosphorylation needs to be performed after digestion of the vector and before separating the fragments via agarose gel.

4.1.10 Gel Extraction

This technique is used to extract DNA fragments gained of previous cloning advances of 70 bp up to 10 kb after they have been separated by gel electrophoresis. The fragments of interest are identified by theoretically cloning of vector and/or insert with Geneious to get their fragment sizes and comparing them with a standard DNA ladder. The expected bands are visualized under UV light and isolated from the gel by using a scalpel (cleaned with EtOH before). Usually, the DNA is then extracted via a spin column extraction kit to remove the accompanying salts and stain. In our case, we used the QIAquick Gel extraction Kit (250) (QIAGEN, Germany) and the including protocol. The kit works on a silica-membrane basis and makes it possible to purify up to 400 mg slices of DNA bands from gels. After several fast binding and washing procedures (description of most used buffer under 3.1.12.1) the DNA is eluted with 30–50 µl elution buffer. Besides the PCR products, which were mostly eluted with 30 µl elution buffer, we usually used 20 µl of elution buffer. The purified DNA fragments are ready for direct use in all applications, including sequencing, ligation and transformation (QIAGEN, Hilden, Germany).

4.1.11 Verification of Correct BioBrick Part Assembly

After production of a new BioBrick vector, there are different possibilities to test the correct assembly of the used BioBrick parts before sending them for sequencing.

4.1.11.1 Test digestion

It is important to be aware of negative controls for the analysis of a test digestion. That means the vector backbone of the particular construct has to be digested with the same enzymes as the assembled BioBrick for comparing the expected bands. The required enzyme volume per sample can be reduced down to 0,5 µl of each enzyme. According to that, an incubation time of 40 min is enough and depending on the size of the expected fragments, the gel runs only about 25 min at 115 V.

4.1.11.2 Colony PCR

Another strategy is that a colony PCR can be performed by using primers that anneal to the verification primer binding sites. When designing these primers, it is important to make several predictions, for example to avoid undesirable pairings of the primers or unspecific bindings to the template. Therefore the primers are designed by choosing the same melting temperature (T_m) as the desired template. According to that they should have a primer length of about 800 bp for a good detection on the gel. With a colony PCR, bacterial colonies are screened directly by PCR. Each colony is picked with a sterile toothpick, which can be transferred not only into a PCR mix, but at the same

time into fresh DYT media preparing for a Mini- or Midiprep. When using a standard polymerase, the PCR is started with an extended denaturation time of 95°C to release the DNA from the cells. After running the program, the samples are loaded on an agarose gel to proof the success of a BioBrick assembly.

4.1.12 Purification of Plasmid DNA

4.1.12.1 Miniprep

We used the QIAprep[®] Spin Miniprep Kit (QIAGEN, Germany) which enables the purification of up to 20 µg molecular biology grade plasmid DNA or cosmid DNA. The procedure was done following the QIAGEN standard protocol including three basic steps. First one is the clearing of the bacterial lysate, then the adsorption onto a membrane and at the end the elution of plasmid DNA. Before clearing the lysate, the bacteria are lysed under alkaline conditions (Buffer 1 with RNase, Buffer P2). Buffer P2 contains SDS, which solubilizes the phospholipid and protein components of the cell membrane, while NaOH denatures the plasmid DNAs and proteins. After that the lysate is subsequently neutralized (N3 Buffer) and exposed to high salt-binding conditions. This leads to precipitation of chromosomal DNA, cellular debris and SDS, while the smaller plasmid DNA renaturates and stays in the solution. As a next step the sample can be applied to the spin column following two washing steps with PB and PE Buffer. Finally, the DNA can be eluted with water or with elution buffer. Unlike the standard protocol, we eluted the DNA with 60 µl Buffer EB instead of using 50 µl. (QIAGEN, Hilden, Germany)

4.1.12.2 Midiprep

The Midipreps were done following the standard protocol of Qiagen using a QIAGEN[®] Plasmid Plus Midi Kit (QIAGEN, Hilden, Germany). These kits enable fast, large-scale purification of up to 250 µg of highly pure plasmid DNA (description of most used buffer under 3.1.12.1). By using a vacuum manifold which replaces the single centrifugation steps up to 24 samples can be prepared in parallel. Therefore we used the vacuum technique for large sample numbers of Midipreps as well as Minipreps. The plasmid DNA obtained is suitable for example to transfect the DNA into sensitive cell lines. (QIAGEN, Hilden, Germany)

4.2 Cell Culture

4.2.1 Cell lines

4.2.1.1 HEK 293 cells

4.2.1.1.1 Overview

The 293 cell line was derived from primary cultures of human embryonic kidney (HEK) cells with sheared fragments of adenovirus (Ad) 5 DNA. HEK 293 cells contain the nucleotides 1-4344 of Ad5 which are located within the pregnancy-specific β -1-glycoprotein 4 (PSG 4) gene. The transforming region of the human adenovirus contains the early region (E1), comprising two transcription units, E1a and E1b, whose products are essential and sufficient for mammalian cell transformation by adenoviruses. Because 293 cells express E1 gene products they are extensively used for the production of E1-deleted Ad viruses.

Adeno-associated viruses (AAVs) belong to the family of *Parvoviridae*, being one of the smallest single-stranded and non-enveloped DNA viruses. AAVss are replication-deficient and have required co-infection with a helper adeno- or herpes virus for productive infection.

The AAV Helper-free system takes advantage of the identification of the specific adenovirus gene products that mediate AAV replication and allows the production of infectious recombinant human adeno-associated virus-2 (AAV-2) virions without the use of a helper virus (AAV Helper-free System Instruction Manual, Agilent Technologies).

Stratagene recommends preparing Adeno-associated virus stocks using the AAV-293 cell line. The AAV-293 cells are derived from the commonly used HEK293 cell line, but produce higher viral titers. These cells also allow production of infectious viral particles when cells are co-transfected with the three AAV Helper-Free System plasmids (ITR containing plasmid, pAAV_RC and pHelper) because the adenovirus E1 gene product is stably expressed in AAV-293 cells.

Thus the AAV-293 cell line is specifically selected for high levels of AAV production in a Helper-Free System and offers several advantages over common HEK293 cells.

4.2.1.1.2 Establishing AAV-293 Cultures from Frozen Cells

For safe treatment of cells, the following steps have to be carried out under sterile conditions. Required materials and chemicals are: DMEM (Dulbecco's Modified Eagle Medium 1x, Invitrogen, Darmstadt, Germany), PBS (Dulbecco's PBS (1x) w/o Ca and Mg, PAA Laboratories GmbH, Pasching, Austria), T75 flask (Nunc, 75 cm² nunclon treated flask, blue filter cap, Roskilde, Denmark), 15 ml falcon, pipett tips

1. Thaw frozen cells within 1-2 minutes by gentle agitation in a 37 °C water bath
2. Transfer the thawed cells suspension into the 15 ml falcon containing 10 ml of DMEM
3. Collect cells by centrifugation at 200 x g for 5 minutes at room temperature (Centrifuge 5702, Eppendorf, Hamburg, Germany)
4. Remove supernatant and resuspend the cells in 3 ml of fresh DMEM by gently pipetting up and down
5. Transfer the 3 ml of cell suspension to a T75 flask containing 17 ml of DMEM
6. Place the cells in a 37 °C incubator at 5 % CO₂.
7. Monitor cell density daily. Cells should be passaged when the culture reaches 50 % confluence.

4.2.1.1.3 Passaging of AAV-293 Cells

Required materials and chemicals: DMEM, PBS, Trypsin-EDTA 0,25 % (Invitrogen, Darmstadt, Germany), T75 flask, 15 ml falcon, pipett tips

1. Prewarm the DMEM to 37 °C in a water bath and trypsin-EDTA solution at room temperature
2. Remove the medium and wash cells once with 10ml of phosphate-buffer saline (PBS)
3. Trypsinize the cells for 1-1.5 minutes in 1 ml of trypsin-EDTA solution
4. Dilute the cells with 10 ml DMEM to inactivate the trypsin and detach the remaining cells by soft resuspending
5. Transfer cells into a 15 ml falcon
6. Collect cells by centrifugation at 200 g for 5 minutes
7. Calculate the cell amount per ml via Neubauer cell chamber
 - a. Mix 95 µl Trypan Blue Stain 0,4 % (Lonza, Walkersville, USA) with 5 µl of the cell suspension
 - b. Mix gently by pipetting up and down

- c. Pipet the solution into the Neubauer chamber
 - d. Trypan stains dead cells blue, living cells appear as white
 - e. Counting of all living cells in four big squares
 - f. Calculate the amount of living cells per ml with the help of following formula:

$$(\text{counted cells} / 4) * 2.2 * 20 * 10.000$$
8. Calculate the cell amount per T75 flask (1.500.000 cells/20 ml DMEM) and transfer the cell suspension to a T75 flask containing fresh DMEM. Place the cells in a 37 °C incubator at 5 % CO₂.

4.2.1.1.4 Transfecting the AAV-293 Cells

Stratagene recommends a calcium phosphate-based protocol, usually resulting in the production of titers $\geq 10^7$ particles/ml when AAV-293 cells were transfected.

To achieve high titers, it is important that AAV-293 cells are healthy and plated at optimal density. It should be taken care to avoid clumping of the cells during passaging and plating for transfection.

Required materials and chemicals: 0.3 M CaCl₂, 2x HBS-Buffer pH 7.1, autoclaved deionized (Millipore) water, 1.5 ml Eppi-tubes

1. Inspect the host cells that were split two days before; they should be approx. 70-80 % confluent
2. Remove the plasmids to be co-transfected from storage at -20 °C. Adjust the concentration of each plasmid to 1 µg/µl in sterile/autoclaved Millipore water.
3. Pipet the required volume of each of the plasmid DNA solution (5 µg of each plasmid) into an 1.5 ml tubes. Fill up to 300 µl with sterile Millipore water.
4. Add 300 µl of 0.5 M CaCl₂ and mix gently.
5. Pipet 600 µl of 2x HBS into a 15 ml falcon.
6. Vortex the falcon gently while pipetting the DNA/CaCl₂ solution dropwise into the falcon.
7. Incubate 20 minutes (precipitate formation).
8. Apply the DNA/CaCl₂/2x HBS solution dropwise to the plate of cells (10 cm dish).
9. Return the cells in a 37 °C incubator at 5 % CO₂ for 6 h.
10. After incubation remove the medium, wash once with PBS and replace it with 10 ml of fresh DMEM growth medium.
11. Return the cells back to the 37 °C incubator for an additional 66-72 h.

4.2.2 HT1080

4.2.3 A431

The A431 cells belong to the fibroblasts and the cell line was established from an epidermal carcinoma of a vulva. The main purpose of fibroblasts is to maintain the structure of connective tissues by continuously secreting precursors of the extracellular matrix. They are the most common cells in connective tissue in animals. The A431 cells show an epithelial morphology, have been used for a lot of different studies in cellbiology and are naturally devoid of a potent tumor suppressor and transcription factor: p53 protein (p53His273 mutation).

The extreme expression of EGF receptors by this cell line is due, at least partly, to the amplification of EGF receptor DNA sequences (30-fold). Normal human cells exhibit a EGF receptor density ranging from 40.000 to 100.000 receptors/cell whereas the A431 cell line has 3×10^6 receptors/cell. (Carpenter & Cohen 1979).

4.2.4 Flow Cytometry

4.2.4.1 Overview

Flow cytometry is a technique for measuring and analyzing multiple physical characteristics of single particles, usually cells, as they flow in a fluid stream through one or more beams of light. The properties measured include the particle's relative size and granularity or internal complexity and relative fluorescence intensity.

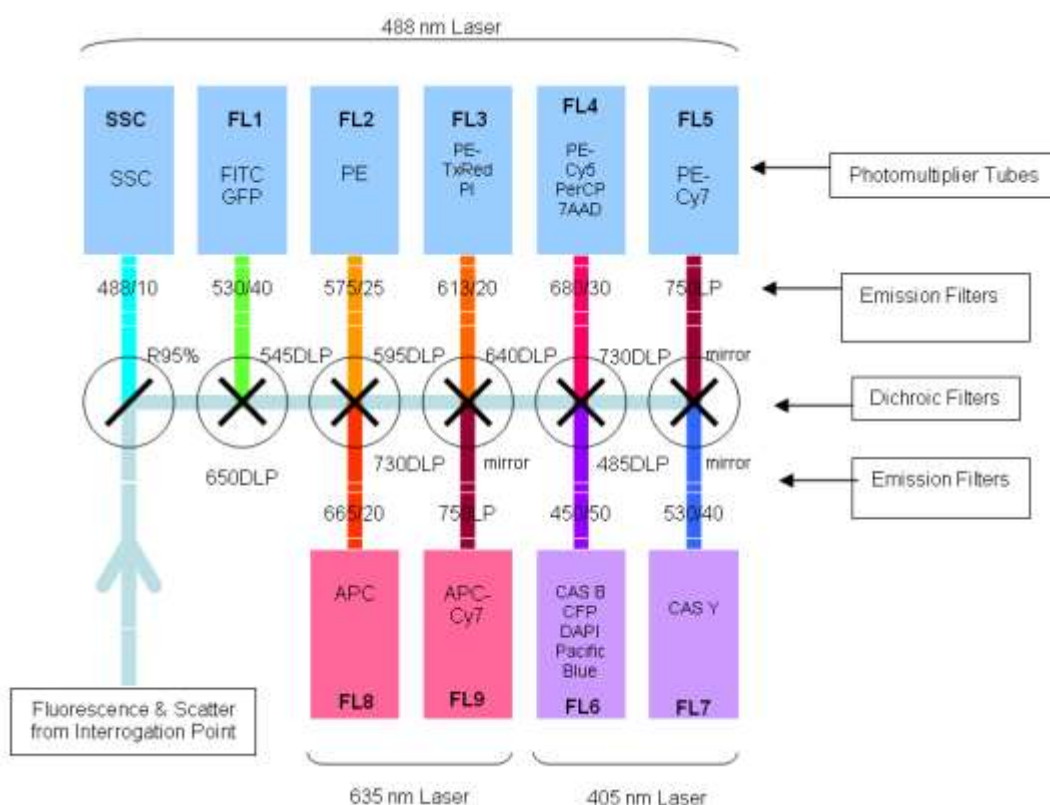


Figure 43: Schematic overview of a typical flow cytometer setup (Beckmann Coulter 2008).

After hydrodynamic focusing (produces a single stream of cells) cells are carried to the laser intercept. When these cells pass through the laser intercept, they scatter laser light. Light that is scattered in the forward direction is collected by a lens known as the forward scatter channel (FSC). The FSC intensity nearly equates to the particle's size and can be used to distinguish between cellular debris and living cells. Light measured perpendicular to the excitation line is called side scatter. The side scatter channel (SSC) provides information about cell complexity or granularity.

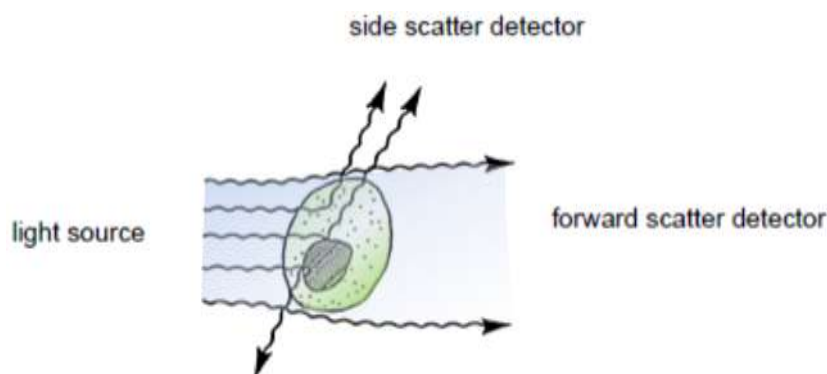


Figure 44: Light-scattering properties of a cell adapted from (Marti, Stetler-Stevenson, Bleesing, & Fleisher, 2001).

Fluorescent labeling allows investigation of cellular structure and functions. Flow cytometers use distinct fluorescence (FL-) channels to detect light emitted. The detection of fluorescent proteins in cells allows to monitor gene expression and to identify fluorescently labeled particles.

There are a lot of fluorescent substances with potential applications in flow cytometry. The most frequently used molecule is the green fluorescent protein (GFP), a biological molecule derived from the jellyfish *Aequorea victoria*. Among GFP variants, yellow fluorescent proteins (YFPs) are relatively acid-sensitive and uniquely quenched by chloride ions (Cl⁻). Found in the Registry of Standard Biological Parts, we used mVenus ([BBa_1757008](#)) as our desired gene of interest which contains a novel mutation at position F46L. SEYFP-F46L (Venus) folds well and forms the chromophore efficiently at 37°C (Nagai et al. 2002). The usage of fluorescent molecules as fusion proteins allows checking the transduction efficiency by determining the fluorescent intensity of YFP in transduced cells. GFP shows excitation and emission maxima at 489nm and 509nm, respectively. SEYFP-F46L's peak excitation and emission wavelengths are 515nm and 528nm. Both GFP and SEYFP-F46L can be excited with a 488 nm blue laser and detected on FL 1.

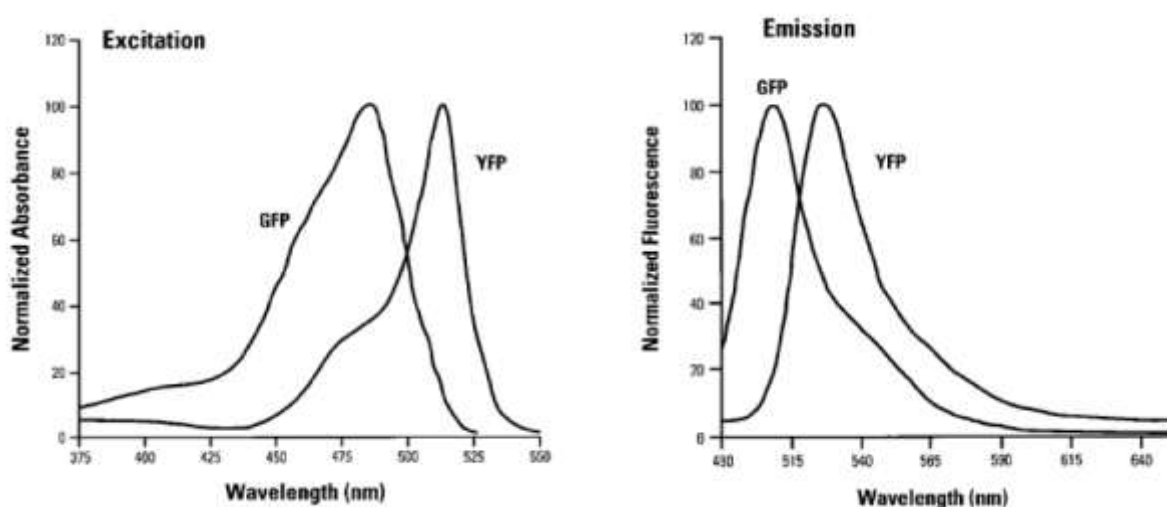


Figure 45: Excitation/emission spectra of GFP and YFP adapted from (Lybarger et al. 1998).

The number of fluorescent proteins that can be detected depends on the instruments and lasers available to the user. The Flow Cytometer CyAn ADP 9 Color from Beckman Coulter (Krefeld, Germany) is equipped with a 488 nm and a 405 nm laser and a 642nm diode which allows the detection of fluorescence of different fluorochromes. We used the 488 nm laser to excite mVenus (YFP) and the fluorescent channel 1 (FL 1) to detect light emitted.

Laser Light Source	Parameters	Fluorochromes
488nm	FL1	GFP, YFP, Alexa Fluor
	FL4	7-AAD, Alexa Fluor
405nm	FL6	CFP

Figure 46: Laser Light Source to excite different Fluorochromes and the adapted fluorescent channels to detect light emitted (Beckmann Coulter 2008).

Data analysis was carried out using Summit 4.3 (Beckman Coulter) software. Forward and side scatter light gating were used to exclude dead cells and debris (Fig. 5). A minimum of 10.000 events was collected for each gate and histogram, respectively.

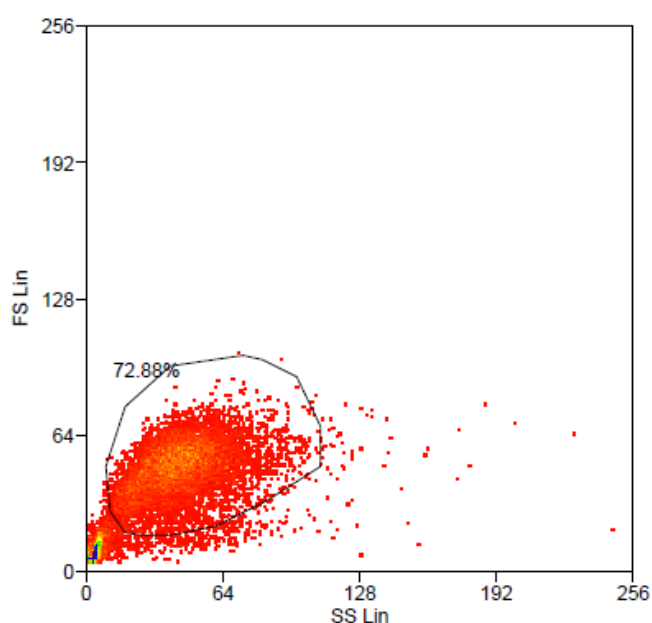


Figure 47: Gating for excluding cell debris

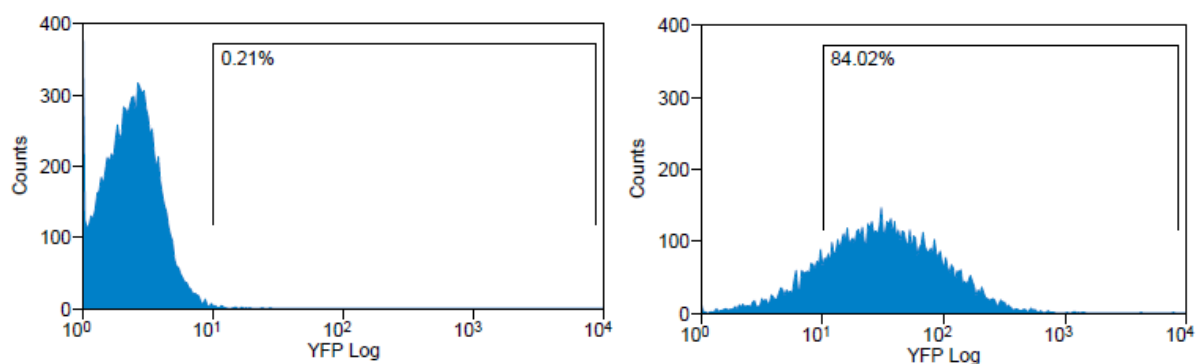


Figure 48: Histogram of negative control cells (left) and YFP-positive transduced cells (right).

Analytical gates were set such that 1% or fewer of negative control cells fell within the positive region (Fig.6 left). The same gate was used to detect the YFP-Expression of transduced cells (Fig.6 right). For transduction we use human tumor cell lines (HT1080 and A431). YFP expression can be correlated with the transduction efficiency of the viral vectors by monitoring measured fluorescence.

4.2.4.2 Sample Preparation for Flow Cytometry

- Harvest cells by trypsinization with 0,25% 1x Trypsin-EDTA (Invitrogen, Darmstadt, Germany)
- Collect cells by centrifugation at 1200 x g for 3 minutes (Heraeus Sepatech, Varifuge 3.0 R, Thermo Scientific, Germany)
- Discard supernatant and wash cells by resuspending cell pellet with 500 µl 1x Dulbecco's PBS without calcium, and magnesium (PAA, Pasching, Austria)
- Centrifuge at 1200 x g for 3 minutes
- Discard supernatant and resuspend cell pellet with 500 µl Dulbecco's PBS
- Centrifuge at 1200 x g for 3 minutes
- Discard supernatant and resuspend cell pellet with 500 µl Dulbecco's PBS
- Centrifuge at 1200 x g for 3 minutes
- Discard supernatant and resuspend cell pellet with 300 µl Dulbecco's PBS for evaluation on flow cytometry
- Use the 488 nm blue laser to excite the fluorochrome YFP and FL-1 to detect light emitted.

4.2.4.3 Cell Staining for Flow Cytometry

- **7-AAD Viability Staining:** 7-AAD has a high DNA binding constant and is efficiently excluded by intact cells. It is useful for DNA analysis and dead cell discrimination during flow cytometric analysis.
- For dead cell exclusion, wash cells threefold with 500 µl of 1x Dulbecco's PBS
- Discard supernatant and resuspend cell pellet in 300 µl of Cell Staining Buffer (BioLegend, BIOZOL Diagnostica, Eching, Germany)
- Add 3 µl of 7-AAD and incubate for 5-10 minutes in the dark before analysis
-
- **Alexa Flour 647 Annexin V:** Annexin V is a member of the annexin family of intracellular proteins that binds to phosphatidylserine (PS) in a calcium-dependent manner. PS is normally only found on the intracellular leaflet of the plasma membrane in healthy cells, but during early apoptosis, membrane asymmetry is lost and PS translocates to the external leaflet. Fluorochrome-labeled Annexin V can then be used to specifically target and identify apoptotic cells.

- Wash cells twice with cold cell staining buffer (BioLegend, BIOZOL Diagnostica, Eching, Germany)
- Resuspend cell pellet in 100 μ l Annexin V binding buffer (BioLegend, BIOZOL Diagnostica, Eching, Germany)
- Add 5 μ l of Alexa Fluor 647 Annexin V (BioLegend, BIOZOL Diagnostica, Eching, Germany)
- Add 10 μ l of PI solution (BioLegend, BIOZOL Diagnostica, Eching, Germany) or 7-AAD (for double-staining)
- Gently vortex the cells and incubate for 15 min at RT in the dark
- Add 400 μ l of Annexin V Binding Buffer (BioLegend, BIOZOL Diagnostica, Eching, Germany) and analyze the samples by flow cytometry

4.2.5 MTT Assay

4.2.5.1 Overview

The MTT-assay is a colorimetric assay, which is able to detect cell proliferation, viability and cytotoxicity. It is based on the metabolic activity of viable cells.

MTT (3-(4,5-Dimethylthiazol-2-yl)-2,5-diphenyltetrazolium bromide) is a yellow tetrazole, which is reduced to purple formazan in the presence of NADH and NADPH.

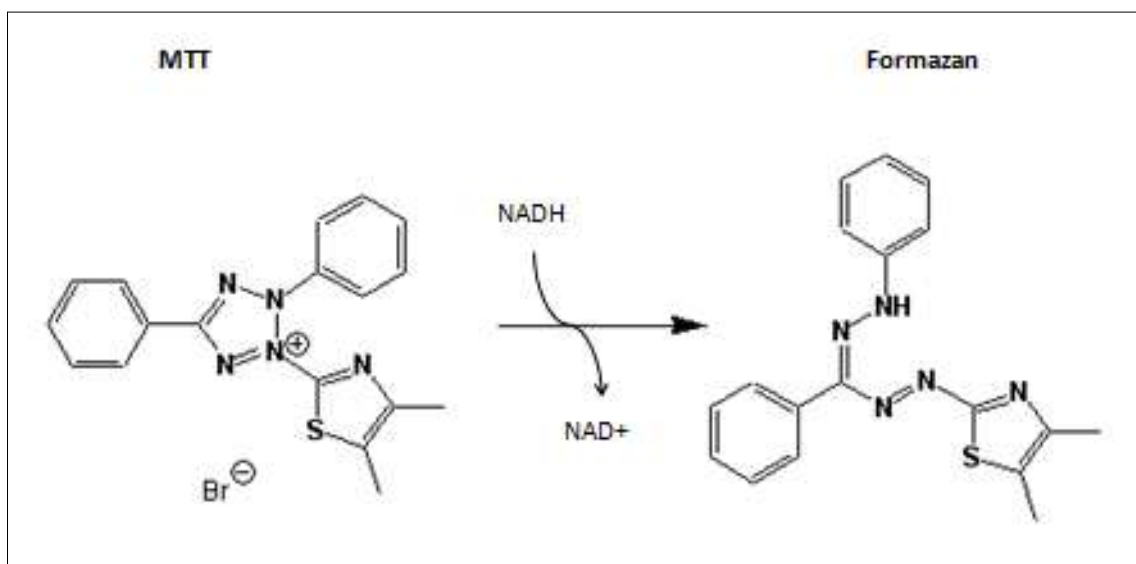


Figure 49 The reaction of the dye MTT (yellow) into the purple product formazan (image from wikipedia)

Viable, metabolic active cells produce in the respiratory chain the pyridine nucleotide cofactors (NADH, NADPH). NADH and NADPH are basically responsible for cellular reductions and therefore responsible for the cleavage of MTT. (Roche n.d.) Our purpose is to use the MTT-assay as a cytotoxicity test, for testing cytotoxicity on the tumor cell lines HT1080 and A431.

The MTT-Assay can easily be performed in 96-well plates. This enables a reduction of the amount of culture medium, cells and plasticware. Furthermore, the dye MTT is a bargain. On balance, it is a cheap and simple method to detect viability.

The colorimetric analysis can simply be carried out via spectrometry. In our case, we are using the ELISA-Reader Tecan Sunrise for reading out our 96-well plates.

In comparison to other viability assays, the product formazan of the MTT-assay unfortunately is water insoluble. That's why an additionally step to solve the formazan has to be performed.

4.2.5.2 Protocol

Sörensen-buffer: 0.1 M Glycine, 0,1 M NaCl, H₂O, pH 10.5

MTT-Solution: 3.65 mg/ml in PBS,

The solution should be kept cold (4°C) and in the dark (Schröter 2009)

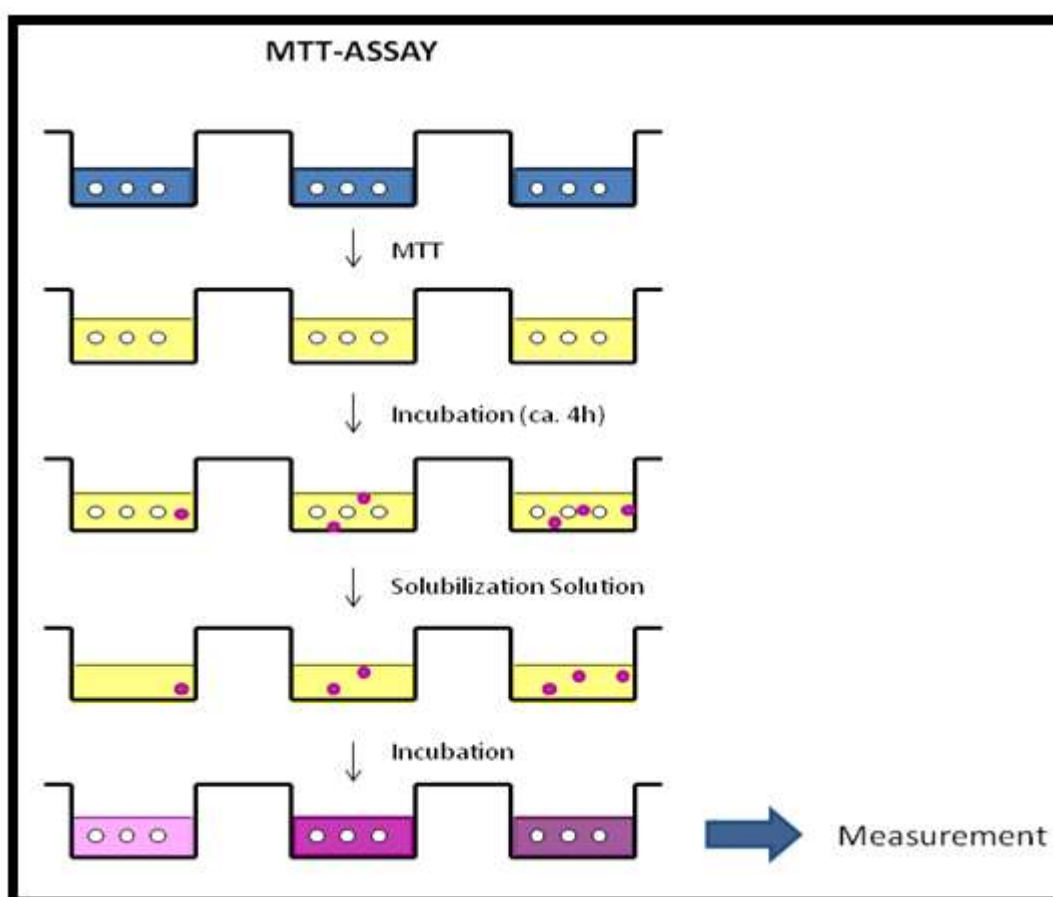


Figure 50: MTT assay

Day one:

- Take the T75 Flask, remove Medium, wash the cells with 8 ml PBS detach cells with 1ml Trypsin (about 30 seconds up to 10 minutes incubation time! Check permanently!). Inactivate Trypsin with 10 ml DMEM medium, transfer the cells into a 15 ml falcon. Centrifugate (200 rcf/g for 5 min).
- Remove supernatant, resuspend pellet with 10 ml DMEM. Count cells via Neubauer Cell Chamber.
- Take the 96 well plates and add 5.000-10.000 cells in each well. Fill up to 200µl with DMEM.
- Leave some wells empty for negative control
- Put the plate into the incubator. Incubate over night, to allow cells to attach to the wells

Day two:

- Remove medium (carefully!)
- Treat cells with the drug
- Final volume should be 200 µl per well
- Incubate 1-3 days

Day three:

- Remove medium (carefully!)
- Fill in 100 µl medium and 25µl MTT solution
- Incubate 4 hours
- Remove medium
- Resuspend in 200µl DMSO and 25 µl Sörensen-buffer
- (take on shaker for 15 minutes) read absorbance at 570 nm

4.2.6 Quantitative real-time PCR

The quantitative real-time polymerase chain reaction (qPCR) represents a beneficial method for monitoring the amplification of a specific DNA sequence. The amount of PCR product is measured after each cycle. By comparing the exponential phase of the samples with a standard curve of known sequence copies, the exact initial DNA-amount can be determined. This method not only provides the possibility of precise quantification but also renders analysis of the products after PCR redundant.

For measuring the sequence copy number one takes advantage of a fluorescent dye that incorporates into double-stranded DNA. The template amplification results in increasing fluorescence signals which can be directly correlated to the amplicons. By illustrating the fluorescence against the cycle number by a diagram, quantification of PCR product can be illustrated over time (Nolan et al. 2006; Invitrogen 2008).

4.2.6.1 SYBR Green

SYBR Green is a nucleic acid stain which preferentially binds within the minor groove of double-stranded DNA. By excitation at $\lambda_{\text{max}} = 488 \text{ nm}$, fluorescence emission can be detected at $\lambda_{\text{max}} = 525 \text{ nm}$. As binding to double-stranded DNA increases fluorescence emission, amplification of DNA can be monitored and correlated to the amount of double-stranded DNA in the original sample.

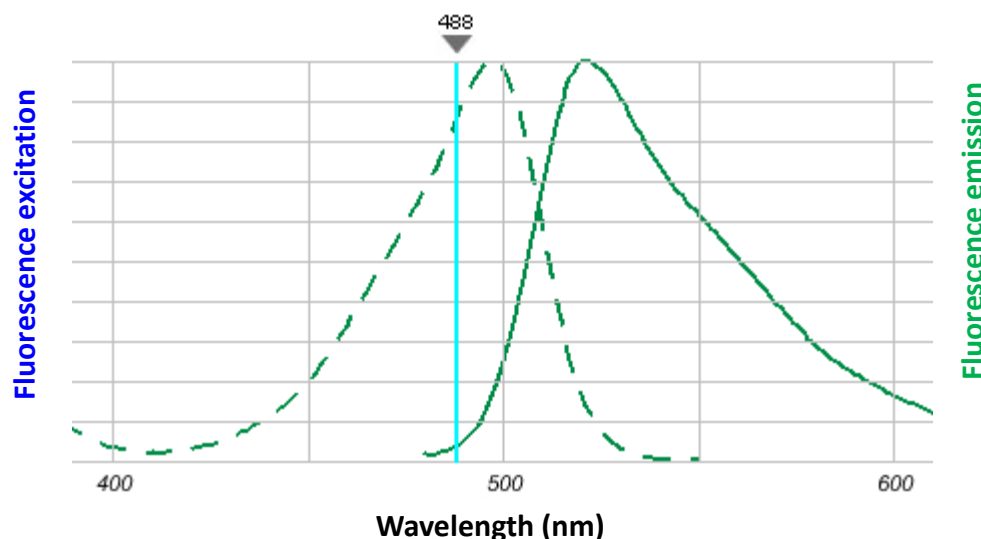


Figure 51: Excitation and Emission Spectra of Sybr Green (adapted from Invitrogen Fluorescence-SpectraViewer; http://tools.invitrogen.com/content/sfs/manuals/cms_039996.pdf)

4.2.6.2 Protocols

We used quantitative real-time PCR to determine genomic virus titers after the transfection of our production cells and after the transduction of our various tumor cell lines with the harvested virus particles.

We followed protocols published by Rohr et al. (Rohr et al. 2002), (Rohr et al. 2005).

4.2.6.2.1 Genomic titer

To measure the titer of assembled virus particles in our harvested production cells, we first digested all cellular and plasmid DNA left in our virus stocks. We therefore treated 5 μ l supernatant from pelleted cell lysate with 7.5 μ l DNase I (Fermentas, Catalogue No. EN0521, 1 u/ μ l) and 5 μ l 50 mM MgCl₂ (end concentration 5 mM) in a final volume of 50 μ l at 37°C for 30 min. We then heat inactivated the enzyme for 10 min at 65°C. PCR reactions were carried out with 2 μ l of our digested samples.

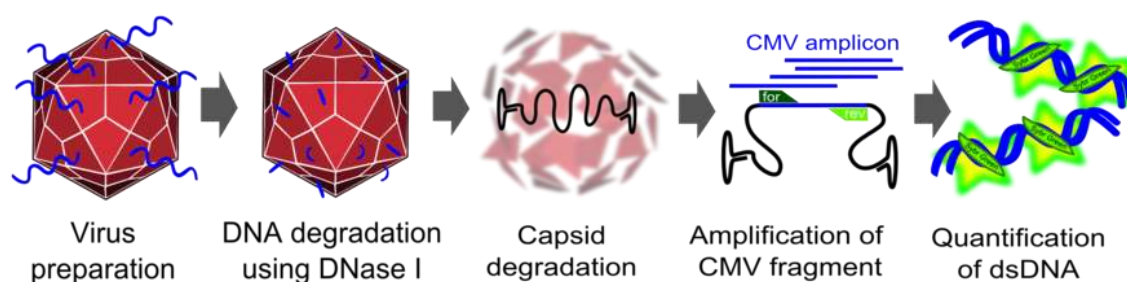


Figure 52: Quantification of virus DNA.

4.2.6.2.2 Infectious titer

To measure the titer of infectious virus particles, we digested our transduced cells with 10 μ g Proteinase K (Sigma Aldrich) for 1 h at 50°C. After inactivation at 97°C for 15 minutes, we centrifuged the lysate at 13.000 g for 10 minutes and digested 10 μ l of the supernatant with 5 μ l S1 nuclease (Promega, 100 u/ μ l) for 30 minutes at 37°C. The enzyme was again inactivated for 15 minutes at 97°C. DNA was diluted 1:100. PCR reactions were carried out with 5 μ l of our digested samples.

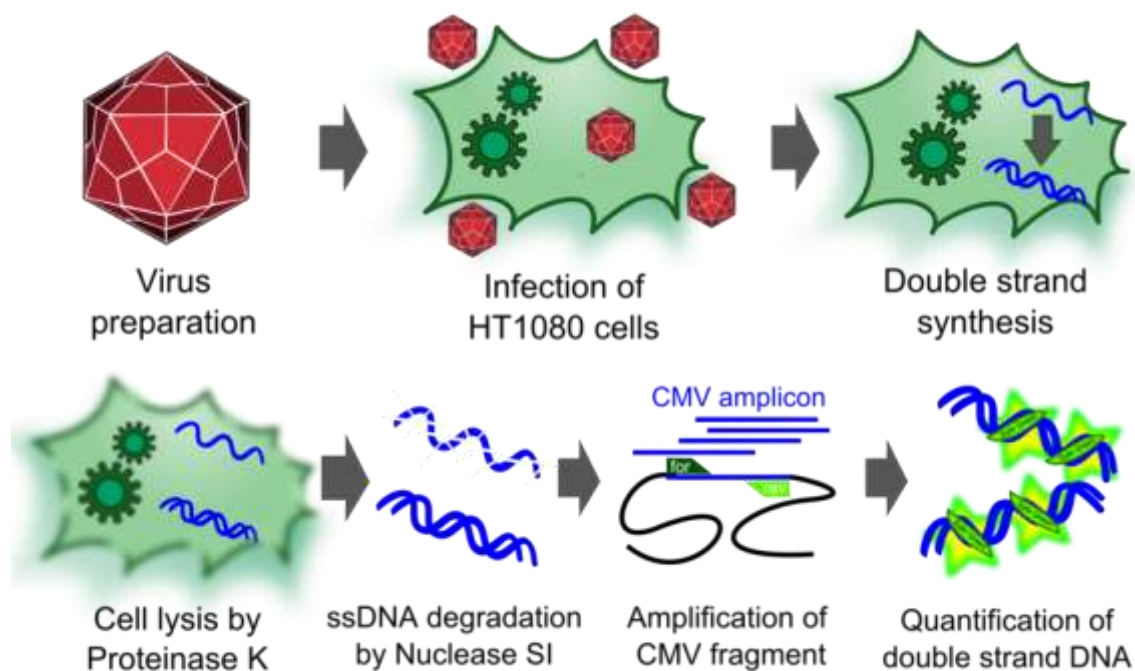


Figure 53: Quantification of DNA in infected cells.

All qPCR reactions were carried out using the QuantiFast SYBR Green PCR Kit from Qiagen, (Catalogue No. 204052), employing the following primers:

- CMV_forward_qPCR: 5' - GGGACTTTCCTACTTGGCA - 3'
- CMV_reverse_qPCR: 5' - GGCGGAGTTGTTACGACA - 3'

The qPCR reactions were run on a Corbett RotorGene 3000 realtime thermal cycler and analyzed with the RotorGene software. The qPCR program was:

Step	Time	Temperature
Initial activation	5 min	95 °C
Two-step cycling		
Denaturation	10 sec	95 °C
Annealing / Extension	30 sec	60 °C
Number of cycles	45	

4.2.7 Fluorescence microscopy

We used the fluorescent proteins: EGFP, CFP, mCherry, and mVenus with the filtersets outlined in table Table 3.

Table 3 Fluorescent protein and filtersets.		
Protein	Filterset	Excitation
EGFP	Nr.1	505 nm
CFP	Nr.2	365 nm
YFP (mVenus)	Nr.2	505 nm
mCerry	Nr.1	555 nm

Filter set 1 : F 66-502, HC-Set AHF, Bp 387/11, Bp 494/20, Bp 575/25 (without exciter), triple beam splitter 436/514/604 D/F/T, triple band-elimination filter 457/530/628 D/F/T.

Filter set 2: F 56-317, ET-Set; 430/24, 500/20 (without exciter), Bp 452-480

The microscope was an inverted research microscope from Carl Zeiss (Axio Observer Z1) optimized for tissue culture and fluorescence microscopy with the following equipment: AxioCam MRm, Zeiss Temp Module S, Zeiss CO2 Module S, Heating Unit XL S, Heating Insert PS1, Colibri.

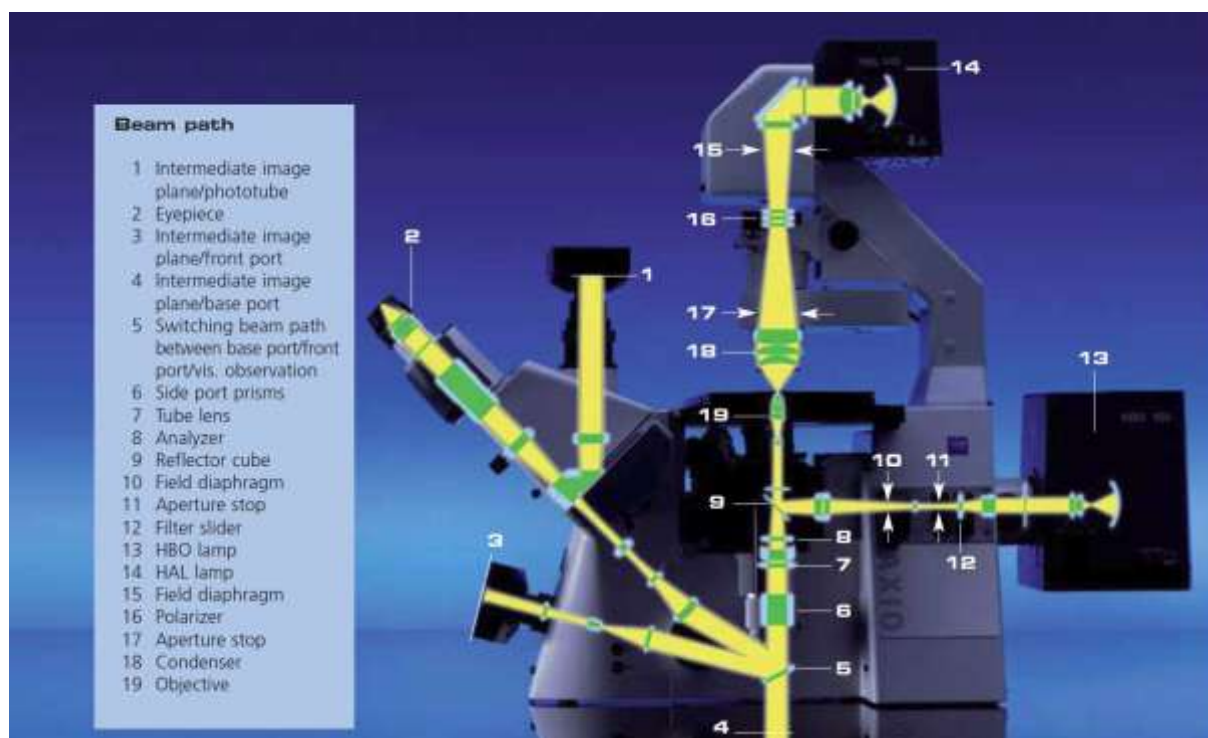


Figure 54 Beam Path of Axio Observer Z1 (c) Carl Zeiss MicroImaging GmbH 07740 Jena, Germany

5 Results

5.1 Modularization

5.1.1 Introduction to Modularization of Vector Plasmid

Producing recombinant virus particles for therapeutical applications is, besides specific cell targeting, purification and quantification assays of AAV-2, one intention of the ‘Virus Construction Kit’ provided by the iGEM team Freiburg_Bioware 2010. For obtaining a modular toolkit, the complex biological system of the Adeno-associated virus serotype 2 was examined by an exhaustive literature search. Subsequently, the essential components for AAV-2 particle production were extracted and redesigned to match the iGEM standard.

The provided tripartite system is independent of a superinfection of Adeno- or herpes simplex viruses since the genes encoding the required helper-proteins are co-transfected. Inside the eukaryotic host cell, the DNA sequence containing the inverted terminal repeats (ITRs) is extracted and later encapsidated into the preformed capsids after production of single-stranded DNA. Consequently, this plasmid is known as the vector plasmid (pGOI). Promoter, *beta-globin* intron and the hGH terminator signal are flanked by the ITRs (ITRs, BBa_K404100 and BBa_K404101) and regulate transgene expression. The vector plasmid containing the desired gene of interest is cotransfected with the RepCap plasmid (BBa_K404001, BBa_K404002 or BBa_K404003) and the pHelper plasmid. To obtain the fully assembled vector plasmid, several assembly steps have to be performed.

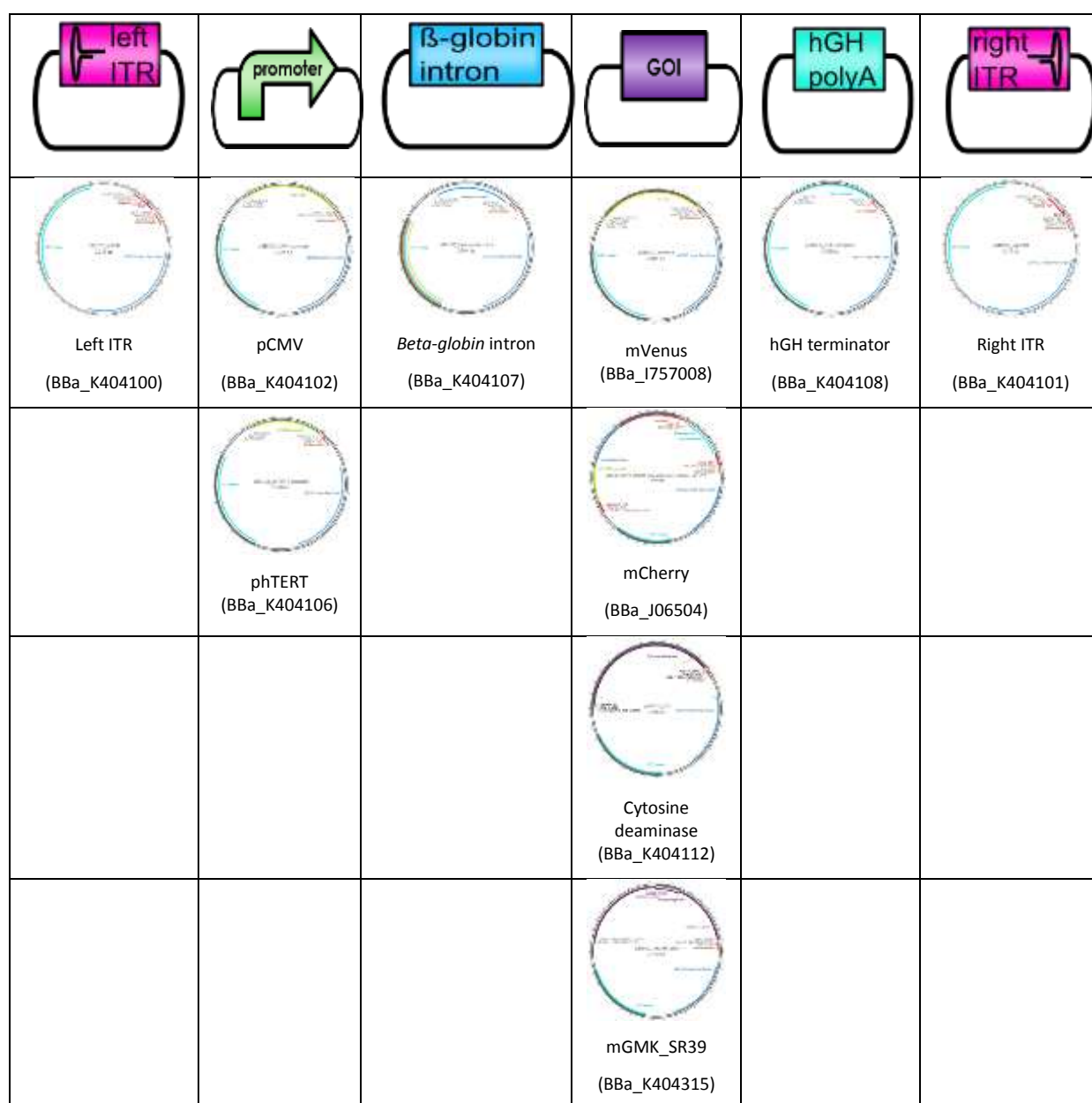
Furthermore, by providing the tumor-specific promoter with the “Virus Vonstruction Kit”, the iGEM Freiburg_Bioware team 2010 ensures another layer of specificity and safety to the recombinant viral vector system. Telomerase activation is a critical step in human tumorigenesis and about $85 \pm 90\%$ of several human tumors show telomerase activity. In most somatic cells, the pHtert promoter is inactive. This prevents expression of the hTERT protein subunit and renders the healthy tissue telomerase negative.

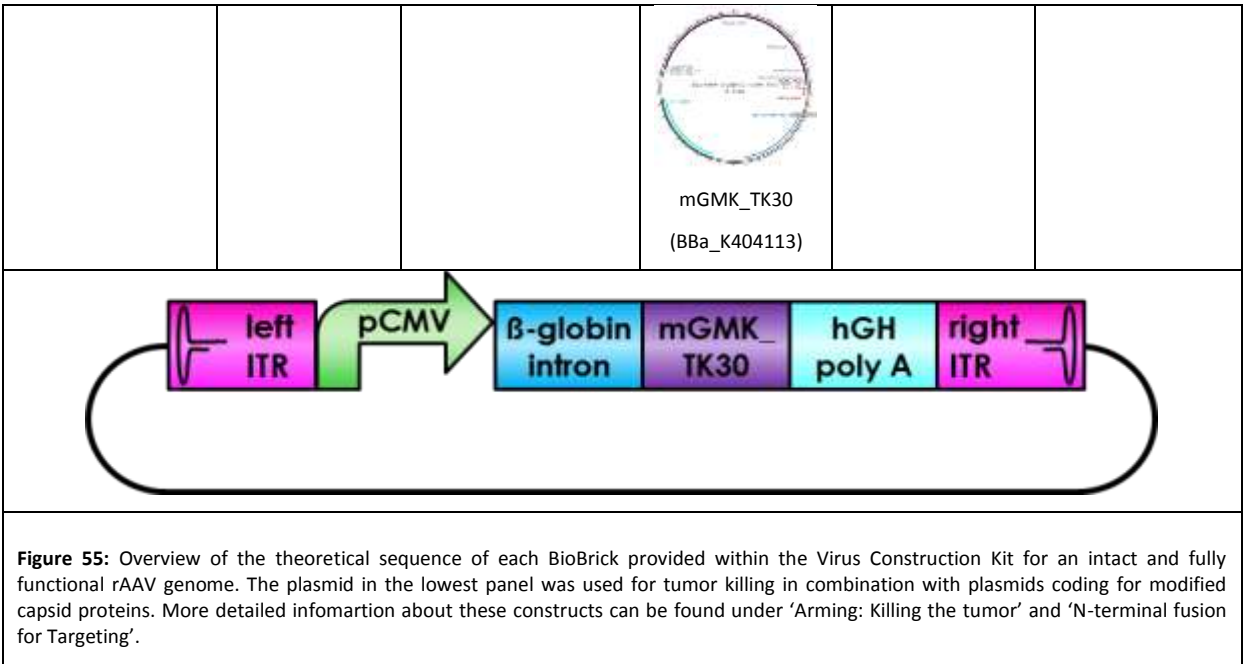
5.1.2 Recombinant and Modular Vectorplasmid Carrying GOI

Recombinant and Modular Vector plasmid Carrying GOI

The iGEM team Freiburg_Bioware 2010 provides a modular ‘Virus Construction Kit’ for therapeutical applications, quantification assays and purification approaches depending on capsid modifications

and the gene of interest flanked by the inverted terminal repeats (ITRs). In order to produce BioBrick-compatible standardized biological parts, we reengineered the plasmids and added new components for gene therapy approaches and analysis of biological activity of assembled BioBrick parts. Each element required for intact and functional plasmids comprising the ITRs, a promoter, a putative enhancer element and the hGH terminator was PCR amplified and fused together *de novo*. As shown in Figure 55, the vector plasmid was assembled with the produced BioBricks consisting of the left and right ITR (BBa_K404100 and BBa_K404101), a promoter (pCMV :BBa_K404102 or phTERT: BBa_K404106) , the beta-globin intron (BBa_K404107), the gene of interests (fluorescent proteins mVenus: BBa_I757008 and mCherry: BBa_J06504, suicide genes mGMK_TK30: BBa_K404112, mGMK_SR39: BBa_K404315 and CD: BBa_K404112) and the hGH terminator (BBa_K404108).





5.1.4 Cloning and Combination Strategies for the Vector Plasmid

Organization of the recombinant viral DNA was modified ensuring several layers of specificity to our systems including a tumor-specific promoter and suicide genes encoding prodrug convertases. In order to modularize the rAAV sequence, each plasmid element (Figure 55) was PCR-amplified and cloned into the iGEM standard plasmid pSB1C3. Furthermore, the iGEM team Freiburg_Bioware 2010 performed three site-directed mutagenesis in the gene of interest TK30 (BBa_K404109) and cytosine deaminase (BBa_K404112) for deletion of PstI and NgoMIV iGEM site (for further information see the results page of ‘Arming – Killing the tumor’). Since the inverted terminal repeats (ITRs) are GC-rich regions forming T-shaped hairpins during replication, PCR amplification was not possible. Hence a cloning strategy was developed by the iGEM team Freiburg in order to provide BioBrick-compatible ITRs (see ‘Method Development of Cloning Strategy for ITRs’).

In Figure 56 the schematic overview of the modularization process can be seen which has been followed to conduct the assembly steps required for functional vector plasmids.

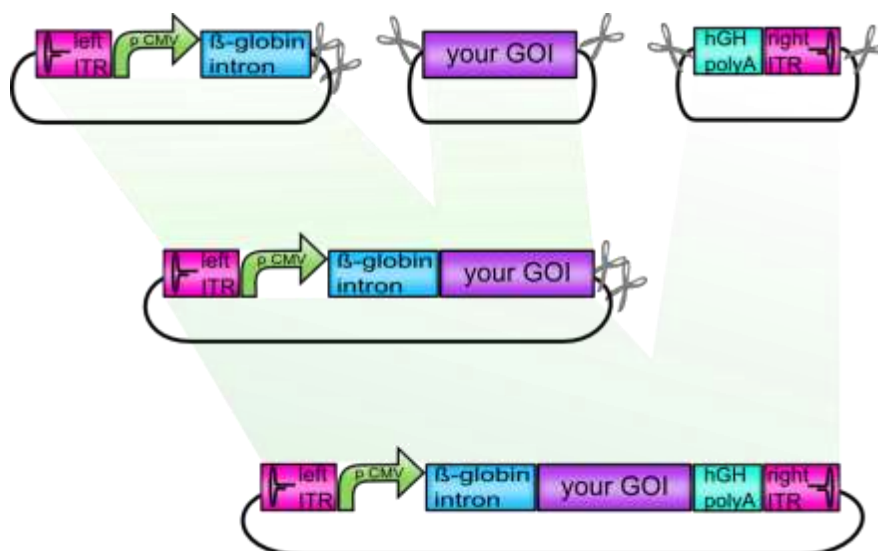


Figure 56: Assembly procedure for fusion of BioBricks and composite parts to a fully assembled and functional plasmid coding for your gene of interest. This plasmid can be cotransfected with two helper plasmids providing protein for assembly and encapsidating of the rAAV genome (your gene of interest) into the capsids.

The iGEM team Freiburg_Bioware provides two examples demonstrating the assembly procedure for constructing vector plasmids. The first representative example is the fusion of the BioBrick part *beta-globin* to the composite parts containing the 5' elements of the plasmids, which are left ITR and CMV or phTERT promoter, respectively.

As shown in **Figure 57** the theoretical cloning performed for assembling the BioBricks *beta-globin* intron and leftITR_CMV together can be observed.

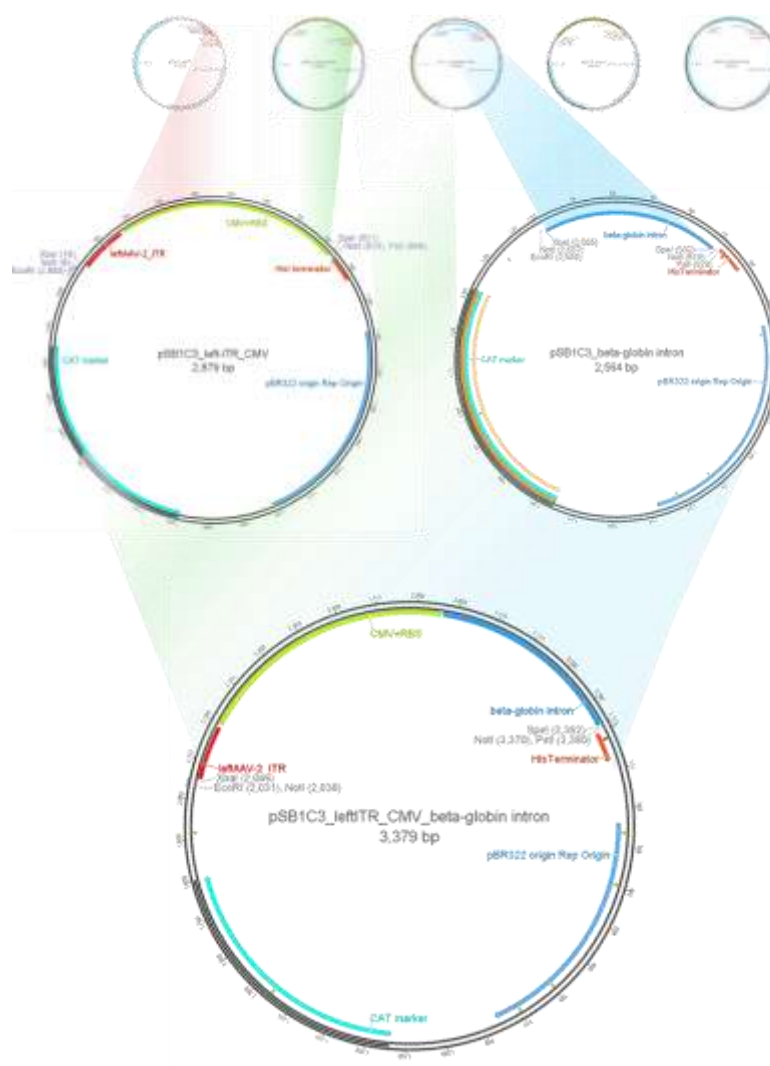


Figure 57: Theoretical cloning of the composite part leftITR_CMV to the *beta-globin* intron BioBrick leading to the plasmid leftITR_CMV_ *beta-globin* intron.

The plasmids were digested with both XbaI and PstI (*beta-globin* intron: Bba_K404107) or SpeI and PstI (leftITR_CMV) and loaded on an agarose gel. As demonstrated in the preparative gel in Figure 57, the expected bands could be detected under UV light and the extracted DNA could be successfully ligated. Each assembly step for producing BioBrick intermediates was conducted following the same strategy.

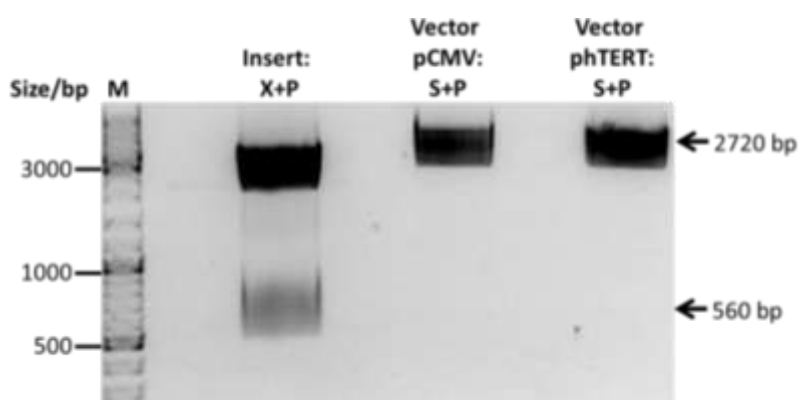


Figure 58: Assembly intermediate in fusion of the vector plasmids containing different promoters. Fusion of the BioBrick part *beta-globin* (BBa_K404107) intron to the composite parts leftITR_pCMV and leftITR_phTERT, respectively, was performed following the BioBrick assembly strategy by digesting the insert with PstI and XbaI and the vectors with SpeI and PstI. The left lane shows the expected fragment at around 560 bp which corresponds to the *beta-globin* intron fragment, in contrast to the two lanes in the center and on the right which correspond to linearized plasmids after digesting with above mentioned iGEM restriction sites. M, GeneRuler DNA ladder mix; Insert, pSB1C3_*beta-globin* intron; Vector pCMV, pSB1C3_leftITR_pCMV; Vector pHtERT, pSB1C3_leftITR_phTERT.

Separated fragments were extracted using the Gel Extraction Kit provided by Qiagen (Hilden, Germany) and ligated with T4-ligase. After ligation has been carried out, *E. coli* XL-1B cells were transformed and incubated over night at 37°C. Picking clones from the transformation plate was performed the following day and DYT medium was inoculated incubating overnight. Plasmid DNA was isolated and test digestion revealed that cloning was successful obtaining the composite part leftITR_CMV_*beta-globin* intron (BBa_K404117).

Plasmid production incorporating all required elements for transgene expression and genome encapsidation into empty viral capsids was performed by fusing the downstream elements consisting of the hGH terminator and right ITR to the intermediate part providing the gene of interest and the promoter fused to the left ITR. **Figure 59** demonstrates the assembly performed with pSB1C3_leftITR_phTERT_*beta-globin* intron_mVenus and pSB1C3_hGH_rightITR (BBa_K404116). The fragment obtained after digestion on the left lane fits to the hGH-terminator_rightITR length. The isolated fragments were ligated and successful assembly was confirmed by test digestion obtaining the vectorplasmid pSB1C3_leftITR_phTERT_*beta-globin* intron_mVenus_hGH_rightITR (BBa_K404124).

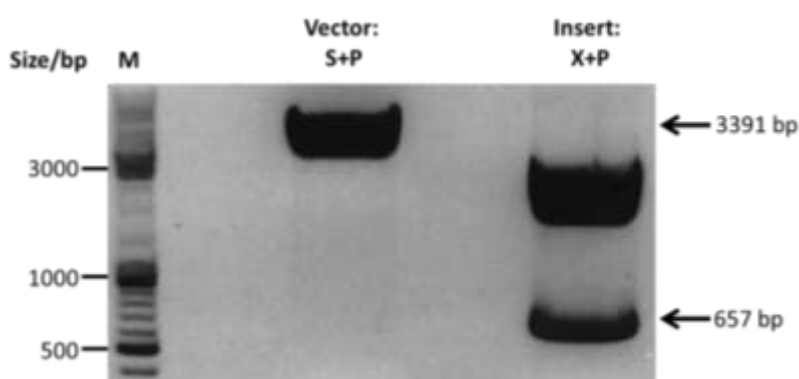


Figure 59: Modularization of the assembled vector plasmid containing the pH_{TERT} promoter and mVenus as gene of interest. Fusion of the composite pSB1C3_leftITR_pH_{TERT}_beta-globin intron_mVenus part to the composite parts pSB1C3_hGH_rightITR was performed following the BioBrick assembly strategy by digesting the insert with XbaI and PstI and the vector with SpeI and PstI. The left lane corresponds to linearized plasmid after digesting with above mentioned iGEM restriction sites whereas the right lane reveals an intensive band at around 650 bp confirming the expected size of 657 bp of hGH_rITR. M, GeneRuler DNA ladder mix; Vector, pSB1C3_leftITR_pH_{TERT}_beta-globin intron_mVenus; Insert, pSB1C3_pSB1C3_hGH_rightITR.

Since cloning does not confirm biological activity, we analyzed the plasmids and their functional components, hGH terminator and *beta-globin* intron, in cell culture. Assembled plasmids have been cotransfected, using AAV-293 cells, which provide the stable integrated E1A and E1B genes, with helper plasmids required for capsid assembly and genome encapsidation (pRC and pHelper) in a molar ratio of 1:1:1 (pGOI:pRC:pHelper). Virus particles containing the single stranded DNA were harvested 72-hours post transfection and HT1080 cells transduced with constant volumes of viral vectors. 48-hours post infection; transduced cells expressing the gene of interest were analyzed by flow cytometry. Facilitating and demonstrating the analysis of functionality of the assembled plasmid, mVenus was used in first place since fluorescent proteins enable facile visualization using fluorescent microscopy and flow cytometry analysis.

5.1.5 Testing functionality of Assembled Vector Plasmid

5.1.5.1 Fluorescence Microscopy of Target Cells Demonstrates GOI Expression

Qualitative analysis of mVenus expression by fluorescence microscopy was conducted using Axio Observer Z1 showing that transduced HT1080 cells and non-transduced cells could be easily distinguished. In **Error! Reference source not found.** cells were excited with 505nm and fluorescence

emission at 536nm was detected. Therefore, successful infection of tumor cells by recombinant viral particles carrying the assembled vectorplasmid coding for mVenus could be demonstrated.

5.1.5.2 Analysis of Target Cells by Flow Cytometry demonstrates GOI Expression

Characterizing the function of the hGH terminator, the *beta-globin* intron and the complete plasmid, several approaches were conducted followed by analysis via flow cytometry.

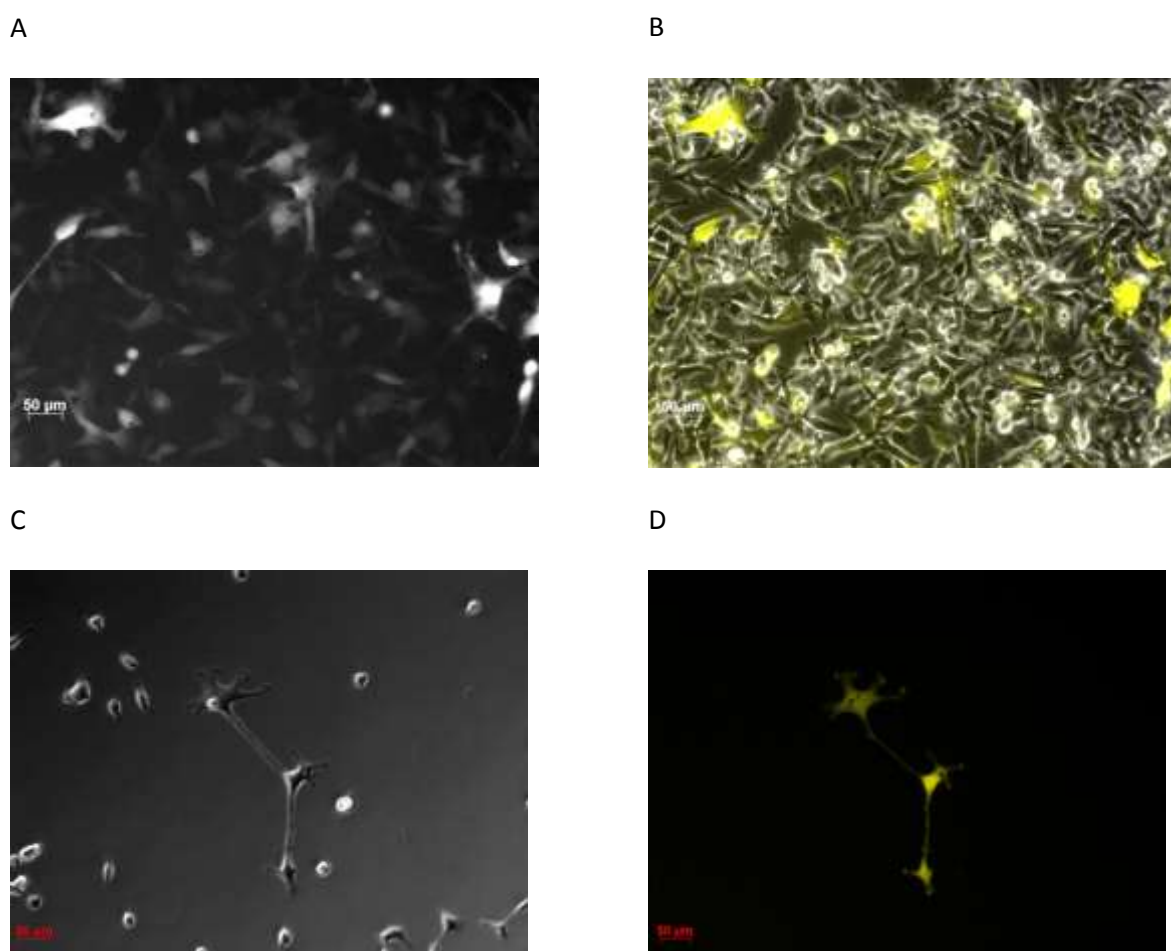


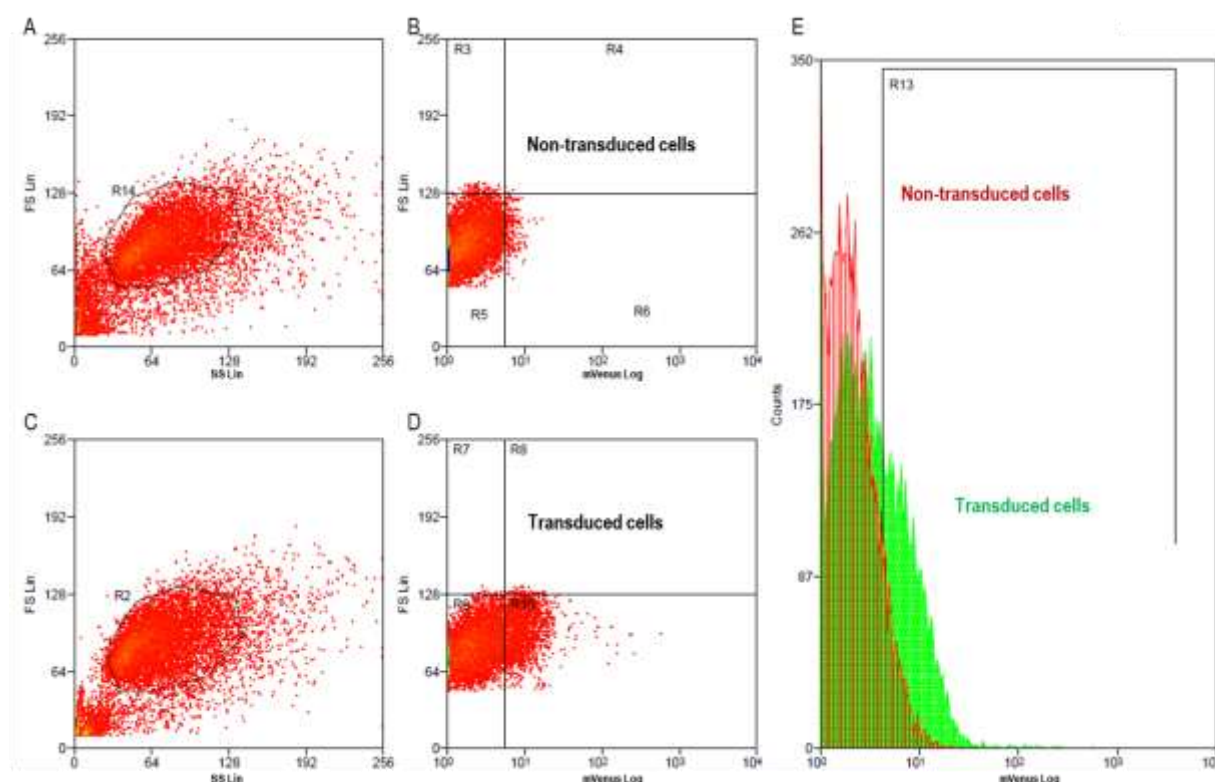
Figure 60: Fluorescence microscopy (Excitation: 505nm, Emission: 536nm) was performed for detection of transduced cell expressing mVenus. AAV-293 cells were transfected with three plasmids (pHelper, pRC and pGOI = mVenus). A: mVenus fluorescence in HT1080 cells B: Overlay of bright field and fluorescence images, sample as in A. C: Brightfield image of xy cells D: mVenus fluorescence, sample as in C.

5.1.5.2.1 Influence of hGH terminator BioBrick on GOI Expression

The iGEM team Freiburg provides the hGH polyadenylation sequence within the 'Virus Construction Kit' due to the fact that almost every eukaryotic mRNA is processed at their 3' and 5' end except for

histone mRNAs (Millevoi et al. 2006). Pre-mRNAs contain two canonical conserved sequences. First, the polyadenylation signal “AATAAA” which is recognized by the multiprotein complex and second the GT-rich region (downstream sequence element, DSE) which is located 30 nucleotides downstream of the cleavage site. The assembled 3′end-processing machinery cleaves the mRNA transcript immediately after a CA-nucleotide therefore defining the cleavage site (Danckwardt et al. 2008). Recombinant vectorplasmids were engineered containing the inverted terminal repeats (ITRs), a strong eukaryotic promoter (CMV promoter: BBa_K404102) and mVenus as gene of interest with and without the hGH terminator signal. Transduction of HT1080 cells with constant volume of viral particles containing the vectorplasmids and measuring mVenus expression 24-hours post infection by flow cytometry demonstrated that transgene expression of the constructs lacking the hGH termination signal is significantly reduced as shown in **Figure 61** and **Figure 62** confirming the expected results that hGH is essential for mRNA processing. The iGEM team Freiburg_Bioware 2010 therefore suggests using the provided hGH termination signal within the Virus Construction Kit for optimal gene expression.

Vectorplasmid lacking hGH termination signal



Vectorplasmid with hGH termination signal

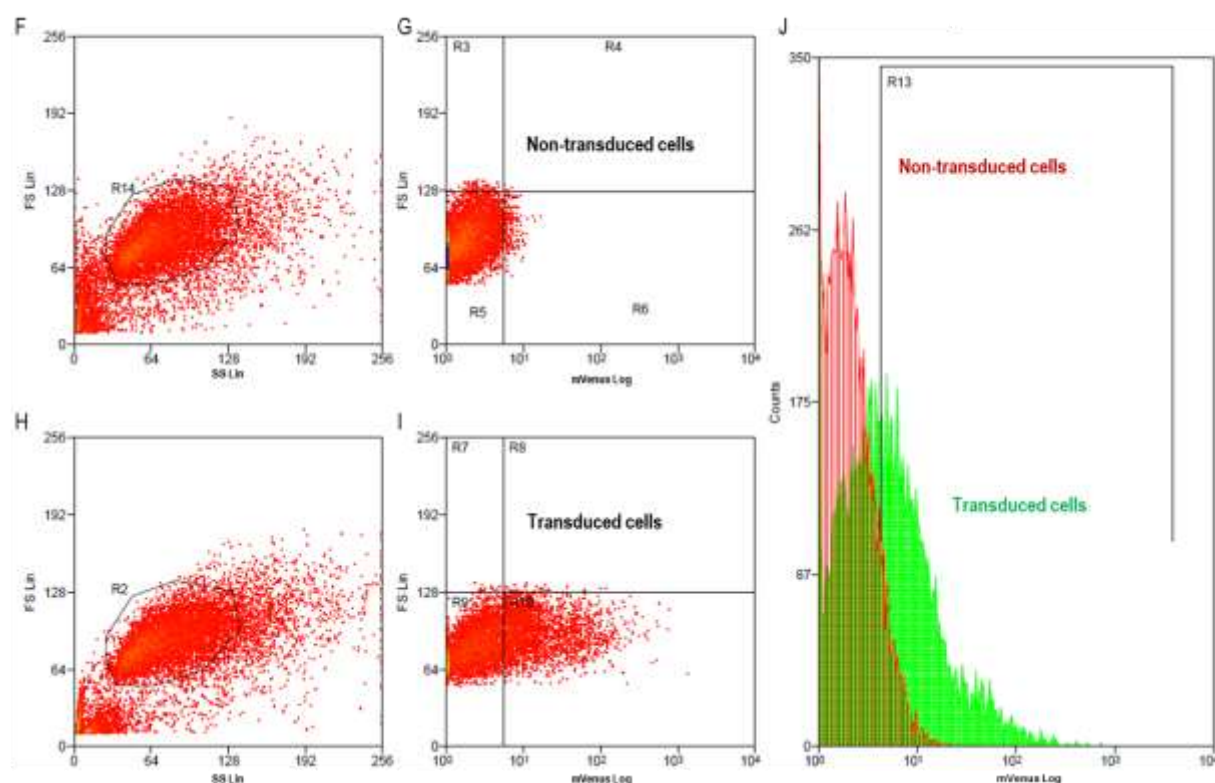


Figure 61: Flow cytometry analysis of vectorplasmids with and without hGH terminator.

A: Gating non transduced cells (control); subcellular debris and clumps can be distinguished from single cells by size, estimated forward scatter (FS Lin) and granularity, estimated side scatter (SS Lin) **B:** Non transduced cells applied against mVenus (Analytical gate was set such that 1% or fewer of negative control cells fell within the positive region (R5). **C:** Gating transduced cells (R2 \triangleq R14) (used plasmids for transfection: GOI: **pSB1C3_IITR_CMV_beta-globin intron_mVenus_rITR (BBa_K404127)**, pHelper, pRC). **D:** Transduced cells plotted against mVenus, R10 comprises transduced cells by detecting mVenus expression. **E:** Overlay of non-transduced (red) and transduced (green) cells applied against mVenus. **F:** Gating non-transduced cells (control) **G:** Non-transduced cells applied against mVenus. **H:** Gating transduced cells (R2 \triangleq R14) (used plasmids for transfection: GOI: reassembled **pSB1C3_IITR_CMV_beta-globin_mVenus_hGH_rITR (BBa_K404119)**, pHelper, pRC). **I:** Transduced cells applied against mVenus, R10 comprised transduced cells, by detecting mVenus expression. **J:** Overlay of non-transduced (red) and transduced (green) cells applied against mVenus.

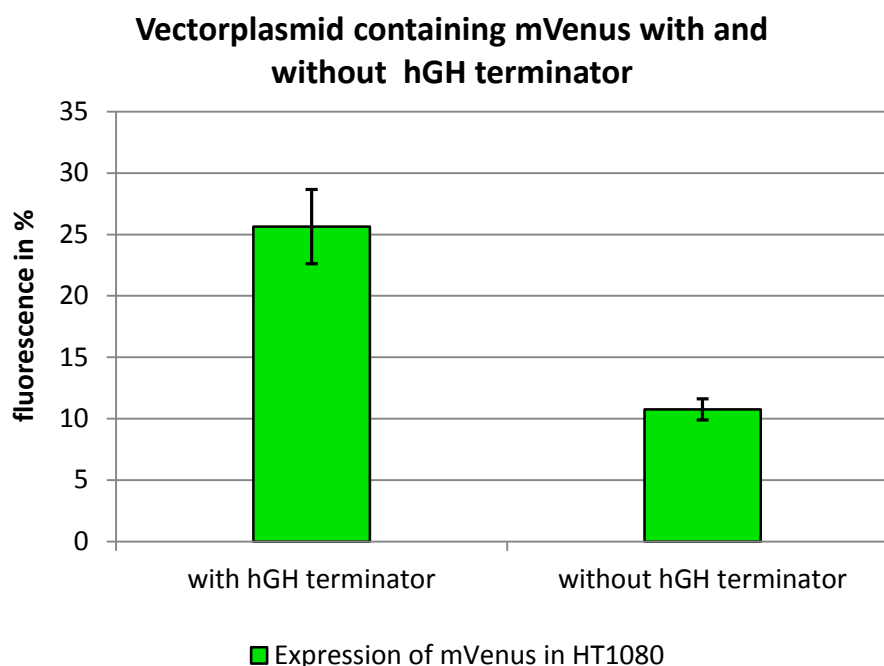
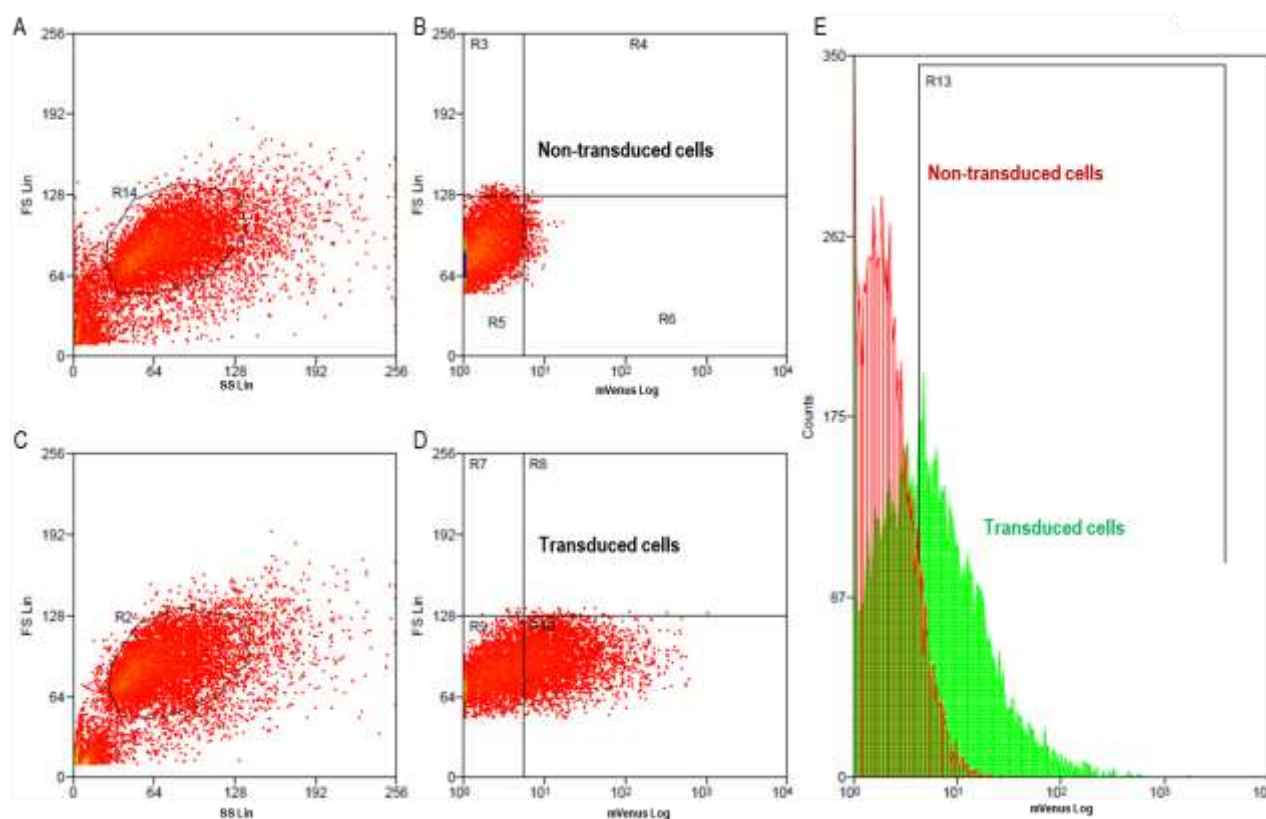


Figure 62: Flow cytometry analysis of vectorplasmids with and without hGH terminator. K: YFP expression of viral genomes was determined by flow cytometry after 24-hour post infection. Results demonstrate that mVenus expression of vectorplasmids lacking the hGH terminator is reduced significantly proving that the polyadenylation signal is essential for viral gene expression using recombinant viral vectors engineered by using components of the Virus Construction Kit.

5.1.5.2.2 Influence of *Beta-globin* intron Biobrick on GOI Expression

Providing an element assumed to be an enhancer of transgene expression (Nott et al. 2003), the iGEM team Freiburg tested a beta-globin intron derived from the human *beta globin* gene which can be fused upstream of the desired gene of interest. The beta-globin intron BioBrick consists of a partial chimeric CMV promoter followed by the intron II of the *beta-globin* gene. The 3' end of the intron is fused to the first 25 bases of human *beta globin* gene exon 3. The *beta globin* intron BioBrick is assumed to enhance eukaryotic gene expression (Nott et al. 2003). Analysis was conducted as described for the hGH terminator experiment (see above). As shown in **Figure 63** and **Figure 64** the vectorplasmid missing the *beta-globin* intron showed a negligible difference in mVenus expression compared to viral genomes containing the *beta-globin* intron. Considering these results and taking into account that a constant volume of viral particles has been used for transduction, the difference between the construct containing and lacking the beta-globin intron is minimal. Since packaging efficiency of the AAV-2 decreases with increasing sizes of the insert (Dong et al. 1996), the iGEM team Freiburg_Bioware suggests using the *beta-globin* intron in dependence on the size of your transgene.

Vectorplasmid lacking *beta-globin* intron



Vectorplasmid containing *beta-globin* intron

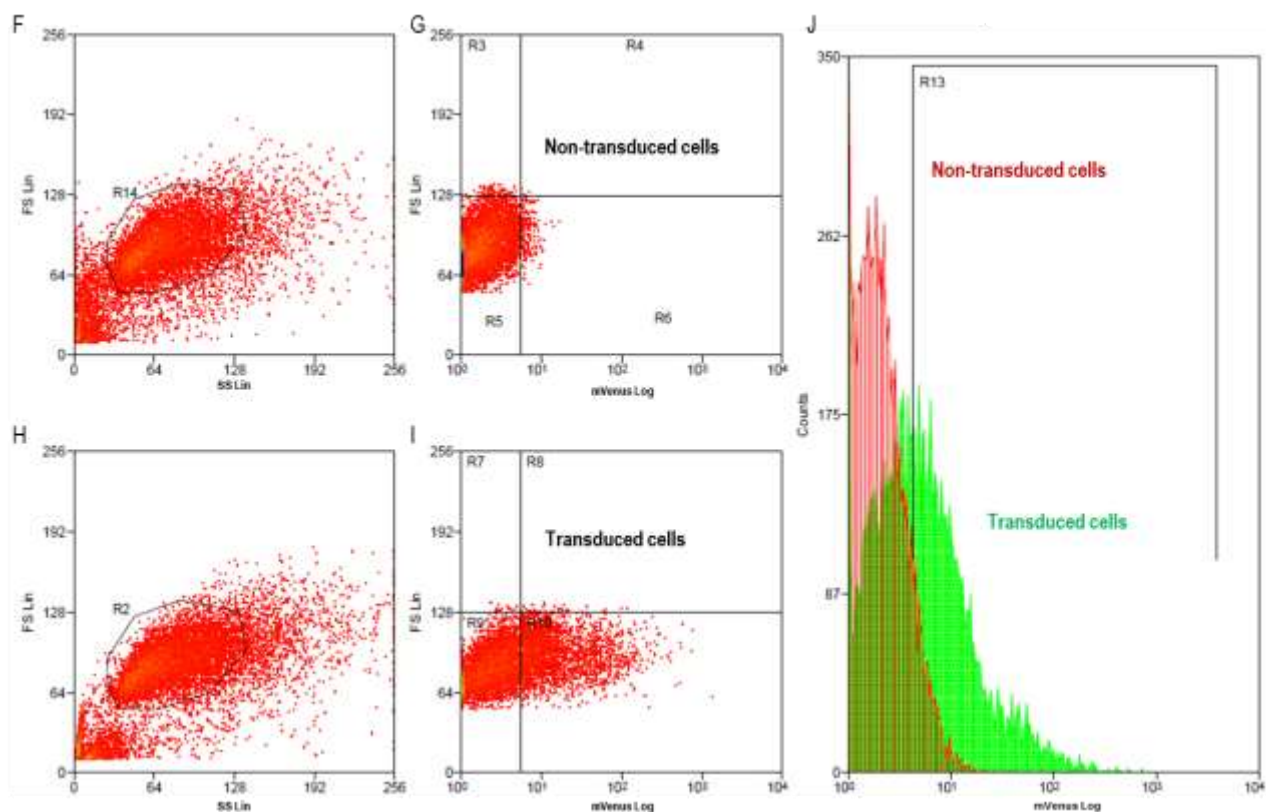


Figure 63: Flow cytometry analysis of vectorplasmids with and without *beta-globin* intron. A: Gating non transduced cells (control); subcellular debris and clumps can be distinguished from single cells by size, estimated forward scatter (FS Lin) and

granularity, estimated side scatter (SS Lin) **B**: Non transduced cells applied against mVenus (Analytical gate was set such that 1% or fewer of negative control cells fell within the positive region (R5). **C**: Gating transduced cells (R2 \triangleq R14) (used plasmids for transfection: GOI: **pSB1C3_IITR_CMV_mVenus_hGH_rITR (BBa_K404128)**, pHelper, pRC). **D**: Transduced cells plotted against mVenus, R10 comprised transduced cells, by detecting mVenus expression **E**: Overlay of non-transduced (red) and transduced (green) cells applied against mVenus **F**: Gating non-transduced cells (control). **G**: Non-transduced cells applied against mVenus (R5). **H**: Gating transduced cells (R2 \triangleq R14) (used plasmids for transfection: GOI: reassembled **pSB1C3_IITR_CMV_beta-globin_mVenus_hGH_rITR (BBa_K404119)**, pHelper, pRC). **I**: Transduced cells applied against mVenus, R10 comprised transduced cells, by detecting mVenus expression. **J**: Overlay of non-transduced (red) and transduced (green) cells applied against mVenus.

K

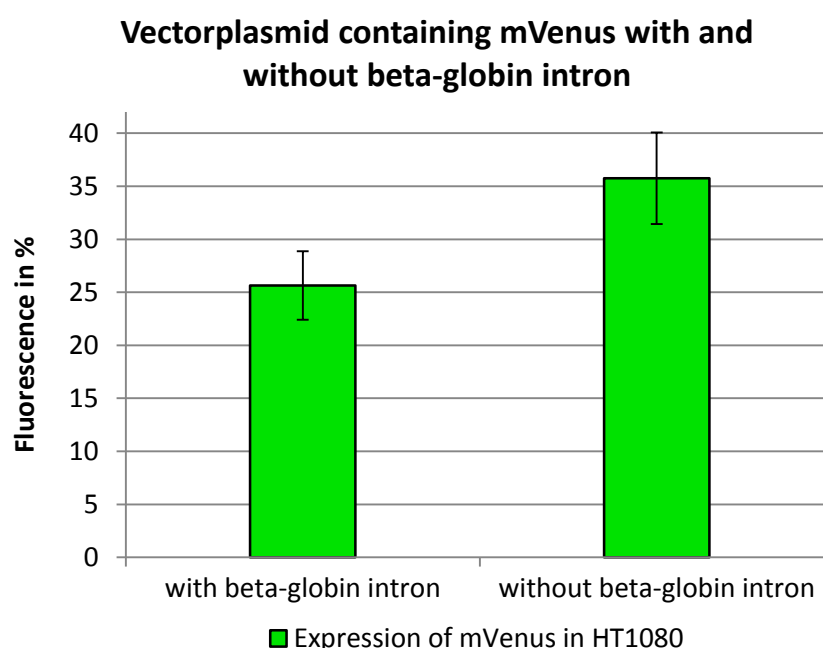


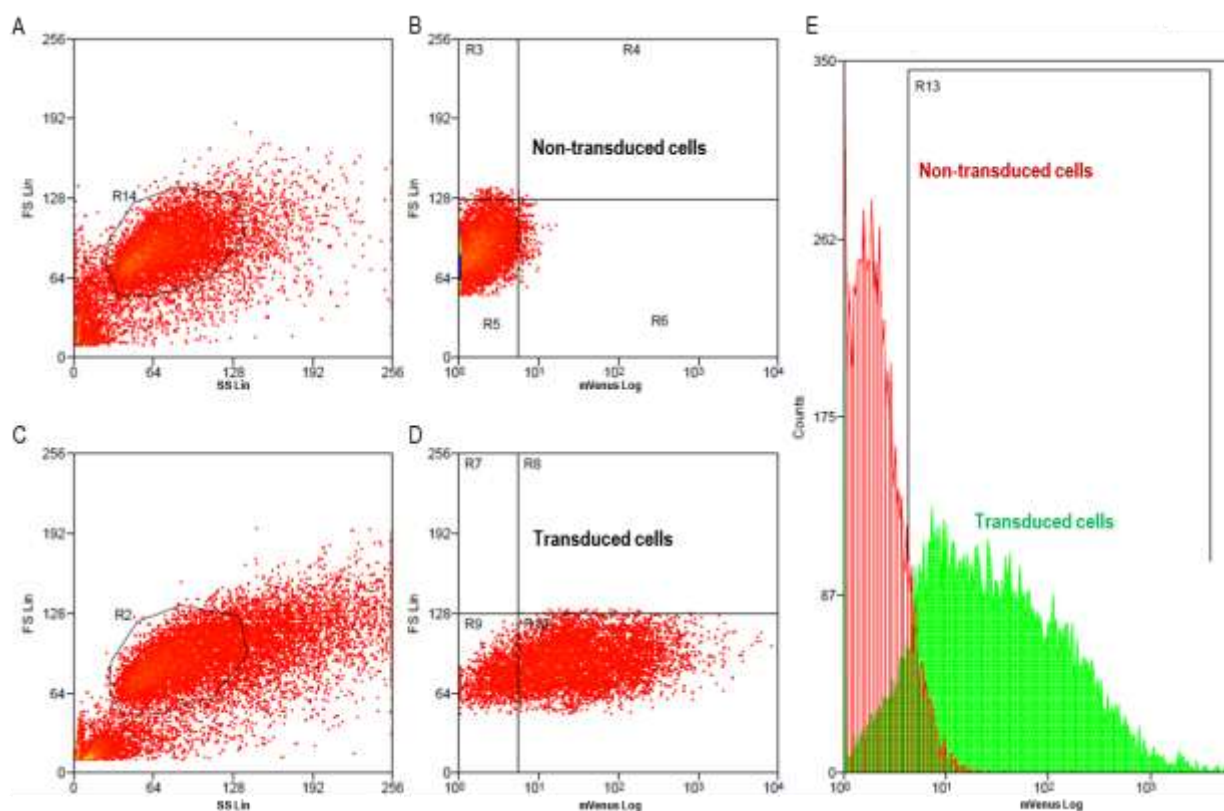
Figure 64: Flow cytometry analysis of vectorplasmids with and without *beta-globin* intron. K: 48-hours post transfection, viral particles were harvested by freeze-thaw lysis and centrifugation followed by HT1080 transduction. YFP expression of vectorplasmids was determined by flow cytometry 24-hours post infection. The vectorplasmid missing the beta-globin intron showed a negligible difference in mVenus expression compared to viral plasmid containing the beta-globin intron.

5.1.5.2.3 Functionality of the Full Assembled Vectorplasmid Demonstrated by GOI Expression

After assembly of plasmids containing all required elements (see **Figure 55**), functionality was tested in cell culture. AAV-293 cells stably expressing E1A and E1B proteins were transfected with three plasmids (pHelper, pRC, pGOI). Virus particles were harvested 72-hours post-transfection and the tumor cell line HT1080 was transduced with the recombinant viral vectors encapsidating the gene of interest mVenus (BBa_I757008).

The iGEM team Freiburg_Bioware 2010 compared the standard-plasmid containing a subcloned mVenus (pAAV_mVenus, derived from the Stratagene system) with the assembled plasmid pSB1C3_lITR_CMV_beta-globin_mVenus_hGH_rITR (pSB1C3_mVenus: BBa_K404119). Fluorescence expression data obtained by flow cytometry analysis are shown in Figure 65 and Figure 66. Comparing mVenus expression of the standard plasmid and the modified, assembled plasmid reveals that biological functionality of the reassembled plasmid was confirmed.

pSB1C3_mVenus (BBa_K404119)



pAAV_mVenus (Reference)

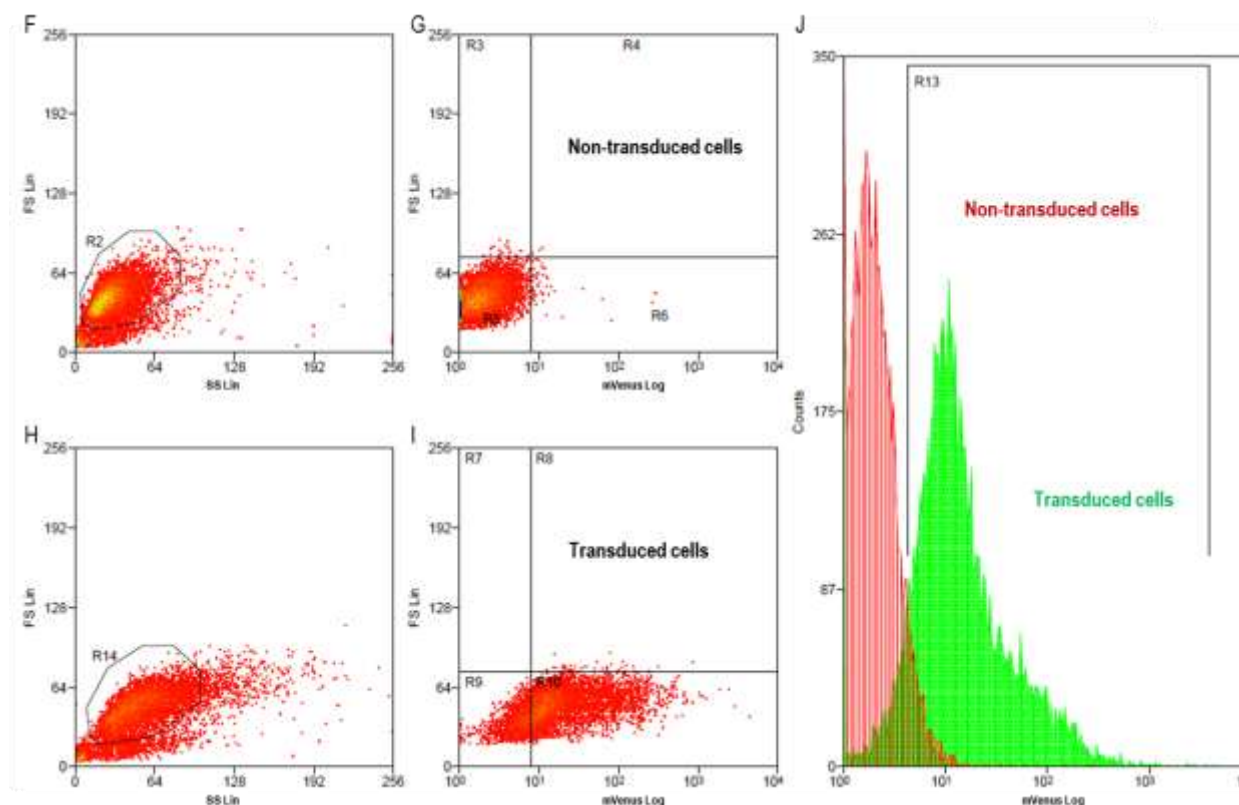


Figure 65: Flow cytometry analysis of fluorescent protein expression in transduced HT1080 cells with and without hGH termination signal. For viral particle production, AAV-293 cells were transfected with the constructs containing hGH and lacking hGH terminator B: Non transduced cells applied against mVenus (Analytical gate was set such that 1% or fewer of negative control cells fell within the positive region (R5). C: Gating transduced cells (R2 \triangleq R14) (used plasmids for transfection: GOI: pSB1C3_lITR_CMV_beta-globin intron_mVenus_rITR (BBa_K404127), pHelper, pRC). D: Transduced cells plotted against cells expressing mVenus. R10 comprises transduced cells detected by mVenus fluorescence. E: Overlay of non-transduced (red) and transduced (green). F: Gating non-transduced cells (control). G: Non-transduced cells plotted against cells expressing mVenus (R5). H: Gating transduced cells (R14 \triangleq R2) (plasmids used for transfection: GOI: reassembled pSB1C3_lITR_CMV_beta-globin_mVenus_hGH_rITR (BBa_K404119), pHelper, pRC). I: Transduced cells plotted against cells expressing mVenus. R10 comprises transduced cells detected by mVenus fluorescence. J: Overlay of non-transduced (red) and transduced (green) cells plotted against mVenus expression.

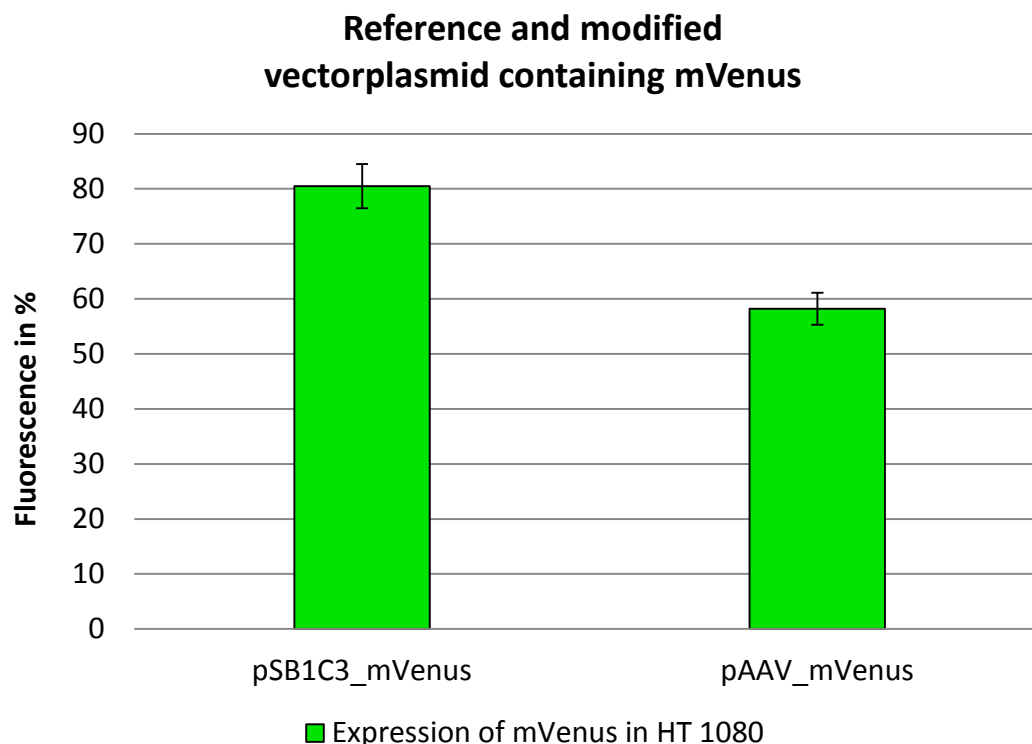


Figure 66: Flow cytometry analysis of reassembled vectorplasmid (BBa_K404119) compared to standard plasmid provided by Stratagene. K: Fluorescence of the standard plasmid pAAV_mVenus (Stratagene) and the recombinant pSB1C3_mVenus (BBa_K404119) construct was measured. As demonstrated mVenus expression is enhanced in the assembled plasmid (pSB1C3_mVenus) compared to the standard pAAV_mVenus construct.

5.1.5.3 Conclusion

Idea of the modular 'Virus Construction Kit' is to provide all required elements for producing recombinant, functional virus particles delivering encapsidated genes of interest to specific cells. First step was to modify and modularize the vector plasmid comprising basically the cis-elements for replication (ITRs), a strong eukaryotic or tissue specific promoter (pCMV or pHRT), the gene of interest (fluorescent proteins or suicide genes) and the hGH termination signal. Each element was successfully cloned and reassembled resulting in functional vector plasmids determined by flow cytometry and fluorescence microscopy analyses. Experiments have been performed with mVenus since measurement of fluorescent proteins can be easily performed and visualized. Considering the results, the iGEM team Freiburg_Bioware 2010 then tested the construct containing the suicide genes thymidine kinase and cytosine deaminase. Further details demonstrating efficient tumor killing, using prodrug-activating systems are provided under results 'Arming' and 'Tumor Killing'.

5.1.6 Modulatization of the RepCap plasmid

5.1.6.1 Overview Modularization: Overview

In our terminology the term “RepVP123” encompasses the whole AAV2 genome excluding the ITRs. The *rep* locus comprises four proteins related to genome replication while the *cap* locus codes for the proteins VP1, VP2, VP3 and the assembly-associated protein (AAP), which are required for viral capsid assembly. Source of the RepVP123 BioBrick supplied within iGEM team Freiburg_Bioware 2010 Virus Construction Kit is the wild-type AAV2 RepVP123, as provided e. g. in the pAAV vector from Stratagene. In order to introduce iGEM standard and additionally enabling the possibility to modify the viral capsid via integration of certain motives within the viral loops 453 and 587 a total of twelve mutations within RepVP123 (see Figure 67) and additionally two mutations within the pSB1C3 backbone were performed either by Site-Directed Mutagenesis (SDM) or by ordering and cloning of specifically designed gene sequences matching the required demands. Modifying the pSB1C3 led to iGEM team Freiburg_Bioware’s variant of this backbone, pSB1C3_001.

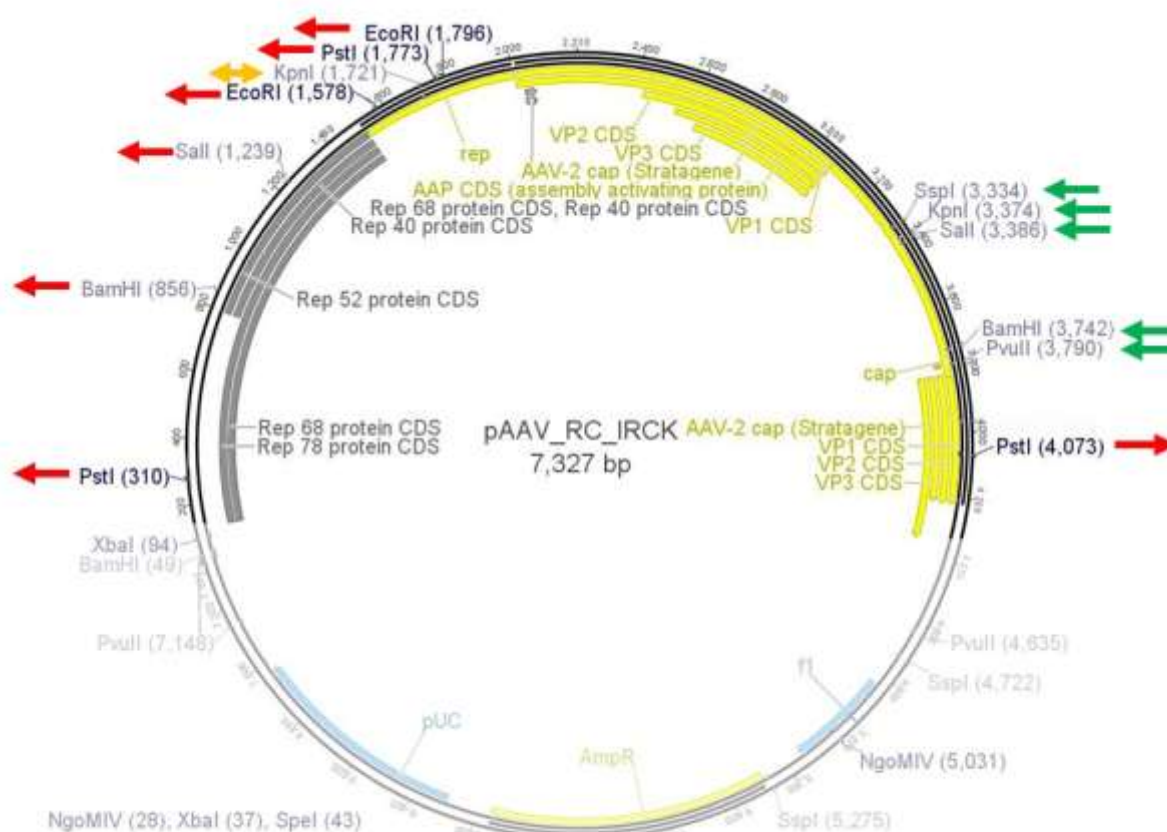


Figure 67 Mutations implemented into *RepVP123* in order to establish both iGEM standard and loop insertion capability. Green arrows indicate integrated restriction sites, red red arrows indicate deleted restriction sites. KpnI was deleted first and reinstated afterwards. (see text).

Table 4: Table contains complete overview about all plasmids containing *RepVP123* which were used by iGEM team Freiburg_Bioware 2010.

Plasmid name:	Functionality (determined in cell culture transduction and flow cytometry):	4x mutations (PstI (310), BamHI (859), Sall (1239), PstI (4073))	inserted <i>rep</i> fragment	inserted <i>cap</i> fragment	reinstated KpnI	pAAV	pSB1C3_001	HSPG-ko
pAAV_RC (wild-type)	yes					x		
pAAV_RC_4x mutant	yes	x				x		
pAAV_RC_inserts	no	x	x	x		x		
pAAV_RC_Cap	yes	x		x		x		
pAAV_RC_RepVP123	yes	x	x	x	x	x		
pSB1C3_RepVP123_p5TATAless	yes	x	x	x	x		x	
pSB1C3_RepVP123_HSPG-ko_p5TATAless	yes	x	x	x	x		x	x

5.1.7 Modularization: Removing iGEM restriction sites and establishing loop insertion capability

5.1.7.1 Modifications in Rep

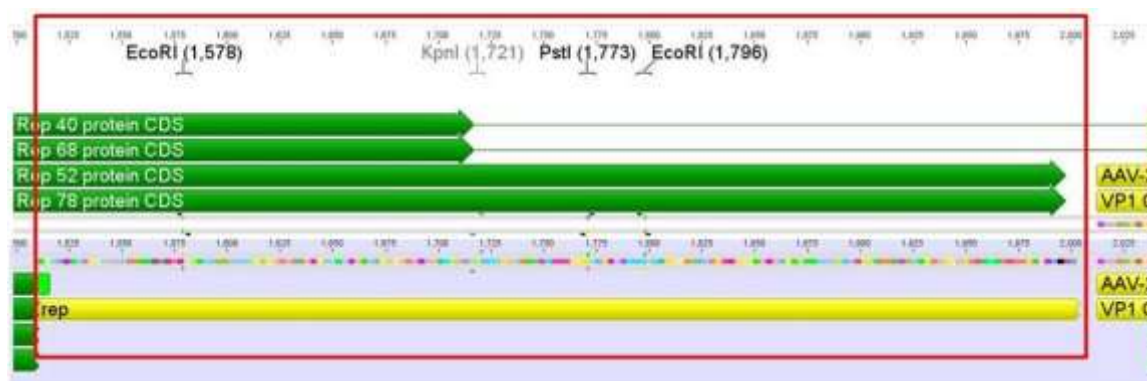


Figure 68 Restriction sites within the wild-type *rep* gene sequence, which were removed via cloning of synthesized *rep* gene fragment into the plasmid. The red box indicates the region spanned by the synthetic sequence.

Making the *RepVP123* wild-type compatible with the iGEM standards required the removal of five restriction sites (see Figure 67). This was achieved using site-directed mutagenesis for PstI (position 310) and PstI (4073). The remaining three iGEM restriction sites EcoRI (1578), PstI (1773) and EcoRI (1796) were replaced by a synthetic gene fragment, since the *rep* ORF contained these restriction sites in close proximity to each other plus an additional KpnI restriction site which was also not desired (see Figure 68). This gene fragment was cloned into the *rep* gene using HindIII and SwaI, which are single-cutting restriction enzymes adjacent to the target area. Additionally, BamHI (859) and Sall (1239) were removed, because these enzymes were required for genetically inserting the loop modifications in VP123.

5.1.7.2 Modifications in VP123

In order to implement the restriction sites necessary for targeting via loop insertions, the gene coding for the VP proteins was modified as well. The introduction of these restriction required up to four base mutations in a row, hence it was decided to synthesize this gene fragment and replace the wild-type sequence in *RepVP123* as well.

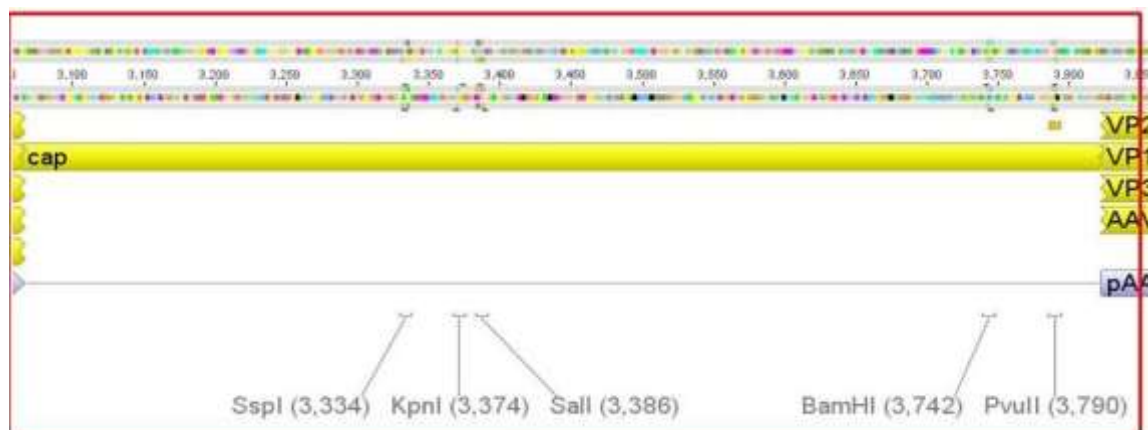


Figure 69 Restriction sites within *cap* sequence showing introduced loop insertion restriction sites into *cap* to enable cloning of targeting or purification motifs into both 453 and 587 loops. Again, the red box indicates gene sequence which was synthesized.

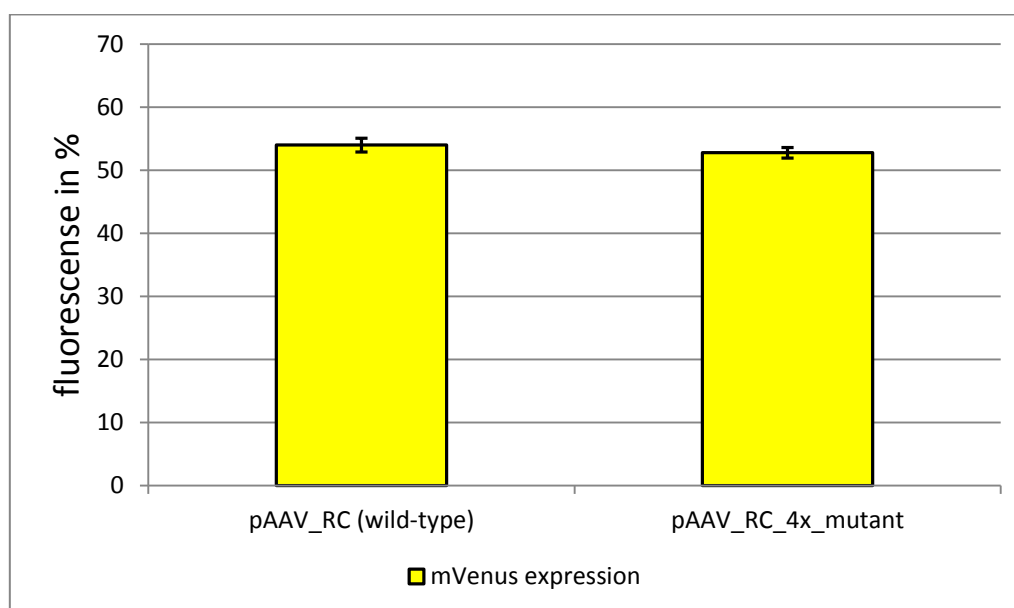


Figure 70 Results for transduction efficiency measured by flow cytometry. The tested *RepVP123* containing four point mutation to delete iGEM and loop insertion restriction sites does not show any difference within mVenus expression compared to the wild-type and therefore can be verified working.

Alongside to creating an iGEM compatible plasmid, infectivity of the modified construct was tested in cell culture via flow cytometry. Then experiments confirmed that single cloning steps did not interfere with natural viral infectivity at first (see Figure 70). But cloning of the synthesized *rep* gene fragment into the plasmid dramatically reduced transduction efficiency as detected by flow

cytometry. Scrutinizing each mutation and its potential impact, suggested that abolished transduction was related to the mutation, which removed the KpnI (1721) site. This site is located within a splice site, which is crucial for the Rep proteins, and thus even silent mutations may interfere with virus production (see extra topic “Rep proteins”).

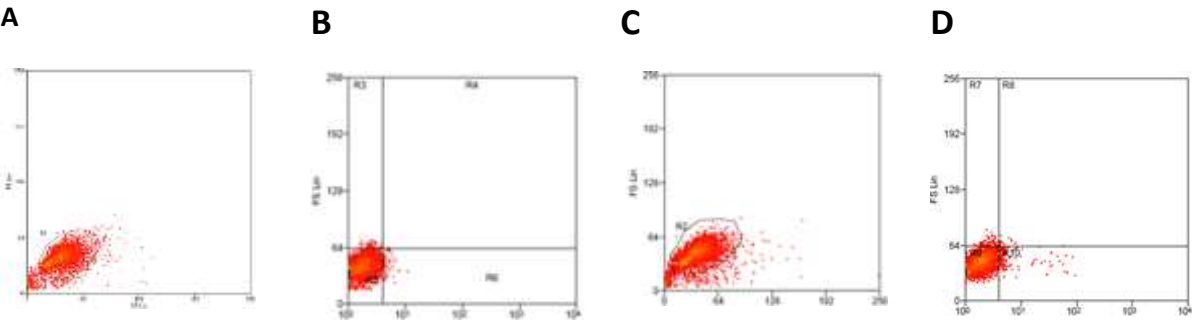


Figure 71 pAAV_RC_inserts (modified)
(original data obtained from flow cytometry)
A: gated cells (control)
B: non transduced cells (control)
C: gated cells (pAAV_RC_inserts)
D: transduced cells (pAAV_RC_inserts)
E: Overlay B + D

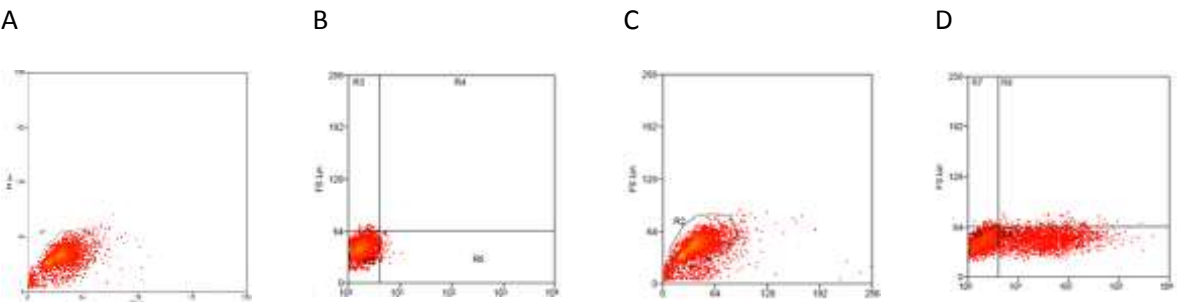
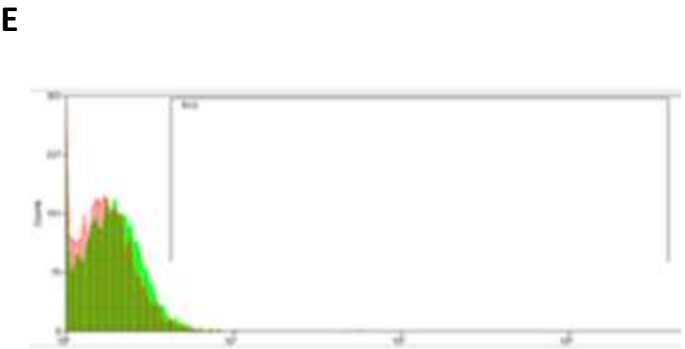
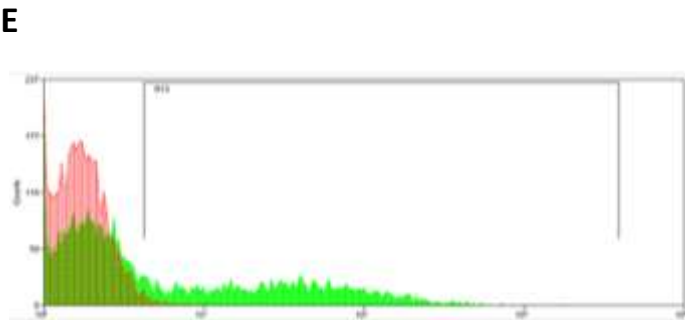


Figure 72 pAAV-RC (wild-type)
(original data obtained from flow cytometry)
A: gated cells (control)
B: non transduced cells (control)
C: gated cells (pAAV_RC)
D: transduced cells (pAAV_RC)
E: Overlay B + D



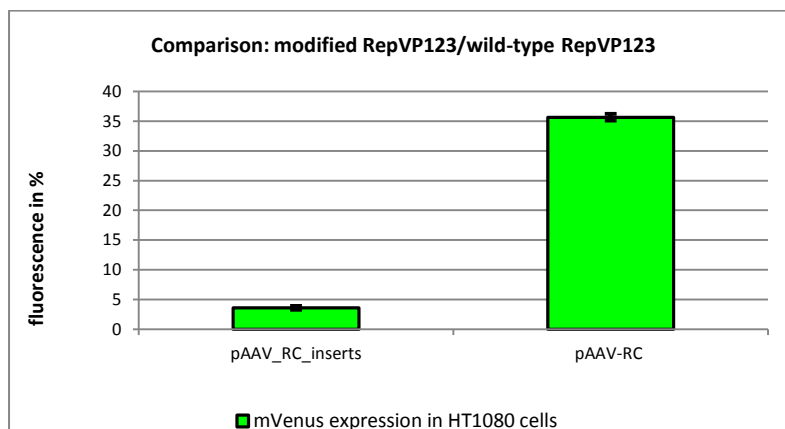


Figure 73 AAV-293 cells were transfected with three plasmids pHelper, pSB1C3_[AAV2]-left-ITR_pCMV_betaglobin_mVenus_hGH_[AAV2]-right-ITR and pAAV_RC_inserts or pAAV_RC providing essential genes and proteins for producing viral particles. After 48-hour post transfection, viral particles were harvested by freeze-thaw lysis and centrifugation followed by HT1080 transduction. mVenus expression of viral genomes was determined by flow cytometry after 24-hour post infection. Results show that insertion of both rep and cap syntheses disrupts viral infectivity.

Therefore, additional constructs were designed containing only the synthetic *cap* sequence or both, the synthesized sequences plus a re-mutation of KpnI (1721), in order to re-establish the wild-type splice site within the *rep* ORF. Results from cell culture obtained via FACS revealed that in fact the poor results were related to the KpnI restriction site deletion. Both constructs showed a transduction efficiency corresponding to the unmodified wild-type *RepVP123*'s transduction efficiency.

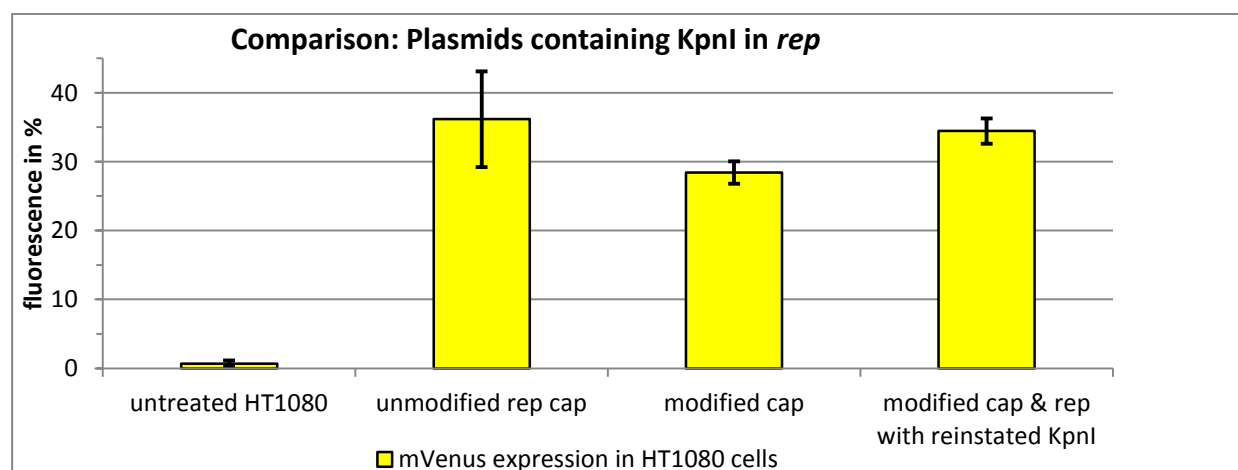


Figure 74 Fluorescence of cells transduced with mVenus carrying rAAV measured by flow cytometry. AAV-293 cells were transfected with three plasmids pHelper, pSB1C3_[AAV2]-left-ITR_pCMV_betaglobin_mVenus_hGH_[AAV2]-right-ITR and *RepVP123* constructs providing essential genes and proteins for producing viral particles. After 48-hour post transfection, viral particles were harvested by freeze-thaw lysis and centrifugation followed by HT1080 transduction. mVenus expression of viral genomes was determined by flow cytometry after 24-hour post infection. Results show that *cap* integration does not influence infectivity. Recreation of KpnI within *rep* splice site recovers transduction efficiency.

5.1.7.3 Modularization: Adapting pSB1C3 to loop insertions – pSB1C3_001

To fulfill iGEM requirements all plasmids need to be submitted in pSB1C3, therefore primers were ordered for amplifying *RepVP123* containing all modifications done so far by PCR and cloning the into pSB1C3. Still, pSB1C3 contains two restriction sites for *SspI* and *PvuII* restriction enzymes in its CAT marker. Since these are necessary for cloning ViralBricks in this vector, the iGEM Team Freiburg_Bioware 2010 decided in agreement with iGEM Headquarters to implement a new standard for the pSB1C3 backbone which was named pSB1C3_001. Both restriction sites interfering with ViralBrick insertions were mutated to make *SspI* and *PvuII* single-cutters (see method development).

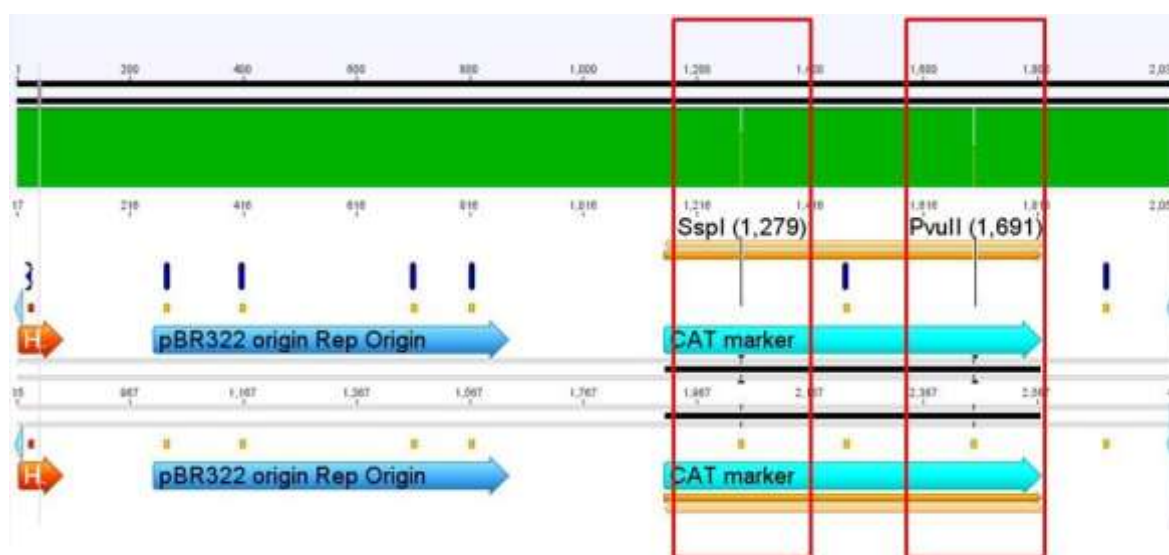


Figure 75 Comparison of pSB1C3 (upper row) and pSB1C3_001 (lower row). Deletions of *SspI* and *PvuII* are marked by red boxes.

RepVP123 containing both *rep* and *cap* synthetic gene fragments including the re-mutation of *KpnI* and the downstream p5TATA-less promotor was cloned into the newly constructed pSB1C3_001. Testing this newly assembled plasmid in cell culture revealed unexpected data. Not only did the newly assembled plasmid work (see Figure 75), but in comparison to pAAV containing the same *RepVP123* construct, pSB1C3_001 showed an about 3 times higher transduction efficiency. Although exact reasons are still unknown, these results are probably related to the reduced length of pSB1C3_001 compared to the original pAAV plasmid of approximately 1000 base pairs.

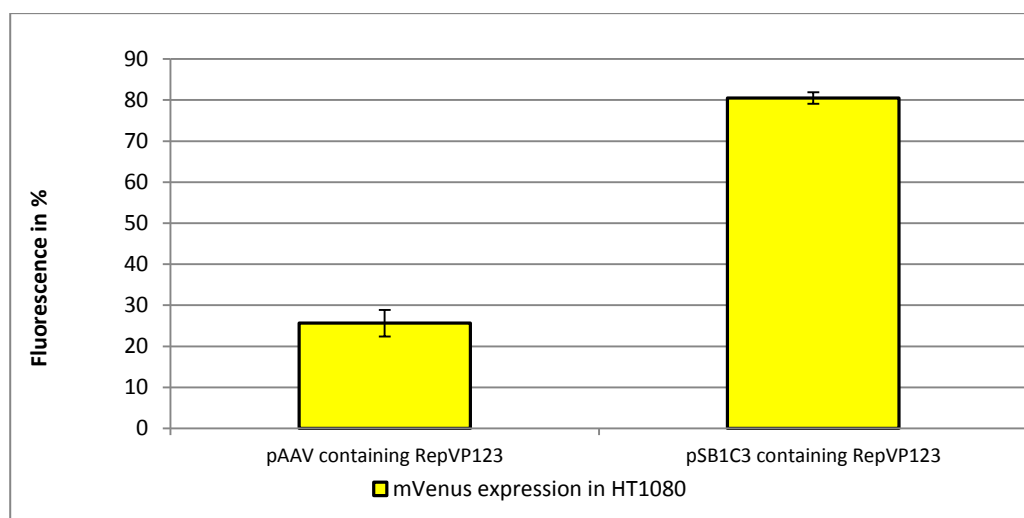


Figure 76 AAV-293 cells were transfected with three plasmids pHelper, pSB1C3_001_[AAV2]-Rep-VP123_p5-TATAless or pAAV_RC_IRCK and pSB1C3_[AAV2]-left-ITR_pCMV_beta-globin_mVenus_hGH_[AAV2]-right-ITR providing essential genes and proteins for producing viral particles. After 48-hour post transfection, viral particles were harvested by freeze-thaw lysis and centrifugation followed by HT1080 transduction. mVenus expression of viral genomes was determined by flow cytometry after 24-hour post infection. Results showed functionality of *RepVP123* within pSB1C3_001 vector and additionally increased transduction efficiency.

5.1.7.4 Turning-off natural tropism: HSPG-knock-out

Shutting-down the natural viral tropism is essential for targeting specifically tumor cells and not infecting healthy cells. Therefore, the iGEM team Freiburg_Bioware 2010 decided to knock-out the viral natural tropism delivered by the heperan sulfate proteoglycan-(HSPG) binding site within the viruses 587 loop. The knock-out was cloned by designing primers containing the required base exchanges and performing a SDM. Like performed before, this *RepVP123* variant was tested in cell culture as well and evaluated by flow cytometry. Results show that mutation of HSPG-binding motif has severe impact on transduction efficiency thus enabling a viral particle carrying this knock-out and additional targeting motifs, e.g. within the loops or presented via N-terminal fusion to bind target cells' receptors and therefore infecting target cells at a much higher rate compared to unspecific infection of other cell types within an organism (seeFigure 78).

To quantify differences in infectivity, the infectious titer of viral particles built-up of *RepVP123* with and without HSPG binding motif was determined by qPCR (see Figure 79) for different cell lines. Results show that the implemented HSPG-ko verifies results obtained from flow cytometry, infectious titers severely compared to *RepVP123* with intact HSPG binding motif.

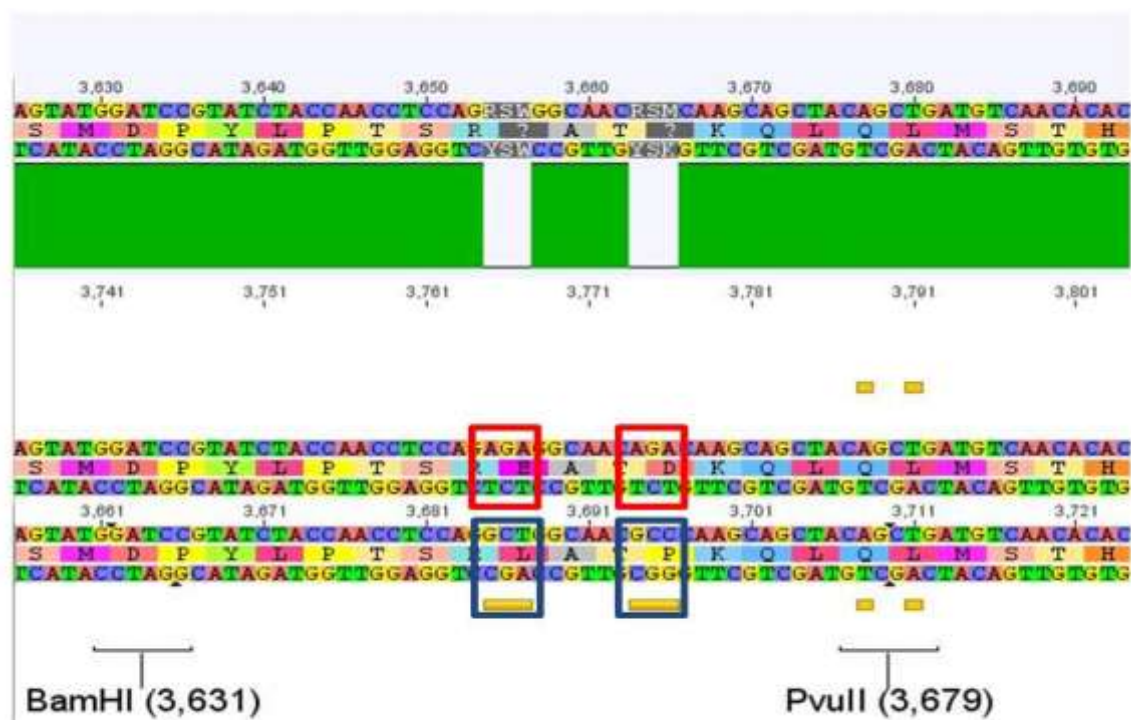


Figure 77 Alignment of 587 loop within viral VP123: The upper sequence shows a strand containing the HSPG binding motif (AGA, in red boxes), the lower sequence contains the HSPG-ko introduced by the iGEM team Freiburg_Bioware 2010 (GCT and GCC, blue boxes).

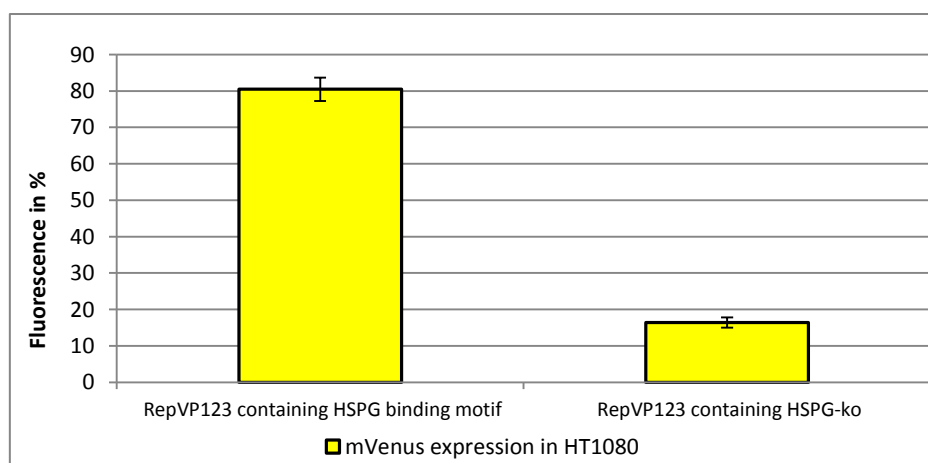


Figure 78 Transduction efficiency of HT1080 cells measured by flow cytometry. Knock-out of HSPG binding motif greatly reduces transduction efficiency compared to *RepVP123* containing the motif.

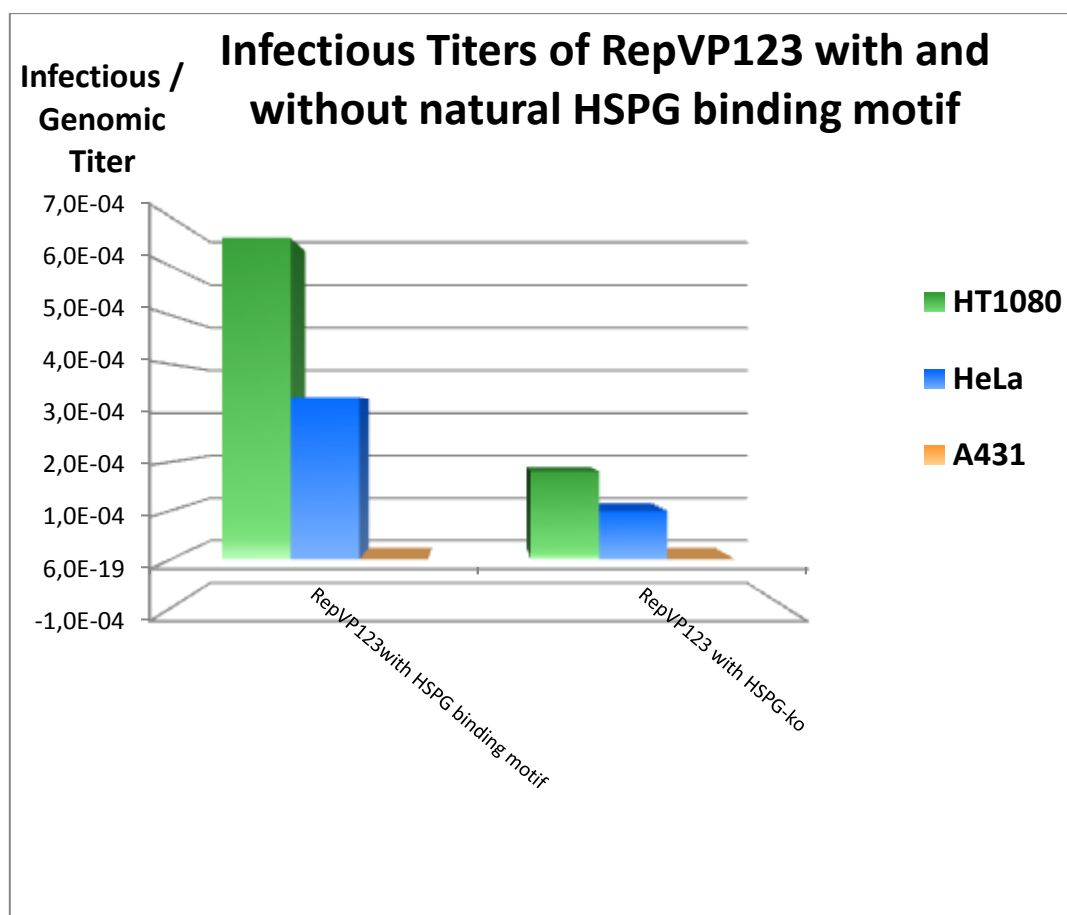


Figure 79 Infectious titers of RepVP123 with and without natural HSPG binding motif tested in different cell lines via qPCR. Shutting-down the HSPG binding motif reduces infectious titer in both HT1080 and HeLa cell lines. For A431 cells, no infectious titer could be detected via qPCR, which is probably related to poor transduction efficiency of A431 cells.

5.2 Targeting

Modifying the viral tropism was approached in two ways. First the loops, which mainly determine the tropism of the wild-type virus, were made amenable to genetic manipulation and functionality of loop replacements was demonstrated. Second N-terminal fusions to the capsid proteins were tested and shown to be functional.

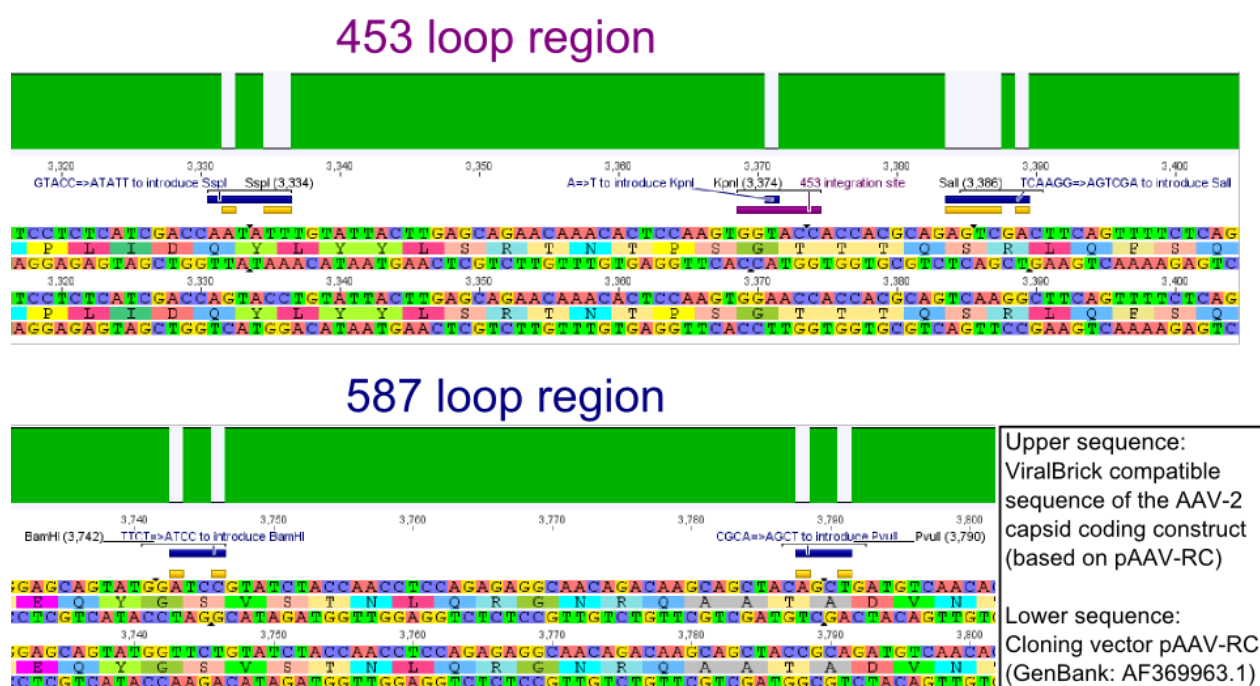
5.3 Loop Insertions for Targeting, Purification, and Biotechnological Applications

The insertion of sequences for functional peptides into the viral capsid is a well established and characterized possibility for retargeting of AAV viral vectors. Over the last decade, different positions in the viral sequence have been evaluated for their suitability to insert small peptides.

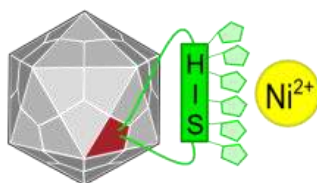
We decided to use the well established 587 and the newly identified 453 integration site (numbrbs give the aminao acid position in the capsid) for our Virus Construction Kit.

To ensure flexibility and usability, we decided to use single cutting restriction sites for exchanging the loop motifs rather than PCR-technology as used by other groups. Our approach provides the advantage that all capsid coding constructs can be modified using our “ViralBricks” in a single cloning step. For the enzyme approach we had to ensure that the functionality of the viral gene is not destroyed by the mutations. Therefore, functionality of the modified version with the introduced single cutting restriction sites was tested in cell culture and the functionality was determined as comparable with the unmodified sequence.

In order to have these single cutting restriction sites two restriction sites had to be removed from the Rep-protein coding region of pAAV-RepCap and the restriction sites had to be introduced into the Capsid coding region as show in the following figure.



5.3.1.1 IMAC purification via Viral Brick: The Histidin Affinity Tag

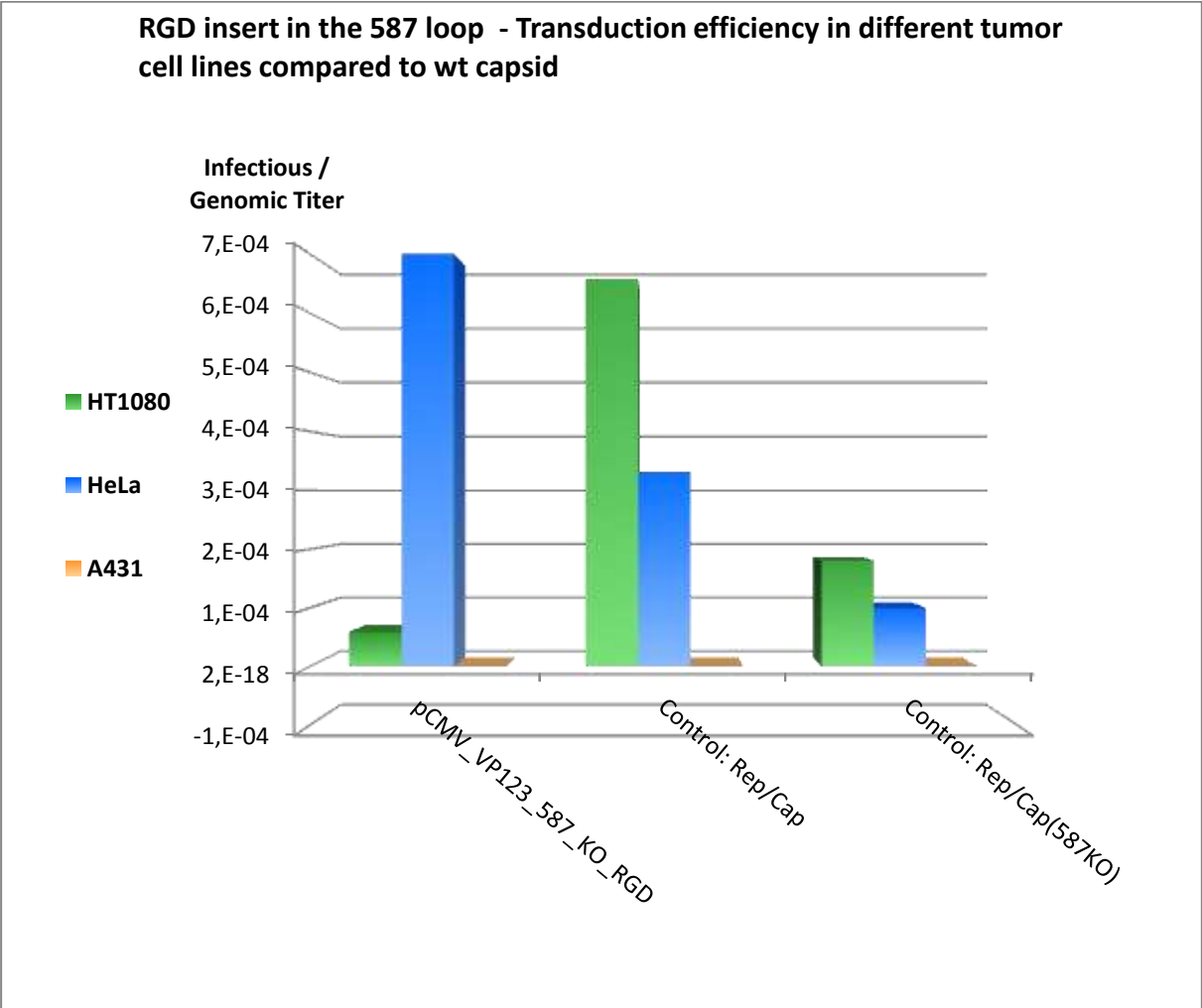


Protein tagging via Histidine Tags is a widely used method for protein purification: Multiple histidine residues (most commonly: Six) are being fused to the end of the targeting protein.

The high binding affinity of Histidine towards metal is being exploited for the purification of proteins via the so called „Immobilized Metal Ion Affinity Chromatography“ (IMAC): Multiple histidine residues (most commonly: Six) are being fused to the end of the targeting protein. A cell extract containing the recombinant protein is then applied to a column containing immobilized Ni^{2+} -Ions. The His-tags covalently bind the Ni-Ions while other cellular proteins can be washed off the column. The purified proteins can then be eluted with Imidazol, which displaces the histidine residues. (M. C. Smith et al. 1988), (Hoffmann & Roeder 1991)

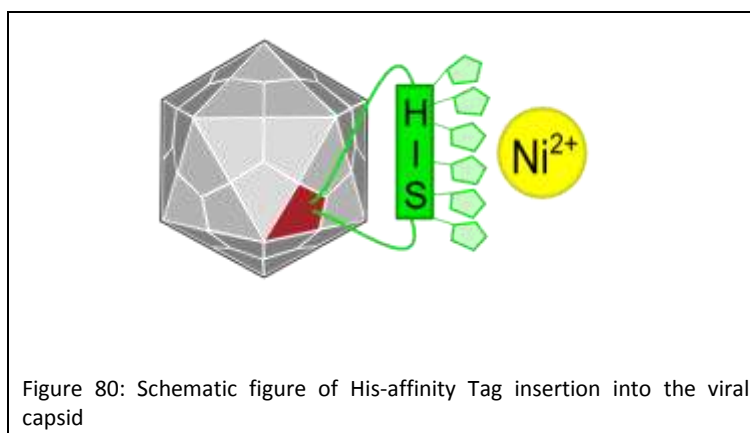
Since the aim behind engineering therapeutic AAV vectors is a safe administration to human patients, it is important to consider a convenient way of purifying the virus particles. Contamination by cellular proteins could cause toxic side effects or a strong immune response. (Korber et al. 2007) have first inserted a His-tag into a surface-exposed loop at amino acid position 587 in the Cap protein and successfully purified recombinant viruses using IMAC. For our Virus Construction Kit, we provide the His-tag motif in the ViralBrick standard, allowing an easy insertion into the 453 and/or 587 loop.

5.3.1.2 qPCR for infectious titer



5.3.2 His-Affinity Tag

5.3.2.1 Theory



The insertion of a His-Affinity Tag into the exposed major surface loops of the viral vectors allows their specific affinity purification employing e.g. Ni-NTA affinity chromatography. This purification method was tested using the cell culture lysate of transfected AAV-293 cells that were either grown in DMEM supplemented with 10% FCS or in the serum-free GIBCO® FreeStyle™ 293 Expression Medium (Invitrogen). The usage of serum-free media is a technological modification meant to facilitate the production of pure viral vectors. Purified viral vectors are important for several applications such as animal models and biophysical characterizations. On the other hand, the elution of the His-tagged viral vectors allows also enrichment of transgene viral vectors. In order to answer the question if and to what degree viral vectors are transferred into the media, the cells were centrifugated, then divided into the pellet fraction and the supernatant. Physical cell lysis was performed for both fractions of the two produced batches (serum-free and FCS media) by performing four cycles of freeze and thaw.

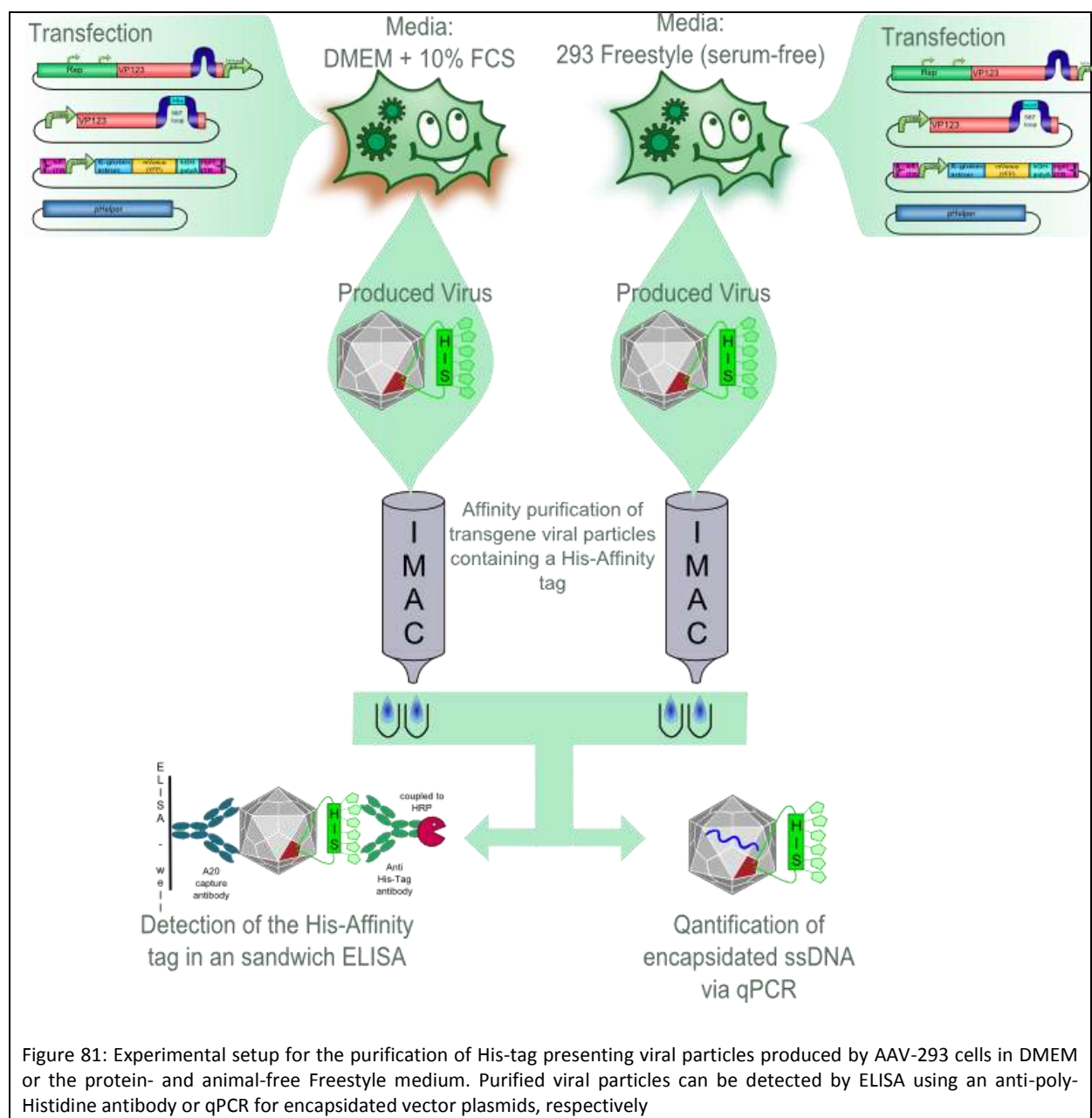


Figure 81: Experimental setup for the purification of His-tag presenting viral particles produced by AAV-293 cells in DMEM or the protein- and animal-free Freestyle medium. Purified viral particles can be detected by ELISA using an anti-poly-Histidine antibody or qPCR for encapsulated vector plasmids, respectively

5.3.2.2 Material and Methods:

Transfection of the AAV-293 producer cells was performed in five 10 cm petri dishes with 3.6×10^6 cells, resulting in a confluency of about 70-80% according to the standard protocol either with cells grown in GIBCO® FreeStyle™ 293 Expression Medium (Invitrogen, protein- and animal-origin free) or in DMEM supplemented with 10% FCS (PAA). For transfection, the composite parts pCMV_VP123(587-His) and RepVP123(587-KO)_p5-TATA-less were used in an 1:1 ratio together with pHelper and [AAV2]-left-ITR_pCMV_betaglobin_mVenus_hGH_[AAV2]-right-ITR. Cells were spun down at $200 \times g$ for five minutes and the samples were divided into the pellet and the supernatant fractions. Physical cell lysis was performed by four cycles of freeze and thaw for all four samples. The cell lysate / supernatant fractions were incubated with 800 μ l of His-Affinity Gel (kindly provided by

Zymo Research, USA) at 4 °C for 18 hours with 200 rpm constant agitation. The beads were then collected in 5 ml gravity-flow columns and washed five times with one column volume of PBS each. The His-affinity gel was subsequently washed with PBS, 25 mM Imidazole to remove unspecifically bound proteins. Elution was performed in a second step with PBS, 500 mM Imidazole to elute the His-tagged viral vectors. The genomic titer of the purified viral vectors was detected via q-PCR. In an ELISA, viral vectors were captured employing the monoclonal antibody A20 (kindly provided by PD Dr. J. Kleinschmidt, DKFZ, Heidelberg) that exclusively recognizes assembled AAV capsids. His-Tags present in assembled viral capsids were subsequently detected with an HRP-tagged secondary anti-His-Tag antibody (1:2000 diluted, A7058, Sigma). HRP presence was detected using the peroxidase substrate ABTS. Generation of blue-green color (absorption at 405 nm) was measured in a Tecan Sunrise plate reader. Sample data were blanked with the average of the non-template controls (NTC).

5.3.2.3 Results and Discussion:

Presence of the His-affinity tag in the viral capsid was detected and the ELISA enabled quantification of the purification procedure efficiency. The absorbance measured for the elution fractions of the 1/10 diluted samples sums up to 2.3 for the DMEM- and 0.5 for the Free Style 293-grown cells, assigning the DMEM-grown cells a five times higher production efficiency. Comparison between the cell pellet and the supernatant fractions revealed that 70 - 80% of the viral particles can be found inside the producer cells.

According to these results, producer cells should be grown in complex media for *in vitro* and cell culture experiments. Use of serum-free produced viral vectors is recommended for mouse or other animal experiments and possible therapeutical applications where even the presence of traces amounts of fetal calf serum should be avoided. Combination with different purification approaches such as gel filtration chromatography using i.e. Superdex 200 columns (GE Healthcare) enables the production of highly purified viral vectors for several different applications.

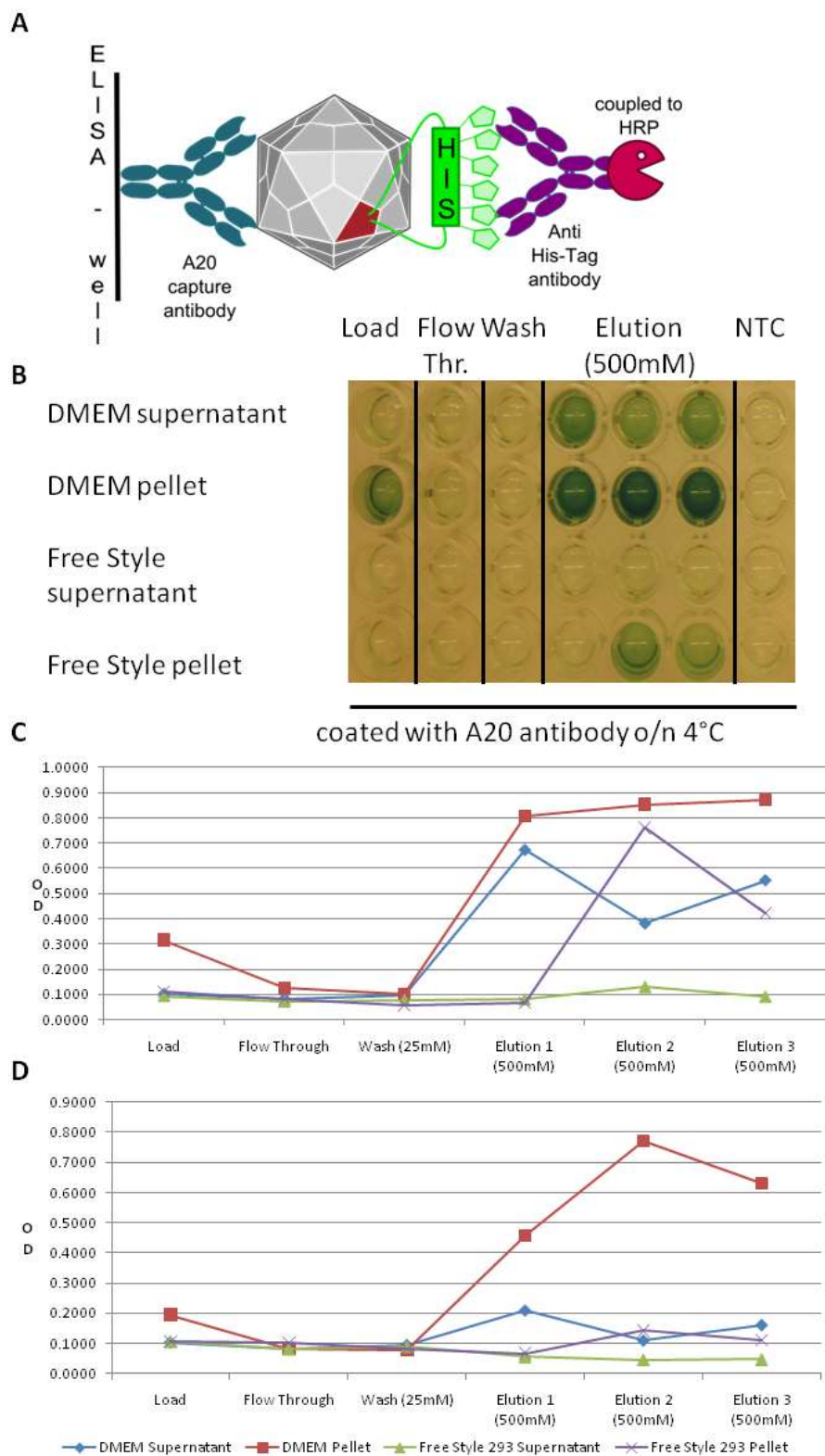


Figure 82:

A: Schematic overview of the sandwich ELISA for the detection of His-tagged viral particles

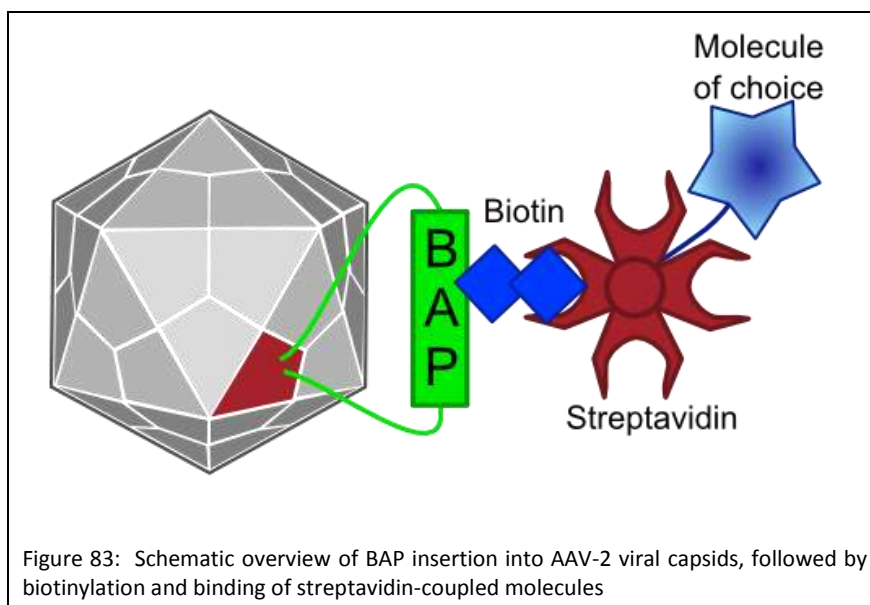
B: ELISA from viral particles produced by AAV-293 cells in DMEM or Free Style medium, divided into cell pellet and cell culture supernatant samples. The particles were purified using Ni-NTA affinity chromatography with Imidazole in PBS as washing and elution agent

C: Absorption measurements from plate shown in B. Undiluted Äkta fractions converted ABTS peroxidase substrate at 405 nm

D: As C, whereas Äkta fractions were 10-fold diluted

5.3.3 Biotinylation Acceptor Peptide (BAP)

5.3.3.1 Theory



The BAP (Biotinylation Acceptor Peptide) included in the Virus Construction Kit is a 15 amino acid peptide identified by Schatz et al. (1993) in a library screening approach and published under the number #85. This peptide with the sequence GLNDIFEAQKIEWHE contains a central lysine residue that can be specifically biotinylated by the prokaryotic holoenzyme biotin synthetase, encoded by the BirA gene of *E. coli*. Specific biotinylation of this peptide sequence can be performed *in vivo* by cotransfecting a plasmid with the BirA gene as described for the AAV by Arnold et al. (2006) or by an *in vitro* coupling approach using the purified *Escherichia coli* enzyme biotin ligase (BirA).

Biotin molecules specifically coupled to the viral loops can either be used to attach Streptavidin-coupled molecules to the viral capsid or to chemically couple molecules with a reactive group to biotin. Consequently, the inserted motif can enable the visualization of single virus particles by coupling fluorophores to the virus capsid empowering further uses of the Virus Construction Kit in fundamental virological research. In addition, targeting molecules such as Streptavidin-coupled affinity molecules (i.e. Antibodies, Nanobodies or Affibodies) can be coupled for manifold targeting approaches.

5.3.3.2 Materials and Methods:

Transfection of the AAV-293 producer cells was performed in five 10 cm petri dishes with 3.4×10^6 cells (grown in DMEM supplemented with 10% FCS) resulting in a confluence of 70-80% according to the standard protocol. Producer cells were harvested and together with the culture supernatant subjected to four cycles of freeze and thaw cell lysis. The cell lysate was centrifuged at 4000 rpm for 15 minutes and concentrated in a VivaSpin VS2002 column with 10 kDa molecular weight cut-off to yield two milliliters. Genomic DNA attached to the virus particles was degraded using 250 units of Benzonase (EC 3.1.30.2, Sigma-Aldrich) at 37 °C for one hour. The concentrated cell lysate was washed three times with 4 ml 20 mM bis-Tris buffer pH 6.0, 100 mM NaCl. From this concentrated sample, 500 µl were loaded on the ÄKTA purifier (GE Healthcare) equipped with a Superdex 200 gel filtration column (GE Healthcare). This purification is also described by Smith et al. (2003). Fractions around the void volume giving a UV absorbance peak were pooled and applied to a Amicon Ultra column (Millipore, size limit 100 kDa, 2 ml loading volume) and concentrated to 500 µl. This purified virus sample was washed four times with 10 mM Tris-buffer pH 8.0 buffer which is recommended for the BirA biotin ligase that was kindly provided by Avidity LCC (Colorado, USA).

The BAP-containing viral vector sample (500 µl) was mixed according to the manufacturer protocol with each 72 µl Biomix A, Biomix B and Biotin. To reach maximal biotinylation, a volume of 5 µl containing 25000 units of the biotin ligase BirA was added to the reaction mixture and incubated for 6 h at 30 °C. In order to remove unbound biotin, the biotinylated viral vectors were washed five times with 10 mM Tris buffer pH 8.0.

Biotinylation was verified with an ELISA as depicted in figure A. For the detection of successfully biotinylated viral vectors, MaxiSorp 96-well plates (Nunc) were coated with 200 ng monoclonal A20 antibody per well for eight hours at 4°C, and blocked over night with PBST + 0.5 % BSA. This plate was incubated for 1 h at room temperature with 100 µl of serial diluted viral vectors. After washing the plates three times, the recommended amount of Streptavidin-HRP conjugate (Sigma-Aldrich) was added to each well for 1 h at room temperature. Again, the plates were washed three times followed by detection of absorbance caused by converted ABTS substrate at 405 nm. Additionally, the genomic AAV-2 titer was determined by qPCR.

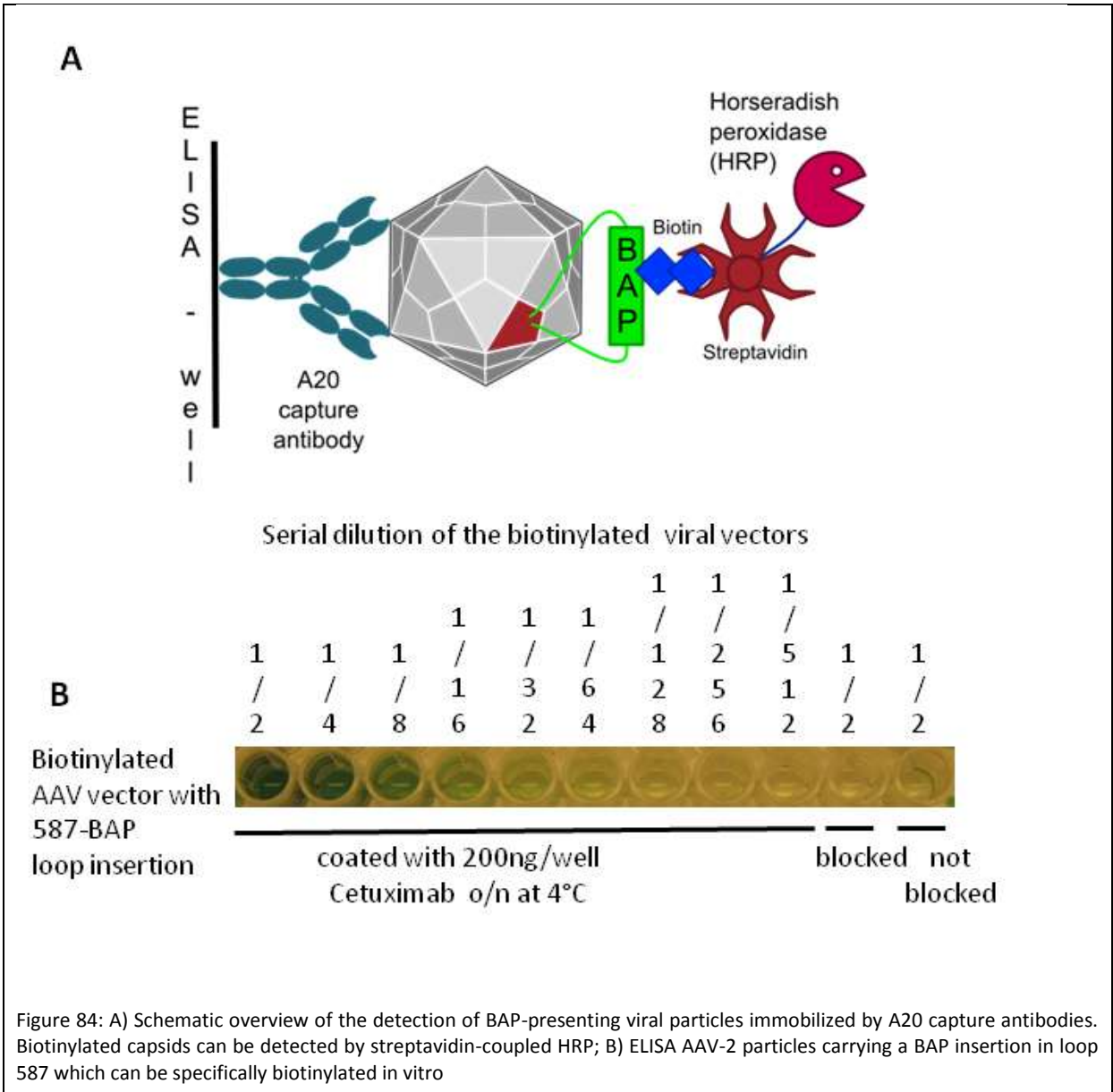


Figure 84: A) Schematic overview of the detection of BAP-presenting viral particles immobilized by A20 capture antibodies. Biotinylated capsids can be detected by streptavidin-coupled HRP; B) ELISA AAV-2 particles carrying a BAP insertion in loop 587 which can be specifically biotinylated in vitro

5.3.3.3 Results and Discussion:

As can be seen in figure B, biotinylation of assembled AAV particles was achieved with the dilution series ranging from 2- to 128-fold. Correlating this assay with the qPCR experiment for the detection of encapsidated vector plasmid (genomic titer using CMV-promoter primers) yields a value of 4.70E+07 DNase-resistant particles (DRP). Consequently, the presence of approximately 3.6x10^5 biotinylated DRPs can be detected using the described ELISA. Compared to the virus particle detection ELISA employing A20 as capture- and detection antibody, the detection limit of the biotinylated viral capsids is about 10fold more sensitive. This may be explained by the higher affinity of streptavidin towards biotin relative to the A20 antibody affinity or multiple biotinylation of a single virus particle.

5.3.4 Miniaturized antibody binding domain (Z34C)

5.3.4.1 Theory for Z34C

5.3.4.2 Material and Methods

Transfection of the AAV-293 producer cells was performed for three different loop insertions of Z34C in each three 10 cm petri dishes with 3.4×10^6 cells resulting in a confluence of about 70-80%. For the transfection, either the composite parts pCMV_VP123(453-Z34C), pCMV_VP123(587KO- Z34C) or pCMV_VP123(587Ko- Z34C-Spacer) were cotransfected with pHelper, [AAV2]-left-ITR_pCMV_betaglobin_mVenus_hGH_[AAV2]-right-ITR and RepVP123(587KO). The producer cells were harvested with the culture supernatant and subjected to four cycles of freeze and thaw cell lysis. The cell lysate was centrifuged at 4000 rpm for 15 minutes and concentrated in a VivaSpin VS2002 (Sartorius Stedem) with a 10 kDa molecular weight cut-off to two milliliters and washed three to five times with 20 mM Bis-Tris buffer, pH 6. The cell lysates were incubated with 250 units of Benzonase (Sigma-Aldrich) to remove contaminant genomic DNA and loaded on an ÄKTA purifier (GE Healthcare) equipped with a Superdex 200 gel filtration column (GE Healthcare). Fractions (500 μ l) around the void volume containing viral particles were collected and used in a sandwich ELISA. 96 well plates were coated with 200 ng Cetuximab (Imclone/Merck/Bristol-Myers Squibb). Detection was performed using the monoclonal antibody A20 (kindly provided by PD Dr. J. Kleinschmidt, DKFZ Heidelberg) that was biotinylated using a Biotinylation kit (Dojindo, Japan) and Streptavidin-HRP (Sigma-Aldrich). The HRP presence was detected by the conversion of the substrate ABTS at 405 nm. The average of the non-template controls (NTC) was subtracted from the sample data.

5.3.4.3 Results and Discussion

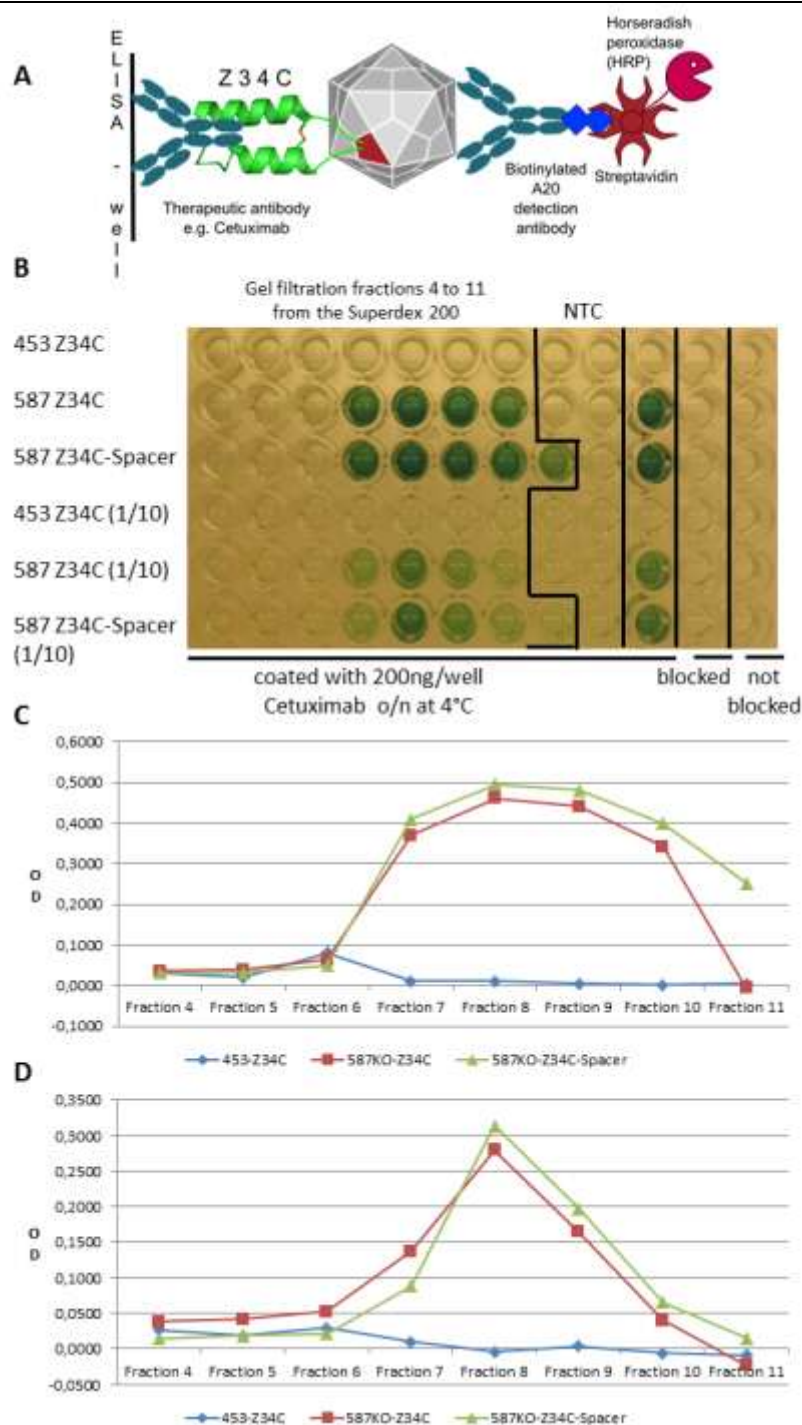


Figure 85: **A**) Sandwich-ELISA scheme for the detection of Z34C-presenting viral particles. Immobilization is achieved by binding a IgG molecule. Intact viral capsids can be specifically bound by the biotinylated A20 antibody which can be detected by Streptavidin-HRP; **B**) ELISA using the principle described in A for loop insertion samples obtained by gel filtration chromatography of 453- and 587-Z34C particles. Undiluted and 10-fold diluted samples were employed **C**) ELISA signals obtained by absorbance measurements from B at 405 nm, undiluted samples; **D**) ELISA signals obtained by absorbance measurements from B at 405 nm, diluted samples

Three samples of different viral particles with insertions of the antibody-binding motif Z34C were successfully purified by the gel filtration chromatography. The fractions around the void volume were

subsequently used in two different sandwich ELISAs. The first one aims at the detection of the particle's ability to bind IgG-antibodies. The therapeutical antibody Cetuximab was employed to test the affinity of the virus particles. As displayed in figure 1A, only Z34C-presenting particles should be immobilized and only assembled viral capsid will be detected due to the affinity of the A20 antibody (as described above). Figure 1B shows that absorbance signal were obtained in case of the 587KO-Z34C and 587KO-Z34C-spacer insertions. Loop 453-Z34C did not yield any significant absorbance signals. In addition, the assay was performed with undiluted samples and those which were 10-fold diluted in PBST + 0.5 % BSA. Signal strengths in the undiluted ELISA samples indicated that the assay was saturated, therefore the diluted sample data were used for evaluation. The ABTS conversion indicates that highest amount of Z34C-presenting viral particles is present in the Äkta fractions 7-9 of the two different 587 insertions. No viral particles with a binding affinity for the IgG antibody were present in the 453 samples.

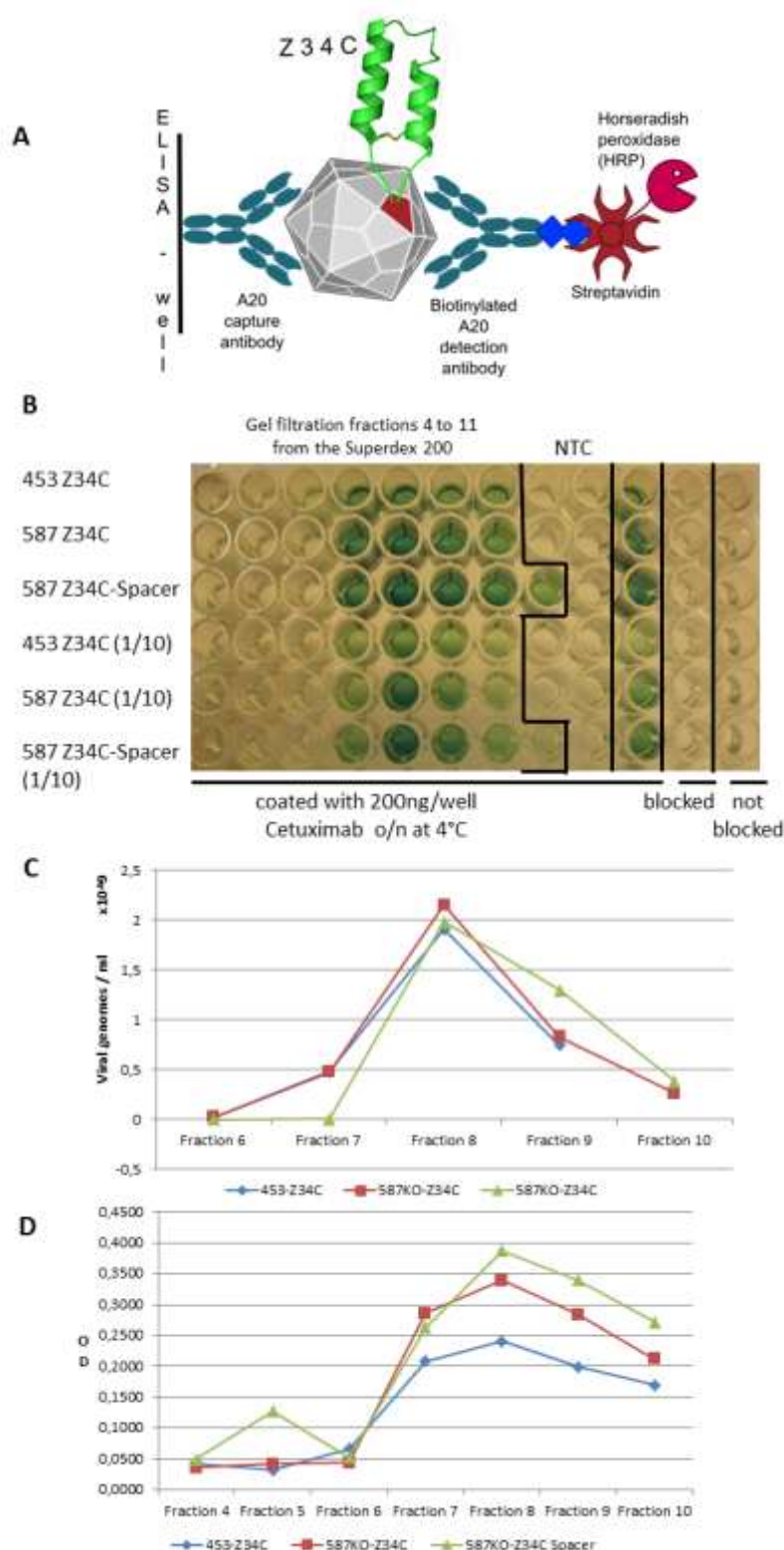
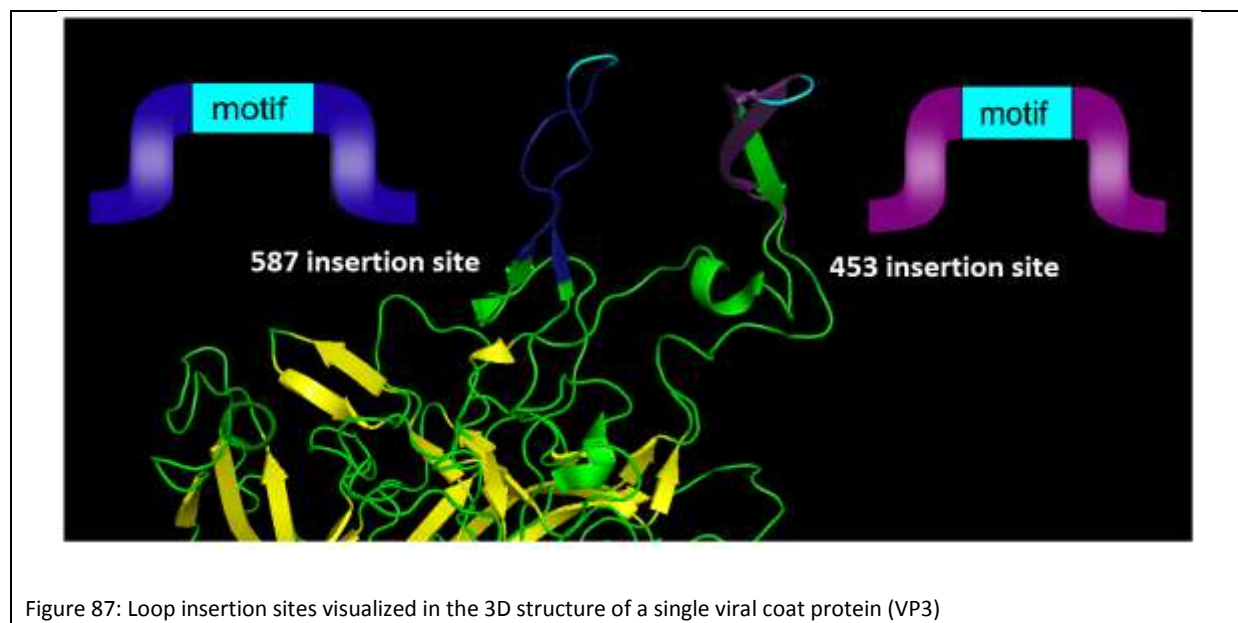


Figure 86: **A)** Sandwich-ELISA scheme for the detection of AAV-2 particles. Immobilization is achieved by binding to the A20 capture molecule which also acts as the biotinylated detection antibody after washing. Intact viral capsids can be specifically detected by Streptavidin-HRP; **B)** ELISA using the principle described in A for loop insertion samples obtained by gel filtration chromatography of 453- and 587-Z34C particles. Undiluted and 10-fold diluted samples were employed; **C)** qPCR data for the CMV-promoter-based DRP-titer determination. Samples as in B; **D)** ELISA signals obtained by absorbance measurements from B at 405 nm, diluted samples

A second approach was conducted to reveal the reason for the absence of Z34C-presenting particles in case of the 453 insertion. The sandwich ELISA, as shown in figure 2A, uses the A20 antibody to capture and detect all assembled viral capsids independent of the presence of a Z34C motif giving the so-called physical AAV titer (see figure 2D). To correlate these measurements, we additionally conducted qPCR measurements to determine the amount of encapsidated vector plasmids, the so-called DRP (DNase-resistant particle) titer (see figure 2C). Comparison reveals that both assays yielded a peak signal around the Äkta fraction 8. The qPCR data indicated that all samples contain approximately 2×10^9 copies of the vector plasmid per milliliter. Assuming equal packaging efficiencies for the vector plasmids, all three loop insertion approaches contain comparable amounts of viral capsids. The sandwich-ELISA yielded a peak around fraction eight for all three loop-insertion approaches. Since the signal strength for the 587KO-Z34C samples is significantly higher, it can be assumed that additionally to the affinity of the A20 antibody for assembled viral capsids, the Z34C-containing viral particles add a high affinity for the Fc-part of the detection antibody. Hence the qPCR-titration only depends on the number of encapsidated AAV-vector plasmids and not on the viral capsid and its degree of modification, it is the more quantitative method of particle titration which proved equal for all three loop insertion approaches.

Summarizing, the insertion of a 34/39 amino acid functional motif into the two most promising integration sites of the AAV-2 capsid (see figure 3) revealed no integration of modified viral capsid proteins (VP1-3) into assembled viral capsids for the 453 integration site. As also seen by the data obtained for the linker-containing insertion, the 587 region tolerates insertions of at least 39 amino acids. For the 453 integration site, either the inserted Z34C motif loses its ability to bind IgG molecules or the influence of the inserted motif causes strong structural changes that disturb the ability of the modified VP proteins to be integrated into the virus capsid.

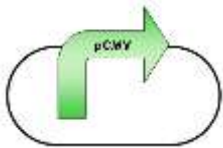

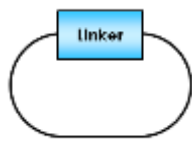





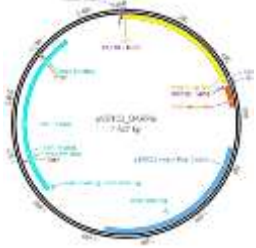


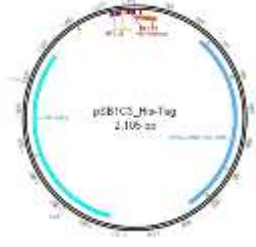

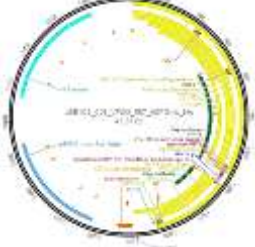




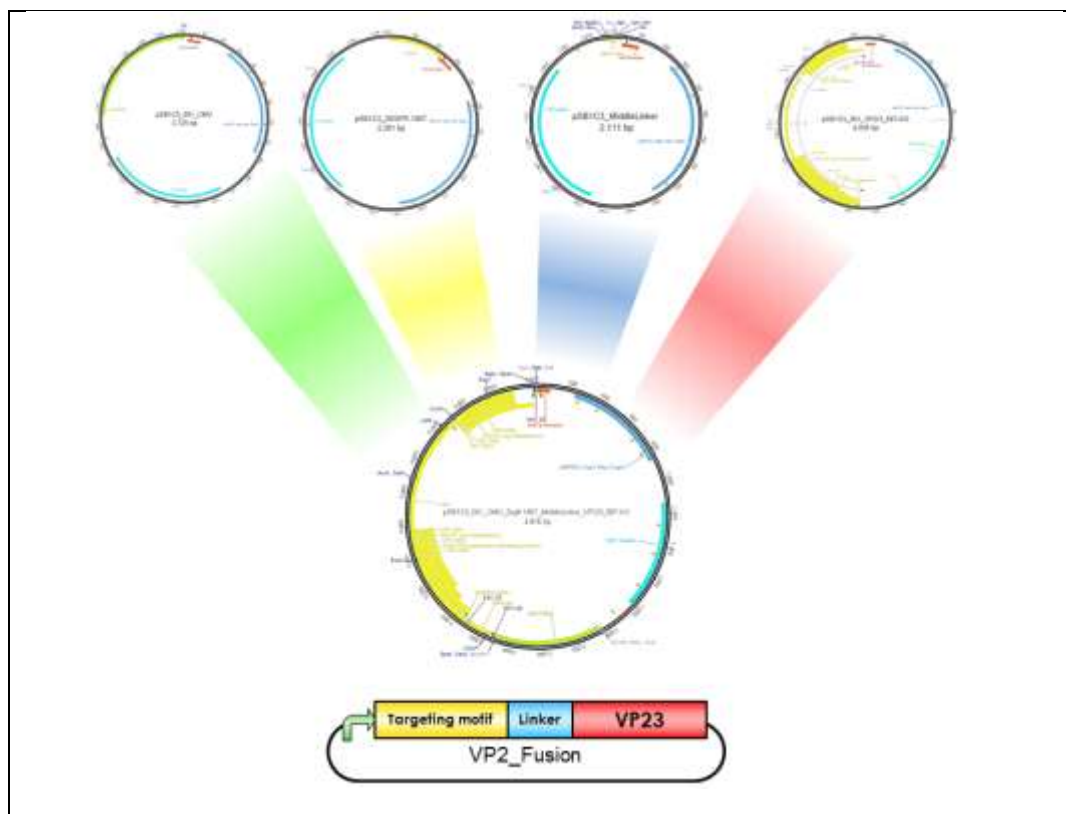
5.4 N-terminal Fusion of Targeting Molecules for Targeting and Tumor Killing

5.4.1 Design of VP2 Fusion

The Freiburg2010 team fused motifs which are desired to be surface exposed to the N-terminus of VP2/3 open reading frame, avoiding steric hindrance by connecting them with linker. We ensured in frame coupling by designing or using the referring parts in the Freiburg RFC25 standard, thus creating fusion constructs via NgoMIV and AgeI. For retargeting AAV2 virus particles towards EGFR over expressing cancer cells we investigated the Z_{EGFR:1907} Affibody and the E01 DARPIn – in combination with VP2/3_587-KO (HSPG knock down) – as surface exposed motifs. We also created so called “all-in-one” virus particles by fusing VP2/3_His-Tag or VP2/3_BAP via Middle Linker to the Affibody. Purification or imaging approaches could be conducted by His-Tag or CFP motifs, respectively. All constructs were cloned downstream of the CMV promoter (Figure 88: Cloning scheme of VP2 fusionFigure 88).

Table 5: List of VP2 fusion parts

Promoter	Motifs	Linker	VP2/3
			
CMV	Affibody Z _{EGFR:1907}	Short Linker	VP2/3_587-KO
			
	DARPin E01	Middle Linker	VP2/3_587-KO_BAP
			
	His-Tag	Long Linker	VP2/3_587-KO_His
			
	CFP	SEG Linker	
			



First of all we fused the Affibody ZEGFR:1907 to the Short-, Middle-, Long- or SEG Linker and cloned the resulting constructs downstream of the CMV promoter. Afterwards either unmodified VP2/3 or HSPG affinity knock down VP2/3 were fused to the different linkers. Further on CFP and His-Tag were coupled to VP2/3 by the Middle Linker (Figure 89).

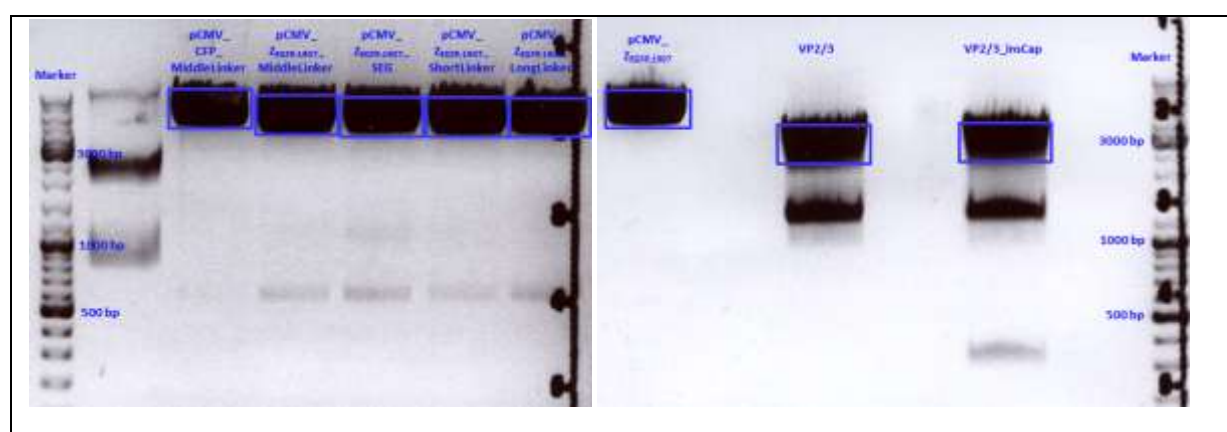
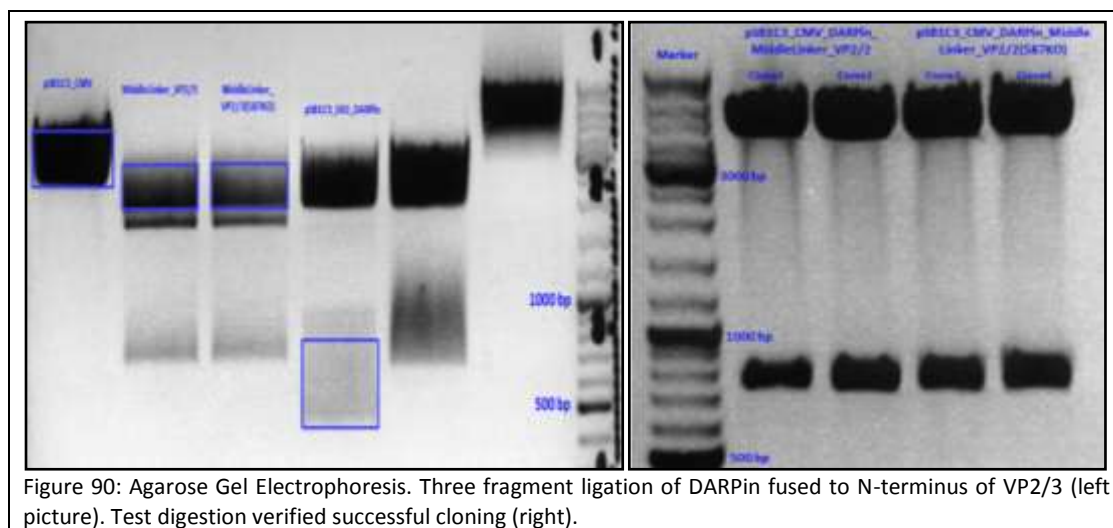
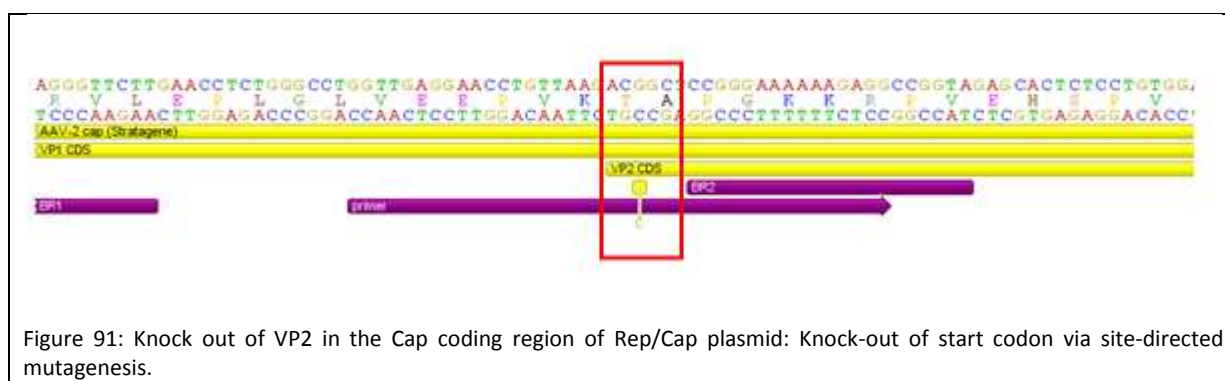


Figure 89: Agarose Gel Electrophoresis. Fusion of VP2/3 to CMV_Affibody_Linker or CMV_CFP_MiddleLinker constructs.

We conducted three fragment ligations with the DARPin E01, MiddleLinker_VP2/3 or MiddleLinker_VP2/3(587KO) and pSB1C3_CMV plasmid (Figure 90).




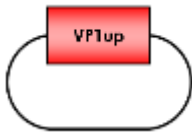
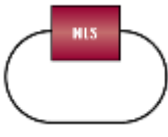

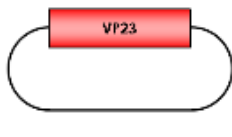

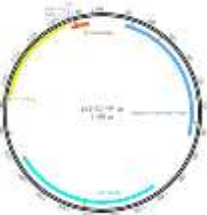
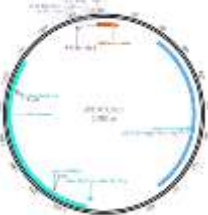
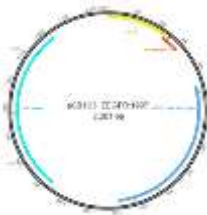
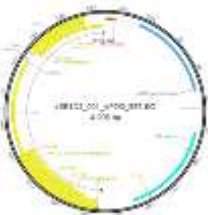
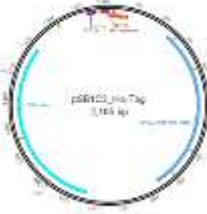

For 100 % replacement of wildtype VP2 the fusion plasmid was co-transfected to the Rep/Cap plasmid which contained a start codon mutation of VP2. Wildtype VP2 knock-out was achieved by site-directed mutagenesis (Figure 91).

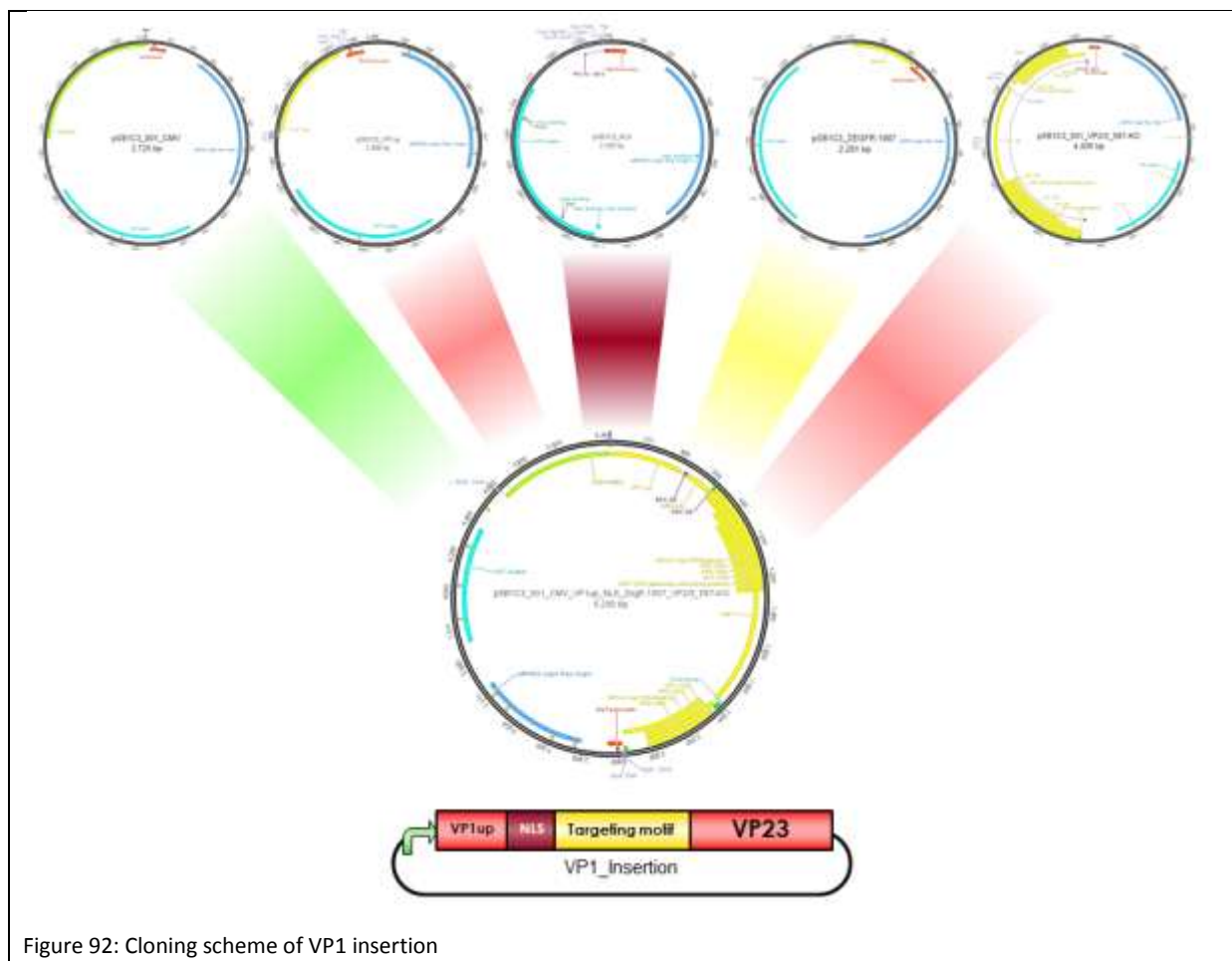


5.4.2 Design of the VP1 Insertion

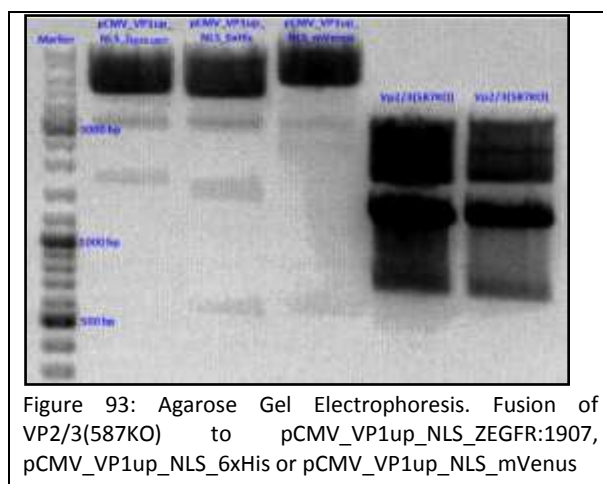
We inserted three different motifs into the VP1 open reading frame. They were fused, together with the unique upstream region of VP1 (VP1up) and a nuclear localization sequence (NLS), according to the RFC25 standard to VP2/3 (Figure 92). Again, all of these parts were driven by CMV promoter.

Table 6: List of VP1 insertion parts

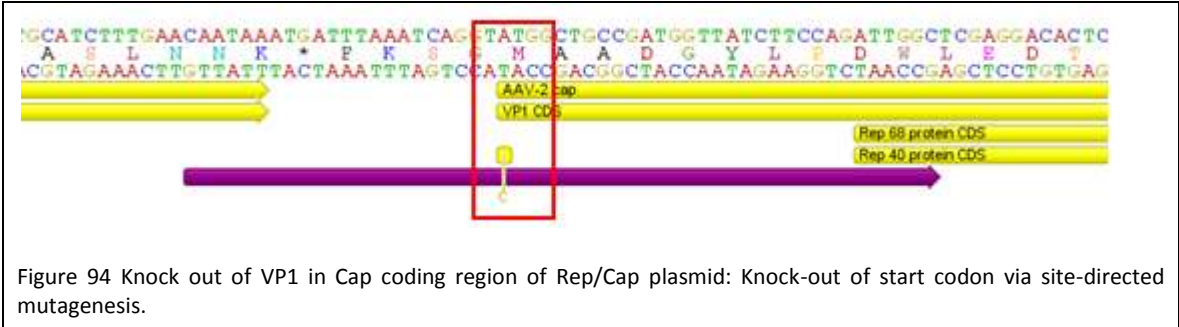
Promoter	VP1up	NLS	Motif	VP2/3
				
CMV 	VP1up 	NLS 	Affibody Z _{EGFR} :1907 	VP2/3_587-KO 
			His-Tag 	
			mVenus 	



First VP1up-NLS was fused to the surface exposed motif – Affibody, His-Tag or mVenus – and the resulting constructs were cloned downstream of the CMV promoter. This was followed by either fusing unmodified VP2/3 or HSPG affinity knock down VP2/3 to the different kinds of motifs (Figure 93).



We designed site-directed mutagenesis primer for the VP1 start codon modification in the Rep/Cap plasmid in order to ensure 100 % replacement with modified VP1 proteins (Fig. 7).



5.4.3 Colony PCR

Big amounts of samples necessitated fast and exact analysis of cloning. For this purpose colony PCR was conducted. We verified successful VP2/3 fusion by using primer that exclusively bound to a specific location in the VP2/3 sequence (**Error! Reference source not found.**). In the case of successful ligation a 880 bp fragment was amplified via Taq polymerase.

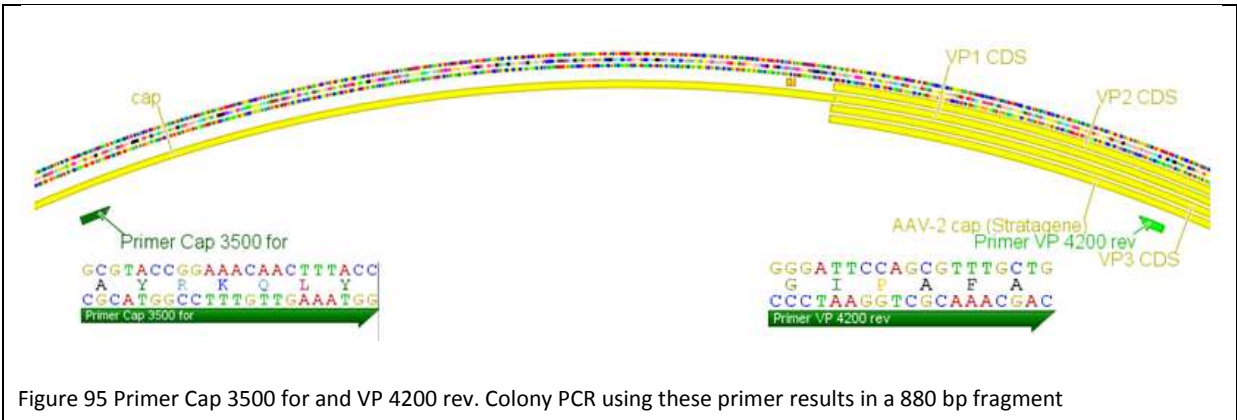
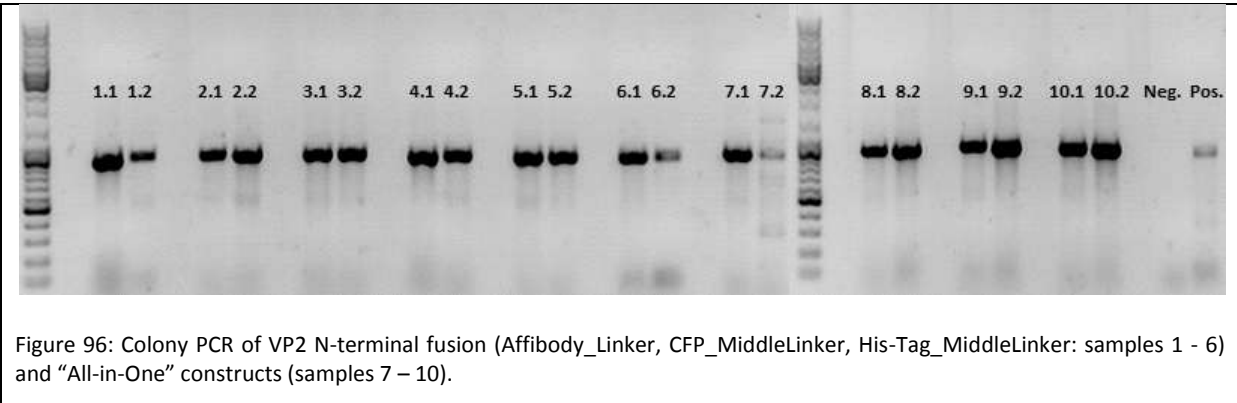
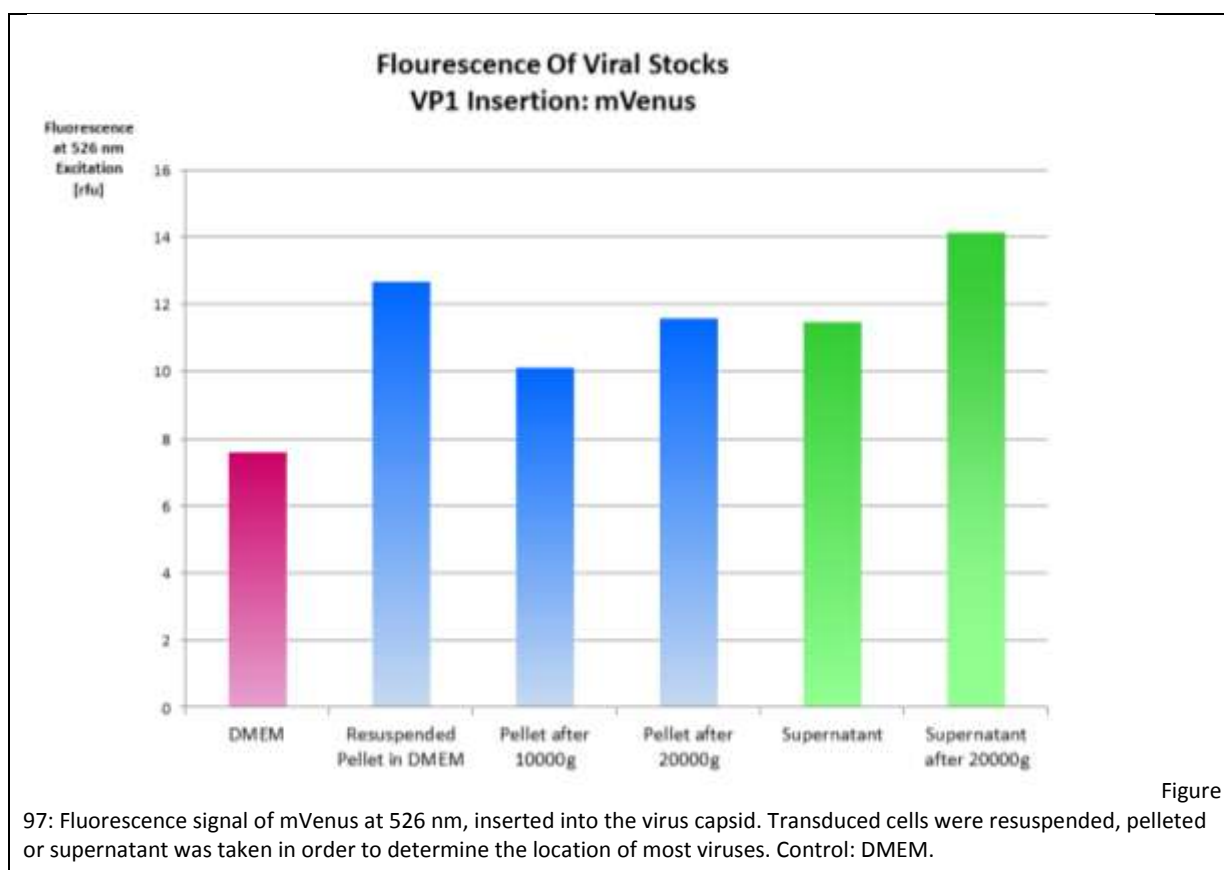


Figure 96 demonstrates a colony PCR example: VP2 fusion constructs containing VP2/3(587) sequence and the so called “All in One” constructs were cloned into pSB1C3_CMV. Successful cloning could be verified (positive control: pAAV_RC; negative control: pSB1C3_IITR)



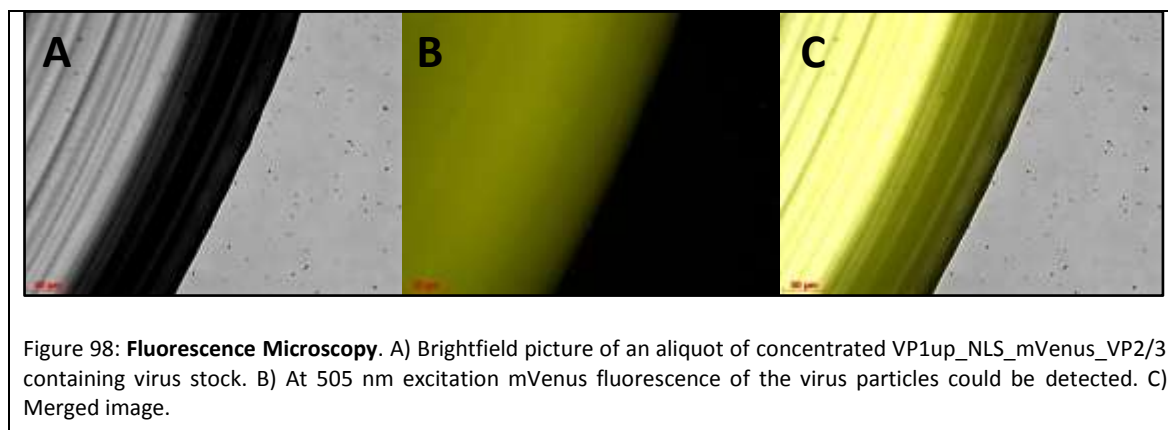
5.4.4 Fluorescence analysis of viral stocks

We wanted to develop a protocol for harvesting as much viruses as possible. For this purpose we took advantage of viruses containing mVenus fused to VP1. In order to find out whether most viruses were located in the cell pellet, cell suspensions were centrifuged at 10.000 g or 20.000 g. Afterwards mVenus fluorescence was measured at 526 nm. The resulting values were compared to cell culture supernatant, 20.000 g centrifuged supernatant and resuspended cell pellet (Figure 97).



5.4.5 Concentrating VP1UP_NLS_mVENUS_VP2/3 Viruses

For further analysis, viral stocks originating from cell culture supernatant needed to be concentrated. Therefore ultrafiltration with protein concentrators (Sartorius VivaSpin 20; 20.000Da MWCO) was conducted. Figure 98 shows fluorescence microscopy image of an aliquot from ultrafiltrated cell culture supernatant / cell lysate containing VP1up_NLS_mVenus_VP2/3 viruses.



5.4.6 Fluorescence microscopy

AAV-293 cells were transfected with a 50:50 ratio of the Rep/Cap(VP1KO) to the CMV_VP1_NLS_mVenus_VP2/3 plasmid. We packaged mCherry, driven by the CMV promoter, into the virus capsids and followed protein expression via fluorescence microscopy. 30 hours post transfection mCherry fluorescence was detectable in the whole cytosol of the successfully transfected cells, demonstrating that DNA located between the AAV2 ITRs is already transcribed in the producer cell line. In contrast to that mVenus fluorescence signal could be observed only in the nuclei (Figure 99). This indicated that the nuclear localization sequence targets the single VP1_NLS_mVenus_VP2/3 proteins efficiently to the cell nucleus, where assembly and packaging of the virus particles takes place.

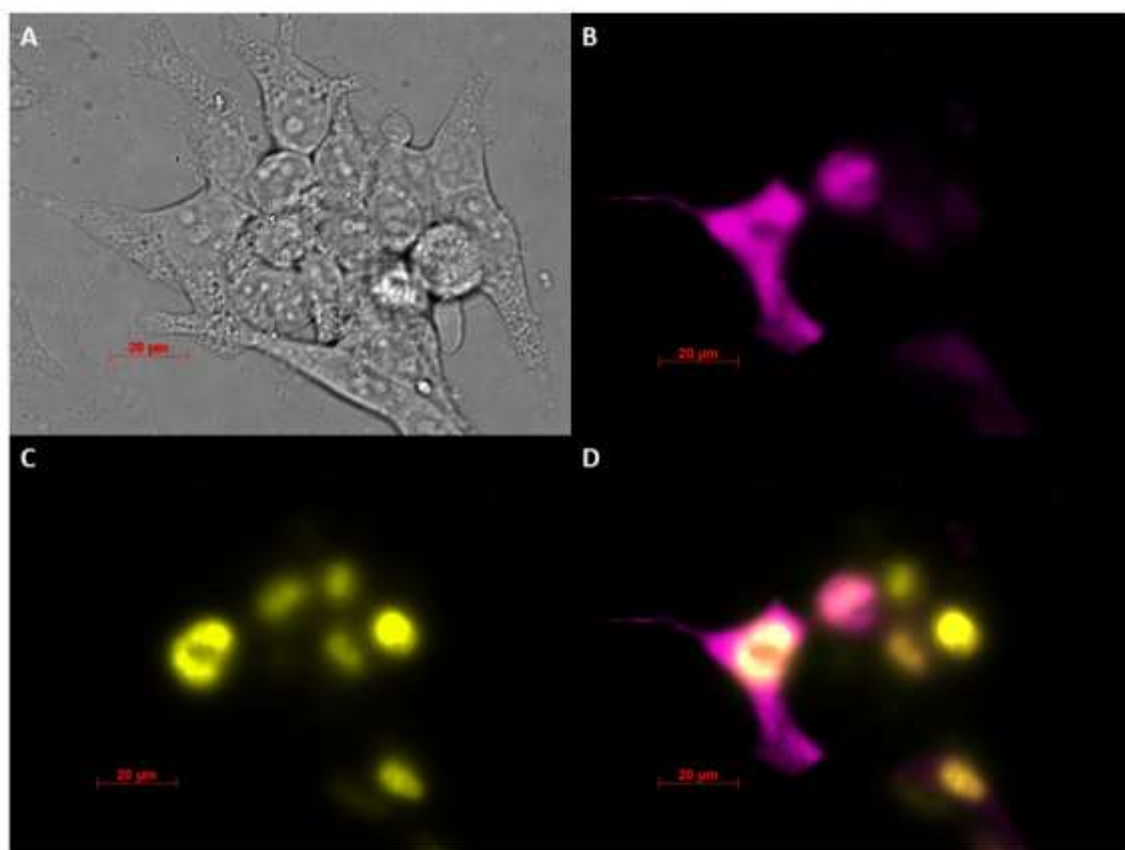
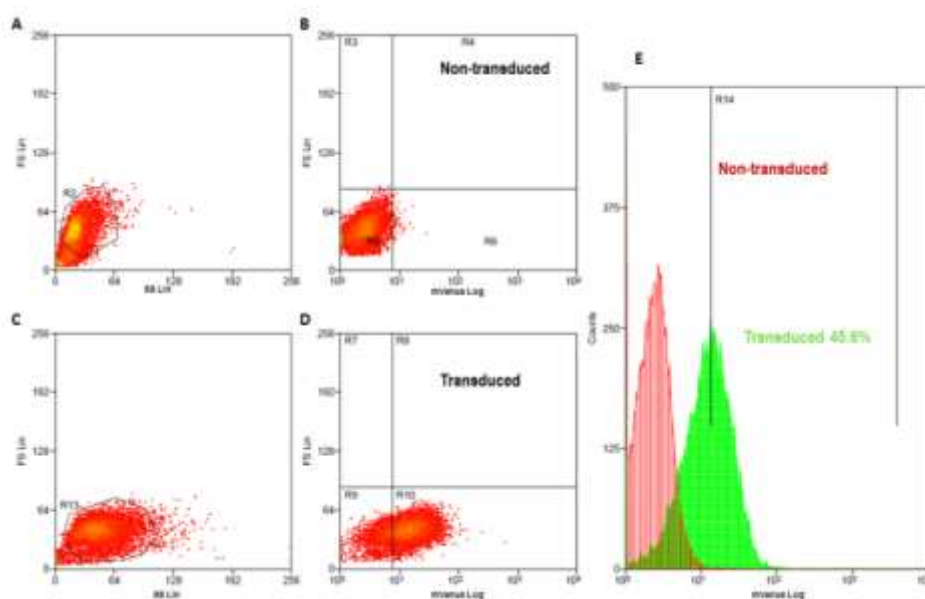


Figure 99: Fluorescence Microscopy. A) Brightfield picture. B) Excitation at 555 nm showed mCherry signal in the cytosol. C) Excitation at 505 nm revealed mVenus fluorescence in the nuclei, indicating functionality of the nuclear localization sequence inserted – together with mVenus – into VP1. D) Merged image

5.4.7 Flow cytometry

For determination of transduction efficacy flow cytometry analysis was conducted. The Affibody $Z_{EGFR:1907}$ was fused with SEG-, middle- and long linker to the VP2/3 open reading frame (ORF) in order to investigate differences in infection efficacy due to different linker lengths. 250.000 AAV-293 cells were transfected with 1 µg total DNA. Different ratios of VP2 fusion constructs in respect to the Rep/Cap plasmid were co-transfected. 72 hours post transfection viruses were harvested and two different cell lines, HT1080 and A431, were transduced with 1 mL virus stock. By encapsulating mVenus coding sequence, the amount of transduced cells could be determined via flow cytometry

HT1080 cells:



A431 cells:

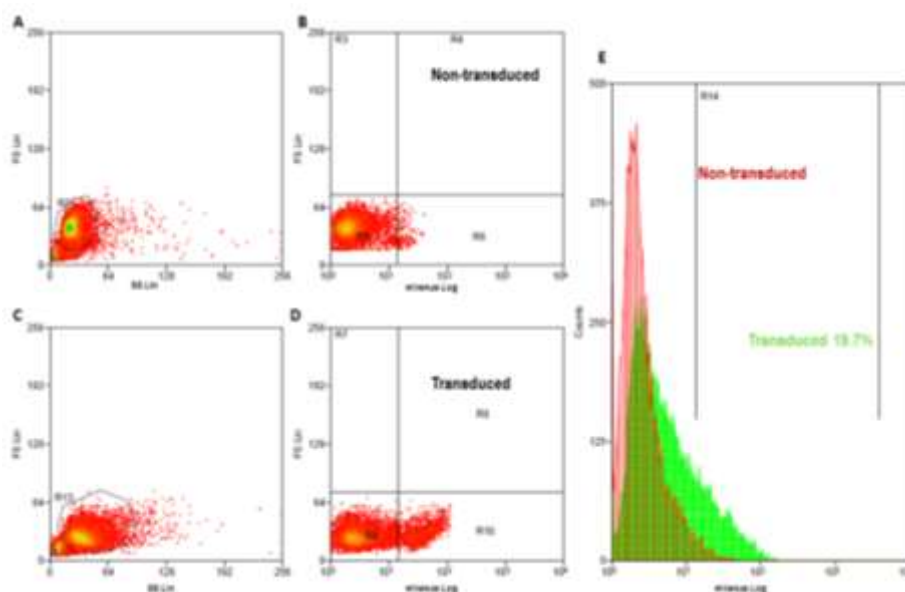


Figure 100: Flow cytometry. Test of transduction efficiency with HT1080 and A431 cells by detecting mVenus expression from **Z_{EGFR:1907}_Middlelinker_VP2/3** virus particles (Transfection ratio: 50:50 in respect to Rep/Cap plasmid). A) Gating non transduced cells (control); subcellular debris and cellular aggregates can be distinguished from single cells by size, estimated via forward scatter (FS Lin) and granularity, estimated via side scatter (SS Lin). B) : Non transduced cells plotted against mVenus fluorescence (Analytical gate was set such that 1% or fewer of negative control cells fell within the positive region (R6)). C) Gating transduced cells. D) Transduced cells plotted against mVenus fluorescence, R10 comprised transduced, mVenus expressing cells. E) Overlay of non-transduced (red) and transduced (green) cells plotted against mVenus fluorescence.

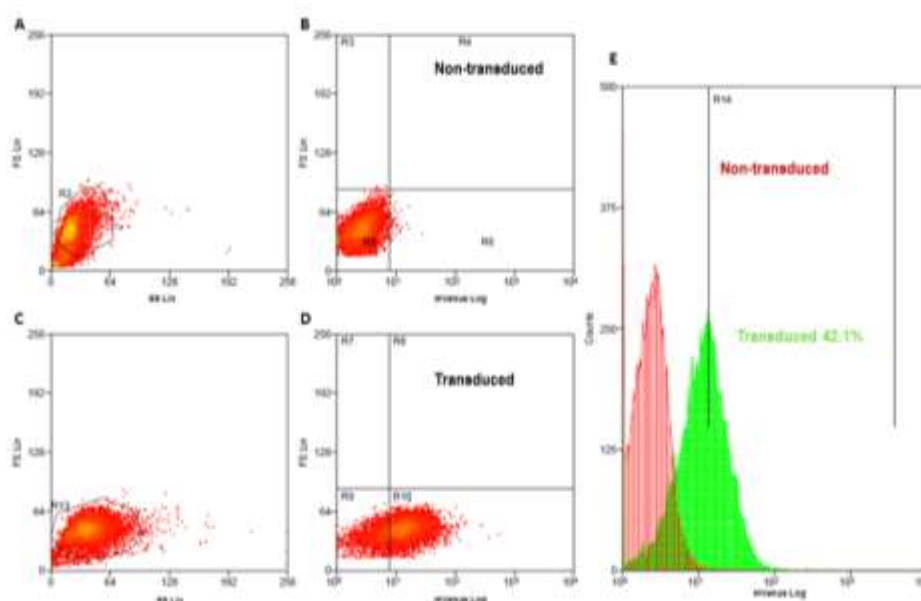
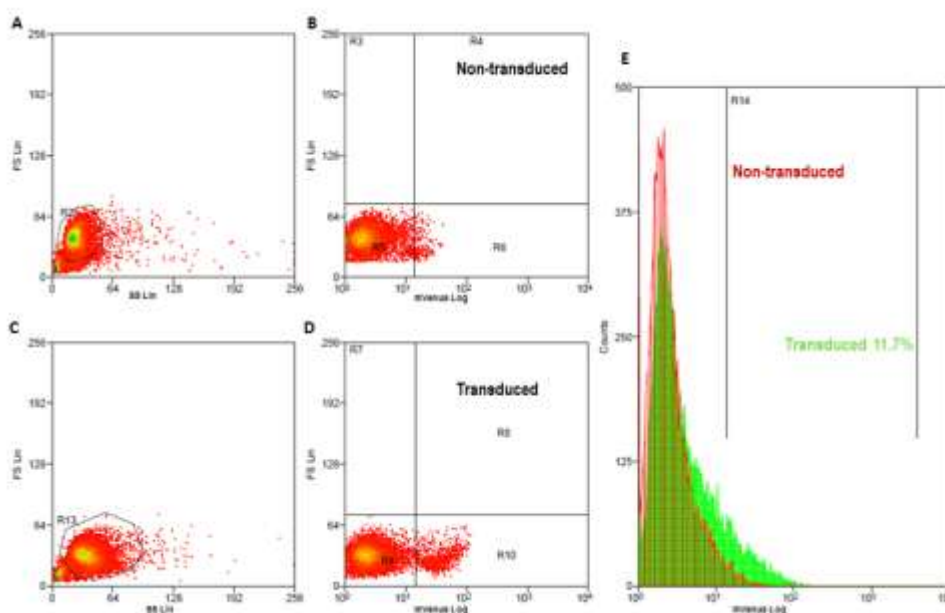
HT1080 cells:**A431 cells:**

Figure 101: Flow cytometry. Investigating transduction efficiency with HT1080 and A431 cells by detecting mVenus expression from **Z_{EGFR:1907}_SEG_VP2/3** virus particles (Transfection ratio: 50:50 in respect to Rep/Cap plasmid). A) Gating non transduced cells (control); subcellular debris and cellular aggregates can be distinguished from single cells by size, estimated via forward scatter (FS Lin) and granularity, estimated via side scatter (SS Lin). B) : Non transduced cells plotted against mVenus fluorescence (Analytical gate was set such that 1% or fewer of negative control cells fell within the positive region (R6). C) Gating transduced cells. D) Transduced cells plotted against mVenus fluorescence, R10 comprised transduced, mVenus expressing cells. E) Overlay of non-transduced (red) and transduced (green) cells plotted against mVenus fluorescence.

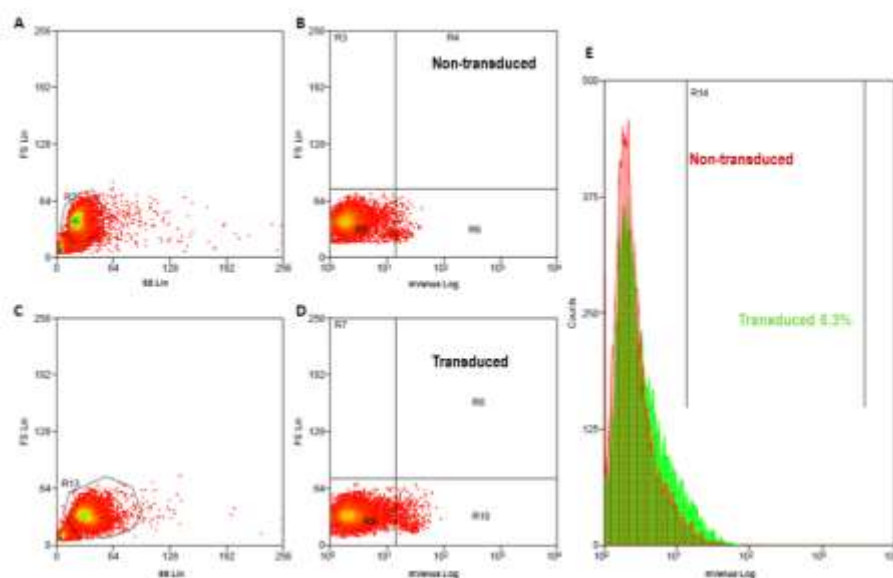
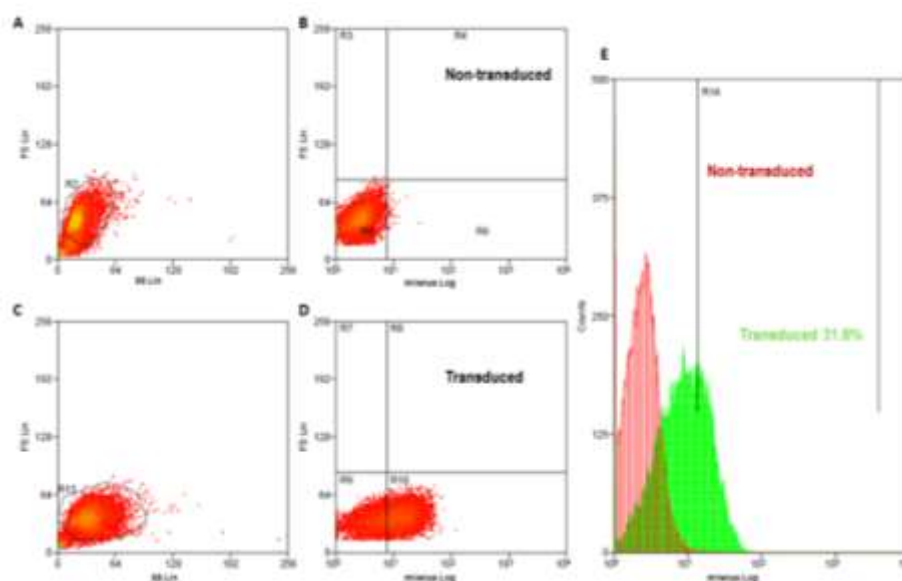
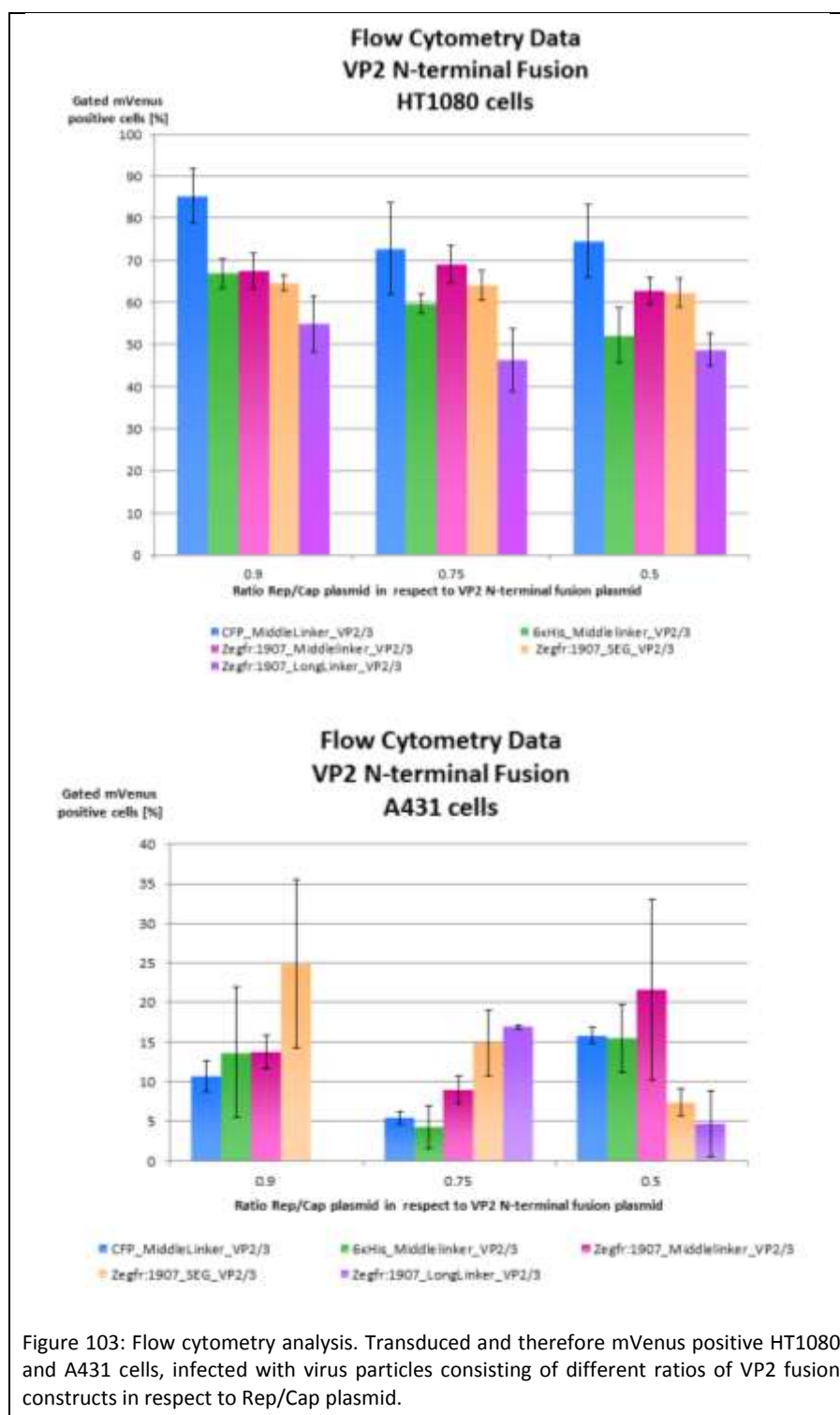
HT1080 cells:**A431 cells:**

Figure 102: Flow cytometry. Investigating transduction efficiency with HT1080 and A431 cells by detecting mVenus expression from **Z_{EGFR:1907}_LongLinker_VP2/3** virus particles (Transfection ratio: 50:50 in respect to Rep/Cap plasmid). A) Gating non transduced cells (control); subcellular debris and cellular aggregates can be distinguished from single cells by size, estimated via forward scatter (FS Lin) and granularity, estimated via side scatter (SS Lin). B) : Non transduced cells plotted against mVenus fluorescence (Analytical gate was set such that 1% or fewer of negative control cells fell within the positive region (R6). C) Gating transduced cells. D) Transduced cells plotted against mVenus fluorescence, R10 comprised transduced, mVenus expressing cells. E) Overlay of non transduced (red) and transduced (green) cells plotted against mVenus fluorescence.

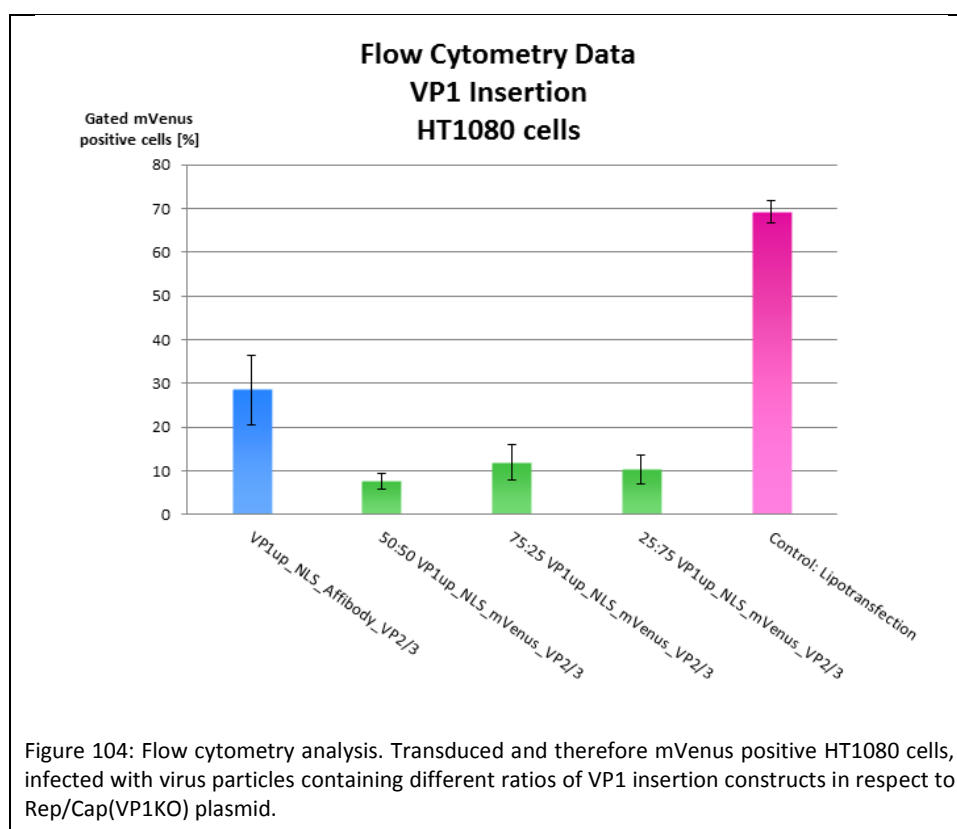
Additionally viruses containing a His-Tag or CFP, fused via Middle Linker to the VP2/3 ORF, were analyzed. Figure 103 overviews transduction efficacy of all constructs, transfected in a 10:90, 25:75 and 50:50 ratio in respect to Rep/Cap plasmid.



Transduction of HT1080 cells revealed that all viral particles regardless of which motifs inserted into the capsids remained infectious with efficacies up to 85 %. In general the amount of mVenus positive cells decreased only slightly when harboring more modified VP2 subunits. This indicates that larger

peptides could be inserted into the AAV2 capsids without affecting virus assembly and packaging. A431 cells, which overexpress EGF receptor, were generally transduced with reduced efficacy.

Further on the Affibody Z_{EGFR:1907} or mVenus were inserted into the VP1 ORF together with a nuclear localization signal. 250.000 AAV-293 cells were transfected with 1 µg total DNA and different ratios of VP1 insertion constructs in respect to the Rep/Cap(VP1KO) plasmid were co-transfected. 72 hours post transfection viruses were harvested and HT1080 and A431 cells were transduced. 48 hours later the number of transduced, or to be precise mVenus positive, cells was determined via flow cytometry (Figure 104, Figure 105).



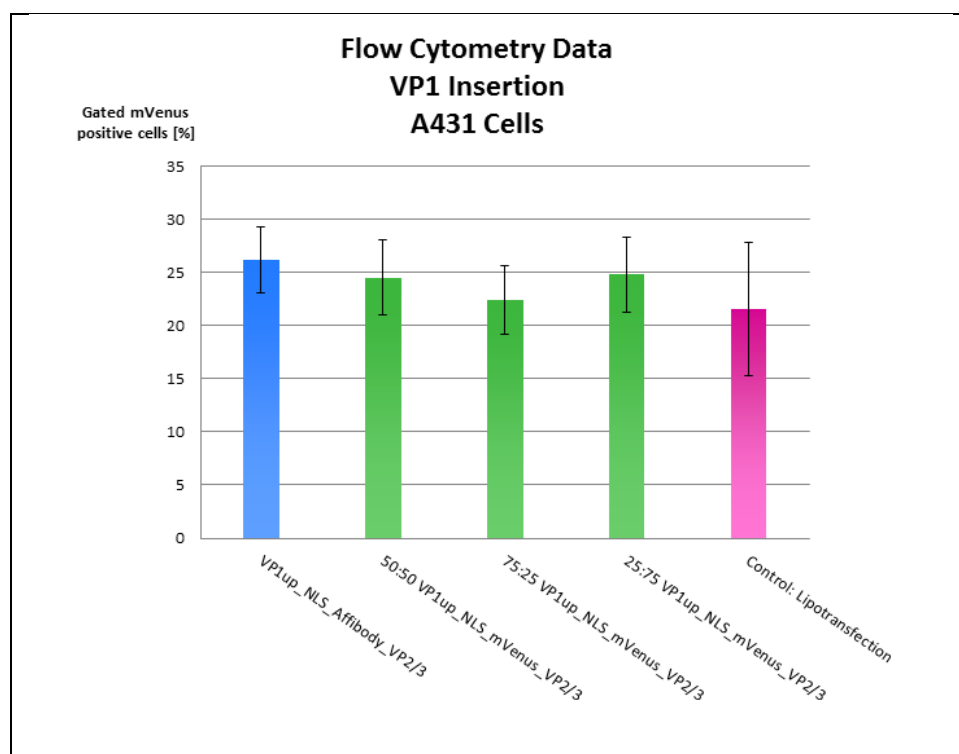


Figure 105: Flow cytometry analysis. Transduced and therefore mVenus positive A431 cells, infected with virus particles containing different ratios of VP1 insertion constructs in respect to Rep/Cap(VP1KO) plasmid.

Again results revealed that all virus particles remained infectious, regardless of whether inserting the Affibody or mVenus. This indicated that VP1 tolerated larger peptides inserted downstream of its unique N-terminal region and that this modification still allowed virus assembly and packaging.

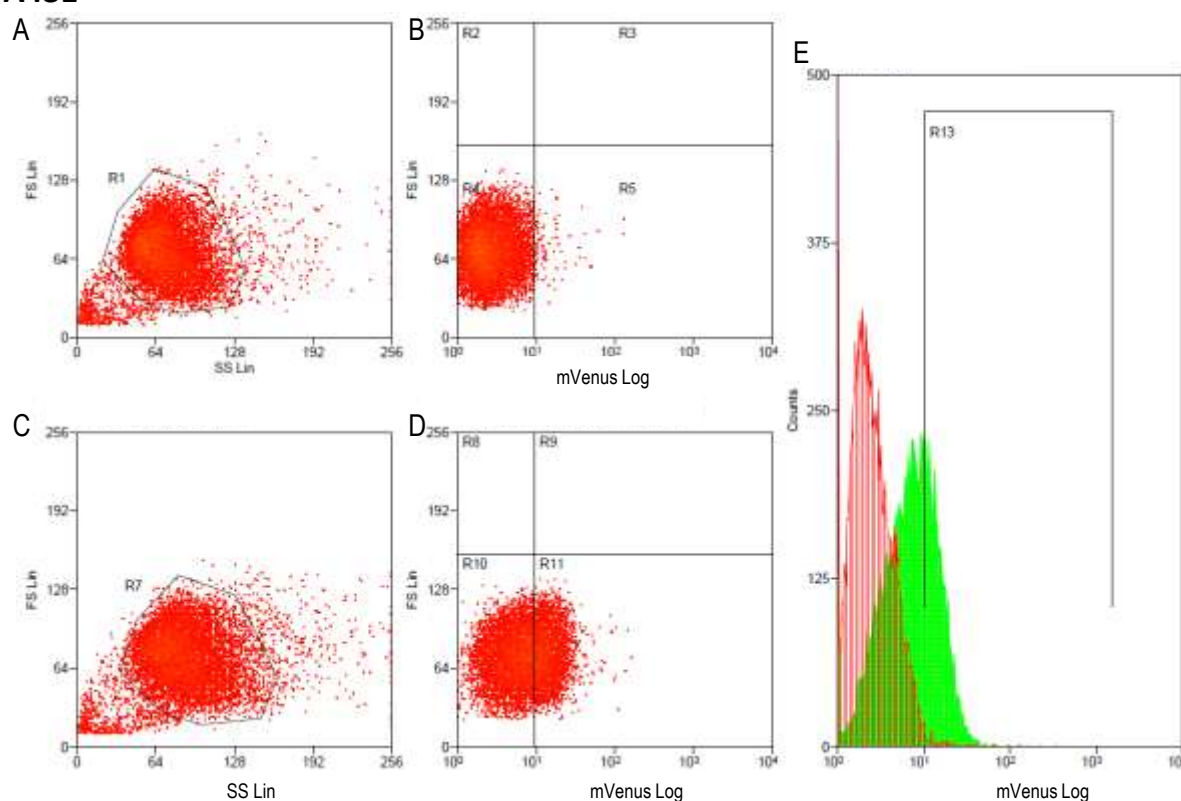
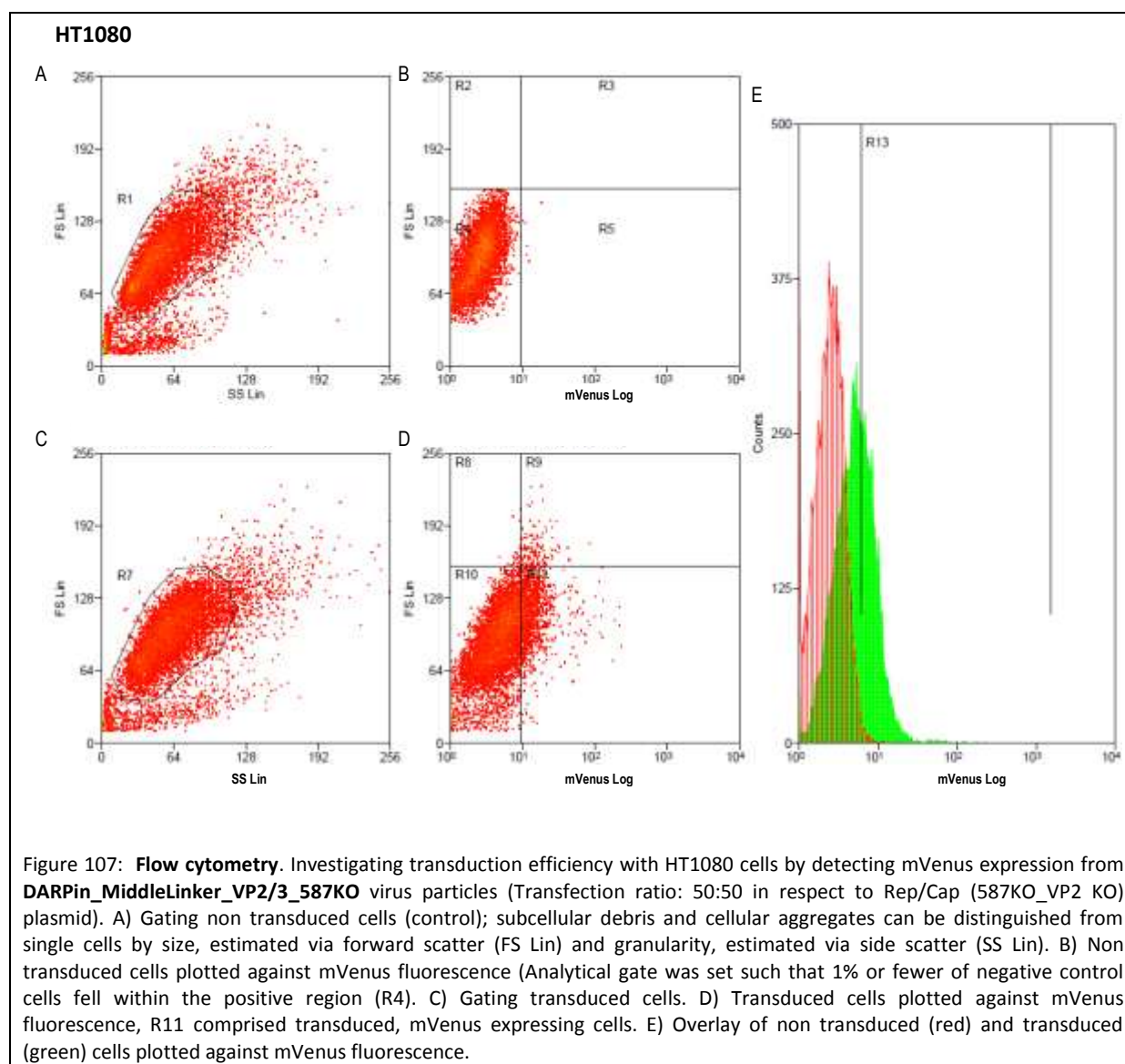
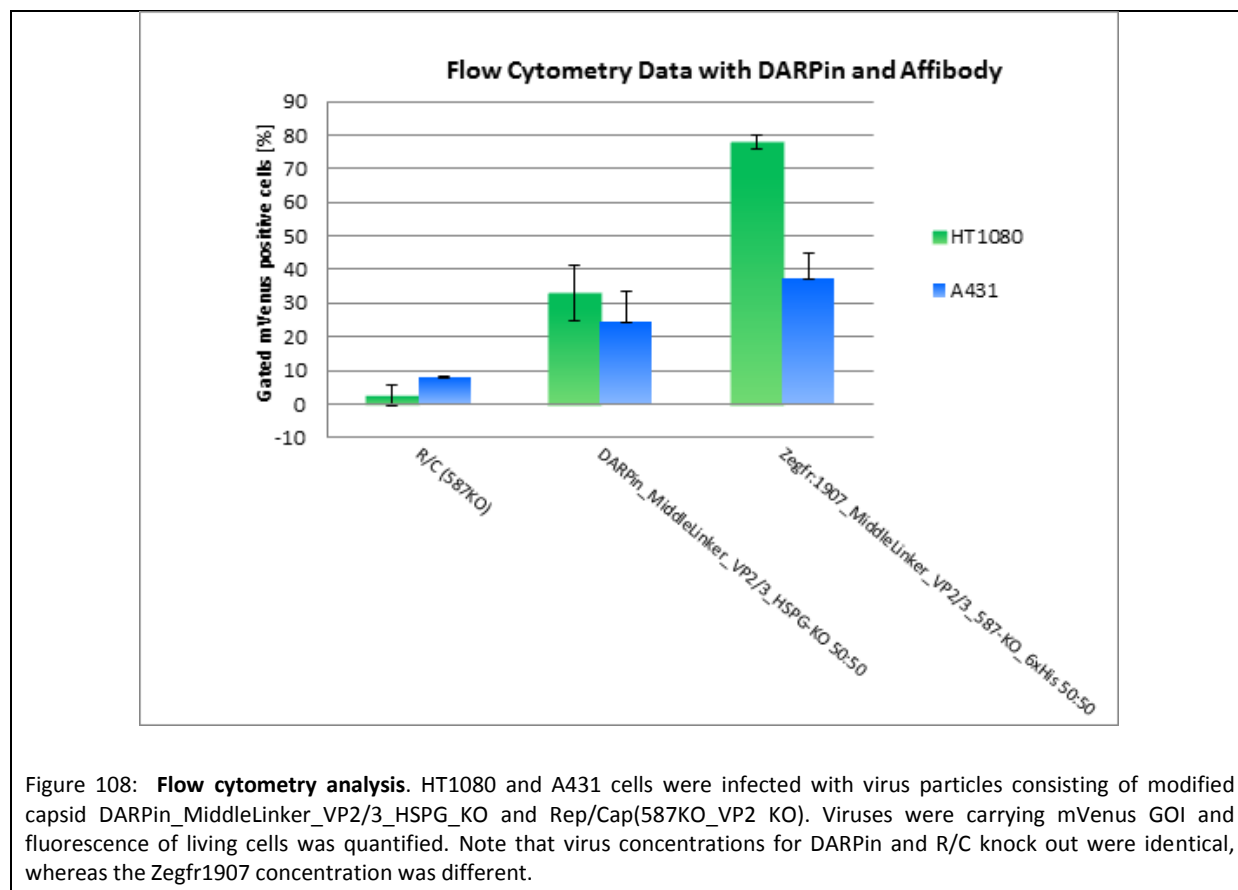
A431

Figure 106: **Flow cytometry.** Investigating transduction efficiency with A431 cells by detecting mVenus expression from **DARPin_MiddleLinker_VP2/3_587KO** virus particles (transfection ratio: 50:50 in respect to Rep/Cap (587KO_VP2 KO) plasmid). A) Gating non transduced cells (control); subcellular debris and cellular aggregates can be distinguished from single cells by size, estimated via forward scatter (FS Lin) and granularity, estimated via side scatter (SS Lin). B) Non transduced cells plotted against mVenus fluorescence (Analytical gate was set such that 1% or fewer of negative control cells fell within the positive region (R4). C) Gating transduced cells. D) Transduced cells plotted against mVenus fluorescence, R11 comprised transduced, mVenus expressing cells. E) Overlay of non transduced (red) and transduced (green) cells plotted against mVenus fluorescence.





Transduction of HT1080 cells revealed that viral particles containing the targeting motifs inserted into the capsids remained infectious with efficacies up to 75 %. A431 cells, which overexpress EGF receptor, were generally transduced with reduced efficacy.

In general, results revealed that the inefficient transfection-rate of the viral particles containing only the HSPG KO included into the capsid can be rescued by insertion of targeting motifs, such as Affibody or DARPin.

As you can see in **Figure 108**, transduction efficiency is up to 4- fold higher by usage of constructs containing targeting motifs.

250.000 AAV-293 cells were transfected with 1 µg total DNA and different targeting constructs in respect to the Rep/Cap(587KO_VP2 KO) plasmid were co-transfected. 72 hours post transfection viruses were harvested and HT1080 and A431 cells were transduced. 48 hours later the number of transduced, or to be precise mVenus positive, cells was determined via flow cytometry (**Figure 106**, **Figure 107**).

To sum up, results revealed that all virus particles maintained infectious. Moreover, insertion of Affibody or DARPin even increases the transduction efficiency.

qPCR

We transfected 250.000 AAV-293 cells with 1 µg of total DNA composed of equal amounts of Rep/Cap, pHelper and vector plasmid. VP2 fusion or VP1 insertion plasmids were co-transfected with two different ratios in respect to Rep/Cap(VP1KO) or Rep/Cap(VP2KO): 25 % VP2 fusion or VP1 insertion proteins allow better assembly and packaging of the virus particles, compared to 50 % VP2 fusion or VP1 insertion proteins which increase the chance of integration into the capsids.

We created viruses containing the Z_{EGFR:1907} Affibody fused to VP2 or inserted into VP1 and the DARPin E01 fused to VP2. These types of AAV2 particles were produced in two versions: With or without HSPG binding affinity knock down (587KO).

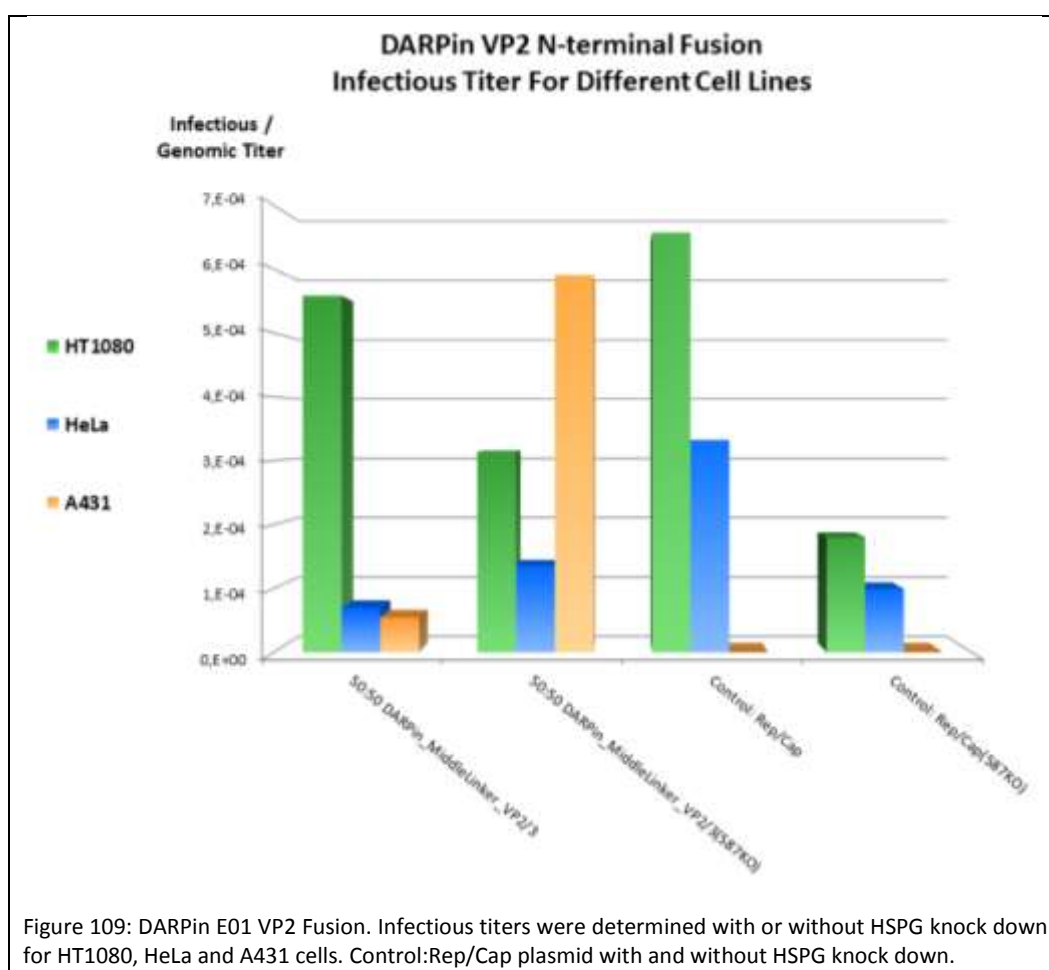
Viruses were harvested three days post transfection. The genomic titer was determined via qPCR by amplification of a specific sequence located in the CMV promoter of the vector plasmid (Table 7).

Table 7: Quantitative Real-Time PCR. Determination of genomic titer. Data were corrected for negative control value.

Co-transfected Construct	Ratio	Genomic Titer /1ml Corrected For Negative Control
Affibody_MiddleLinker_VP2/3	25:75	2,20E+08
Affibody_MiddleLinker_VP2/3	50:50	2,39E+08
Affibody_MiddleLinker_VP2/3(587KO)	25:75	1,17E+09
Affibody_MiddleLinker_VP2/3(587KO)	50:50	5,44E+08
CFP_MiddleLinker_VP2/3(587KO)	25:75	3,63E+09
CFP_MiddleLinker_VP2/3(587KO)	50:50	1,67E+09
6xHis_MiddleLinker_VP2/3(587KO)	25:75	3,37E+09
6xHis_MiddleLinker_VP2/3(587KO)	50:50	1,38E+09
VP1up_NLS_Affibody_VP2/3	25:75	3,52E+09
VP1up_NLS_Affibody_VP2/3	50:50	1,50E+09
VP1up_NLS_Affibody_VP2/3(587KO)	25:75	6,98E+08
VP1up_NLS_Affibody_VP2/3(587KO)	50:50	5,30E+08
VP1up_NLS_6xHis_VP2/3(587KO)	25:75	5,25E+09
VP1up_NLS_6xHis_VP2/3(587KO)	50:50	1,65E+09
DARPin_MiddleLinker_VP2/3	25:75	4,36E+08
DARPin_MiddleLinker_VP2/3	50:50	3,93E+08
DARPin_MiddleLinker_VP2/3(587KO)	25:75	1,00E+09
DARPin_MiddleLinker_VP2/3(587KO)	50:50	3,99E+08
Control: Rep/Cap	100%	1,55E+08
Control: Rep/Cap(587KO)	100%	5,39E+08

We investigated transduction of different cell lines. For this purpose 100.000 HT1080, HeLa or A431 cells were seeded and transduced with 50 μ L virus stock and harvested 24 hours later. Infectious titers were determined via qPCR and normalized to the genomic titers.

Figure 109 shows infection efficacy of DARPin exposing viruses. Transduction of HT1080 cells was almost not affected as long as binding to HSPG was not knocked down. HeLa cells were also infected less efficient compared to the controls. However, A431 cells which overexpress EGFR were not infected by the controls. Transduction is rescued by integration of the DARPin into the virus capsid. By additionally knocking down the HSPG binding affinity these cells are transduced 10 times better, reaching wild type capsid HT1080 infection efficacy. These results indicated that specific re-targeting of AAV2 virus particles towards EGFR over expressing tumor cells was achieved by N-terminal fusion of targeting motifs to VP2.



We additionally obtained similar results for Affibody exposing viruses: A431 cell transduction could also be rescued by capsid integration of the Affibody. Again infection efficacy was increased by knocking down the natural tropism of the AAV2 viruses towards HSPG (Figure 110). These data

emphasized the functionality of the VP2 fusion constructs for specifically targeting tumor cells for therapeutic or imaging applications.

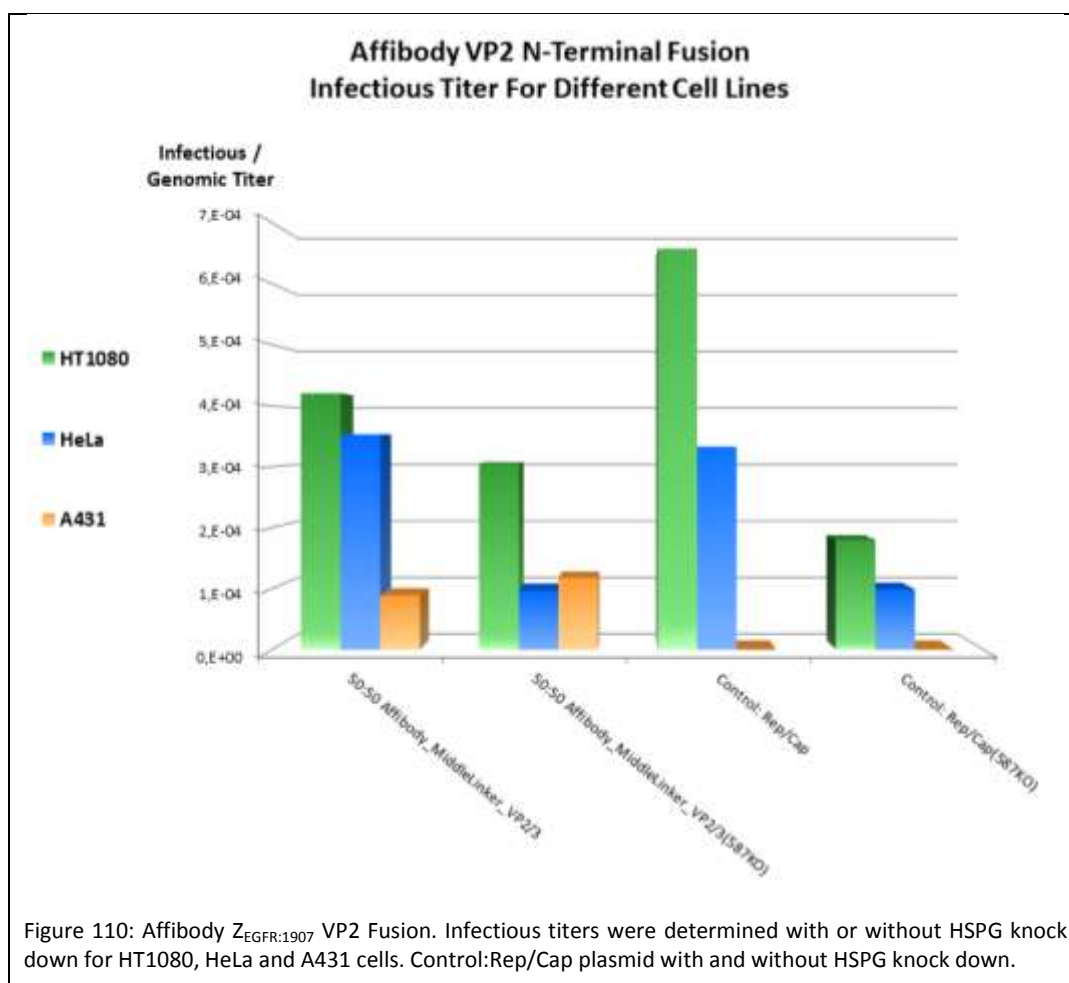
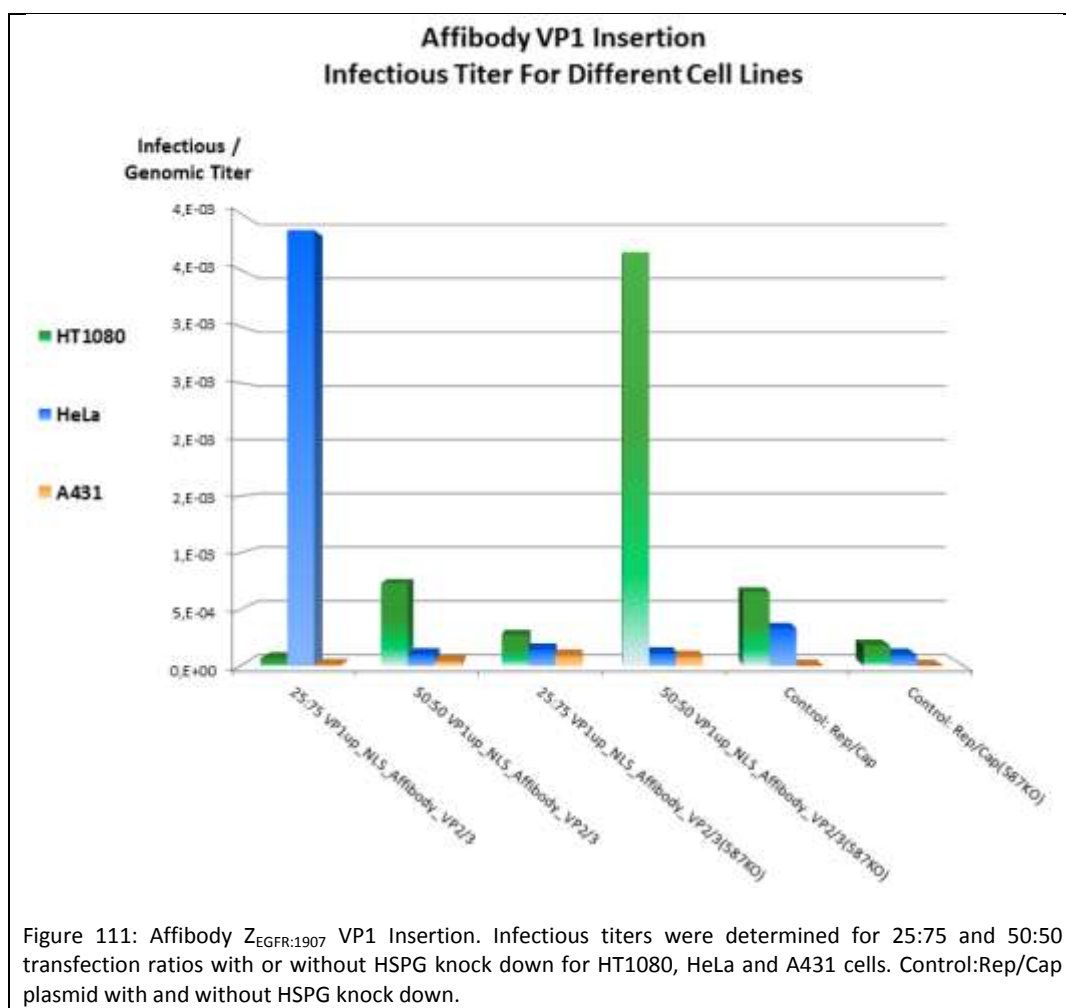


Figure 111 represents the infectivity of viruses containing VP1 inserted Affibody molecules in respect to three different cell types (HT1080, HeLa, A431). The data clearly shows that virus capsids assembled and remained infectious. These AAV2 particles also featured specific binding properties to A431 cells, validating the functionality of the VP1 insertion strategy. The two outlier (HeLa VP1up_NLS_Affibody_VP2/3 25:75 & HT1080 VP1up_NLS_Affibody_VP2/3(587KO) 50:50) should be left unconsidered.



5.4.8 Time laps

HT1080 and A431 cells were transduced with so called “All-in-One” viruses containing the Affibody $Z_{EGFR:1907}$ fused to VP2/3(587KO_His-Tag) and packaged with the guanylate kinase fused to the thymidine kinase coding sequence (GMK-TK). A time series of pictures was started directly after adding 20 μ M Ganciclovir (Figure 112).

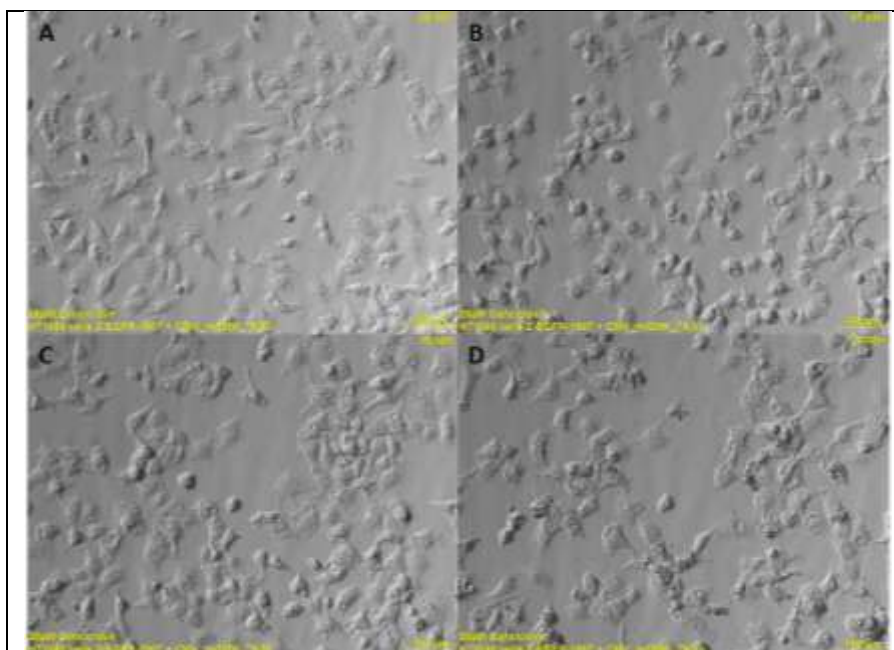


Figure 112: Time-lapse. HT1080 (control) cells transduced with GMK-TK packaged viruses and treated with 20 μ M Ganciclovir A) 0 hours, B) 7 hours, C) 15 hours and D) 23 hours post transduction.

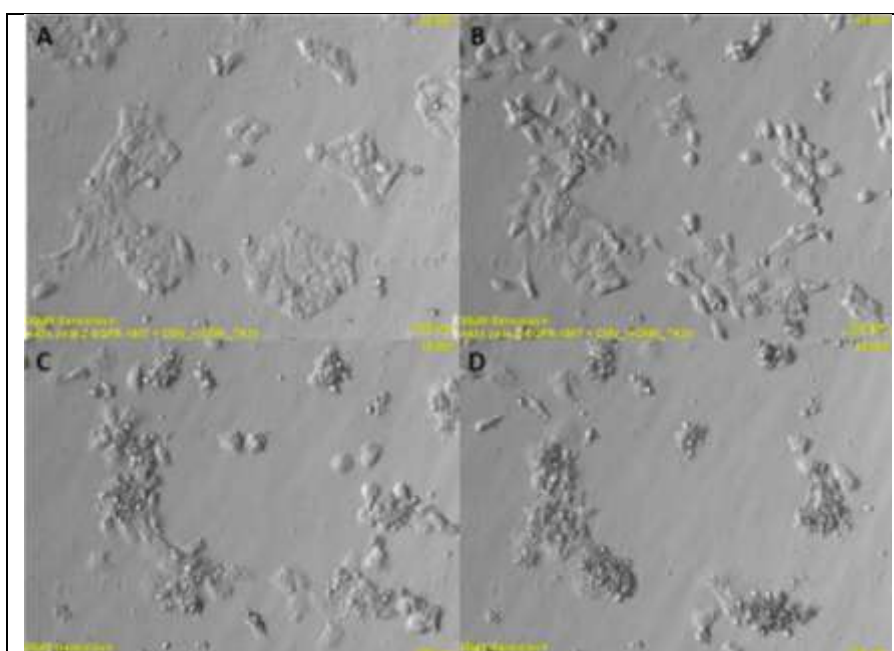


Figure 113: Time-lapse. A431 cells transduced with GMK-TK packaged viruses and treated with 20 μ M Ganciclovir A) 0 hours, B) 7 hours, C) 15 hours and D) 23 hours post transduction.

Virus and Ganciclovir treatment only slightly affect the morphology of HT1080 cells. After 23 hours of incubation in 20 μ M Ganciclovir the cells had almost the same appearance as at time point zero (Fig. 20 a). In comparison to that A431 epidermoid carcinoma cells were efficiently killed after transduction and Ganciclovir add-on: After 23 hours nearly all cells were lysed (Figure 113). These

results clearly demonstrate that we were able to specifically target EGFR over-expressing tumor cells via capsid integrated Affibody and that these transduced cells were efficiently killed by expressing the GMK-TK which converted prodrug Ganciclovir into its cell-toxic monophosphate.

5.5 Arming: Suicide Genes as GOIs

5.5.1 Introduction

Gene delivery using viral vectors to specifically target tumor cells gained increasing attention in the last years being efficient in combination with suicide gene approaches (Willmon et al. 2006). Several prodrug/enzyme combinations have been reported. Two systems - ganciclovir (GCV)/herpes simplex virus thymidine kinase (HSV-TK) (A Ardiani et al. 2010) and 5-fluorocytosine/cytosine deaminase (CD) (Fuchita et al. 2009) – have been widely used and their therapeutic benefit was demonstrated in preclinical studies (Greco & Dachs 2001). Adeno-associated viruses (AAV) as delivery vectors are commonly used in suicide gene therapy. The suicide gene flanked by the inverted terminal repeats (ITRs) is encapsulated into the virus particles and delivered to the target cells where suicide gene expression is mediated by cellular proteins.

The iGEM team Freiburg_Bioware 2010 provides both the cytosine deaminase (CD, BBa_K404112) and an improved guanylate kinase - thymidine kinase fusion gene (mGMK_TK, BBa_K404113) within the Virus Construction Kit as effective suicide genes. We demonstrate efficient and specific killing of tumor cells by enzymatic cytotoxicity assays, flow cytometry, as well as phase contrast microscopy. HT1080 cancer cell lines were transduced with directed viral particles containing the suicide genes packaged into the viral capsids.

5.5.2 Successful Assembly of Vector Plasmids Carrying Suicide Genes via Cloning

To create the functional vector plasmids, assembly of the constructs carrying the suicide genes was performed following the BioBrick Standard Assembly. All plasmids contain the enhancer-element human *beta-globin* intron (BBa_K404107) and the *human growth hormone* terminator signal (hGH, BBa_K404108) flanked by the inverted terminal repeats (ITRs, BBa_K404100 and BBa_K404101). Assembled suicide genes are either under the control of the CMV promoter (BBa_J52034) or the tumor-specific telomerase promoter pHtert (BBa_K404106).

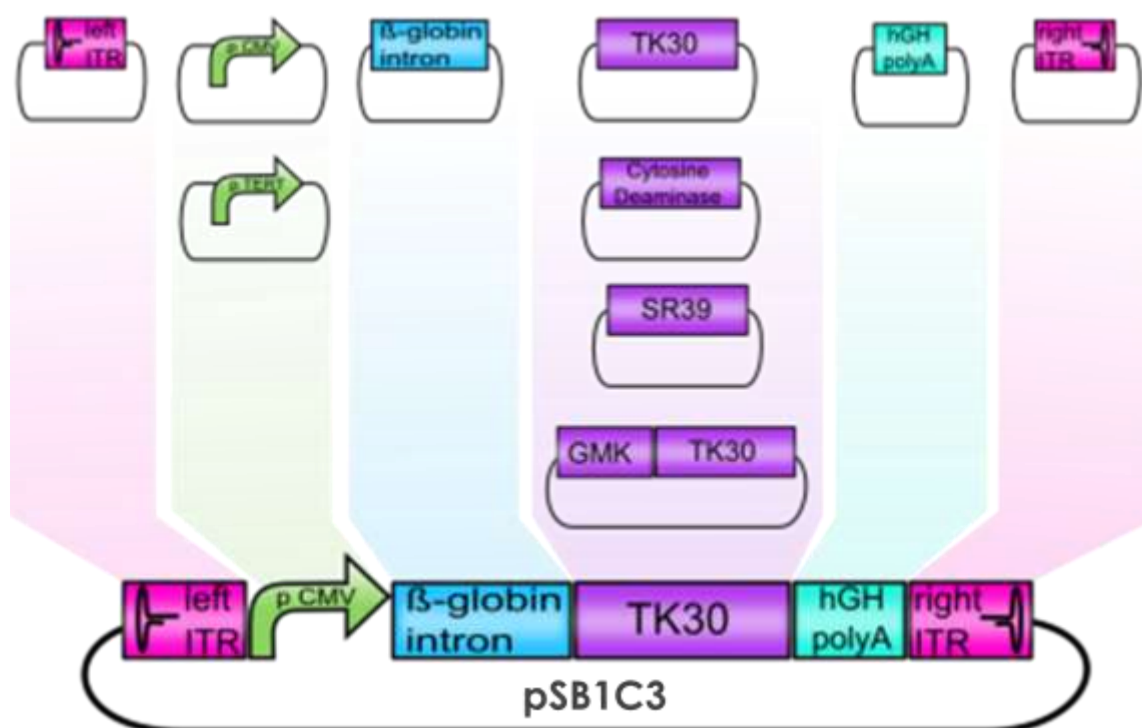


Figure 114: BioBrick-compatible assembly of functional vector plasmids containing the suicide genes. The schematic figure shows the cloning strategy of the guanylate kinase – thymidine kinase fusion gene (mGMK_TK30).

To enable modularization of the thymidine kinase mutants TK30 and SR39 (BBa_K404109 and BBa_K404110) according to the BioBrick standard, the fusion genes mGMK_TK30 and mGMK_SR39 (BBa_K404113 and BBa_K404315) and CD (BBa_K404112) were modified using the QuikChange Lightning Site-Directed Mutagenesis Kit (Stratagene) for deletion of iGEM RFC10 pre- and suffix restriction sites. Figure 114 demonstrates one example of successful deletion of a PstI restriction site located within the mGMK_TK30 sequence at position 3109. A point mutation was introduced replacing the nucleotide G by A, resulting in the deletion of the restriction site while maintaining the encoded amino acid glutamine. Exchange of guanine to adenine was confirmed by sequencing (Figure 115).

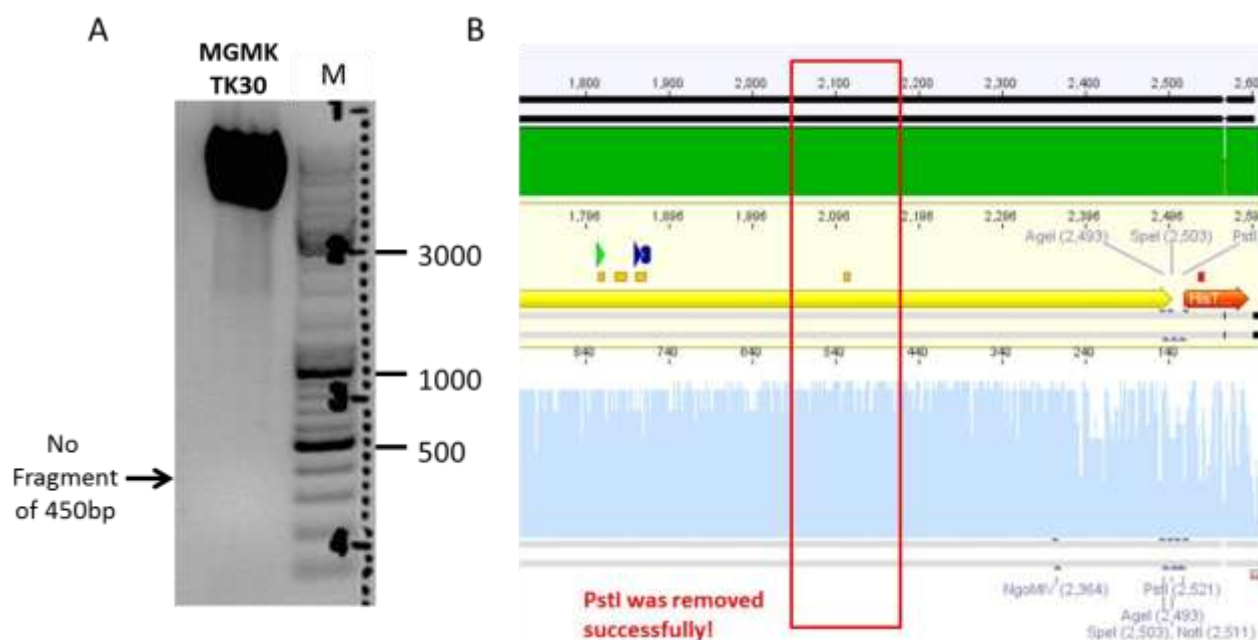


Figure 115: Cytosine to guanine exchange by site-directed mutagenesis using QuikChange Lightning Kit provided by Stratagene was successful as demonstrated by (A) test digestion linearizing the plasmid with PstI and (B) by sequencing.

Furthermore, assembly of BioBrick-compatible vector plasmids was performed. An example for the last assembly step of mGMK_TK30 and hGH_rITR is shown in Figure 116. The plasmids were digested with both XbaI and PstI (New England Biolabs, Insert: BBa_K404116: hGH_rITR) or SpeI and PstI (Vector) and loaded on an agarose gel. As demonstrated in the preparative gel in Figure 116, the expected bands were detected under UV light and the extracted, subsequently purified DNA was successfully ligated and transformed into *E. coli*. Each assembly step for producing the BioBricks was conducted following the iGEM BioBrick standard.

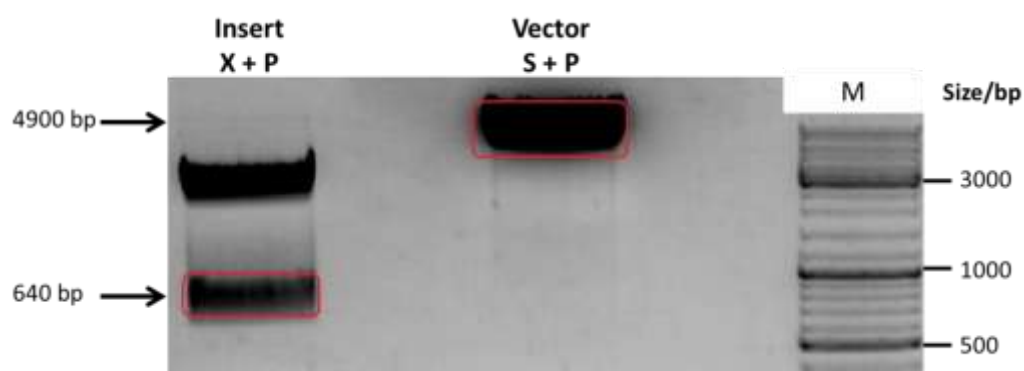


Figure 116: Assembly of mGMK_TK30 (vector molecule, in pSB1C3) and hGH-terminator_rightITR (insert molecule). The digested fragments were visualized under UV-light and correspond to the expected sizes.

5.5.3 Monitoring Efficient Tumor Killing by Phase-Contrast Microscopy

Tumor cells, transduced with viral particles encapsidating the effector constructs containing the mGMK_TK30 driven by the CMV promoter, were cultured both in presence and absence of ganciclovir (Roche). Morphological changes were monitored via phase-contrast microscopy for 48 hours post infection. As it can be seen in Figure 117, non-transduced tumor cells treated with ganciclovir and transduced cells without ganciclovir did not show significant cell ablation. In contrast, transduced cells expressing the guanylate kinase - thymidine kinase fusion protein showed significant cell death after incubation with ganciclovir for 48 hours post infection.

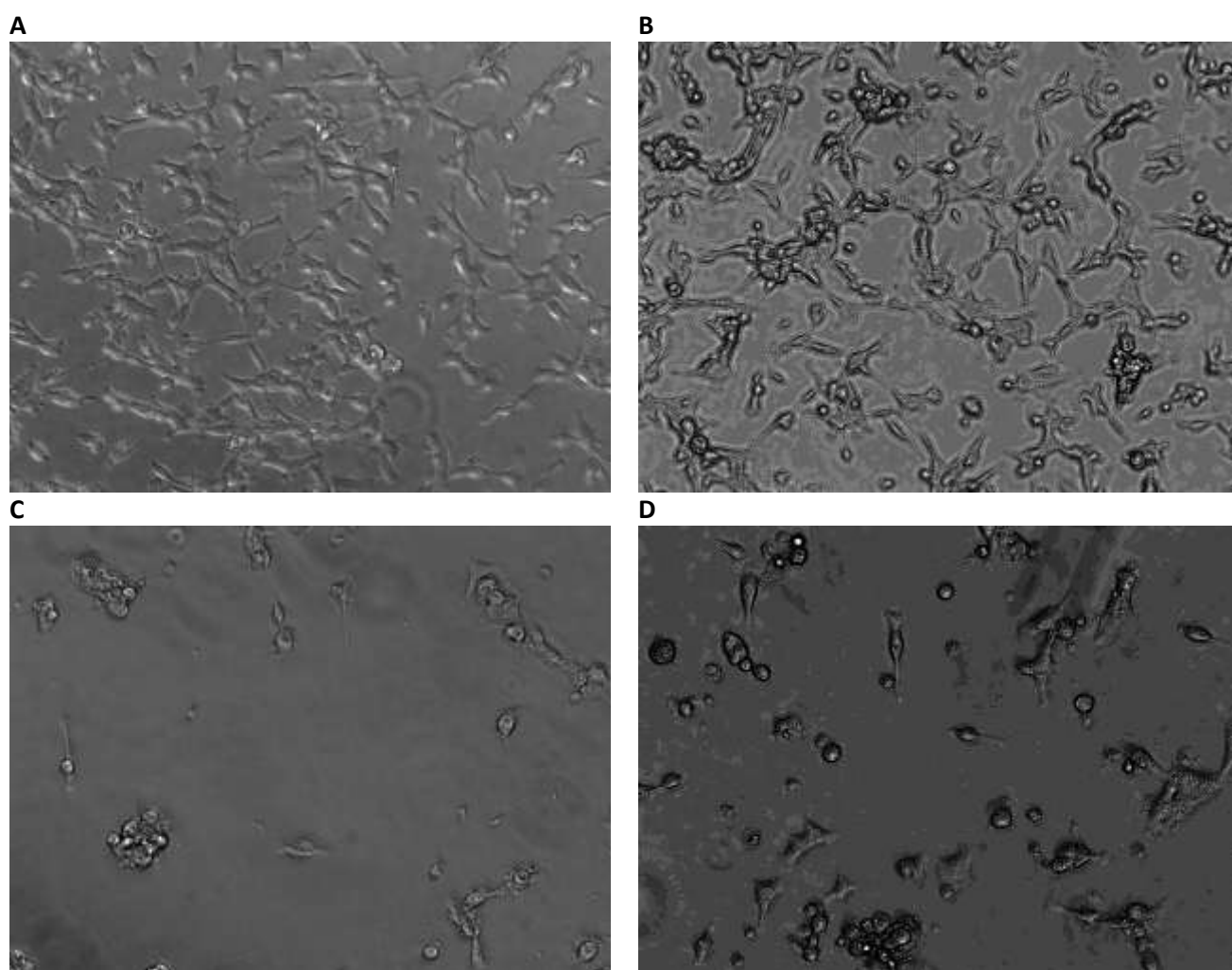


Figure 117: Qualitative analysis of cell death induced by conversion of ganciclovir to ganciclovir-triphosphate by virus-delivered guanylate - thymidine kinase (mGMK_TK30). A: Non-transduced HT1080 cells incubated in the presence of ganciclovir not exhibiting cell death. B: Untreated transduced HT1080 cells showing a high survival rate. C: HT1080 cells transduced with 300 µL viral particles and incubated with ganciclovir leading to tumor cell ablation. D: HT1080 cells transduced with 600 µL viral particles and incubated with ganciclovir leading to ablation of tumor cells.

Suicide gene therapy is based on the localized conversion of non-toxic prodrugs to toxic substances (Greco & Dachs 2001), promoting cell death in the tumor tissue (Figure 118). Directed gene delivery

is achieved by using recombinant viral vectors as provided by the iGEM team Freiburg_Bioware 2010 within the Virus Construction Kit.

Non-transduced cells can survive in the presence of ganciclovir since the prodrug is not toxic for

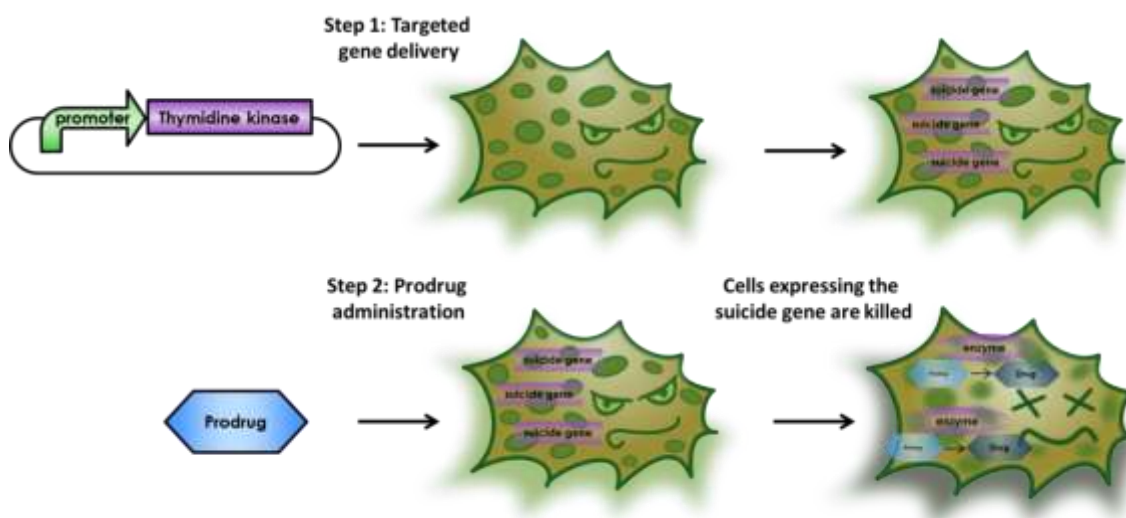


Figure 118: Overview of the suicide gene therapy approach. Non-toxic prodrugs are converted into toxic effector molecules leading to cell death of the tumor cells.

these cells (Figure 117A). The demonstration that transduced cells are viable in the absence of ganciclovir confirms that cell killing is indeed induced by combination of the delivered thymidine kinase and treatment with ganciclovir. Viral particles encapsidating the suicide construct mGMK_TK30 are efficient in directed gene delivery, thus leading to cell death of transduced cells due to overexpression of mGMK_TK30 and prodrug conversion. The cell-toxic ganciclovir-triphosphate is incorporated into the nascent DNA chain leading to replication termination and finally resulting in death of dividing cells.

5.5.4 Quantitative Analysis of Cell Death by Flow Cytometry

Quantitative analysis of the cytotoxic effect induced by mGMK_TK30 was first conducted by flow cytometry analysis 72 hours post transduction. HT1080 cells were stained with 7-AAD and Annexin V. 7-AAD intercalates in double-stranded DNA after penetrating cell membranes of dead cells, whereas Annexin V specifically binds phosphatidylserine which is only accessible during apoptosis. Figure 119 demonstrates the relation between cell death and ganciclovir concentration.

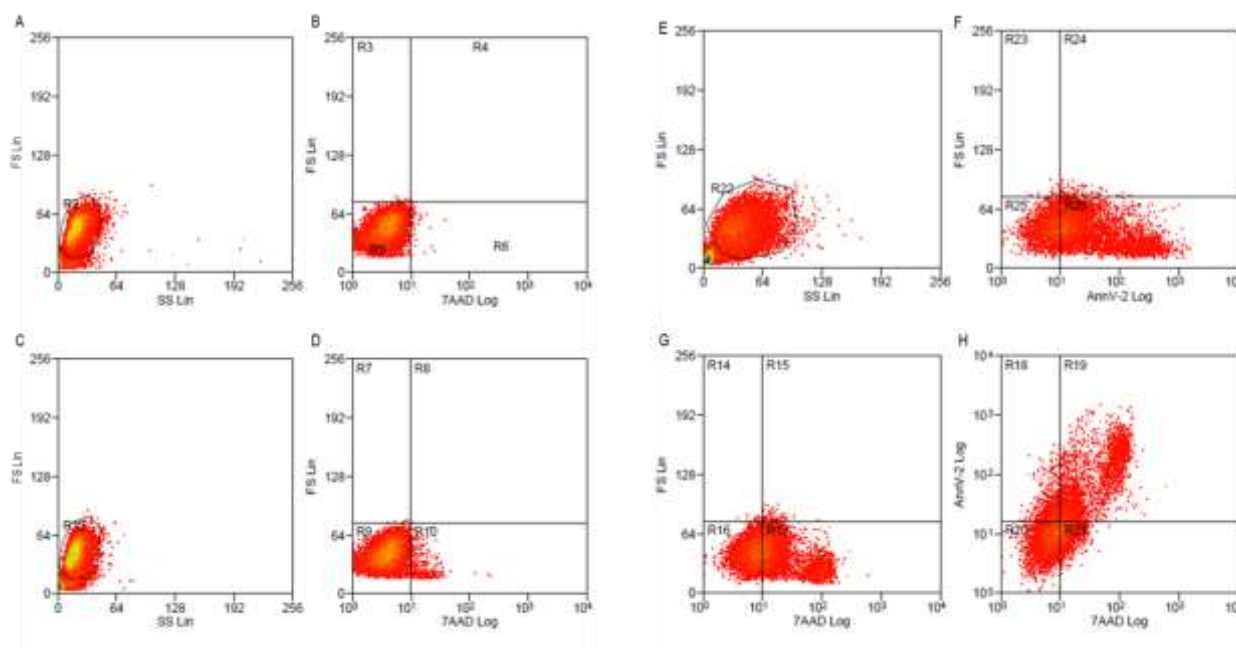


Figure 119: Flow cytometry data analysis. A: Gating non-transduced HT1080 cells (control). B: Non-transduced cells without staining plotted against 7-AAD. C: Gating non-transduced cells stained with 7-AAD. D: Non-transduced, 7-AAD-stained cells plotted against 7-AAD. E: Gating transduced cells (GOI: mGMK_TK30) treated with 485 μ M ganciclovir. F: Gated, Annexin-V stained cells plotted against AnnV-2 Log. G: Gated cells plotted against 7-AAD. H: Gated, 7-AAD and Annexin-V stained cells plotted against 7-AAD and Annexin-V. Gate R19 comprised Annexin-V and 7-AAD positive cells.

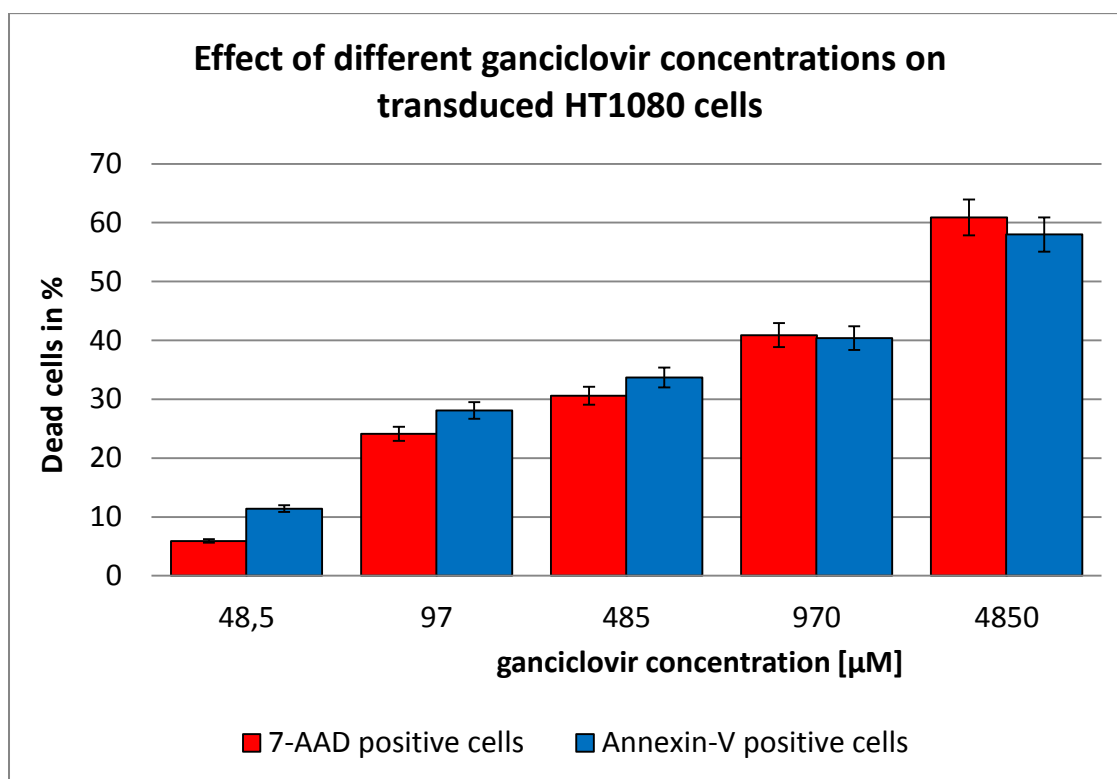


Figure 120: Quantification of flow cytometry data provided in Figure 119. With increasing ganciclovir concentration, the survival rate of cells decreases. 60 % of HT1080 cells treated with 4.85 mM ganciclovir show tumor ablation, however even lower amounts of ganciclovir lead to significant cell death.

The effect of different ganciclovir concentrations on transduced HT1080 sarcoma cells was investigated. Transduction was performed with recombinant viral particles encapsidating the mGMK_TK30 prodrug gene. 72 hours post infection, cells were stained with 7-AAD and Annexin V. As Figure 120 shows, the fraction of killed transduced cells is proportional to the applied ganciclovir concentration.

5.5.5 Titrating Ganciclovir Concentrations for Efficient Cell Killing by Cytotoxicity Assays

Further analysis of the cytotoxic effect induced by thymidine kinase converting ganciclovir to the toxic anti-metabolite has been performed using MTT assays. 3-(4,5-Dimethylthiazol-2-yl)-2,5diphenyltetrazolium bromide), also known as MTT, is a yellow-colored tetrazole, which is reduced to purple insoluble formazan in the presence of NADH and NADPH (Roche n.d.). Colorimetric analysis can be carried out via spectrometry. HT1080 cells were transduced with the recombinant viruses carrying the linear DNA construct coding for mGMK-TK30 regulated by the CMV promoter and subsequently treated with ganciclovir. 48 and 72 hours post infection, cells were incubated with MTT and fresh DMEM. After cell lysis by DMSO, absorbance of formazan at 570 nm was quantified using a Tecan Sunrise plate reader.

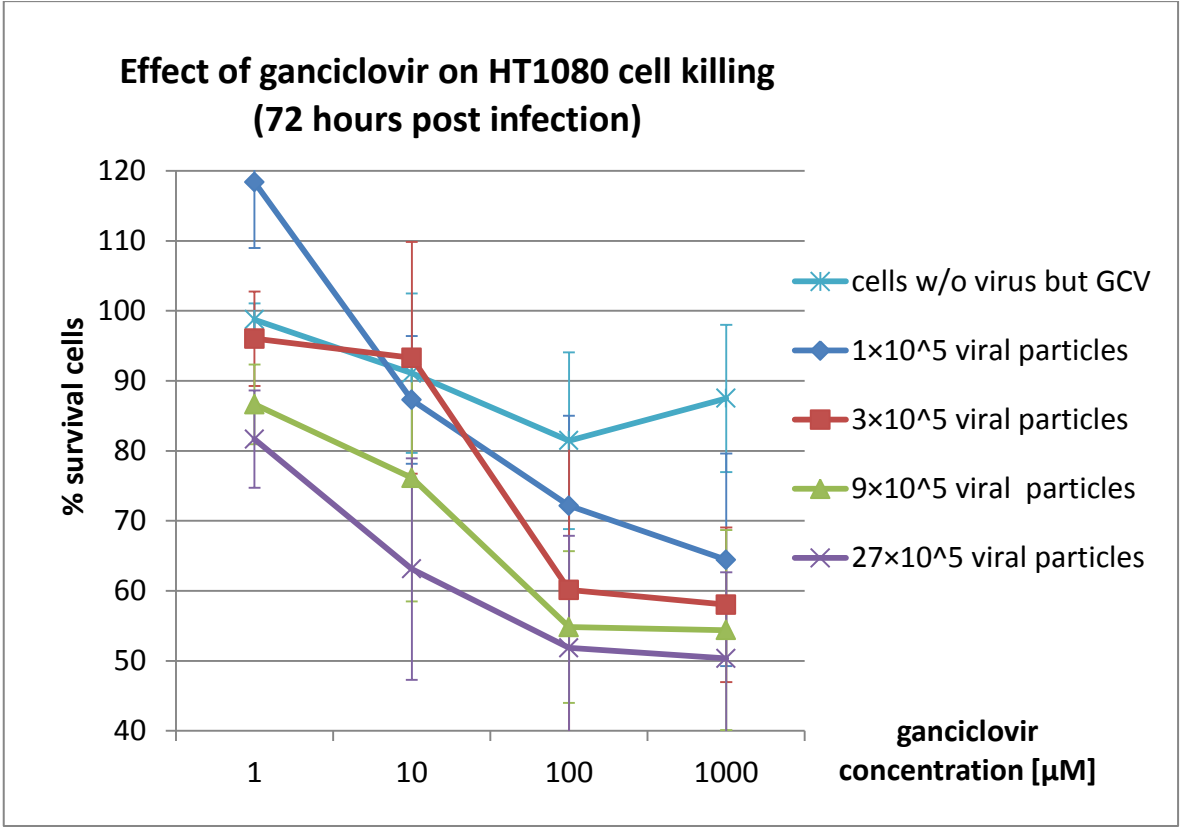


Figure 121: Effect of ganciclovir on HT1080 cell killing

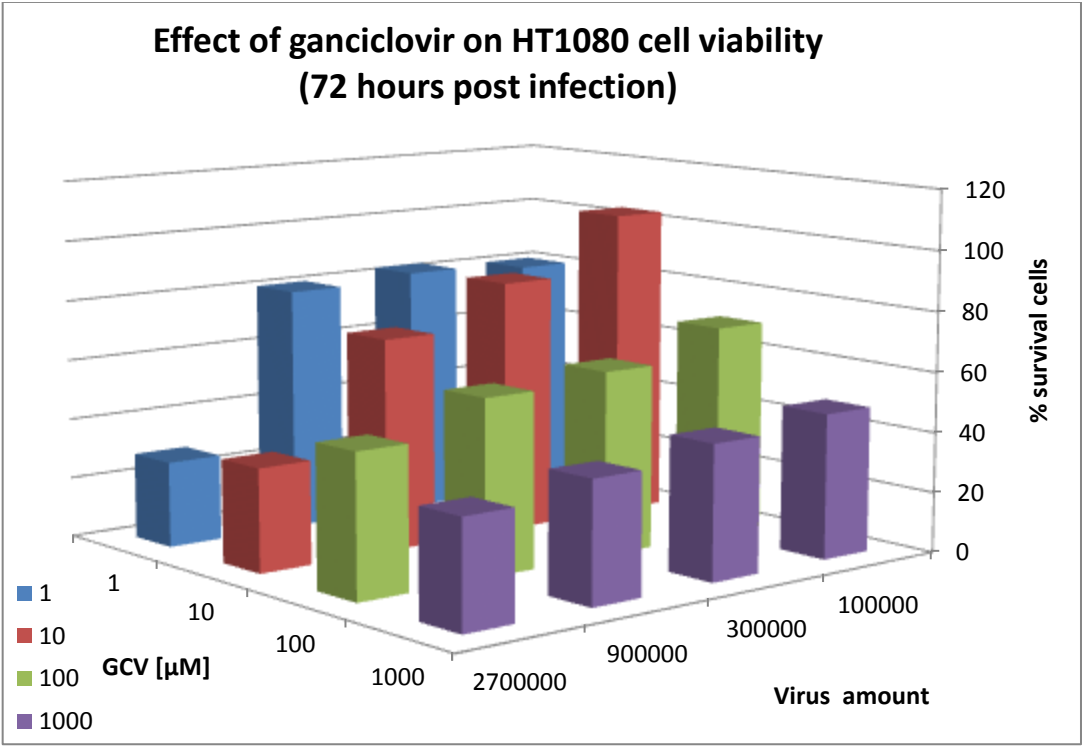


Figure 122: Effect of ganciclovir on HT1080 cell survival 72 hours post infection as (A) two dimensional plot of survival of cells and (B) three-dimensional plot of ganciclovir, virus particles and cell survival.

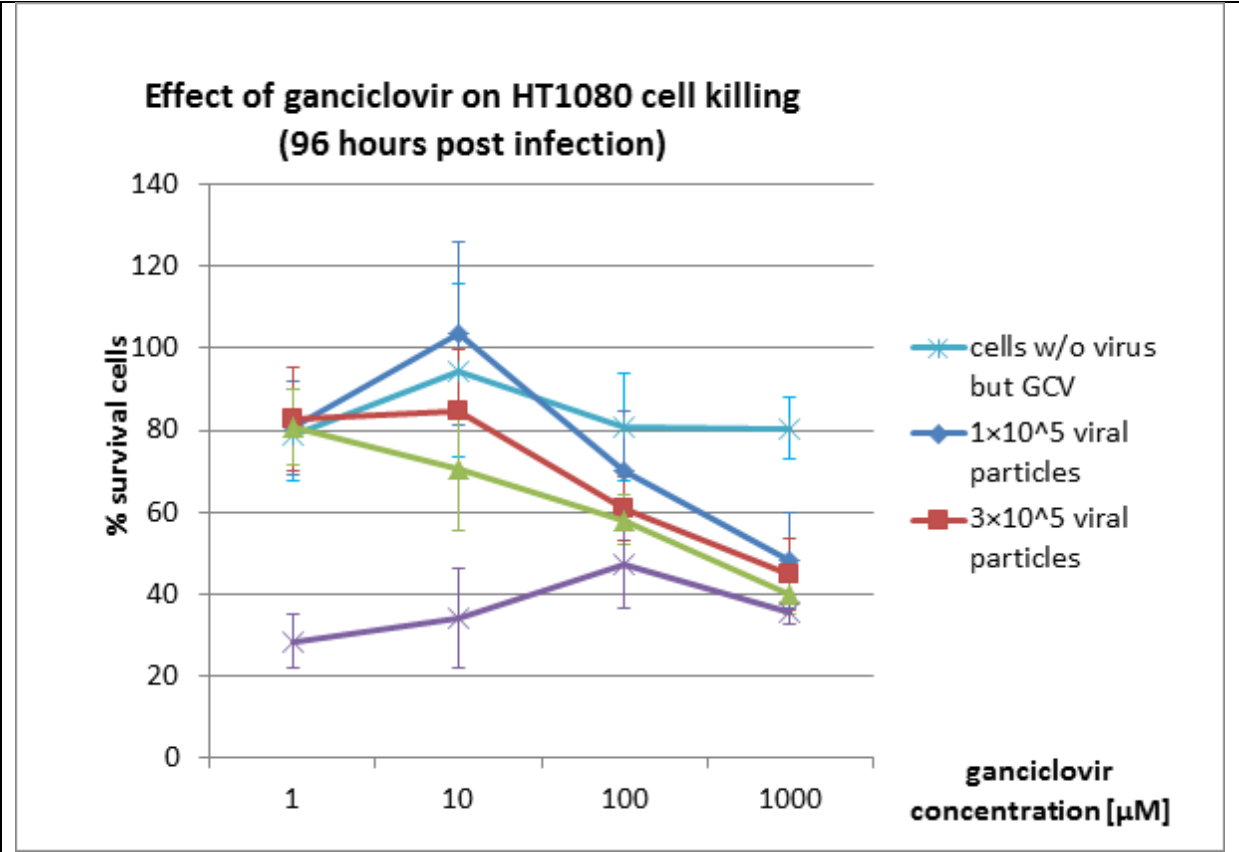
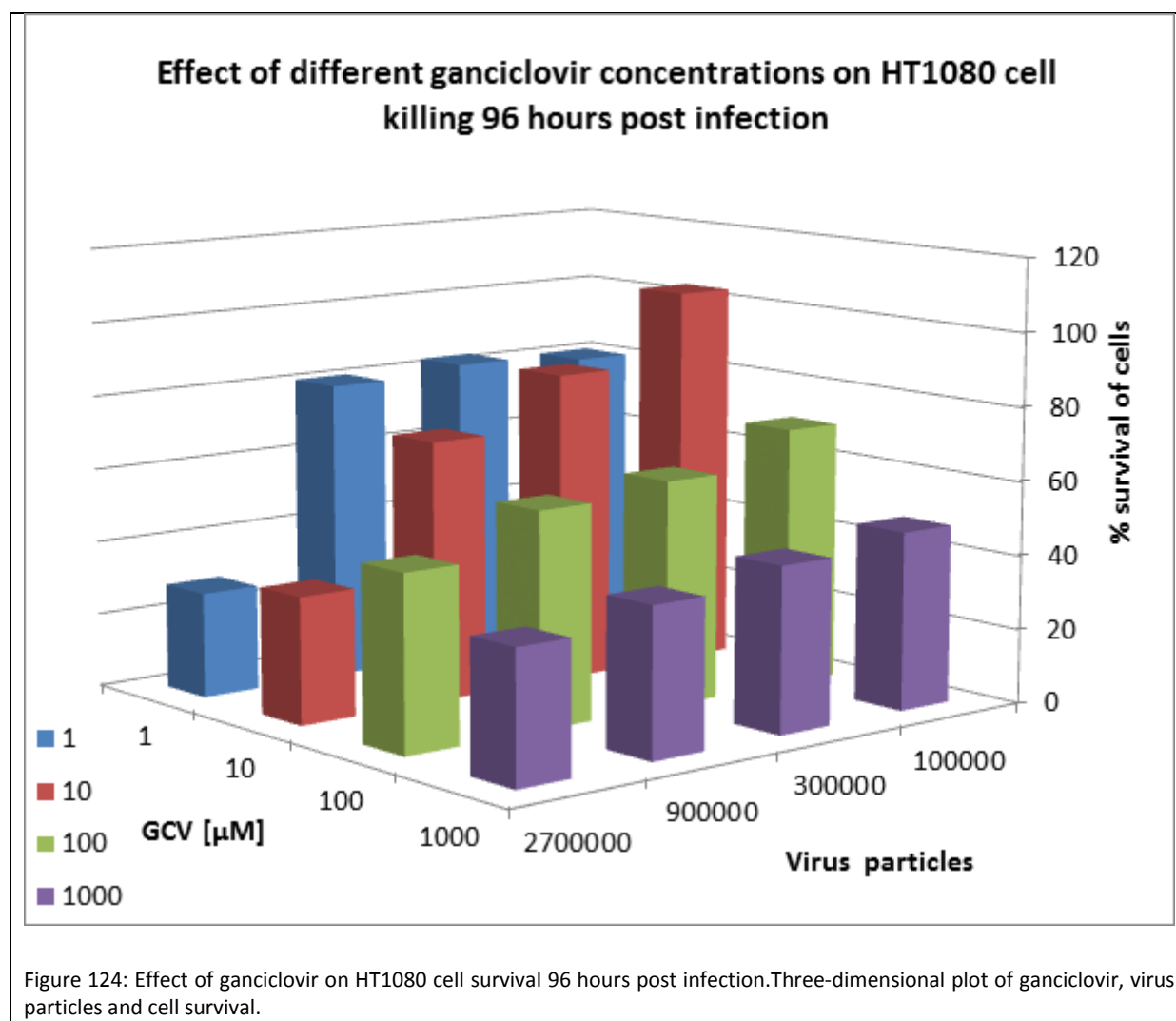


Figure 123: Effect of ganciclovir four days post transduction. Two dimensional plot of cell survival is plotted.



Data of MTT assay quantification are shown in Figure 122 and HT1080 cells were infected with viral particles containing the mGMK_TK30 transgene. 72 h- and 96 h post infection and addition of ganciclovir, cells were incubated with MTT. Changes in absorbance were measured and survival of cells plotted against ganciclovir concentration. Figure 122A demonstrates the correlation between increasing ganciclovir concentrations and percentage of cell survival. Furthermore, different virus particle concentrations were used for transduction. Figure 122B shows that the highest amount of viral particles combined with the highest ganciclovir concentration led to significant HT1080 apoptosis 72 hours post transduction.

Additionally, 96 hours post infection cells were incubated with MTT and absorbance was quantified via spectrometry. Again, survival of HT1080 cells was plotted against increasing ganciclovir concentrations.

5.5.6 Killing Non-transduced Tumor Cells via Bystander Effect

The bystander effect was first reported by Moolten (1986) showing that prodrug convertase negative cells surrounded by suicide enzyme positive cells did not survive prodrug treatment. Besides efficient killing of targeted tumor cells, neighboring, non-transduced cells are killed as well, providing an important effect in cancer treatment. Since 5-Fluorouracil is soluble and can diffuse into adjacent cells (Huber et al. 1993) (Huber et al. 1994), the bystander effect was demonstrated using cytosine deaminase as gene of interest.

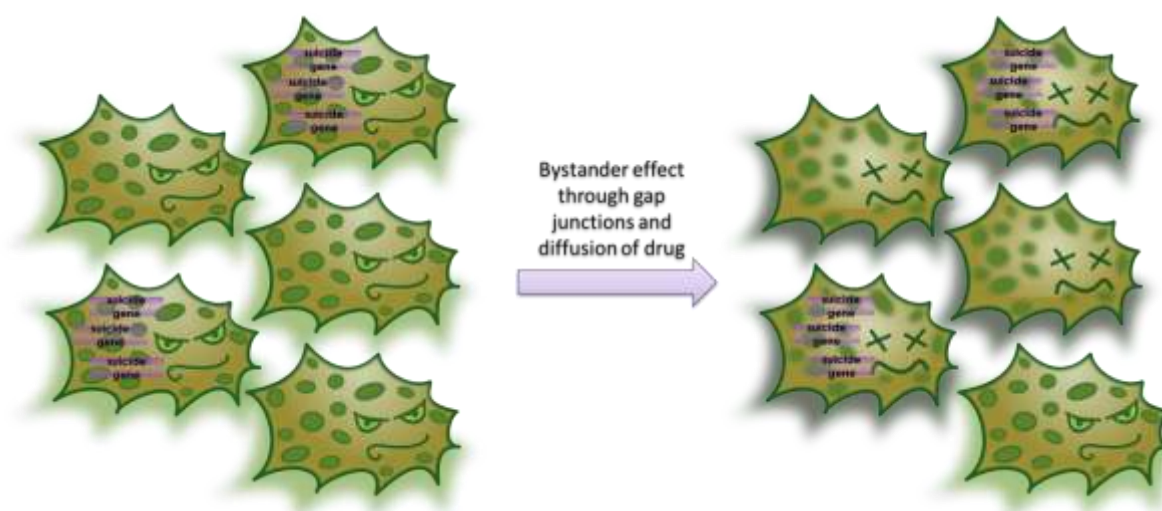


Figure 125: Schematic overview of the Bystander effect.

The aim was to investigate if the modified AAV-2 is able to kill tumor cells with the cytosine deaminase (CD) as gene of interest. The viral particles were produced according to the standard protocol using the following plasmids:

- pHelper
- Rep/Cap: pSB1C3_001_[AAV2]-Rep-VP123(ViralBrick-587KO-empty)_p5-TATAless
- Gene of interest: pSB1C3_[AAV2]-left-ITR_pCMV_betaglobin_CD_hGH_[AAV2]-right-ITR

90 % confluent HT1080 cells were transduced in T75 flasks with 9 ml of viral stock. In parallel, another T75 flask was transduced with a viral stock packaged with the mVenus coding sequence to assess transgene expression.

24 hours before harvesting the CD-transduced cells, two six well plates with 200.000 cells per well were seeded. After 30 hours, mVenus expression was observed and the CD-transduced HT1080 were harvested. To minimize the influence of viral particles in the medium, the cells were washed four times with PBS. The cells were counted via a Neubauer cell chamber and 100.000 cells per well of a

six well plate were seeded. Additionally, 100.000 of the CD-transduced cells were seeded onto previously seeded untransduced HT1080.

The incubation with the prodrug 5-fluorocytosine (5-FC) was performed at a final concentration of 53 mM. According to Fuchita *et al.*, this amount should be sufficient to show the functionality of the CD (Fuchita et al. 2009). As demonstrated in **Error! Reference source not found.**, cytotoxicity of 5-FC is remarkable.

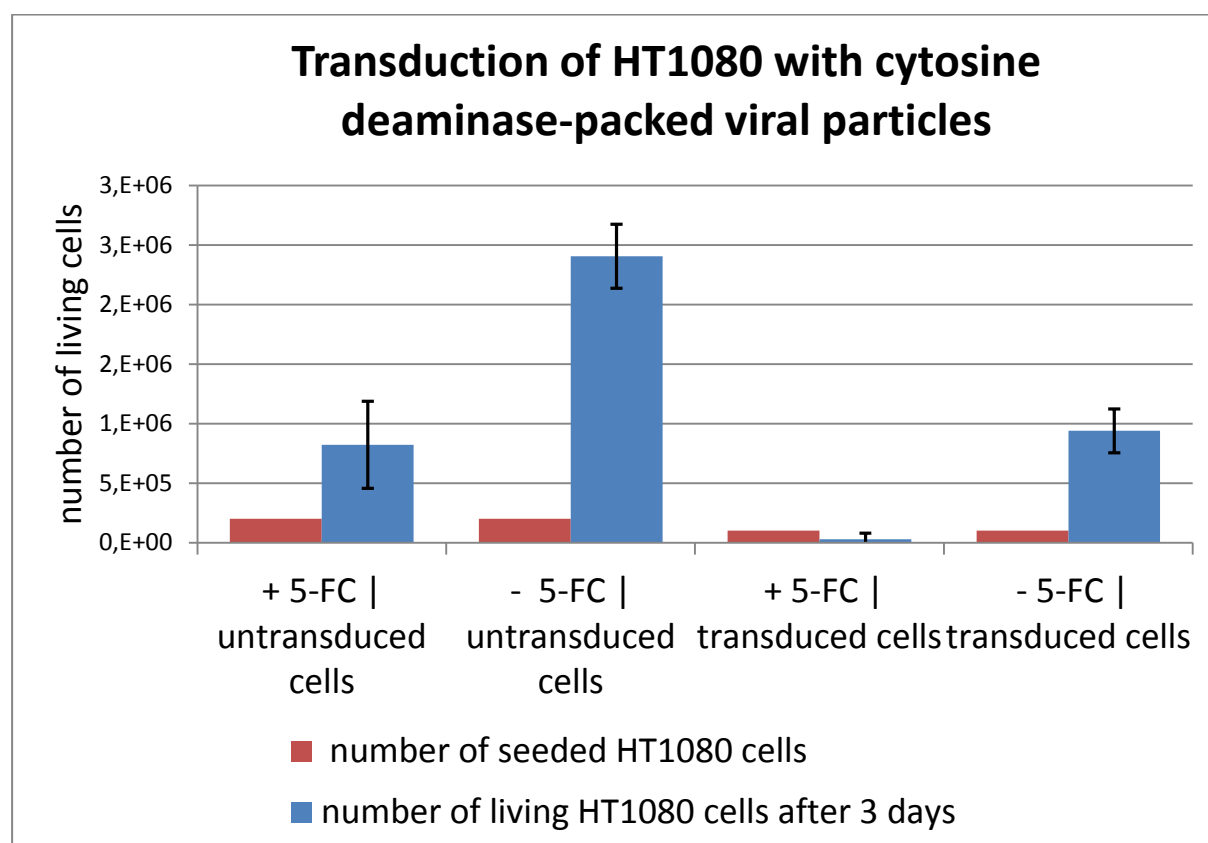


Figure 126: Transduction of HT1080 with cytosine deaminase-packed viral particles. 5-FC: 5-fluorocytosine (53 mM)

After three days of incubation in 5-fluorocytosine, the cells were washed, detached with Trypsin, centrifuged at 200 g for 5 min followed by two washing steps with PBS and finally resuspended with 200 µl DMEM. Living cells were then counted via Trypan blue staining.

After this successful qualitative demonstration of an AAV2-mediated cytosine deaminase treatment, the bystander effect was quantified as well. The activated 5-FC molecules are able to diffuse through the plasma membrane and thus effect cells that are not transduced (Figure 127). The bystander effect was tested with untransduced HT1080 cells, which were mixed with the CD-transduced HT1080 cells.

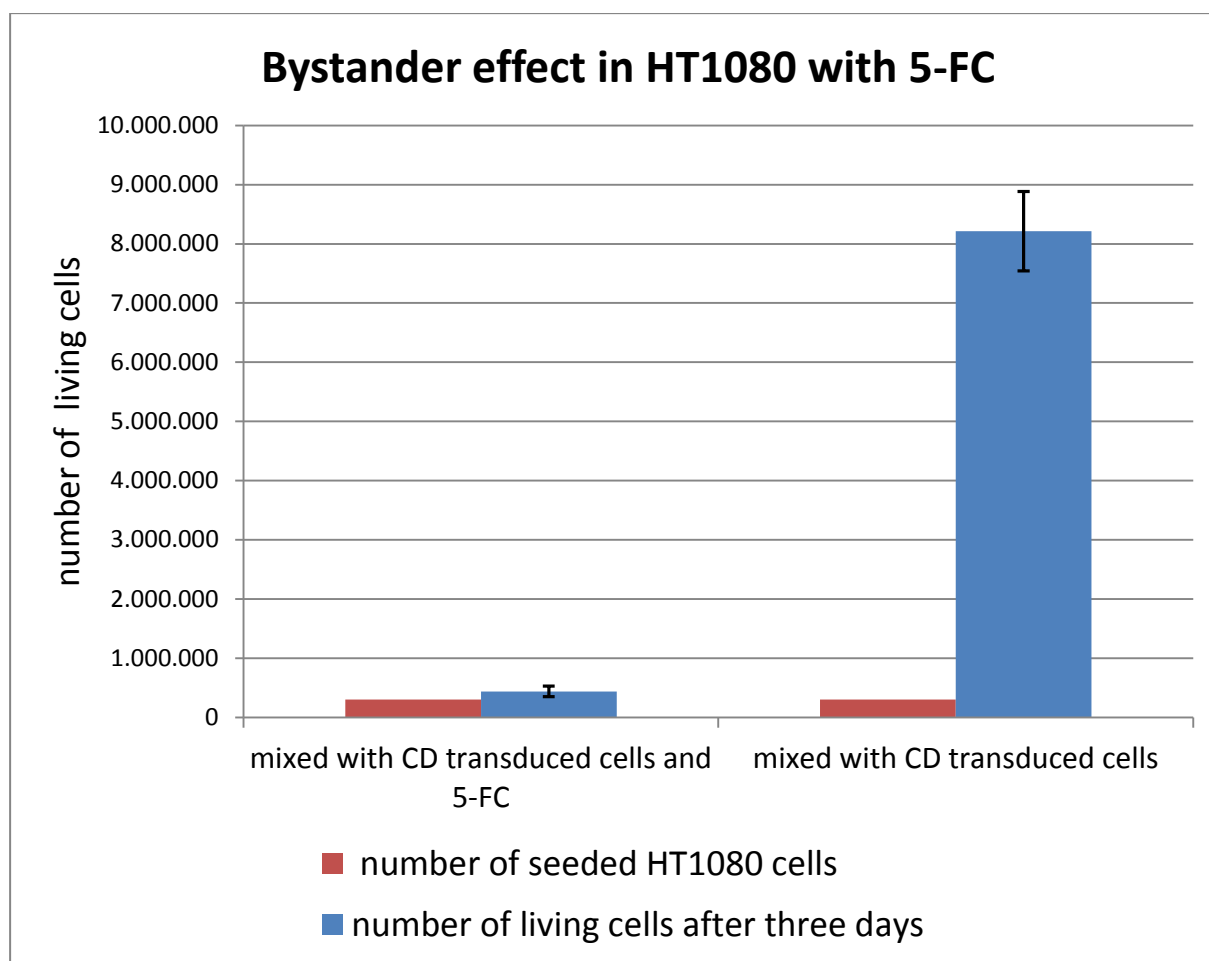


Figure 127: Quantifying the bystander effect on HT1080 cells 5-FC: 5-fluorocytosine (53 mM)

The cytosine deaminase expressing cells have an obvious effect on the viability of the non-transduced cells. As shown in the graph we were able to demonstrate that cytosine deaminase mediated cancer cell death is also fatal for non-transduced cells in close proximity.

5.5.7 Conclusions

Efficient and tissue-specific tumor killing is one major challenge in cancer therapy (M E Black et al. 1996). Gene-directed enzyme prodrug therapy (GDEPT) is based on the conversion of non-toxic substances into toxic drugs resulting in tumor cell death. The iGEM team Freiburg_Bioware 2010 provides several functional suicide genes within the Virus Construction Kit, thus offering a feasible and modular tool to the growing field of personalized medicine and the iGEM community. We successfully demonstrated cancer cell death caused by the introduction of cytosine deaminase and modified fusion genes consisting of guanylate and thymidine kinases.

To prevent systemic toxic side effects of conventional chemotherapy, the iGEM team Freiburg_Bioware 2010 took a leap and efficiently retargeted the viral vector for directed suicide

gene delivery towards tumor cells. Capsid engineering was successfully demonstrated by the iGEM team Freiburg_Bioware 2010. Further details can be found under Results – Targeting.

5.6 Modeling

5.6.1 Model for Virus Production

5.6.1.1 Reaction Scheme

Reducing the complexity of virus production we divide the cell into three compartments: the extracellular matrix (all quantities with the index *ext*), the cytoplasm (*cyt*) and the nucleus (*nuc*). Four plasmids are transfected - the plasmid coding for the helper proteins (*helper*), the gene of interest (*goi*) and two types of plasmids coding for the capsid proteins (*capwt* [wild type], *capmod* [modified]).

The plasmids are transported into the nucleus where gene expression is initiated. Processed mRNA is transported into the cytoplasm and proteins (*phelper*, *pcapwt*, *pcapmod*) are produced. Containing a nuclear localization sequence proteins are relocated into the nucleus where capsid assembly occurs. The viral capsid is composed of 60 subunits of viral coat proteins. Titration of the two plasmids coding for the capsid proteins leads to virus surfaces with different ratios of wild type and modified capsid proteins.

The gene of interest is replicated by cellular polymerases and single stranded DNA (*ssDNA*) is encapsidated into the preformed capsids (*capsid*) forming infectious viral particles (*V*).

Finally the recombinant viruses are released into the extracellular matrix and can be harvested for transduction.

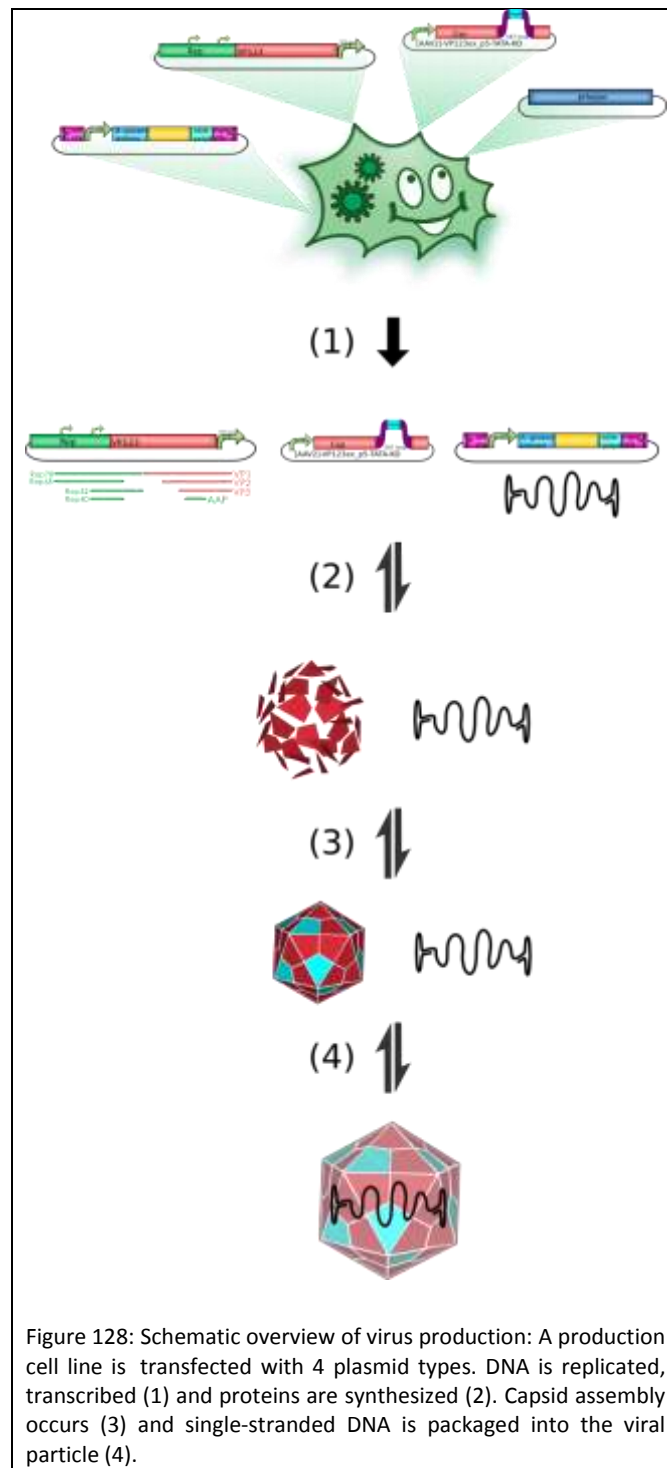
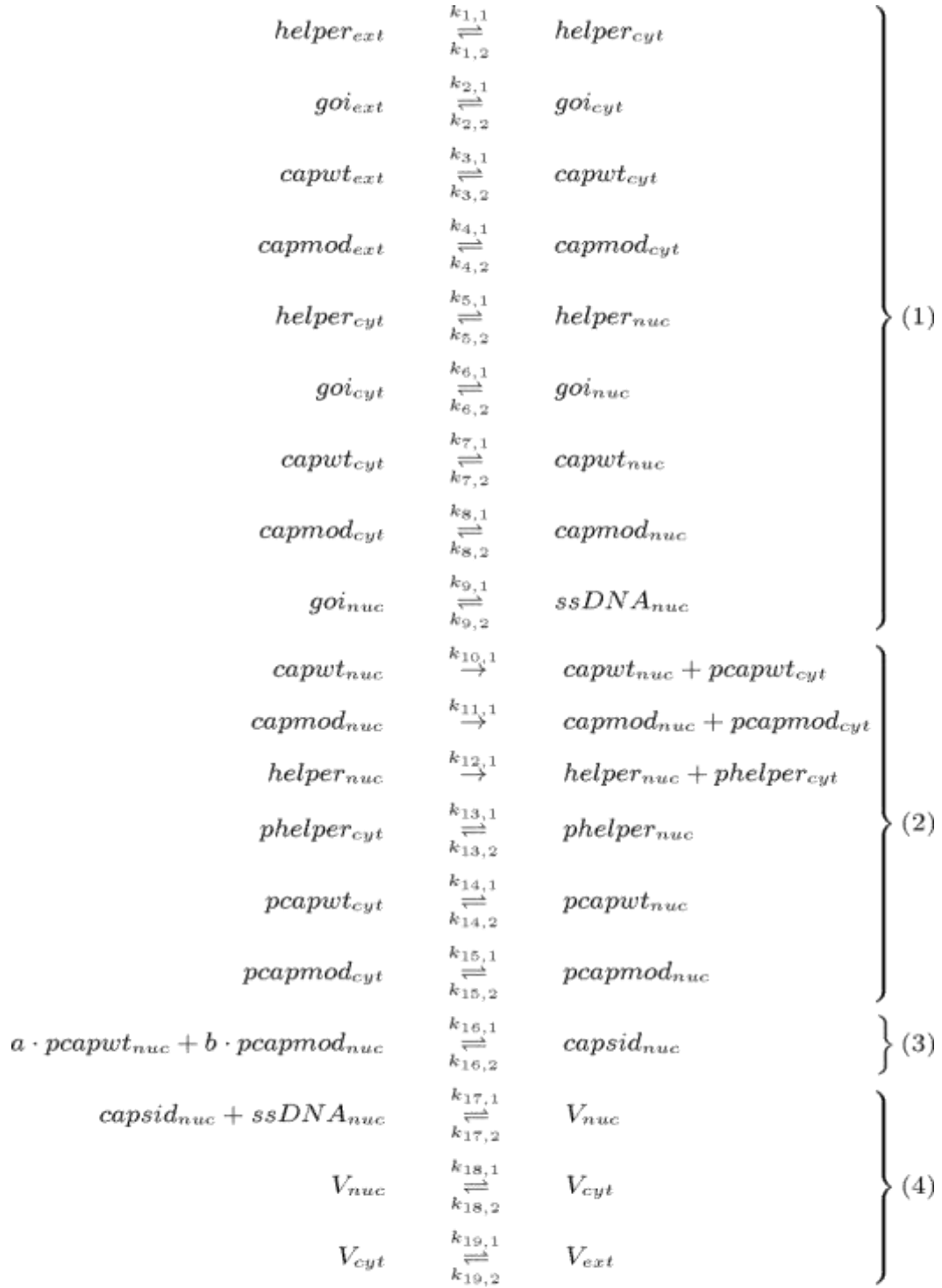


Figure 128: Schematic overview of virus production: A production cell line is transfected with 4 plasmid types. DNA is replicated, transcribed (1) and proteins are synthesized (2). Capsid assembly occurs (3) and single-stranded DNA is packaged into the viral particle (4).

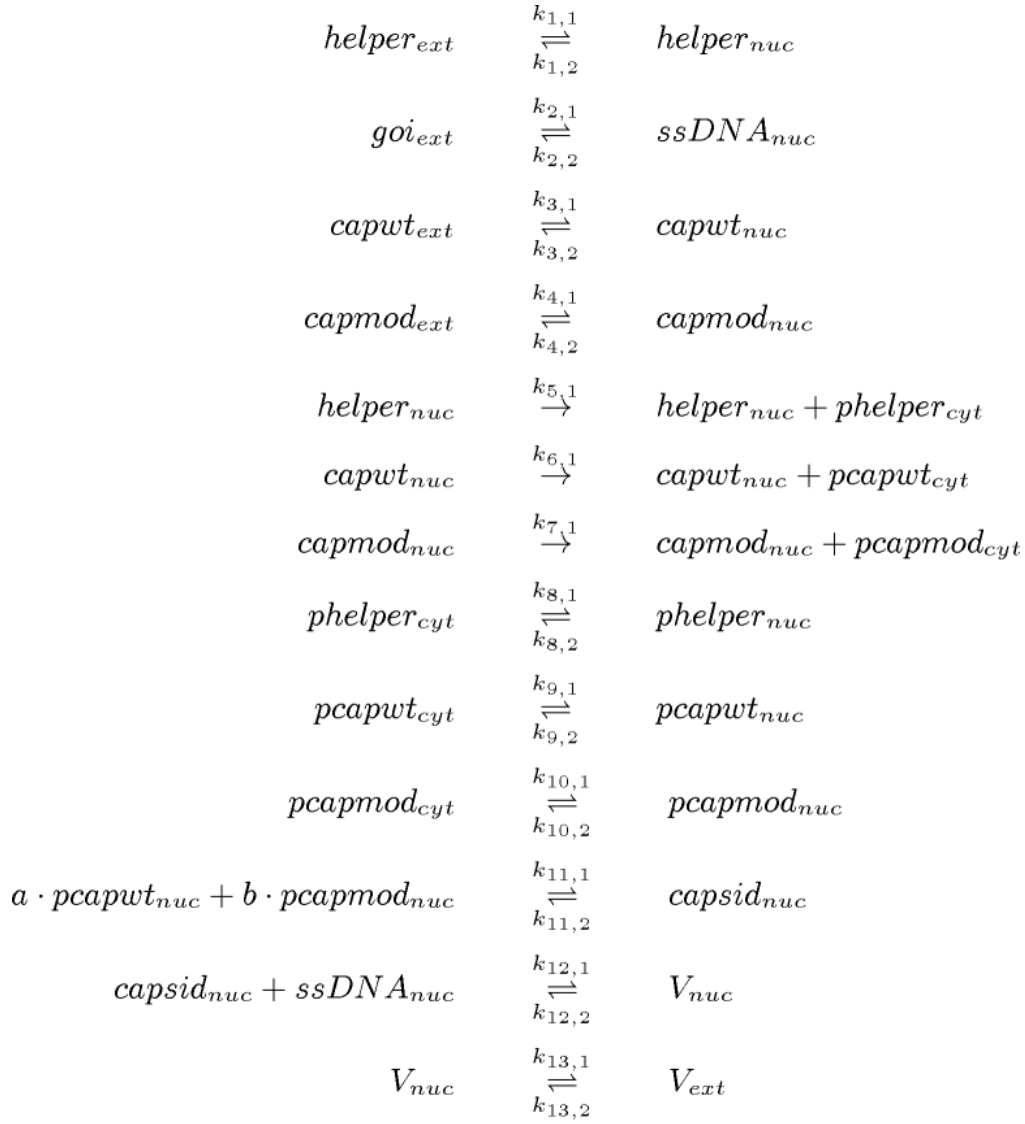


(with $a + b = 60$; $a, b \in \mathbb{N}_0$)

5.6.1.2 Reduced Reaction Scheme

Even the coarse model for virus production described in the previous paragraph would still consist of 24 ODEs containing 39 parameters (35 rate constants and 4 initial plasmid

concentrations). Taking into account the linearity of the law of mass action (LMA) for simple transport processes we can neglect these fast reactions and for this reason reduce the model to the rate limiting steps like protein synthetization, capsid formation and virus packaging.



(with $a + b = 60$; $a, b \in \mathbb{N}_0$)

5.6.1.3 Differential Equations

The 13 reactions for the virus production are represented in a system of 17 coupled ODEs.

In addition to the terms provided by the law of mass action we considered the following terms:

a linear degradation of *ssDNA* in the nucleus with the rate constant $k_{14,1}$

replication of *ssDNA* in the nucleus with the rate constant $k_{15,1}$

$$\begin{aligned}
\frac{d[\text{helper}_{ext}]}{dt} &= -k_{1,1}[\text{helper}_{ext}] + k_{1,2}[\text{helper}_{nuc}] \\
\frac{d[\text{goi}_{ext}]}{dt} &= -k_{2,1}[\text{goi}_{ext}] + k_{2,2}[\text{ssDNA}_{nuc}] \\
\frac{d[\text{capwt}_{ext}]}{dt} &= -k_{3,1}[\text{capwt}_{ext}] + k_{3,2}[\text{capwt}_{nuc}] \\
\frac{d[\text{capmod}_{ext}]}{dt} &= -k_{4,1}[\text{capmod}_{ext}] + k_{4,2}[\text{capmod}_{nuc}] \\
\frac{d[\text{helper}_{nuc}]}{dt} &= -k_{1,2}[\text{helper}_{nuc}] + k_{1,1}[\text{helper}_{ext}] - k_{14,1}[\text{helper}_{nuc}] \\
\frac{d[\text{ssDNA}_{nuc}]}{dt} &= -k_{2,2}[\text{ssDNA}_{nuc}] + k_{2,1}[\text{goi}_{ext}] - k_{12,1}[\text{capsid}_{nuc}] \cdot [\text{ssDNA}_{nuc}] \\
&\quad + k_{12,2}[V_{nuc}] - k_{14,1}[\text{ssDNA}_{nuc}] + k_{15,1}[\text{ssDNA}_{nuc}] \\
\frac{d[\text{capwt}_{nuc}]}{dt} &= -k_{3,2}[\text{capwt}_{nuc}] + k_{3,1}[\text{capwt}_{ext}] - k_{14,1}[\text{capwt}_{nuc}] \\
\frac{d[\text{capmod}_{nuc}]}{dt} &= -k_{4,2}[\text{capmod}_{nuc}] + k_{4,1}[\text{capmod}_{ext}] - k_{14,1}[\text{capmod}_{nuc}] \\
\frac{d[\text{phelper}_{cyt}]}{dt} &= -k_{8,1}[\text{phelper}_{cyt}] + k_{5,1}[\text{helper}_{nuc}] + k_{8,2}[\text{phelper}_{nuc}] \\
\frac{d[\text{pcapwt}_{cyt}]}{dt} &= -k_{9,1}[\text{pcapwt}_{cyt}] + k_{6,1}[\text{capwt}_{nuc}] + k_{9,2}[\text{pcapwt}_{nuc}] \\
\frac{d[\text{pcapmod}_{cyt}]}{dt} &= -k_{10,1}[\text{pcapmod}_{cyt}] + k_{7,1}[\text{capmod}_{nuc}] + k_{10,2}[\text{pcapmod}_{nuc}] \\
\frac{d[\text{phelper}_{nuc}]}{dt} &= -k_{8,2}[\text{phelper}_{nuc}] + k_{8,1}[\text{phelper}_{cyt}] \\
\frac{d[\text{pcapwt}_{nuc}]}{dt} &= -k_{9,2}[\text{pcapwt}_{nuc}] + k_{9,1}[\text{pcapwt}_{cyt}] - k_{11,1}a \cdot [\text{pcapwt}_{nuc}]^a \cdot [\text{pcapmod}_{nuc}]^b \\
&\quad + k_{11,2}a \cdot [\text{capsid}_{nuc}] \\
\frac{d[\text{pcapmod}_{nuc}]}{dt} &= -k_{10,2}[\text{pcapmod}_{nuc}] + k_{10,1}[\text{pcapmod}_{cyt}] - k_{11,1}b \cdot [\text{pcapwt}_{nuc}]^a \cdot [\text{pcapmod}_{nuc}]^b \\
&\quad + k_{11,2}b \cdot [\text{capsid}_{nuc}] \\
\frac{d[\text{capsid}_{nuc}]}{dt} &= -k_{12,1}[\text{capsid}_{nuc}] \cdot [\text{ssDNA}_{nuc}] + k_{11,1}[\text{pcapwt}_{nuc}]^a \cdot [\text{pcapmod}_{nuc}]^b \\
&\quad - k_{11,2}[\text{capsid}_{nuc}] + k_{12,2}[V_{nuc}] \\
\frac{d[V_{nuc}]}{dt} &= -k_{13,1}[V_{nuc}] - k_{12,2}[V_{nuc}] + k_{12,1}[\text{capsid}_{nuc}] \cdot [\text{ssDNA}_{nuc}] + k_{13,2}[V_{ext}] \\
\frac{d[V_{ext}]}{dt} &= -k_{13,2}[V_{ext}] + k_{13,1}[V_{nuc}]
\end{aligned}$$

5.6.1.4 Methods and Simulation

The ODE model was implemented in MathWorks® MATLAB R2010b. Integration of the differential equations was achieved using the stiff integrator *ode15s* with automatic integration step size management.

In order to adjust the dynamical model to biological data we extracted the average intensity out of the time lapse recordings of fluorescence experiments as well as published values for the rate constants. For initial conditions we took the plasmid concentrations we used in experiments.



Figure 129: Fluorescence microscopy of transfected cells. mVenus is included to the modified capsid plasmid i.e. fluorescence intensity reflects capsid protein concentration.

The image on the left shows one snapshot out of the time lapse recorded over a period of 1560 minutes (26 hours) after transfection. The bright spots correspond to the fluorescence intensity of *mVenus* in the upper and of *mCherry* in the lower picture.

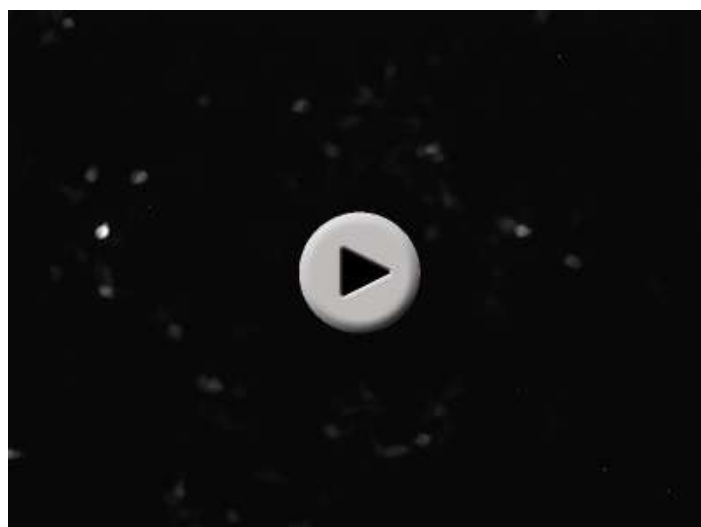
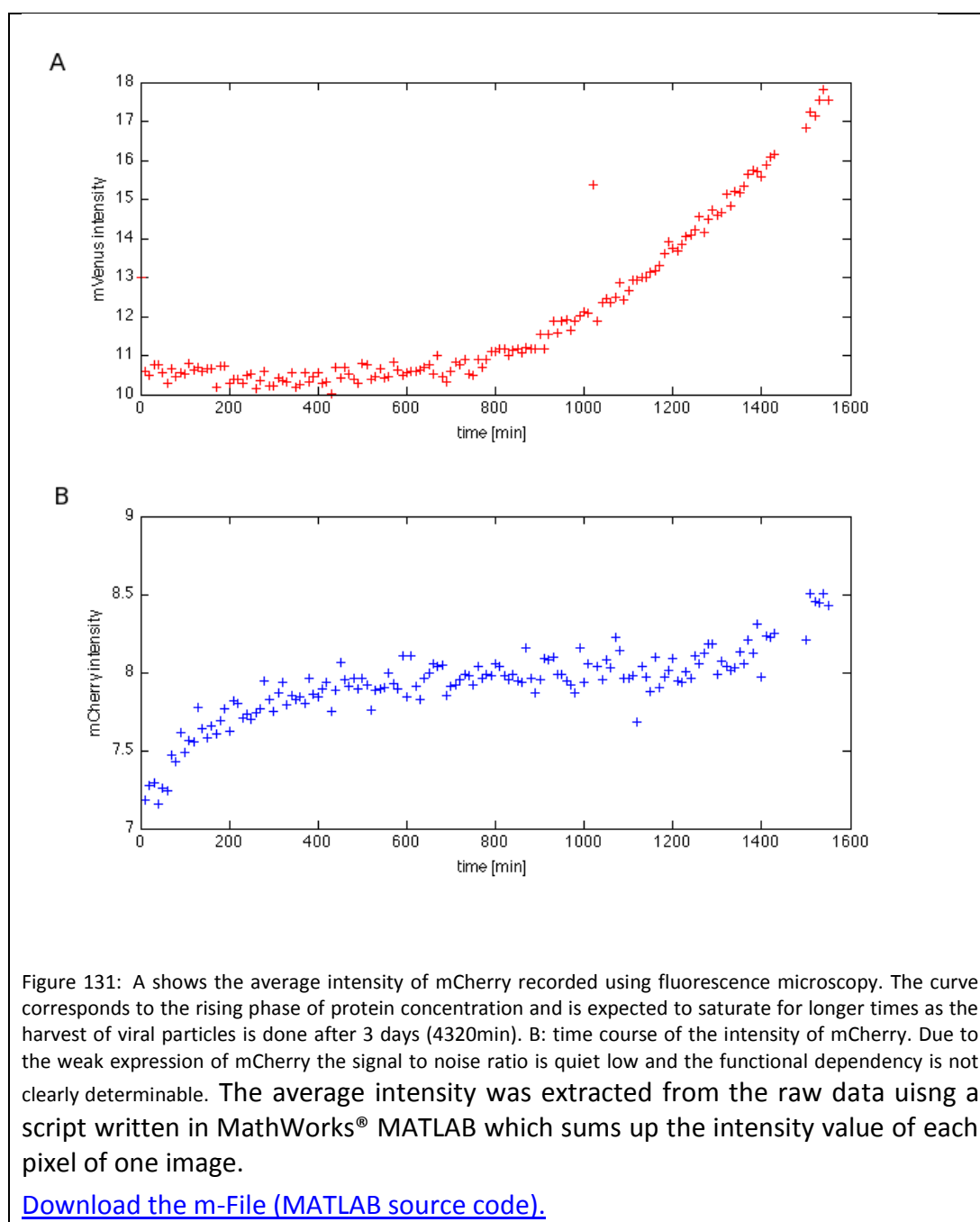


Figure 130: Fluorescence microscopy of transfected cells. Viral particles containing mCherry as gene of interest are visible.



The used model parameters are given in the table below.

Table 8: Rate constants for the virus production model. Generally forward reactions were assumed to be faster than reverse ones. Replication of ssDNA is slower than its degradation.

forward rate constant	value	reverse rate constant	value
$k_{1,1}$	0.500	$k_{1,2}$	0.010
$k_{2,1}$	0.500	$k_{2,2}$	0.010
$k_{3,1}$	0.500	$k_{3,2}$	0.010
$k_{4,1}$	0.500	$k_{4,2}$	0.010
$k_{5,1}$	0.350	—	—
$k_{6,1}$	0.350	—	—
$k_{7,1}$	0.350	—	—
$k_{8,1}$	0.500	$k_{8,2}$	0.010
$k_{9,1}$	0.500	$k_{9,2}$	0.010
$k_{10,1}$	0.500	$k_{10,2}$	0.010
$k_{11,1}$	0.500	$k_{11,2}$	0.000
$k_{12,1}$	0.500	$k_{12,2}$	0.000
$k_{13,1}$	0.500	$k_{13,2}$	0.010
$k_{14,1}$	0.007	—	—
$k_{15,1}$	0.002	—	—

[Download the m-File \(MATLAB source code\).](#)

5.6.1.5 Results and Discussion

Figure 5 shows the time course of the model for virus production. The initial plasmid concentrations were chosen to 20 μ M for the *helper*, *goi*, and *capsid-wt* plasmids and 10 μ M of the modified capsid plasmid. After the short peaks of the intranuclear plasmid concentrations proteins are synthesized and capsids are formed. The ssDNA enters the capsid through a pore and infectious virus particles are released to the cytoplasm from where they are transported out of the cell.

The concentrations reach a steady state as a result of ssDNA degradation inside the nucleus.

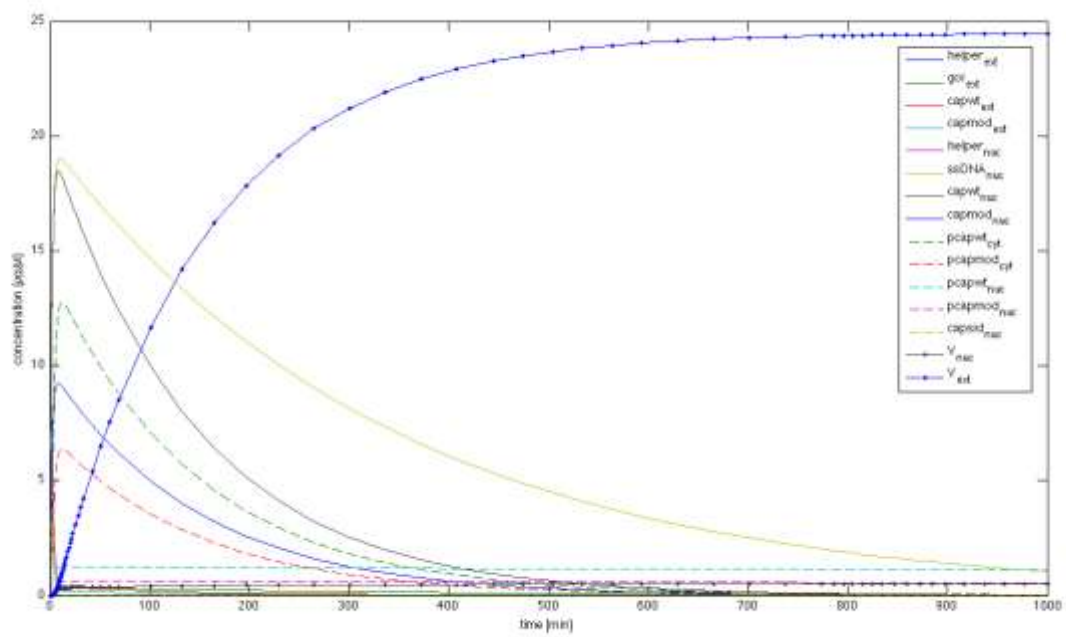


Figure 132 A model extension was made taking into account the production efficiency dependent on the level of modification. The resulting curves are plotted in figure 6.

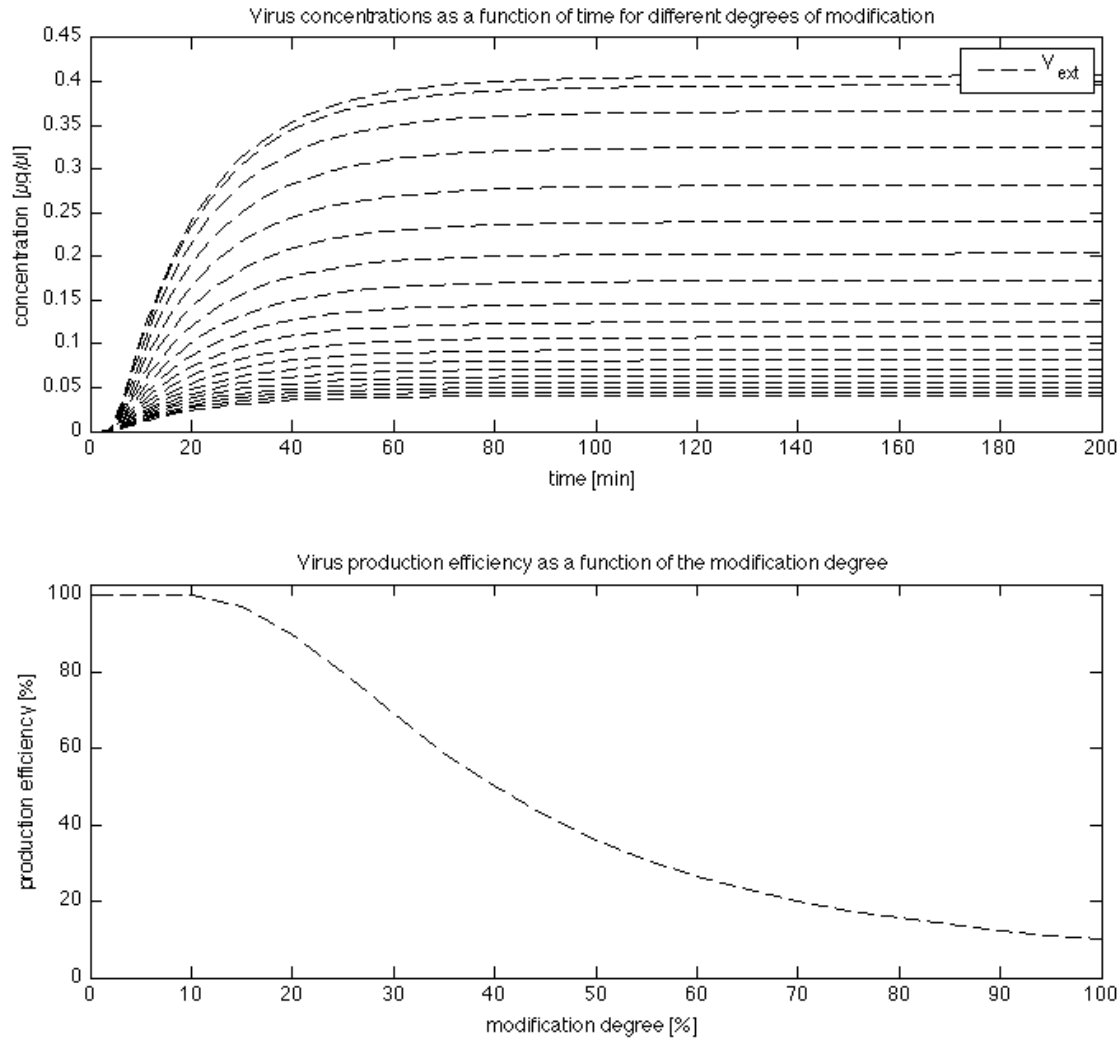
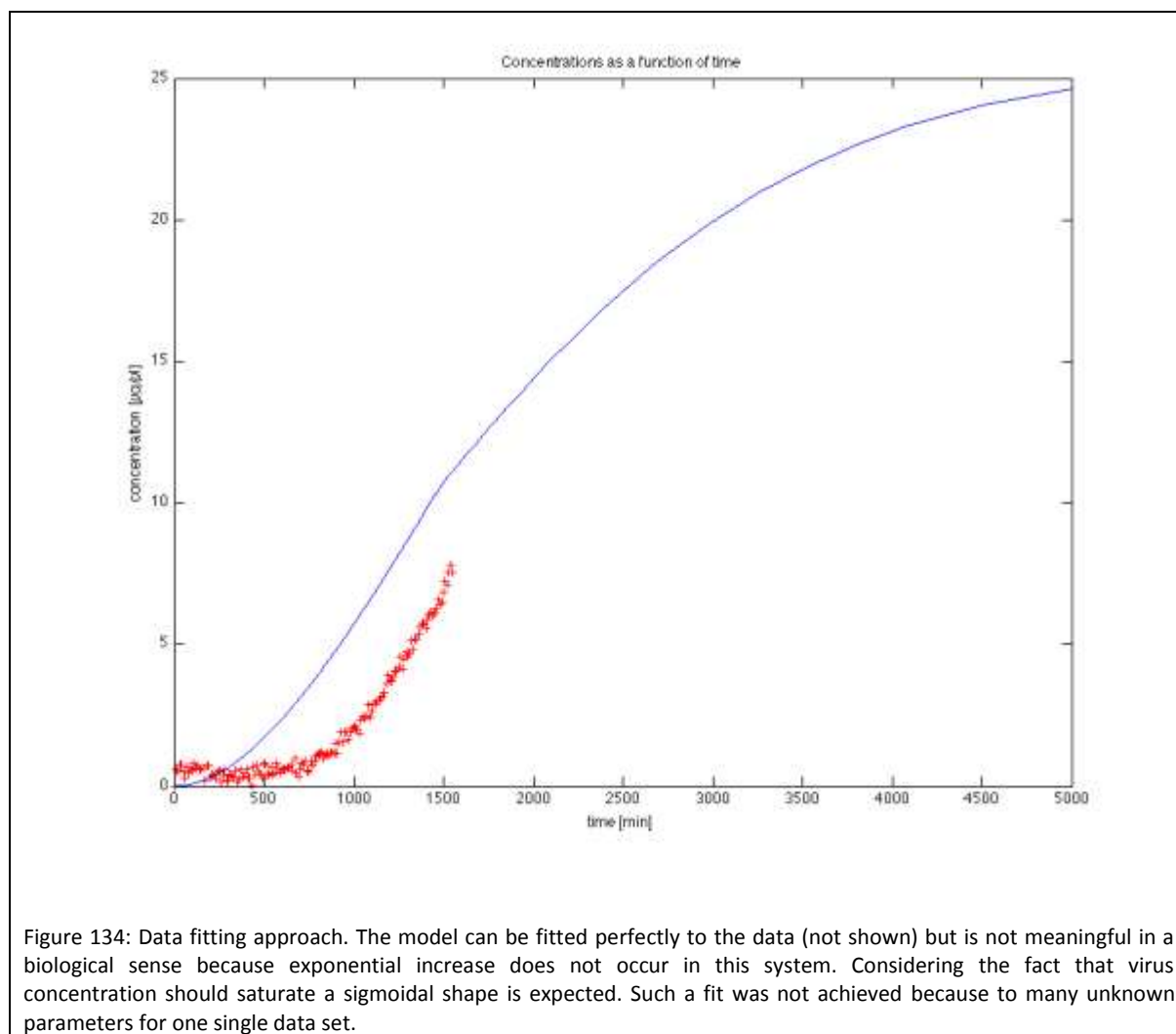


Figure 133: Enzyme concentration depending on different degrees of modification. B: production efficiency as a function of modification degree m .

Fitting the model to the data obtained from the fluorescence experiment was performed by the method of least squares in logarithmic parameter space. Unfortunately only one data set quantifying the single protein, capsid and virus concentration was available so that the optimization problem was clearly under-determined and no explicit ideal parameter set could be found without losing the biological significance. More precisely, the data was fitted by an exponential increase while the biological system is expected to saturate for large time values because no more virus is produced if its plasmid is completely degraded. Figure 7 shows more realistic model characteristics where the blue line represents the sum of all concentrations containing mVenus and the red dots describe the mVenus intensity data set.

Thereby the desired simoidal shape was achieved though the chi-square value and consequently the quality of the fit is not optimal.

In order to improve the predictive capability of this mathematical model one has to perform further adjustments and more experimental data is needed accordingly.



6 Outlook

6.1 Other strategies

6.1.1 Evolutionary Self Coating Approach (ESCA)

The motivation of ESCA is to optimize the viral surface for targeting a specific cell line with an evolutionary method and restrict the superior transduction efficiency on the VP protein of choice. Limiting the optimization on VP proteins is advantageous for introducing a characterized system in gene therapy.

To implement this ability, each viral particle needs to carry the information of its own targeting component. Successful transduction is detected via qPCR and following sequencing of the gene of interest (GOI), which encodes for the capsid structure.

An essential part of ESCA is the stable-transfected producer cell line, which offers the genetic information for the viral particles, except one VP protein under control of an inducible promoter. Transfecting the GOI triggers the synthesis of viral particles. Due to the CMV promoter the GOI gets transcribed by the cellular RNA polymerase. After translation, the targeting VP protein travels into the nucleus and infectious viral particles assemble. The GOI then gets packed into the capsid.

After harvesting, the target cells get transduced by the viral particles which is quantified via qPCR. The infectious virus capsids are able to insert their GOI into the target cell line, after sequencing of the extracted genes of interest it is possible to examine the mutations that are responsible for the superior targeting.

It is not guaranteed that each cell gets transduced by only one GOI. This way it is possible that the individual viral particles do not carry the GOI which encodes for their targeting VP protein. To minimize these stochastic fluctuations and make it truly evolutionary, multiple runs of ESCA have to be performed.

6.1.2 RNA interference (RNAi) approach

One of the most promising fields for future gene therapy is the specific knockdown of mRNA translation via small interfering RNAs. The knockdown is performed by RNA-induced silencing complex (RISC), which incorporates an active strand of RNA to target complementary sequences. The

target mRNA gets cleaved by the Argonaute-2 protein (Ago-2) and finally degraded by intracellular RNases.

Since the discovery of RNA interference in 2001/2002 (Elbashir et al. 2001),(McCaffrey et al. 2002) several groups investigate efficient methods for tissue-specific transport of RNAi. Beside liposomal transport (Zimmermann et al. 2006) various viral vectors are currently under development.

According to Grimm et al “...AAVs might actually approach our idea of an optimal vector, for several reasons.” This statement is based on the low immune response and the possibility to mediate high amounts of viral particles.

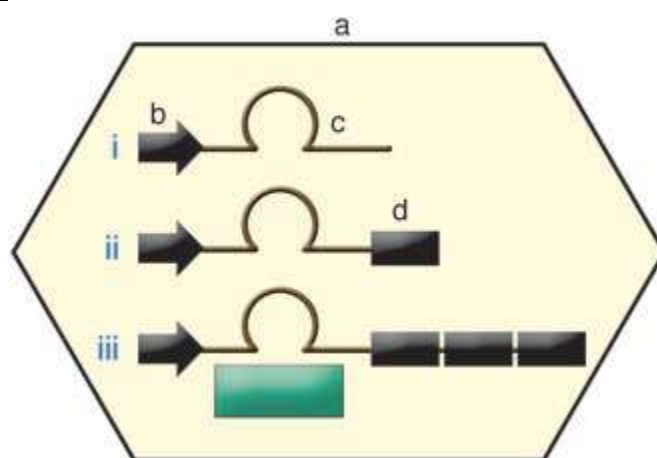


Figure 135: Levels of control over RNAi expression with viral vectors. Through binding to cellular receptors, the viral capsid (a) will determine the tropism of the RNAi vector, i.e., the tissue and cell type that will be infected. This occurs regardless of the vector insert. In a conventional shRNA expression cassette (i), the promoter (b) can further contribute to specificity by being active only in desired tissue or cell types. Alternatively, promoters can be made regulatable via exogenous triggers. Ideally, both properties are combined to permit spatiotemporal control over shRNA expression. Moreover, the shRNA itself (c) is a major determinant of specificity and control and should be designed to selectively bind to the target mRNA. (ii) Theoretically, it should be possible to create hybrid vector genomes in which an shRNA cassette is fused with a binding site for a particular miRNA (d; black box). This would allow the restriction of shRNA expression only to cells in which this miRNA is not expressed, thus helping to minimize off-target effects. (iii) Alternatively, the hybrid genome (or a vector expressing a cDNA; green box) could be fused with multiple tandem sites for miRNA binding and then be used to sequester, and thus inactivate, this miRNA from the cellular pool. This strategy is useful to block miRNAs that are involved in pathogenic processes such as tumorigenesis (Dirk Grimm & Kay 2007)

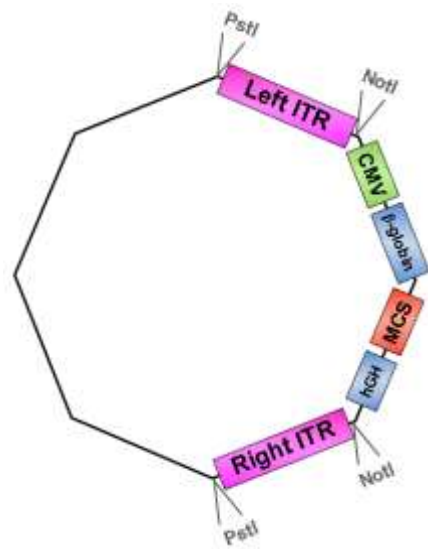
After years of investigation of viral RNAi the viral mediated approach seems to be more promising than ever. It appears that controllable, tissue specific RNAi expression is crucial for minimizing the toxic side effects of the medication. {Document not in library}

Combining our optimized vectors with miRNA coding gene of interests would be an exciting application for future works.

7 Appendix

7.1 *Dear diary* (– a Story on ITRs),

once upon a time there were two inverted terminal repeats (ITRs) – the left and the right ITR. They flanked a CMV promoter, followed by a β -globin intron, a multiple cloning site and a hGH polyA site in order to be packaged into Adeno-associated virus serotype 2 particles.



One day some biology students, participating at the iGEM competition, wanted to produce BioBricks of these two DNA sequences.

26.05.2010

For this purpose they designed and ordered primers in order to delete the PstI restriction sites which flank the ITRs via site-directed mutagenesis.

02.06.2010

Primers for removal of NotI restriction sites, which also flank the ITRs, were designed and ordered.

10.06.2010

The students conducted the first attempt of removing the PstI restriction sites: The **1st** PCR for site-directed mutagenesis was performed...

... but didn't yield any results.

18.06.2010

The team encountered a problem: The designed primers bound to both ITRs, thus amplification of just one ITR was not possible. So they hit upon the idea of digesting the plasmid with AlwNI in order to produce two different-sized fragments. Prior to PCR these two sequences could be separated by electrophoresis.

25.06.2010

Plasmid was digested with AlwNI.

28.06.2010

The **2nd** site-directed mutagenesis PCR was performed...

... but again didn't work.

The students didn't bury their head in the sand: New primers with higher annealing temperatures were designed and ordered.

30.06.2010



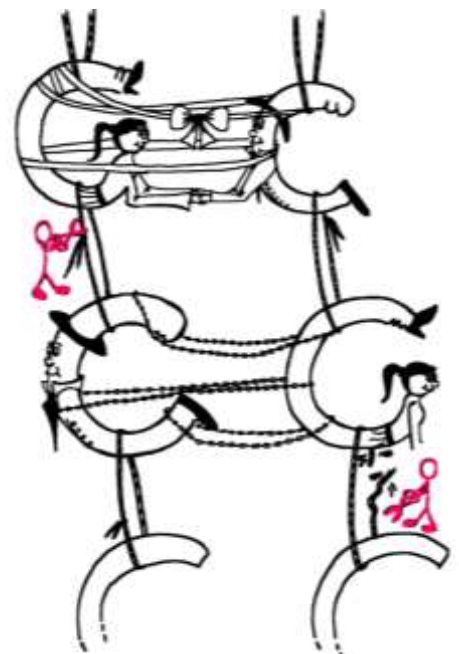
Simultaneously the eager FreiGEMs figured out an alternative plan for the ITR BioBrick production, which required no PCR steps (!): They wanted to take advantage of the NotI and PstI restriction sites flanking the ITRs. For this purpose special oligos needed to be designed: After hybridization they should deliver NotI or PstI overhangs in that way that these restriction sites become removed after ligation. By providing RFC10 restriction sites the ITR_oligo construct could be cloned into the iGEM standard plasmid resulting in ITR BioBrick. This alternative plan was named the "ITR fancy method".



05.07.2010

The "ITR fancy method" was specified:

Oligos were designed which needed to be hybridized and provided necessary RFC10 prefix or suffix restriction sites. They possessed compatible overhangs to the PstI and NotI restriction sites of the ITRs but shouldn't generate new restriction sites after ligation.



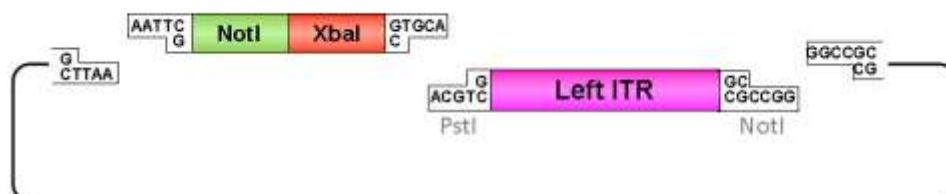
7.2 ITR Methods

ITR fancy method:

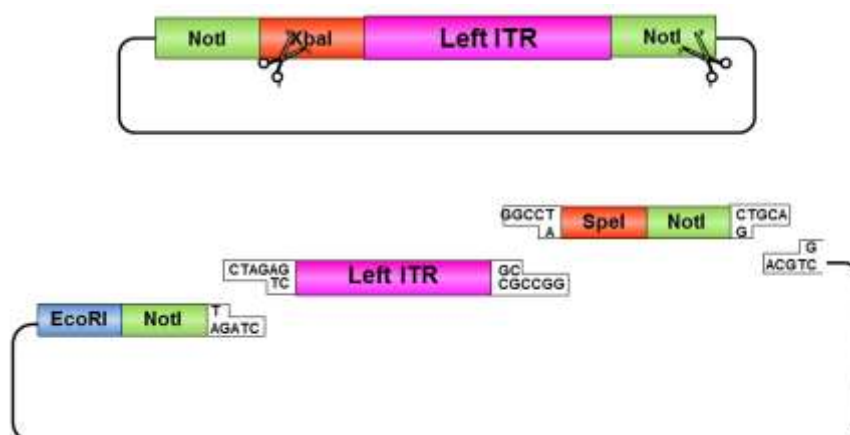
Digestion of pAAV_MCS with AlwNI: results in one large fragment (2982 bp) containing the right ITR and one small fragment (1674 bp) containing the left ITR.

Left ITR:

- Digestion of left ITR fragment with PstI and NotI
- Digestion of pSB1C3 with EcoRI and NotI
- Ligation of left ITR with prefix and pSB1C3

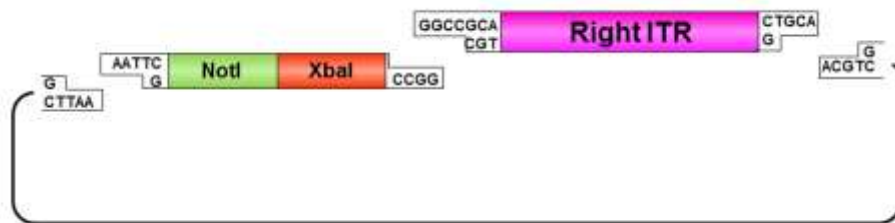


- Digestion of pSB1C3_prefix_leftITR with XbaI and NotI
- Digestion of pSB1C3 with PstI and XbaI
- Ligation of left ITR with suffix and pSB1C3

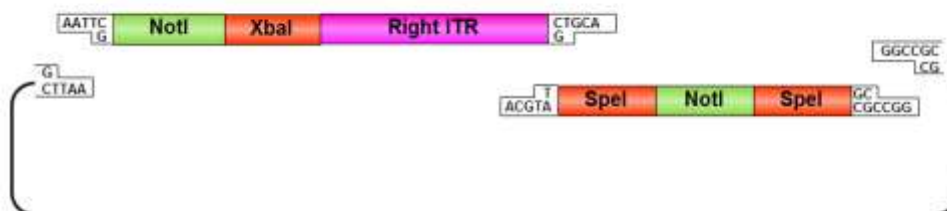


Right ITR:

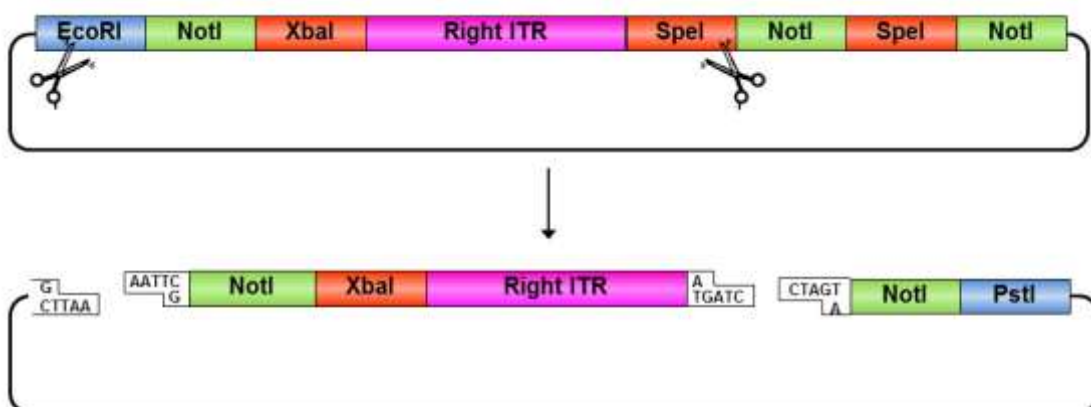
- Digestion of right ITR fragment with NotI and PstI
- Digestion of pSB1C3 with XbaI and PstI
- Ligation of right ITR with prefix and pSB1C3



- Digestion of pSB1C3_rightITR with EcoRI and NotI
- Digestion of pSB1C3 with EcoRI and NotI
- Ligation of right ITR with special suffix and pSB1C3



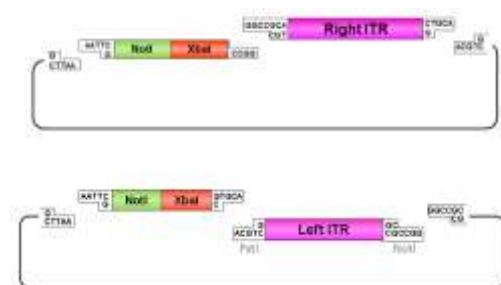
- Digestion of pSB1C3_prefix_rightITR_specialsuffix with EcoRI and SpeI
- Digestion of pSB1C3 with EcoRI and SpeI
- Ligation of pSB1C3 with right ITR



On the same day the **3rd** PCR attempt with new primers was conducted. Two reactions per ITR were performed – one without and one with 10% DMSO... but again no PCR product was detectable.

12.07.2010

First steps of the “ITR fancy method” were performed.



Result: ITRs with RFC10 prefix.

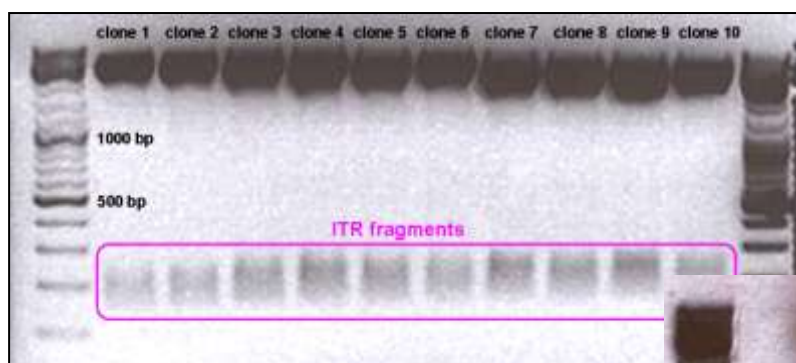
14.07.2010

The ambitious students wanted to play safe and also ordered the left ITR according to the RFC10 standard at a gene synthesis company. Nevertheless they continued with PCR and cloning, because they knew by experience that DNA synthesis could possibly take long.

15.07.2010

Unfortunately it turned out that the first try of the “ITR fancy method” didn’t work. The students were not surprised: Digestion of plasmid, gel extraction, followed by second digestion and gel extraction of just 150 bp small ITR fragments leaves nearly no DNA for ligation. Nevertheless cloning was repeated.

17.07.2010



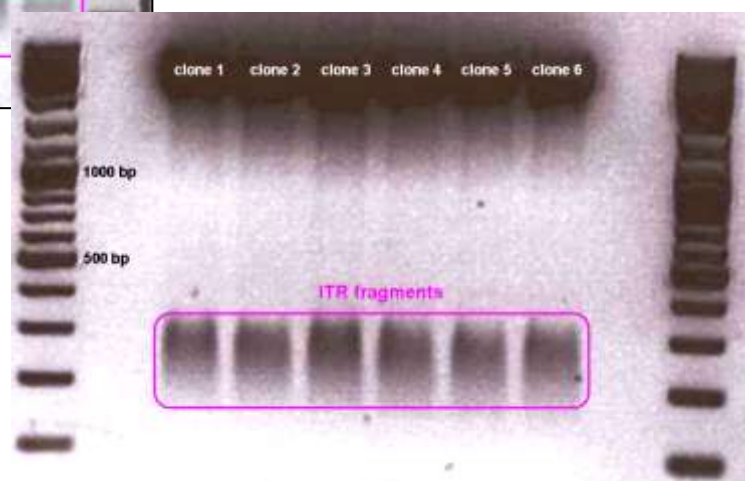
Test digestion revealed: RFC10 prefix was successfully fused to the left ITR.

19.07.2010

Test digested of the right ITR also revealed positive results: Right ITR was provided with RFC10 prefix.

Some team impressions:

“Yes, that’s great! Finally something



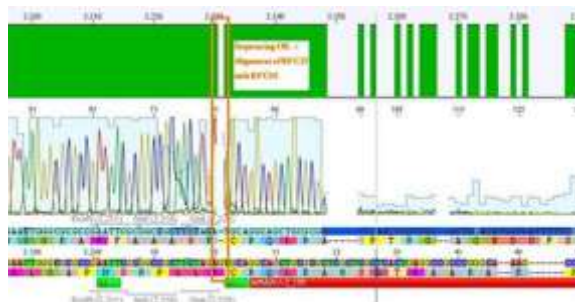
worked with our ITRs!” (Bea)

*“The most astonishing test digestion gel of our entire working time!”
(Adrian)*

21.07.2010

Sequencing not only revealed that the prefixes were successfully fused to the ITRs, but also that besides site-directed mutagenesis also sequencing of the ITRs following the standard procedure does not work.

The students concluded that the polymerase isn't able to read through and that their ITRs must fulfil a great job in forming very strong secondary structures!



It turned out that a “G” was missing in the prefix of the left ITR. Therefore new oligos were designed and ordered.

26.07.2010

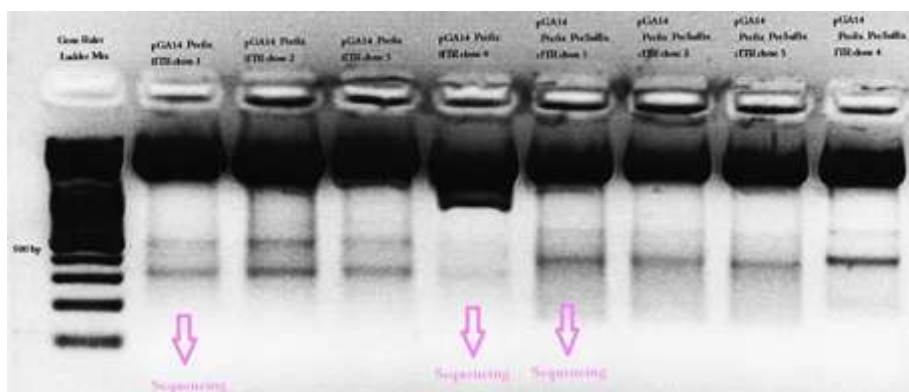


The left ITR fancy method was started again with the newly arrived oligos.

In addition to that cloning of the right ITR was continued: Fusion of special suffix to right ITR.

29.07.2010

pGA14_newPrefix_leftITR and pGA14_prefix_rightITR_specialSuffix was prepared and test digested. The ITR bands didn't exactly match to the expected fragment size. In addition a second band could be detected at about 500 bp. The students weren't able to explain this and sent three samples for sequencing.



31.07.2010

Left ITR:

The sequencing company didn't manage to read through the left ITR samples until now. The FreiGEMs interpreted this as good news: Problems with sequencing indicated very strong secondary structures – caused by (for example) ITRs!

☺

Therefore "ITR fancy method" was continued: Suffix was fused to left ITR.

Right ITR:



Sequencing results confirmed test digestion: The right ITR was provided with RFC10 prefix. However due to short chromatogram range it was not possible to validate that the "special" suffix was fused to the ITR.

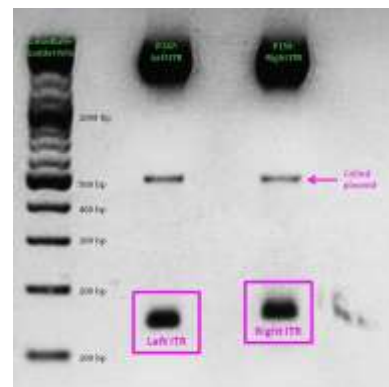
The students didn't bounce back and continued with the last step of their ITR fancy method: The right ITR needed to be subcloned into a plasmid providing the iGEM restriction sites, resulting in RFC10 suffix downstream of the ITR.



02.08.2010

Last mini-prep and test digestion was conducted: The expected fragment sizes (156 resp. 157) could be detected in the referring range between 100 and 200 bp.

Now the students wanted to verify these results and sent the samples for sequencing – this time following special procedures.



04.08.2010



Eight sequencing files (which needed to be analyzed base by base "per hand") later,

alignments showed that the ITRs are OK and were successfully converted into the RFC10 BioBrick standard.

After subcloning the ITRs into the iGEM pSB1C3 plasmid, the students were happy and proud of their success.

So they all lived happily ever after and had much fun with their new ITR BioBricks.

By the way: The students obtained satisfaction, because the ordered rebellious ITRs didn't arrive until now – even DNA synthesis seems to be difficult....

I guess the lesson is clear: Never perform PCR with ITRs, nor try to order them from gene synthesis companies. And: Better do not try to sequence them! ☺

Good luck!

7.3 Protocols

7.3.1 Recipes for stock solutions

7.3.1.1 Antibiotics

Ampicillin (Amp)

Stock solution: 100 mg/ml

In 70% EtOH

Working concentration: 20-100 µg/ml (50 µg/ml)

Cloramphenicol (Cm)

Stock solution: 25 mg/ml

In 70% EtOH

Working concentration: 25-170 µg/ml (100 µg/ml)

Kanamycin (Kana)

Stock solution: 50 mg/ml

Filter in H₂O (Millipore)!

Working concentration: 10-50 µg/ml (30 µg/ml)

Tetracycline (Tet)

Stock solution: 25 mg/ml

In 70% EtOH

Working concentration: 10-50 µg/ml (10 µg/ml in liquid culture; 12,5 µg/ml in Plates)

Be careful: Light sensitive, take aluminium foil and wrap tube!

7.3.1.2 Buffers and Solutions

2× HBS

280 mM NaCl

1.5 mM Na₂HPO₄

50 mM HEPES*

Adjust the pH to 7.10 with NaOH

N-2-hydroxyethylpiperazine- N'-2ethanesulfonic acid 100ml

Na₂HPO₄: M= 177,99 g/mol -> 0.027g

NaCl : M= 58.44 g/mol -> 1,636g

HEPES

M= 238,31 g/mol -> 1,19155g

Add approx. 50ml H₂O (Milipore)

pH 7.10 titrate with NaOH (start with 5M and use 1M afterwards)

Fill up to 100ml

Sterile filtrate (small filtration)

TAE (50x) (1 l)

242 g tris base

57.1 ml glacial acetic acid

100 ml 0.5 M EDTA

Fill up to 1 l using H₂O (Millipore)

CaCl₂ (1 M)

110,98 g CaCl₂

1 l H₂O milipore

For 1 l:

CaCl₂ x 2 H₂O : M= 147,02 g/mol

Molecular weight 147,02 g

fill up to 1000 ml with Milipore H₂O

sterile filtration (Big Filtration)

TE Buffer (1×) (100 ml)

10 mM Tris-HCl (pH 7.5) -> M= 121,14 g/m

1 mM EDTA -> c=0,5M

Autoclave

1,2114g Tris + 0,2 ml EDTA (0,5M)

add 70 ml H₂O (Milipore)

titrate with HCl to pH 7,50

ad 100 ml H₂O (Milipore)

filter

Glycerol

fill Glycerol into a flask

autoclave

IPTG

MW= 238,3 g/mol

1M Stock solution: 238,3g in 1l H₂O

- 20ml: 4,766g in 20ml H₂O
- filtern ("sterilize by filtration)
- aliquot in 1 ml portions and store at -20°C

7.3.1.3 Media

DYT

5 Liter:

80 g Bactotrypton

50 g Bacto yeast

25 g NaCl

- add 2 l Millipore-H₂O

- add the magnetic stir bar
- add 5 l Millipore H₂O
- fill into a jar
- autoclave

LB-Medium + Agar

Only start to prepare the LB Medium if it will be autoclaved on the same day (8:00 am, 10:00 am, 12:00 am, 14:00 pm).

Take a 1 L flask and fill in:

- 10 g Bactotryptone
- 10 g NaCl
- 5 g Bactoyeast
- Add 500 ml Millipore H₂O and dissolve the three substances.
- While dissolving, prepare 19 or 20 100 ml flasks and fill in 0,75 g Agar (0,015 g Agar/ml).
- Label it with your name, the date and LB+Agar.
- As soon as the substances are dissolved in 500 ml Millipore H₂O add another 500 ml.
- Then fill 50 ml LB-medium in each 100 ml flask and autoclave it.

7.3.1.4 E. coli culture

7.3.1.4.1 Competent E-coli-cells

Preparation rules

- Work always sterile, fast and on ice
- All volumes deal with the common cell line
- The centrifuge should cool down to 4 °C early enough
- Prepare 1,5 ml tubes and cool down to -80 °C before using
- Use Milipore filter for preparation of sterile CaCl₂

Main steps:

- Prepare 15 ml LB-Medium (or DYT) with the specific antibiotic (XL1-blue Tetracycline, BL21 none!), inoculate and incubate over night
- Prepare 200 ml LB-Medium (or DYT) with the specific antibiotic, inoculate with 2ml of the over-night-culture
- Wait until culture reaches OD₆₀₀ 0,2-0,5

- Keep cell suspension in sterile falcons (50 ml) 20 min on ice, then centrifuge for 20 min at
- 4 °C; 2500 g
- Discard supernatant, carefully resuspend on ice with 2,5 ml cold 80 mM CaCl₂ solution per falcon
- Pool every resuspended aliquot
- Add 40 ml CaCl₂ solution (total volume 50ml)
- Keep falcon for 30 min on ice
- Centrifuge for 20 min; 4 °C; 2500 g
- Discard supernatant, carefully resuspend pellet in 5,5 ml CaCl₂ (80 mM) /Glycerol (≥ 99,5%)
- Prepare 60 µl aliquots in 1,5 ml tubes and store immediately at - 80 °C
- Preparation of 80 mM CaCl₂ solution:
- Mix 2,94 g calcium chloride (+ 2H₂O) with 250 ml Milipore H₂O (80 mM)
- Filtrate the solution with Milipore filter in another 250ml-flask
- Preparation of CaCl₂/Glycerol solution:
- 4,12 ml CaCl₂ (80 mM)
- 1,38 ml Glycerol (≥ 99,5%)
- Vortex and put on ice afterwards

Check for competent Cells

- PUC18 50pg/µl -> 2 µl to 1 1,5 ml tubes of cells
- Test-Trafo
- 1 Kan +1 Amp –additional plate with untransfected cells for control

7.3.2 Cell culture protocols

For safe treatment of cells, the following steps have to be carried out under sterile conditions.

7.3.2.1 Establishing AAV-293 Cultures from Frozen Cells

Required materials and chemicals: DMEM (Dulbecco's Modified Eagle Medium 1x, Invitrogen, Darmstadt, Germany), PBS (Dulbecco's PBS (1x) w/o Ca and Mg, PAA Laboratories GmbH, Pasching, Austria), T75 flask (

Nunc, 75 cm² nunclon treated flask, blue filter cap, Roskilde, Denmark), 15 ml falcon, pipett tips

- Thaw frozen cells within 1-2 minutes by gentle agitation in a 37 °C water bath

- Transfer the thawed cells suspension into the 15 ml falcon containing 10 ml of DMEM
- Collect cells by centrifugation at 200 g for 5 minutes at room temperature (Centrifuge 5702, Eppendorf, Hamburg, Germany)
- Remove supernatant and resuspend the cells in 3 ml of fresh DMEM by gently pipetting up and down
- Transfer the 3 ml of cell suspension to a T75 flask containing 17 ml of DMEM
- Place the cells in a 37 °C incubator at 5 % CO₂.
- Monitor cell density daily. Cells should be passaged when the culture reaches 50 % confluence.

7.3.2.2 Passaging of AAV-293 Cells

Required materials and chemicals: DMEM, PBS, Trypsin-EDTA 0,25 % (Invitrogen, Darmstadt, Germany), T75 flask, 15 ml falcon, pipett tips

- Prewarm the DMEM to 37 °C in a water bath and trypsin-EDTA solution at room temperature
- Remove the medium and wash cells once with 10ml of phosphate-buffer saline (PBS)
- Trypsinize the cells for 1-1.5 minutes in 1 ml of trypsin-EDTA solution
- Dilute the cells with 10 ml DMEM to inactivate the trypsin and detach the remaining cells by soft resuspending
- Transfer cells into a 15 ml falcon
- Collect cells by centrifugation at 200 g for 5 minutes
- Calculate the cell amount per ml via Neubauer cell chamber
- Mix 95 µl Trypan Blue Stain 0,4 % (Lonza, Walkersville, USA) with 5 µl of the cell suspension
- Mix gently by pipetting up and down
- Pipet the solution into the Neubauer chamber
- Trypan stains dead cells blue, living cells appear as white
- Counting of all living cells in four big squares
- Calculate the amount of living cells per ml with the help of following formula:
- $((\text{counted cells})/4) * 2.2 * 20 * 10.000 = \text{cells per ml}$
- Calculate the cell amount per T75 flask (1.500.000 cells/20 ml DMEM) and transfer the cell

- suspension to a T75 flask containing fresh DMEM. Place the cells in a 37 °C incubator at 5 % CO₂.

7.3.2.3 Transfecting the AAV-293 Cells

Stratagene recommends a calcium phosphate-based protocol, usually resulting in the production of titers $\geq 10^7$ particles/ml when AAV-293 cells were transfected. To achieve high titers, it is important that AAV-293 cells are healthy and plated at optimal density. Clumping of the cells should be avoided during passaging and plating for transfection.

Required materials and chemicals: 0,5 M CaCl₂ , 2x HBS-Buffer pH 7.112 , autoclaved millipore water, falcons, 1,5 ml tubes

- Inspect the host cells that were split two days before; they should be approx. 70-80 % confluent
- Remove the plasmids to be co-transfected from storage at -20 °C. Adjust the concentration of each plasmid to 1 µg/µl in sterile/autoclaved Millipore water.
- Pipet the required volume of each of the plasmid DNA solution (5 µg of each plasmid) into an 1,5 ml tubes. Fill up to 300 µl with sterile Millipore water.
- Add 300 µl of 0.5 M CaCl₂ and mix gently.
- Pipet 600 µl of 2x HBS into a 15 ml falcon.
- Vortex the falcon gently while pipetting the DNA/CaCl₂ solution dropwise into the falcon.
- Incubate 20 minutes (precipitate formation)
- Apply the DNA/CaCl₂/2x HBS solution dropwise to the plate of cells (10 cm dish)
- Return the cells in a 37 °C incubator at 5 % CO₂ for 6 hours
- After incubation remove the medium, wash once with PBS and replace it with 10 ml of fresh DMEM growth medium
- Return the cells back to the 37 °C incubator for an additional 66-72 hours

8 Acknowledgment

9 References:

- Adachi, Y. et al., 2000. Experimental gene therapy for brain tumors using adenovirus-mediated transfer of cytosine deaminase gene and uracil phosphoribosyltransferase gene with 5-fluorocytosine. *Human gene therapy*, 11(1), pp.77-89. Available at: <http://www.ncbi.nlm.nih.gov/pubmed/10646641>.
- Aghi, M. et al., 1998. Synergistic anticancer effects of ganciclovir/thymidine kinase and 5-fluorocytosine/cytosine deaminase gene therapies. *Journal of the National Cancer Institute*, 90(5), pp.370-80. Available at: <http://www.ncbi.nlm.nih.gov/pubmed/9498487>.
- Albelda, S.M. et al., 1990. Integrin distribution in malignant melanoma: association of the beta 3 subunit with tumor progression. *Cancer research*, 50(20), pp.6757-64. Available at: <http://www.ncbi.nlm.nih.gov/pubmed/2208139>.
- Andrei, G. et al., 2005. Characterization of herpes simplex virus type 1 thymidine kinase mutants selected under a single round of high-dose brivudin. *Journal of virology*, 79(9), pp.5863-9. Available at: <http://www.pubmedcentral.nih.gov/articlerender.fcgi?artid=1082774&tool=pmcentrez&rendertype=abstract>.
- Ardiani, a, Sanchez-Bonilla, M. & Black, M.E., 2010. Fusion enzymes containing HSV-1 thymidine kinase mutants and guanylate kinase enhance prodrug sensitivity in vitro and in vivo. *Cancer gene therapy*, 17(2), pp.86-96. Available at: <http://www.pubmedcentral.nih.gov/articlerender.fcgi?artid=2808426&tool=pmcentrez&rendertype=abstract>.
- Asokan, A. et al., 2006. Adeno-associated virus type 2 contains an integrin alpha5beta1 binding domain essential for viral cell entry. *Journal of virology*, 80(18), pp.8961-9. Available at: <http://www.pubmedcentral.nih.gov/articlerender.fcgi?artid=1563945&tool=pmcentrez&rendertype=abstract>.
- AVIGEN, I., 1997. WO9706272A3.pdf.
- Beaton, a, Palumbo, P. & Berns, K I, 1989. Expression from the adeno-associated virus p5 and p19 promoters is negatively regulated in trans by the rep protein. *Journal of virology*, 63(10), pp.4450-4. Available at: <http://www.pubmedcentral.nih.gov/articlerender.fcgi?artid=251068&tool=pmcentrez&rendertype=abstract>.
- Beckmann Coulter, 2008. CyAnADP Instructions for Use. *CyAN ADP*, (June).
- Berg, O.G. et al., 2001. Interfacial enzymology: the secreted phospholipase A(2)-paradigm. *Chemical reviews*, 101(9), pp.2613-54. Available at: <http://www.ncbi.nlm.nih.gov/pubmed/11749391>.

- Berthet, C. et al., 2005. How adeno-associated virus Rep78 protein arrests cells completely in S phase. *Proceedings of the National Academy of Sciences of the United States of America*, 102(38), pp.13634-9. Available at: <http://www.pubmedcentral.nih.gov/articlerender.fcgi?artid=1224635&tool=pmcentrez&rendertype=abstract>.
- Binz, H.K. et al., 2003. Designing Repeat Proteins: Well-expressed, Soluble and Stable Proteins from Combinatorial Libraries of Consensus Ankyrin Repeat Proteins. *Journal of Molecular Biology*, 332(2), pp.489-503. Available at: <http://linkinghub.elsevier.com/retrieve/pii/S0022283603008969>.
- Black, M.E., Kokoris, M.S. & Sabo, P., 2001. Herpes simplex virus-1 thymidine kinase mutants created by semi-random sequence mutagenesis improve prodrug-mediated tumor cell killing. *Cancer research*, 61(7), pp.3022-6. Available at: <http://www.ncbi.nlm.nih.gov/pubmed/11306482>.
- Black, M.E. et al., 1996. Creation of drug-specific herpes simplex virus type 1 thymidine kinase mutants for gene therapy. *Proceedings of the National Academy of Sciences of the United States of America*, 93(8), pp.3525-9. Available at: <http://www.pubmedcentral.nih.gov/articlerender.fcgi?artid=39643&tool=pmcentrez&rendertype=abstract>.
- Bleker, S., Pawlita, M. & Kleinschmidt, J.A., 2006. Impact of capsid conformation and Rep-capsid interactions on adeno-associated virus type 2 genome packaging. *Journal of virology*, 80(2), pp.810-20. Available at: <http://www.pubmedcentral.nih.gov/articlerender.fcgi?artid=1346863&tool=pmcentrez&rendertype=abstract>.
- Bleker, S., Sonntag, F. & Kleinschmidt, A., 2005. Mutational Analysis of Narrow Pores at the Fivefold Symmetry Axes of Adeno-Associated Virus Type 2 Capsids Reveals a Dual Role in Genome Packaging and Activation of Phospholipase A2 Activity. *Society*, 79(4), pp.2528-2540.
- Bleker, S., Sonntag, F. & Kleinschmidt, J.A., 2005. Mutational analysis of narrow pores at the fivefold symmetry axes of adeno-associated virus type 2 capsids reveals a dual role in genome packaging and activation of phospholipase A2 activity. *Journal of virology*, 79(4), pp.2528-40. Available at: <http://www.pubmedcentral.nih.gov/articlerender.fcgi?artid=546590&tool=pmcentrez&rendertype=abstract>.
- Bork, P., 1993. Hundreds of ankyrin-like repeats in functionally diverse proteins: mobile modules that cross phyla horizontally? *Proteins*, 17(4), pp.363-74. Available at: <http://www.ncbi.nlm.nih.gov/pubmed/8108379>.
- BRODSKY, F. et al., 1991. Clathrin light chains: arrays of protein motifs that regulate coated-vesicle dynamics. *Trends in Biochemical Sciences*, 16, pp.208-213. Available at: <http://linkinghub.elsevier.com/retrieve/pii/096800049190087C>.
- Büning, Hildegard et al., 2008. Recent developments in adeno-associated virus vector technology. *The journal of gene medicine*, 10(7), pp.717-33. Available at: <http://www.ncbi.nlm.nih.gov/pubmed/18452237>.

- Carter, B.J., Antoni, B. a & Klessig, D.F., 1992. Adenovirus containing a deletion of the early region 2A gene allows growth of adeno-associated virus with decreased efficiency. *Virology*, 191(1), pp.473-6. Available at: <http://www.ncbi.nlm.nih.gov/pubmed/1329332>.
- Cassinotti, P., Weitzand, M. & Tratschin, J.D., 1988. Organization of the adeno-associated virus (AAV) capsid gene: mapping of a minor spliced mRNA coding for virus capsid protein. *Virology*, 167(1), pp.176-84. Available at: <http://www.ncbi.nlm.nih.gov/pubmed/18644583>.
- Chang, L.S., Shi, Y. & Shenk, Thomas, 1989. Adeno-associated virus P5 promoter contains an adenovirus E1A-inducible element and a binding site for the major late transcription factor. *Journal of virology*, 63(8), pp.3479-88. Available at: <http://www.pubmedcentral.nih.gov/articlerender.fcgi?artid=250925&tool=pmcentrez&rendertype=abstract>.
- Clark, K.R. et al., 1999. Highly purified recombinant adeno-associated virus vectors are biologically active and free of detectable helper and wild-type viruses. *Human gene therapy*, 10(6), pp.1031-9. Available at: <http://www.ncbi.nlm.nih.gov/pubmed/10223736>.
- Collaco, R.F. et al., 2003. A biochemical characterization of the adeno-associated virus Rep40 helicase. *The Journal of biological chemistry*, 278(36), pp.34011-7. Available at: <http://www.ncbi.nlm.nih.gov/pubmed/12824181>.
- Collins, B.M. et al., 2002. Molecular Architecture and Functional Model of the Endocytic AP2 Complex. *Cell*, 109(4), pp.523-535. Available at: <http://linkinghub.elsevier.com/retrieve/pii/S0092867402007353>.
- Colquhoun, a J. & Mellon, J.K., 2002. Epidermal growth factor receptor and bladder cancer. *Postgraduate medical journal*, 78(924), pp.584-9. Available at: <http://www.pubmedcentral.nih.gov/articlerender.fcgi?artid=1742539&tool=pmcentrez&rendertype=abstract>.
- Damjanovich, L. et al., 1992. Distribution of integrin cell adhesion receptors in normal and malignant lung tissue. *American journal of respiratory cell and molecular biology*, 6(2), pp.197-206. Available at: <http://www.ncbi.nlm.nih.gov/pubmed/1540382>.
- Damon, L.E., Cadman, E. & Benz, C., 1989. Enhancement of 5-fluorouracil antitumor effects by the prior administration of methotrexate. *Pharmacology & therapeutics*, 43(2), pp.155-85. Available at: <http://www.ncbi.nlm.nih.gov/pubmed/2675132>.
- Danckwardt, S., Hentze, M.W. & Kulozik, A.E., 2008. 3' end mRNA processing: molecular mechanisms and implications for health and disease. *The EMBO journal*, 27(3), pp.482-98. Available at: <http://www.ncbi.nlm.nih.gov/pubmed/18256699>.
- Davis, M.D., Wu, J. & Owens, R.A., 2000. Mutational analysis of adeno-associated virus type 2 Rep68 protein endonuclease activity on partially single-stranded substrates. *Journal of virology*, 74(6), pp.2936-42. Available at: <http://www.pubmedcentral.nih.gov/articlerender.fcgi?artid=111789&tool=pmcentrez&rendertype=abstract>.

- DiPrimio, N. et al., 2008. Surface loop dynamics in adeno-associated virus capsid assembly. *Journal of virology*, 82(11), pp.5178-89. Available at: <http://www.pubmedcentral.nih.gov/articlerender.fcgi?artid=2395211&tool=pmcentrez&rendertype=abstract>.
- Dong, J.Y., Fan, P.D. & Frizzell, R.A., 1996. Quantitative analysis of the packaging capacity of recombinant adeno-associated virus. *Human gene therapy*, 7(17), pp.2101-12. Available at: <http://www.ncbi.nlm.nih.gov/pubmed/8934224>.
- Douar, A., Poulard, K. & Stockholm, D., O., 2001. Intracellular trafficking of adeno-associated virus vectors: routing to the late endosomal compartment and proteasome degradation. *Journal of Virology*, 75(4), pp.1824-1833. Available at: <http://jvi.asm.org/cgi/content/abstract/75/4/1824>.
- Elbashir, S.M. et al., 2001. Duplexes of 21-nucleotide RNAs mediate RNA interference in cultured mammalian cells. *Nature*, 411(6836), pp.494-8. Available at: <http://www.ncbi.nlm.nih.gov/pubmed/11373684>.
- FARBER, S., 1949. Some observations on the effect of folic acid antagonists on acute leukemia and other forms of incurable cancer. *Blood*, 4(2), pp.160-7. Available at: <http://www.ncbi.nlm.nih.gov/pubmed/18107667>.
- Freeman, S.M. et al., 1993. The "bystander effect": tumor regression when a fraction of the tumor mass is genetically modified. *Cancer research*, 53(21), pp.5274-83. Available at: <http://www.ncbi.nlm.nih.gov/pubmed/8221662>.
- Friedman, M. et al., 2008. Directed evolution to low nanomolar affinity of a tumor-targeting epidermal growth factor receptor-binding affibody molecule. *Journal of molecular biology*, 376(5), pp.1388-402. Available at: <http://www.ncbi.nlm.nih.gov/pubmed/18207161>.
- Gentry, B.G. et al., 2005. GCV phosphates are transferred between HeLa cells despite lack of bystander cytotoxicity. *Gene therapy*, 12(13), pp.1033-41. Available at: <http://www.ncbi.nlm.nih.gov/pubmed/15789060>.
- Girod, A. et al., 2002. The VP1 capsid protein of adeno-associated virus type 2 is carrying a phospholipase A2 domain required for virus infectivity. *The Journal of general virology*, 83(Pt 5), pp.973-8. Available at: <http://www.ncbi.nlm.nih.gov/pubmed/11961250>.
- Gladson, C.L. & Cheresch, D.A., 1991. Glioblastoma expression of vitronectin and the alpha v beta 3 integrin. Adhesion mechanism for transformed glial cells. *The Journal of clinical investigation*, 88(6), pp.1924-32. Available at: <http://www.pubmedcentral.nih.gov/articlerender.fcgi?artid=295768&tool=pmcentrez&rendertype=abstract>.
- Gonçalves, M. a F.V., 2005. Adeno-associated virus: from defective virus to effective vector. *Virology journal*, 2, p.43. Available at: <http://www.pubmedcentral.nih.gov/articlerender.fcgi?artid=1131931&tool=pmcentrez&rendertype=abstract>.

- Greco, O. & Dachs, G.U., 2001. Gene directed enzyme/prodrug therapy of cancer: historical appraisal and future perspectives. *Journal of cellular physiology*, 187(1), pp.22-36. Available at: <http://www.ncbi.nlm.nih.gov/pubmed/11241346>.
- Grieger, J.C. et al., 2007. Surface-exposed adeno-associated virus Vp1-NLS capsid fusion protein rescues infectivity of noninfectious wild-type Vp2/Vp3 and Vp3-only capsids but not that of fivefold pore mutant virions. *Journal of virology*, 81(15), pp.7833-43. Available at: <http://www.pubmedcentral.nih.gov/articlerender.fcgi?artid=1951316&tool=pmcentrez&rendertype=abstract>.
- Grignet-Debrus, C. et al., 2000. The role of cellular- and prodrug-associated factors in the bystander effect induced by the Varicella zoster and Herpes simplex viral thymidine kinases in suicide gene therapy. *Cancer gene therapy*, 7(11), pp.1456-68. Available at: <http://www.ncbi.nlm.nih.gov/pubmed/11129288>.
- Grimm, Dirk & Kay, M.A., 2007. Review series Therapeutic application of RNAi : is mRNA targeting finally ready for prime time ? *Gene*, 117(12), pp.3633-3641.
- Göstring, L. et al., 2010. Quantification of internalization of EGFR-binding Affibody molecules: Methodological aspects. *International Journal of Oncology*, 36(4), pp.757-763. Available at: <http://www.spandidos-publications.com/ijo/36/4/757>.
- Halperin, E.C., 2006. Particle therapy and treatment of cancer. *The lancet oncology*, 7(8), pp.676-85. Available at: <http://www.ncbi.nlm.nih.gov/pubmed/16887485>.
- Hermonat, P L et al., 1998. The adeno-associated virus Rep78 major regulatory protein binds the cellular TATA-binding protein in vitro and in vivo. *Virology*, 245(1), pp.120-7. Available at: <http://www.ncbi.nlm.nih.gov/pubmed/9614873>.
- Hirsch, F.R. et al., 2003. Epidermal growth factor receptor in non-small-cell lung carcinomas: correlation between gene copy number and protein expression and impact on prognosis. *Journal of clinical oncology : official journal of the American Society of Clinical Oncology*, 21(20), pp.3798-807. Available at: <http://www.ncbi.nlm.nih.gov/pubmed/12953099>.
- Hoffmann, a & Roeder, R.G., 1991. Purification of his-tagged proteins in non-denaturing conditions suggests a convenient method for protein interaction studies. *Nucleic acids research*, 19(22), pp.6337-8. Available at: <http://www.pubmedcentral.nih.gov/articlerender.fcgi?artid=329157&tool=pmcentrez&rendertype=abstract>.
- Huber, B.E. et al., 1993. In vivo antitumor activity of 5-fluorocytosine on human colorectal carcinoma cells genetically modified to express cytosine deaminase. *Cancer research*, 53(19), pp.4619-26. Available at: <http://www.ncbi.nlm.nih.gov/pubmed/8402637>.
- Huber, B.E. et al., 1994. Metabolism of 5-fluorocytosine to 5-fluorouracil in human colorectal tumor cells transduced with the cytosine deaminase gene: significant antitumor effects when only a small percentage of tumor cells express cytosine deaminase. *Proceedings of the National Academy of Sciences of the United States of America*, 91(17), pp.8302-6. Available at:

- <http://www.pubmedcentral.nih.gov/articlerender.fcgi?artid=44594&tool=pmcentrez&rendertype=abstract>.
- Hutchison, C. a et al., 1978. Mutagenesis at a specific position in a DNA sequence. *The Journal of biological chemistry*, 253(18), pp.6551-60. Available at: <http://www.ncbi.nlm.nih.gov/pubmed/681366>.
- Hüser, D. et al., 2010. Integration preferences of wildtype AAV-2 for consensus rep-binding sites at numerous loci in the human genome. *PLoS pathogens*, 6(7), p.e1000985. Available at: <http://www.pubmedcentral.nih.gov/articlerender.fcgi?artid=2900306&tool=pmcentrez&rendertype=abstract>.
- Im, D.S. & Muzyczka, N, 1990. The AAV origin binding protein Rep68 is an ATP-dependent site-specific endonuclease with DNA helicase activity. *Cell*, 61(3), pp.447-57. Available at: <http://www.ncbi.nlm.nih.gov/pubmed/2159383>.
- Jing, X.J. et al., 2001. Inhibition of adenovirus cytotoxicity, replication, and E2a gene expression by adeno-associated virus. *Virology*, 291(1), pp.140-51. Available at: <http://www.ncbi.nlm.nih.gov/pubmed/11878883>.
- Johnson, J.S. et al., 2010. Mutagenesis of adeno-associated virus type 2 capsid protein VP1 uncovers new roles for basic amino acids in trafficking and cell-specific transduction. *Journal of virology*, 84(17), pp.8888-902. Available at: <http://www.pubmedcentral.nih.gov/articlerender.fcgi?artid=2918992&tool=pmcentrez&rendertype=abstract>.
- Kapeller, R. & Cantley, L.C., 1994. Phosphatidylinositol 3-kinase. *BioEssays : news and reviews in molecular, cellular and developmental biology*, 16(8), pp.565-76. Available at: <http://www.ncbi.nlm.nih.gov/pubmed/8086005>.
- Kelley, K.W., 2008. Effect of inhibition of dynein function and microtubule-altering drugs on AAV2 transduction. *Brain, behavior, and immunity*, 22(5), p.629. Available at: <http://www.ncbi.nlm.nih.gov/pubmed/18554561>.
- Kilstrup, M. et al., 1989. Genetic evidence for a repressor of synthesis of cytosine deaminase and purine biosynthesis enzymes in Escherichia coli. *Journal of bacteriology*, 171(4), pp.2124-7. Available at: <http://www.pubmedcentral.nih.gov/articlerender.fcgi?artid=209866&tool=pmcentrez&rendertype=abstract>.
- King, J. a et al., 2001. DNA helicase-mediated packaging of adeno-associated virus type 2 genomes into preformed capsids. *The EMBO journal*, 20(12), pp.3282-91. Available at: <http://www.pubmedcentral.nih.gov/articlerender.fcgi?artid=150213&tool=pmcentrez&rendertype=abstract>.
- Koechlin, B.A. et al., 1966. THE METABOLISM OF 5-FLUOROCYTOSINE-214C AND OF CYTOSINE-14C I N THE RAT A N D THE DISPOSITION OF 5-FLUOROCYTOSINE-214C I N MAN. *Metabolism Clinical And Experimental*, 15, pp.435-446.

- Koerber, J.T. et al., 2007. Engineering adeno-associated virus for one-step purification via immobilized metal affinity chromatography. *Human gene therapy*, 18(4), pp.367-78. Available at: <http://www.ncbi.nlm.nih.gov/pubmed/17437357>.
- Kohl, A. et al., 2003. Designed to be stable: crystal structure of a consensus ankyrin repeat protein. *Proceedings of the National Academy of Sciences of the United States of America*, 100(4), pp.1700-5. Available at: <http://www.pubmedcentral.nih.gov/articlerender.fcgi?artid=149896&tool=pmcentrez&rendertype=abstract>.
- Kronenberg, S. et al., 2005. A conformational change in the adeno-associated virus type 2 capsid leads to the exposure of hidden VP1 N termini. *Journal of virology*, 79(9), pp.5296-303. Available at: <http://www.pubmedcentral.nih.gov/articlerender.fcgi?artid=1082756&tool=pmcentrez&rendertype=abstract>.
- Labow, M.A., Hermonat, Paul L & Berns, K I, 1986. Positive and negative autoregulation of the adeno-associated virus type 2 genome. *Journal of virology*, 60(1), pp.251-8. Available at: <http://www.pubmedcentral.nih.gov/articlerender.fcgi?artid=253923&tool=pmcentrez&rendertype=abstract>.
- Lackner, D.F. & Muzyczka, Nicholas, 2002. Studies of the mechanism of transactivation of the adeno-associated virus p19 promoter by Rep protein. *Journal of virology*, 76(16), pp.8225-35. Available at: <http://www.pubmedcentral.nih.gov/articlerender.fcgi?artid=155137&tool=pmcentrez&rendertype=abstract>.
- Lehman, I.R., 1974. DNA ligase: structure, mechanism, and function. *Science (New York, N.Y.)*, 186(4166), pp.790-7. Available at: <http://www.ncbi.nlm.nih.gov/pubmed/4377758>.
- Lessey, B.A. et al., 1995. Distribution of integrin cell adhesion molecules in endometrial cancer. *The American journal of pathology*, 146(3), pp.717-26. Available at: <http://www.pubmedcentral.nih.gov/articlerender.fcgi?artid=1869177&tool=pmcentrez&rendertype=abstract>.
- Levy, H.C. et al., 2009. Heparin binding induces conformational changes in Adeno-associated virus serotype 2. *Journal of structural biology*, 165(3), pp.146-56. Available at: <http://www.ncbi.nlm.nih.gov/pubmed/19121398>.
- Li, E. et al., 1998. Adenovirus endocytosis requires actin cytoskeleton reorganization mediated by Rho family GTPases. *Journal of virology*, 72(11), pp.8806-12. Available at: <http://www.pubmedcentral.nih.gov/articlerender.fcgi?artid=110297&tool=pmcentrez&rendertype=abstract>.
- Linden, R M et al., 1996. Site-specific integration by adeno-associated virus. *Proceedings of the National Academy of Sciences of the United States of America*, 93(21), pp.11288-94. Available at: <http://www.pubmedcentral.nih.gov/articlerender.fcgi?artid=38050&tool=pmcentrez&rendertype=abstract>.

- Lusby, E., Fife, K.H. & Berns, K I, 1980. Nucleotide sequence of the inverted terminal repetition in adeno-associated virus DNA. *Journal of virology*, 34(2), pp.402-9. Available at: <http://www.pubmedcentral.nih.gov/articlerender.fcgi?artid=288718&tool=pmcentrez&rendertype=abstract>.
- Lux, K. et al., 2005. Green Fluorescent Protein-Tagged Adeno-Associated Virus Particles Allow the Study of Cytosolic and Nuclear Trafficking. *Journal of Virology*, 79(18), pp.11776-11787.
- Lybarger, L. et al., 1998. Dual-color flow cytometric detection of fluorescent proteins using single-laser (488-nm) excitation. *Cytometry*, 31(3), pp.147-52. Available at: <http://www.ncbi.nlm.nih.gov/pubmed/9515713>.
- Mansilla-Soto, J. et al., 2009. DNA structure modulates the oligomerization properties of the AAV initiator protein Rep68. *PLoS pathogens*, 5(7), p.e1000513. Available at: <http://www.pubmedcentral.nih.gov/articlerender.fcgi?artid=2702170&tool=pmcentrez&rendertype=abstract>.
- Marti, G.E. et al., 2001. Introduction to flow cytometry. *Seminars in hematology*, 38(2), pp.93-9. Available at: <http://www.ncbi.nlm.nih.gov/pubmed/11309691>.
- McCaffrey, A.P. et al., 2002. RNA interference in adult mice. *Nature*, 418(6893), pp.38-9. Available at: <http://www.ncbi.nlm.nih.gov/pubmed/12097900>.
- Michelfelder, S. & Trepel, M., 2009. *Tissue-Specific Vascular Endothelial Signals and Vector Targeting, Part A*, Elsevier. Available at: <http://www.ncbi.nlm.nih.gov/pubmed/19914449>.
- Millevoi, S. et al., 2006. An interaction between U2AF 65 and CF I(m) links the splicing and 3' end processing machineries. *The EMBO journal*, 25(20), pp.4854-64. Available at: <http://www.ncbi.nlm.nih.gov/pubmed/17024186>.
- Modrow, S. et al., 2003. *Molekulare Virologie*,
- Moolten, F.L., 1986. Tumor chemosensitivity conferred by inserted herpes thymidine kinase genes: paradigm for a prospective cancer control strategy. *Cancer research*, 46(10), pp.5276-81. Available at: <http://www.ncbi.nlm.nih.gov/pubmed/3019523>.
- Mullen, C.A., Kilstrupt, M. & Blaese, R.M., 1992. Transfer of the bacterial gene for cytosine deaminase to mammalian cells confers lethal sensitivity to 5-fluorocytosine : A negative selection system. *Cell*, 89(January), pp.33-37.
- Murphy, M. et al., 2007. Adeno-associated virus type 2 p5 promoter: a rep-regulated DNA switch element functioning in transcription, replication, and site-specific integration. *Journal of virology*, 81(8), pp.3721-30. Available at: <http://www.pubmedcentral.nih.gov/articlerender.fcgi?artid=1866101&tool=pmcentrez&rendertype=abstract>.

- Nagai, T. et al., 2002. A variant of yellow fluorescent protein with fast and efficient maturation for cell-biological applications. *Nature biotechnology*, 20(1), pp.87-90. Available at: <http://www.ncbi.nlm.nih.gov/pubmed/11753368>.
- Nash, K. et al., 2009. Identification of cellular proteins that interact with the adeno-associated virus rep protein. *Journal of virology*, 83(1), pp.454-69. Available at: <http://www.pubmedcentral.nih.gov/articlerender.fcgi?artid=2612328&tool=pmcentrez&rendertype=abstract>.
- Nolan, T., Hands, R.E. & Bustin, S. a, 2006. Quantification of mRNA using real-time RT-PCR. *Nature protocols*, 1(3), pp.1559-82. Available at: <http://www.ncbi.nlm.nih.gov/pubmed/17406449>.
- Nord, K. et al., 1997. Binding proteins selected from combinatorial libraries of an alpha-helical bacterial receptor domain. *Nature biotechnology*, 15(8), pp.772-7. Available at: <http://www.ncbi.nlm.nih.gov/pubmed/9255793>.
- Nott, A., Meislin, S.H. & Moore, M.J., 2003. A quantitative analysis of intron effects on mammalian gene expression. *RNA (New York, N.Y.)*, 9(5), pp.607-17. Available at: <http://www.ncbi.nlm.nih.gov/pubmed/12702819>.
- Ohno, H. et al., 1995. Interaction of tyrosine-based sorting signals with clathrin-associated proteins. *Science (New York, N.Y.)*, 269(5232), pp.1872-5. Available at: <http://www.ncbi.nlm.nih.gov/pubmed/7569928>.
- Opie, S., Jr, K.W. & Agbandje-, M., 2003. Identification of amino acid residues in the capsid proteins of adeno-associated virus type 2 that contribute to heparan sulfate proteoglycan binding. *Journal of Virology*, 77(12), pp.6995-7006. Available at: <http://jvi.asm.org/cgi/content/abstract/77/12/6995>.
- Orlova, A. et al., 2007. Synthetic affibody molecules: a novel class of affinity ligands for molecular imaging of HER2-expressing malignant tumors. *Cancer research*, 67(5), pp.2178-86. Available at: <http://www.ncbi.nlm.nih.gov/pubmed/17332348>.
- Panja, S. et al., 2008. How does plasmid DNA penetrate cell membranes in artificial transformation process of Escherichia coli ? *Transformation*, 25(August). Available at: <http://informahealthcare.com/doi/abs/10.1080/09687680802187765>.
- Pereira, D.J. & Muzyczka, N, 1997. The adeno-associated virus type 2 p40 promoter requires a proximal Sp1 interaction and a p19 CArG-like element to facilitate Rep transactivation. *Journal of virology*, 71(6), pp.4300-9. Available at: <http://www.pubmedcentral.nih.gov/articlerender.fcgi?artid=191646&tool=pmcentrez&rendertype=abstract>.
- Philpott, N.J. et al., 2002. A p5 integration efficiency element mediates Rep-dependent integration into AAVS1 at chromosome 19. *Proceedings of the National Academy of Sciences of the United States of America*, 99(19), pp.12381-5. Available at: <http://www.pubmedcentral.nih.gov/articlerender.fcgi?artid=129453&tool=pmcentrez&rendertype=abstract>.

- Pope, I., 1997. The role of the bystander effect in suicide gene therapy. *European Journal of Cancer*, 33(7), pp.1005-1016. Available at: <http://linkinghub.elsevier.com/retrieve/pii/S0959804996004832>.
- Reardon, J.E., 1989. Herpes simplex virus type 1 and human DNA polymerase interactions with 2'-deoxyguanosine 5'-triphosphate analogues. Kinetics of incorporation into DNA and induction of inhibition. *The Journal of biological chemistry*, 264(32), pp.19039-44. Available at: <http://www.ncbi.nlm.nih.gov/pubmed/2553730>.
- Robinson, M.S., 2004. Adaptable adaptors for coated vesicles. *Trends in cell biology*, 14(4), pp.167-74. Available at: <http://www.ncbi.nlm.nih.gov/pubmed/15066634>.
- Roche, Apoptosis , Cell Death and Cell Proliferation.
- Rohr, U.-P. et al., 2005. Quantitative real-time PCR for titration of infectious recombinant AAV-2 particles. *Journal of virological methods*, 127(1), pp.40-5. Available at: <http://www.ncbi.nlm.nih.gov/pubmed/15893564>.
- Rohr, U.-P. et al., 2002. Fast and reliable titration of recombinant adeno-associated virus type-2 using quantitative real-time PCR. *Journal of virological methods*, 106(1), pp.81-8. Available at: <http://www.ncbi.nlm.nih.gov/pubmed/12367732>.
- Samulski, R J, 1993. Adeno-associated virus: integration at a specific chromosomal locus. *Current opinion in genetics & development*, 3(1), pp.74-80. Available at: <http://www.ncbi.nlm.nih.gov/pubmed/8384035>.
- Samulski, R J & Shenk, T, 1988. Adenovirus E1B 55-Mr polypeptide facilitates timely cytoplasmic accumulation of adeno-associated virus mRNAs. *Journal of virology*, 62(1), pp.206-10. Available at: <http://www.pubmedcentral.nih.gov/articlerender.fcgi?artid=250520&tool=pmcentrez&rendertype=abstract>.
- Sanlioglu, S. et al., 2000a. Endocytosis and nuclear trafficking of adeno-associated virus type 2 are controlled by rac1 and phosphatidylinositol-3 kinase activation. *Journal of virology*, 74(19), pp.9184-96. Available at: <http://www.pubmedcentral.nih.gov/articlerender.fcgi?artid=102117&tool=pmcentrez&rendertype=abstract>.
- Sanlioglu, S. et al., 2000b. Endocytosis and nuclear trafficking of adeno-associated virus type 2 are controlled by rac1 and phosphatidylinositol-3 kinase activation. *Journal of virology*, 74(19), pp.9184-96. Available at: <http://www.pubmedcentral.nih.gov/articlerender.fcgi?artid=102117&tool=pmcentrez&rendertype=abstract>.
- Schröter, A.K., 2009. Untersuchung der Wechselwirkung zwischen dem EGFR-Rezeptor und potenziell an den Rezeptor bindenden Molekülen.
- Schultz, B.R. & Chamberlain, J.S., 2008. Recombinant adeno-associated virus transduction and integration. *Molecular therapy : the journal of the American Society of Gene Therapy*, 16(7), pp.1189-99. Available at: <http://www.ncbi.nlm.nih.gov/pubmed/18500252>.

- Seisenberger, G. et al., 2001. Real-time single-molecule imaging of the infection pathway of an adeno-associated virus. *Science (New York, N.Y.)*, 294(5548), pp.1929-32. Available at: <http://www.ncbi.nlm.nih.gov/pubmed/11729319>.
- Sinnis, P. et al., 2007. Mosquito heparan sulfate and its potential role in malaria infection and transmission. *The Journal of biological chemistry*, 282(35), pp.25376-84. Available at: <http://www.pubmedcentral.nih.gov/articlerender.fcgi?artid=2121605&tool=pmcentrez&rendertype=abstract>.
- Smith, M.C. et al., 1988. Chelating peptide-immobilized metal ion affinity chromatography. A new concept in affinity chromatography for recombinant proteins. *The Journal of biological chemistry*, 263(15), pp.7211-5. Available at: <http://www.ncbi.nlm.nih.gov/pubmed/3284883>.
- Smith, R.H. & Kotin, R.M., 1998. The Rep52 gene product of adeno-associated virus is a DNA helicase with 3'-to-5' polarity. *Journal of virology*, 72(6), pp.4874-81. Available at: <http://www.pubmedcentral.nih.gov/articlerender.fcgi?artid=110039&tool=pmcentrez&rendertype=abstract>.
- Smythe, W.R. et al., 1995. Integrin expression in non-small cell carcinoma of the lung. *Cancer metastasis reviews*, 14(3), pp.229-39. Available at: <http://www.ncbi.nlm.nih.gov/pubmed/8548871>.
- Sonntag, F. et al., 2006. Adeno-associated virus type 2 capsids with externalized VP1/VP2 trafficking domains are generated prior to passage through the cytoplasm and are maintained until uncoating occurs in the nucleus. *Journal of virology*, 80(22), pp.11040-54. Available at: <http://www.pubmedcentral.nih.gov/articlerender.fcgi?artid=1642181&tool=pmcentrez&rendertype=abstract>.
- Srivastava, A., 2008. Adeno-associated virus-mediated gene transfer. *Journal of cellular biochemistry*, 105(1), pp.17-24. Available at: <http://www.ncbi.nlm.nih.gov/pubmed/18500727>.
- Steiner, D., Forrer, P. & Plückthun, A., 2008a. Efficient selection of DARPins with sub-nanomolar affinities using SRP phage display. *Journal of molecular biology*, 382(5), pp.1211-27. Available at: <http://www.ncbi.nlm.nih.gov/pubmed/18706916>.
- Steiner, D., Forrer, P. & Plückthun, A., 2008b. Efficient selection of DARPins with sub-nanomolar affinities using SRP phage display. *Journal of molecular biology*, 382(5), pp.1211-27. Available at: <http://www.ncbi.nlm.nih.gov/pubmed/18706916>.
- Stratagene, AAV Helper-Free System. *Manual*, Revision A.
- Summerford, C. & Samulski, R J, 1998. Membrane-associated heparan sulfate proteoglycan is a receptor for adeno-associated virus type 2 virions. *Journal of virology*, 72(2), pp.1438-45. Available at: <http://www.pubmedcentral.nih.gov/articlerender.fcgi?artid=124624&tool=pmcentrez&rendertype=abstract>.

- Tratschin, J.D. et al., 1984. A human parvovirus, adeno-associated virus, as a eucaryotic vector: transient expression and encapsidation of the procaryotic gene for chloramphenicol acetyltransferase. *Molecular and cellular biology*, 4(10), pp.2072-81. Available at: <http://www.pubmedcentral.nih.gov/articlerender.fcgi?artid=369024&tool=pmcentrez&rendertype=abstract>.
- Trepel, M. et al., 2009. A heterotypic bystander effect for tumor cell killing after adeno-associated virus/phage-mediated, vascular-targeted suicide gene transfer. *Molecular cancer therapeutics*, 8(8), pp.2383-91. Available at: <http://www.pubmedcentral.nih.gov/articlerender.fcgi?artid=2871293&tool=pmcentrez&rendertype=abstract>.
- Trepel, M., Vectors, A.-associated V. & Receptors, C.-type S., 2009. Adeno-Associated Viral Vectors and Their Redirection to Cell-Type Specific Receptors. *Advances*, 67, pp.29-60.
- Walker, R. a & Dearing, S.J., 1999. Expression of epidermal growth factor receptor mRNA and protein in primary breast carcinomas. *Breast cancer research and treatment*, 53(2), pp.167-76. Available at: <http://www.ncbi.nlm.nih.gov/pubmed/10326794>.
- Ward, P. et al., 1998. Role of the adenovirus DNA-binding protein in in vitro adeno-associated virus DNA replication. *Journal of virology*, 72(1), pp.420-7. Available at: <http://www.pubmedcentral.nih.gov/articlerender.fcgi?artid=109390&tool=pmcentrez&rendertype=abstract>.
- Warrington, K.H. et al., 2004. Adeno-associated virus type 2 VP2 capsid protein is nonessential and can tolerate large peptide insertions at its N terminus. *Journal of virology*, 78(12), pp.6595-609. Available at: <http://www.pubmedcentral.nih.gov/articlerender.fcgi?artid=416546&tool=pmcentrez&rendertype=abstract>.
- West, M.H. et al., 1987. Gene expression in adeno-associated virus vectors: the effects of chimeric mRNA structure, helper virus, and adenovirus VA1 RNA. *Virology*, 160(1), pp.38-47. Available at: <http://www.ncbi.nlm.nih.gov/pubmed/2820138>.
- Wikman, M. et al., 2004. Selection and characterization of HER2/neu-binding affibody ligands. *Protein engineering, design & selection : PEDS*, 17(5), pp.455-62. Available at: <http://www.ncbi.nlm.nih.gov/pubmed/15208403>.
- Yang, L. et al., 1998. Intercellular communication mediates the bystander effect during herpes simplex thymidine kinase/ganciclovir-based gene therapy of human gastrointestinal tumor cells. *Human gene therapy*, 9(5), pp.719-28. Available at: <http://www.ncbi.nlm.nih.gov/pubmed/9551619>.
- Ybe, J.A. et al., 1999. Clathrin self-assembly is mediated by a tandemly repeated superhelix. *Nature*, 399(6734), pp.371-5. Available at: <http://www.ncbi.nlm.nih.gov/pubmed/10360576>.
- Yue, Y.-bo et al., 2010. Functional differentiation between Rep-mediated site-specific integration and transcriptional repression of the adeno-associated viral p5 promoter.

Human gene therapy, 21(6), pp.728-38. Available at:
<http://www.ncbi.nlm.nih.gov/pubmed/20070175>.

Zimmermann, T.S. et al., 2006. RNAi-mediated gene silencing in non-human primates.
Nature, 441(7089), pp.111-4. Available at:
<http://www.ncbi.nlm.nih.gov/pubmed/16565705>.